UNIVERSIDADE ESTADUAL PAULISTA

"Júlio de Mesquita Filho"

Instituto de Geociências e Ciências Exatas

Câmpus de Rio Claro

REGIANE ANDRADE FUMES

PETROCHRONOLOGY OF HIGH-PRESSURE AMPHIBOLITE TO GRANULITE FACIES ROCKS FROM THE SOUTHERN BRASÍLIA OROGEN: EXAMPLES FROM THE CARRANCAS AND ARAXÁ GROUPS

Orientador: Prof. Dr. George Luiz Luvizotto

Rio Claro – SP

2021

UNIVERSIDADE ESTADUAL PAULISTA

"Júlio de Mesquita Filho"

Instituto de Geociências e Ciências Exatas

Câmpus de Rio Claro

REGIANE ANDRADE FUMES

PETROCHRONOLOGY OF HIGH-PRESSURE AMPHIBOLITE TO GRANULITE FACIES ROCKS FROM THE SOUTHERN BRASÍLIA OROGEN: EXAMPLES FROM THE CARRANCAS AND ARAXÁ GROUPS

Tese de doutorado apresentada ao Instituto de Geociências e Ciências Exatas do Câmpus de Rio Claro, da Universidade Estadual Pau- lista Júlio de Mesquita Filho, como parte dos requisitos para obtenção do título de Doutor em Geociências e Meio Ambiente

Orientador: Prof. Dr. George Luiz Luvizotto

Rio Claro – SP

2021

F977p

Fumes, Regiane Andrade

Petrochronology of high-pressure amphibolite to granulite facies rocks from the Southern Brasília Orogen: examples from the Carrancas and Araxá Groups / Regiane Andrade Fumes. -- Rio Claro, 2021

221 p. : il., tabs., fotos

Tese (doutorado) - Universidade Estadual Paulista (Unesp), Instituto de Geociências e Ciências Exatas, Rio Claro

Orientador: Prof. Dr. George Luiz Luvizotto

1. Zr-em-rutilo. 2. Ti-em-quartzo. 3. datação de monazita. 4. XMapTools. 5. THERMOCALC. I. Título.

Sistema de geração automática de fichas catalográficas da Unesp. Biblioteca do Instituto de Geociências e Ciências Exatas, Rio Claro. Dados fornecidos pelo autor(a).

Essa ficha não pode ser modificada.

REGIANE ANDRADE FUMES

PETROCHRONOLOGY OF HIGH-PRESSURE AMPHIBOLITE TO GRANULITE FACIES ROCKS FROM THE SOUTHERN BRASÍLIA OROGEN: EXAMPLES FROM THE CARRANCAS AND ARAXÁ GROUPS

Tese de Doutorado apresentada ao Instituto de Geociências e Ciências Exatas do Câmpus de Rio Claro, da Universidade Estadual Paulista "Júlio de Mesquita Filho", como parte dos requisitos para obtenção do título de Doutor em Geociências e Meio Ambiente

Comissão Examinadora

Prof. Dr. George Luiz Luvizotto
Prof. Dr. Rudolph Allard Johannes Trouw
Profa. Dra. Eliza Inez Nunes Peixoto
Profa. Dra. Mahyra Tedeschi
Prof. Dr. Rafael Gonçalves Da Motta

Conceito: Aprovado.

Rio Claro/SP, 9 de Setembro de 2021

Acknowledgements

Here I would like to thank the people who were fundamental during this PhD.

To my advisor Prof. Dr. George Luvizotto and to Prof. Dr. Renato de Moraes for their dedication and patience in helping me since the beginning of the master's and for believing our project. I would like to thank all the lessons learned over all these years.

To my parents (Mário and Atilana), my brother Leandro, my aunt Eliane and my grandfather Margarida for their total support during all these years of academic life.

Thaynara for always accompanying me throughout these years.

To my graduate friends, Juliana, Marli, Otávio and Lucas for always accompanying me and making the work environment more productive and fun.

To co-authors Pierre Lanari, Claudio de Morisson Valeriano, Luiz Sérgio Amarante Simões, Monica Heilbron, Silvio Roberto Farias Vach, Thomas Zack, Mark J. Caddick and Lara A. Patto for their valuable collaboration in the works.

To the members of the defense panel, Prof. Dr. George Luiz Luvizotto, Prof. Dr. Rudolph Allard Johannes Trouw, Profa. Dra. Eliza Inez Nunes Peixoto, Profa. Dra. Mahyra Tedeschi, Prof. Dr. Rafael Gonçalves Da Motta for the grandiose discussion about the work and geology of the studied area.

To the members of the qualifying panel, Maurício Pavan Silva and Cauê Rodrigues Cioffi, for their contributions and tips to the work.

National Council for Scientific and Technological Development (CNPq) (grant-141604/2018-2) for PhD scholarship is acknowledged. This study was financed in part by the Coordenação de Aperfeiçoamento de Pessoal de Nível Superior - Brasil (CAPES) - Finance Code 001. Part of this thesis was funded by São Paulo Research Foundation (FAPESP), through grant 15/05230-0.

Agradecimentos

Gostaria de agradecer aqui as pessoas que foram fundamentais para a execução deste doutorado.

Ao meu orientador George Luvizotto e ao Renato de Moraes pela dedicação e paciência em me ajudar desde o início do mestrado e por acreditar nosso projeto. Gostaria de agradecer a todos os aprendizados adquiridos ao longo de todos esses anos.

Aos meus pais (Mário e Atilana), ao meu irmão Leandro, a minha tia Eliane e a minha avó Margarida pelo total apoio durante todos esses anos de vida acadêmica.

À Thaynara por sempre me acompanhar ao longo desse anos.

Aos amigos da pós-graduação, Juliana, Marli, Otávio e Lucas por sempre me acompanharem e tornarem o ambiente de trabalho mais produtivo e divertido.

Aos co-autores Pierre Lanari, Claudio de Morisson Valeriano, Luiz Sérgio Amarante Simões, Monica Heilbron, Silvio Roberto Farias Vach, Thomas Zack, Mark J. Caddick e Lara A. Patto pela valiosa colaboração nos trabalhos.

Aos membros da banca de defesa, Prof. Dr. George Luiz Luvizotto, Prof. Dr. Rudolph Allard Johannes Trouw, Profa. Dra. Eliza Inez Nunes Peixoto, Profa. Dra. Mahyra Tedeschi, Prof. Dr. Rafael Gonçalves Da Motta pela grandiosa discussão sobre o trabalho a geologia da área estudada.

Aos membros da banca de qualificação, Maurício Pavan Silva e Cauê Rodrigues Cioffi, pelas contribuições e dicas ao trabalho.

À capoeira (Prof. Baiano), terapia (Regina) e aos Orixás e entidades que me ajudaram ao longo dos anos.

Por fim, deixo também meu agradecimento a todos que, direta ou indiretamente, apoiaram este trabalho.

O Conselho Nacional de Desenvolvimento Científico e Tecnológico (CNPq) (processo-141604/2018-2) é agradecido pela bolsa de doutorado. O presente trabalho foi realizado com apoio da Coordenação de Aperfeiçoamento de Pessoal de Nível Superior - Brasil (CAPES) - Código de Financiamento 001. Parte desta tese foi financiada pela Fundação de Amparo à Pesquisa do Estado de São Paulo (FAPESP), através do projeto 15/05230-0.

Abstract

Rocks from the southern Brasília Orogen record subduction and collisional processes associated with the Western Gondwana collage, resulting from the convergence between the São Francisco Plate and the Paranapanema Plate. This continental collision led to the formation of east-verging Ediacaran-Cambrian nappe systems. Two nappes from these nappe systems were studied in this work: the Luminárias Nappe and the Passos Nappe. The Luminárias Nappe is composed of quartzites from São Tomé das Letras Unit, metapelites from the Carrancas Unit and the metagreywackes from the Santo Antônio Unit. The metamorphic rocks from this nappe register a metamorphic gradient varying from lower-amphibolite facies (580 ± 4 ^{o}C and ∼0.9 GPa - 644 ^{o}C/GPa) in the northern portion; to high-pressure amphibolite facies (600 ± 15 ^{o}C and 1.1 ± 0.3 GPa - 545 ^{o}C/GPa - Carrancas Unit and ∼630 ^{o}C and ∼0.9 Gpa - Santo Antônio Unit) in the central portion (peak conditions at 615 ± 6 Ma); to eclogite facies (630 ± 13 ^{o}C and 1.4 ± 0.6 GPa - 450 ^{o}C/GPa) in the southern portion (peak conditions at 632 ± 4 Ma). Clockwise P–T–t paths are documented for rocks from the Carrancas and Santo Antônio units. Data from Zr-in-rutile in the quartzite layer from the Luminárias Nappe indicates that the Zr content in detrital rutile may re-equilibrate in quartzite at minimum conditions of ∼630 ± 30 ^{o}C and 1.4 ± 0.6 GPa. In the Passos Nappe, an inverted metamorphic gradient varying from greenschist facies in the base to high-pressure granulite facies in the top is observed. Metamorphic studies were carried out on the high-pressure granulitic rocks and indicate a clockwise P–T–t path. The peak conditions are ∼830 ^{o}C and 1.2 GPa and took place at 630 Ma. Retrograde conditions of ∼600 ^{o}C and 0.9 GPa occurred at 590 Ma and the petrochronological data indicate a slow cooling rates. The high-pressure granulitic rocks from Passos Nappe can be correlated with the high-pressure granulitic rocks from the Andrelândia Nappe System (south of Passos Nappe). The metamorphic peak conditions and age obtained for rocks from the Luminárias and Passos nappes indicate that they formed under a continental-continental collision setting during the neoproterozoic, associated with the Gondwana formation.

Keywords: Zr-in-rutile, Ti-in-quartz, Monazite dating, XMapTools, THERMOCALC

Resumo

O Orógeno Brasília Meridional registra ambientes tectônicos de subdução e colisão associados à colagem do Gondwana Oeste, como resultado de um limite convergente entre as Placas do Sãofranciscana Paranapanema. Nessa colisão continental foram formados diversos sistemas de nappes Ediacaranas-Cambrianas com vergência para o leste. Duas nappes, dentre esses sistemas, foram estudadas neste trabalho: a Nappe de Luminárias e a Nappe de Passos. A Nappe de Luminárias é composta por quartzitos da Unidade São Tomé das Letras, metapelitos da Unidade Carrancas e de metagrauvacas da Unidade Santo Antônio. As rochas metamórficas da Nappe de Luminárias registram um gradiente metamórfico variando de fácies anfibolito inferior de alta pressão na porção norte (580 $\pm$ 4 ^{o}C e $\sim$0.9 GPa - 644 ^{o}C/GPa); de anfibolito de alta pressão (600 $\pm$ 15 ^{o}C e 1.1 $\pm$ 0.3 GPa - Unidade Carrancas e $\sim$630 ^{o}C - 545 ^{o}C/GPa e $\sim$0.9 Gpa - Unidade Santo Antônio) na porção central em 615 $\pm$ 6 Ma; e de fácies eclogito (630 $\pm$ 13 ^{o}C e 1.4 $\pm$ 0.6 GPa - 450 ^{o}C/GPa) na porção sul em 632 $\pm$ 4 Ma. Trajetórias *P–T–t* horárias são observadas nas rochas da Nappe de Luminárias. Dados de Zr-no-rutilo no quartzito da nappe indicam que os teores de Zr em rutilo detrítico devem se reequilibrar em condições mínimas de 630 $\pm$ 30 ^{o}C em condições de pressão de 1.4 $\pm$ 0.6 GPa. Na Nappe de Passos é observado um gradiente metamórfico invertido variando de fácies xisto verde na base a fácies granulito no topo. Em tais rochas granulíticas, que ocorrem no topo da Nappe de Passos, é registrada trajetória metamórfica *P–T–t* horária com condições de pico de 830 ^{o}C e 1.2 GPa em 630 Ma e condições retrometamórficas de $\sim$600 ^{o}C e 0.9 GPa em 590 Ma. Esses dados de petrocronologia indicam taxas de resfriamento lentas para o granulito. Essas rochas granulíticas da Nappe de Passos provavelmente se correlacionam com o granulito do sistema de Nappes Andrelândia (sul da Nappe de Passos). Baseado nas condições de pico metamórfico da Nappe de Luminárias e da Nappe de Passos é possível correlacionar com um ambiente tectônico de colisão entre continente-continente durante o fim do neoproterozóico associado a formação do Gondwana.

Palavras-chave: Zr-em-rutilo, Ti-em-quartzo, datação de monazita, XMapTools, THERMOCALC.

List of illustrations

List of tables

Summary

1 General Introduction

1.1 Preface

The southern Brasília Orogen is one of the collisional Ediacaran-Cambrian orogens associated with the Western Gondwana formation, as a product of the collision between the São Francisco and the Paranapanema plates (FUCK et al., 1994; BRITO NEVES; CAMPOS NETO; FUCK, 1999; CAMPOS NETO, 2000; TROUW et al., 2000; FUCK et al., 2017; HEILBRON; CORDANI; ALKMIM, 2017). The southern Brasília Orogen occurs in the southeastern and central of Brazil and is composed of a pile of sub-horizontal nappes with an inverted metamorphism pattern, varying from greenschist to granulite facies, with pressure conditions higher than those of a typical Barrowian Gradient (CAMPOS NETO; CABY, 1999; CAMPOS NETO, 2000; TROUW et al., 2000).

Although several studies regarding the rocks from southern Brasília Orogen have recently been published (COELHO et al., 2017; RENO et al., 2009; RENO et al., 2012; ROCHA et al., 2017; ROCHA et al., 2018; CIOFFI et al., 2012; CIOFFI et al., 2019; TEDESCHI et al., 2017; TEDESCHI et al., 2018; SILVA; SIMÕES; DUFRANE, 2019, among others), some open questions regarding the regional tectonic evolution of the orogen are still to be answered. The Luminárias Nappe and Passos Nappe are key areas to assess these questions, since detailed metamorphic studies using updated methods are not available for these areas. Some examples of questions are: what are the metamorphic peak conditions and age of metamorphism of the Luminárias and Passos nappes from southern Brasília Orogen? In what tectonic setting were the rocks formed? What are the processes responsible for the exhumation of the nappes?

In order to answers the questions presented above, a series of up to date tools were applied in this thesis. In the last decade, trace element thermobarometers have greatly expanded the ability to assess the pressure (P) and temperature (T) conditions of individual minerals associated with specific textures in metamorphic rocks (CRUZ-URIBE et al., 2018). In this sense, Ti-in-quartz and Zr-in-rutile thermobarometers have been applied in the present study. It is noteworthy that the application of trace element thermobarometers in natural samples/systems are more complex and dynamic than synthesis experiments (KENDRICK; INDARES, 2018). In the experiments the equilibrium among the phases is clearly evidence, however in natural samples the equilibration among all phases is not always maintained. Here, natural samples from high pressure amphibolite to eclogite facies and granulite facies (Luminárias Nappe and Passos Nappe, respectively) are analyzed in order to constrain the use of trace element thermometers in a wide range of metamorphic conditions.

Quantitative compositional mapping by electron probe micro-analyzer (EPMA) with advanced standardization function and the metamorphic modelling using phase diagram for a given bulk composition are further examples of up to date and useful tools that were applied in this study (POWELL; HOLLAND, 2008; LANARI et al., 2014; LANARI; ENGI; BERN, 2017; LANARI; DUESTERHOEFT, 2019). Furthermore, it is crucial to take into account the concept of the petrocronology (ENGI, 2017), since more than a single part of the *P–T–t* path is usually recorded in these rocks. In this sense, the use compositional mapping, pseudosection modelling, trace element thermobarometers, U-Pb-Th_T monazite and U-Pb rutile dating allow for a precise and accurate characterization of the metamorphic evolution of the rocks from Passos Nappe and Luminárias Nappe. These data are indispensable to evaluate the tectonic evolution of collisional belts.

1.2 Aim of the thesis

The aim of this work is to carry out petrochronological studies on high-pressure (HP) metamorphic rocks from Southern Brasília Orogen (Luminárias and Passos nappes), characterizing their metamorphic *P–T–t* paths and discussing the implication of the results on the tectonic evolution of the area. To reach the objectives, the metamorphic conditions and ages of the metamorphic peak and retrograde metamorphism processes in the rocks metamorphosed under HP-lower amphibolite, eclogite and granulite facies, are explored in the present work. The results are obtained through metamorphic modeling using pseudosections, quantitative compositional mapping, trace element thermobarometers (Ti-in-quartz and Ti-in-rutile), and U-Pb-Th_T monazite dating (by EPMA).

1.3 Thesis Structure

This work is composed of thesis chapters and scientific articles as follows:

- *Chapter 1 - General Introduction* - this chapter contains a general introduction to the thesis, a brief contextualization of the covered themes, the aim and the structure of the work.
- *Chapter 2 - Evolution of the geological knowledge of the studied area* - this chapter presents the geological background of the studied areas (Luminárias and Passos Nappe from the Southern Brasília Orogen).
- *Chapter 3 - Petrochronology of high-pressure granulite facies rocks from Southern Brasília Orogen* - a manuscript that is accepted for publication in the Journal of Metamorphic Geology. This article presents data on the metamorphic characterization

of HP granulitic rocks from Passos Nappe, discussing the metamorphic *P-T*-t path, the usage of single element geothermometers and the age of metamorphism.

- *Chapter 4 - Metamorphic modeling and petrochronology of metapelitic rocks from the Luminárias Nappe, southern Brasília orogen (SE Brazil)* - a scientific article published in the Brazilian Journal of Geology (FUMES et al., 2019). In this work is presented the metamorphic modeling from high-pressure lower amphibolite facies to eclogite metapelitic rocks from Luminárias Nappe and the petrochronology. This is a follow up work of the masters dissertation of Fumes (2017), that includes new petrochronological data where the U-Pb-Th$_T$ EPMA in monazite data were acquired during this PhD project.

- *Chapter 5 - The potential for using metagreywacke to study metamorphism* - this chapter presents data on the metamorphic modelling of the metagreywacke of the Santo Antônio Unit in the Luminárias Nappe and a comparison between metapelite protoliths. This manuscript is published in the Journal Mineralogy and Petrology (FUMES et al., 2021).

- *Chapter 6 - Changes in rutile geochemistry in quartzite through increasing P-T conditions* - a manuscript that will be submitted in Journal of South American Earth Sciences, where we investigate changes in trace element composition in rutile from quartzite through increasing metamorphic conditions using as an example rocks from the Luminárias Nappe.

- *Chapter 7 Overall Discussions* - this chapter contains the discussions regarding all the data presented in this thesis. The individual discussions of manuscripts are integrated in order to add information on the geological evolution of the southern Brasília orogen and the application of trace element thermometers.

- *Chapter 8 - Conclusions* - in this section the main conclusions of this thesis are presented.

- *Supplementary Material* - this section provides the links the supplementary referenced in the previous chapters.

- *Appendix* - this section presents conference abstracts that were presented during the doctorate work.

Reference

BRITO NEVES, B. B. de; CAMPOS NETO, M. D. C.; FUCK, R. A. From Rodinia to Western Gondwana: as Aproach to the Brasiliano-Pan African Cycle and orogenic collage. *Episodes-Newsmagazine of International Union of Geological Science*, v. 22, n. 155-166, 1999.

CAMPOS NETO, M. D. C. Orogenic Systems from Southwestern Gondwana: An Approach to Brasiliano-Pan African Cycle and Orogenic Collage in Southeastern Brazil. In: CORDANI, U. G. et al. (Ed.). *Tectonic Evolution of South America*. 1. ed. Rio de Janeiro: COMPANHIA DE PESQUISA DE RECURSOS MINERAIS, 2000. p. 335–365.

CAMPOS NETO, M. D. C.; CABY, R. Neoproterozoic high-pressure metamorphism and tectonic constraint from the nappe system south of the Sao Francisco Craton, southeast Brazil. *Precambrian Research*, v. 97, n. 1-2, p. 3–26, 1999. ISSN 03019268.

CIOFFI, C. R. et al. Geochemical signatures of metasedimentary rocks of high-pressure granulite facies and their relation with partial melting: Carvalhos Klippe, Southern Brasília Belt, Brazil. *Journal of South American Earth Sciences*, v. 40, p. 63–76, 2012. ISSN 08959811.

CIOFFI, C. R. et al. Titanite petrochronology of the southern Brasília Orogen basement: Effects of retrograde net-transfer reactions on titanite trace element compositions. *Lithos*, Elsevier, v. 344, p. 393–408, 2019.

COELHO, M. B. et al. Constraining timing and P-T conditions of continental collision and late overprinting in the Southern Brasília Orogen (SE-Brazil): U-Pb zircon ages and geothermobarometry of the Andrelândia Nappe System. *Precambrian Research*, Elsevier B.V., v. 292, p. 194–215, 2017. ISSN 03019268. Avaible form internet: <http://linkinghub.elsevier.com/retrieve/pii/S0301926816305496>.

CRUZ-URIBE, A. M. et al. Assessing trace element (dis)equilibrium and the application of single element thermometers in metamorphic rocks. *Lithos*, Elsevier B.V., v. 314-315, p. 1–15, 2018. ISSN 18726143. Avaible form internet: <https://doi.org/10.1016/j.lithos.2018.05.007>.

ENGI, M. Petrochronology Based on REE-Minerals: Monazite, Allanite, Xenotime, Apatite. *Reviews in Mineralogy and Geochemistry*, v. 83, n. 1, p. 365 LP – 418, 2017. Avaible form internet: <http://rimg.geoscienceworld.org/content/83/1/365.abstract>.

FUCK, R. et al. Compartimentação tectônica da porção oriental da Província Tocantins. In: *SBG, Congresso Brasileiro de Geologia*. [S.l.: s.n.], 1994. v. 38, n. 1, p. 215–216.

FUCK, R. A. et al. The Northern Brasília Belt. In: HEILBRON, M.; CORDANI, U. G.; ALKMIM, F. F. (Ed.). *São Francisco Craton, Eastern Brazil Tectonic Genealogy of a Miniature Continent*. [S.l.]: Springer Berlin Heidelberg, 2017. p. 205–220.

FUMES, R. A. *Modelagem metamórfica e geotermobarometria de elementos traço em metapelitos e quartzitos: exemplo da Nappe de Luminárias-MG*. Dissertação (Mestrado) — São Paulo State University, January 2017.

FUMES, R. A. et al. Metamorphic modeling and petrochronology of metapelitic rocks from the Luminárias Nappe, southern Brasília belt (SE Brazil). *Brazilian Journal of Geology*, v. 49, n. 2, 2019.

FUMES, R. A. et al. The potential for using metagreywacke to study metamorphism of amphibolite facies conditions: a comparison study within the luminárias nappe, southern brasília orogen (southeastern brazil). *Mineralogy and Petrology*, Springer, p. 1–16, 2021.

HEILBRON, M.; CORDANI, U. G.; ALKMIM, F. F. *São Francisco Craton, Eastern Brazil: Tectonic Genealogy of a Miniature Continent*. [S.l.: s.n.], 2017. 331 p. ISBN 9783319017143.

KENDRICK, J.; INDARES, A. The Ti Record of Quartz in Anatectic Aluminous Granulites. *Journal of Petrology*, n. July, p. 1–23, 2018. ISSN 0022-3530.

LANARI, P.; DUESTERHOEFT, E. Modeling Metamorphic Rocks Using Equilibrium Thermodynamics and Internally Consistent Databases: Past Achievements, Problems and Perspectives. *Journal of Petrology*, v. 60, n. 1, p. 19–56, 2019. ISSN 14602415.

LANARI, P.; ENGI, M.; BERN, C. Local Bulk Composition Effects on Metamorphic Mineral Assemblages. *Reviews in Mineralogy and Geochemistry*, v. 83, p. 55–93, 2017.

LANARI, P. et al. Xmaptools: A matlab©-based program for electron microprobe x-ray image processing and geothermobarometry. *Computers & Geosciences*, Elsevier, v. 62, p. 227–240, 2014.

POWELL, R.; HOLLAND, T. J. B. On thermobarometry. *Journal of Metamorphic Geology*, v. 26, n. 2, p. 155–179, 2008. ISSN 02634929.

RENO, B. L. et al. Eclogite–high-pressure granulite metamorphism records early collision in West Gondwana: new data from the Southern Brasília Belt, Brazil. *Journal of the Geological Society*, Geological Society of London, v. 166, n. 6, p. 1013–1032, 2009.

RENO, B. L. et al. In situ monazite (U-Th)-Pb ages from the Southern Brasília Belt, Brazil: Constraints on the high-temperature retrograde evolution of HP granulites. *Journal of Metamorphic Geology*, v. 30, n. 1, p. 81–112, 2012. ISSN 02634929.

ROCHA, B. C. et al. Timing of anatexis and melt crystallization in the Socorro – Guaxupé Nappe , SE Brazil : Insights from trace element composition of zircon , monazite and garnet coupled to U — Pb geochronology. v. 277, p. 337–355, 2017.

ROCHA, B. C. et al. Magmatic inheritance vs. UHT metamorphism: Zircon petrochronology of granulites and petrogenesis of charnockitic leucosomes of the Socorro–Guaxupé nappe, SE Brazil. *Lithos*, v. 314-315, p. 16–39, 2018. ISSN 18726143.

SILVA, A. J. C. A.; SIMÕES, L. S. A.; DUFRANE, S. A. Tectonic implications of U-Pb ages of detrital zircon grains in metasedimentary rocks of the northwestern sector of the Passos Nappe, southern Brasília Belt, Brazil. *Journal of South American Earth Sciences*, Elsevier, n. 95, p. 1–24, 2019.

TEDESCHI, M. et al. Reconstruction of multiple PTt stages from retrogressed mafic rocks: Subduction versus collision in the Southern Brasília orogen (SE Brazil). *Lithos*, Elsevier, v. 294, p. 283–303, 2017.

TEDESCHI, M. et al. Protracted zircon geochronological record of UHT garnet-free granulites in the Southern Brasília orogen (SE Brazil): Petrochronological constraints on magmatism and metamorphism. *Precambrian Research*, Elsevier, v. 316, n. August, p. 103–126, 2018. ISSN 03019268. Avaible form internet: <https://doi.org/10.1016/j.precamres.2018.07.023>.

TROUW, R. A. J. et al. The Central Segment of the Ribeira Belt. In: CORDANI, U. G. et al. (Ed.). *Tectonic Evolution of South America*. 1. ed. [S.l.]: COMPANHIA DE PESQUISA DE RECURSOS MINERAIS, 2000. p. 287–310.

2 Evolution of the geological knowledge of the studied areas

The Brasília Orogen is a N-S striking Neoproterozoic orogen that occurs in the central and southeastern of Brazil, where it extends for more than 1,1000 km. It records the convergence and collision that took place during the Brasiliano orogeny in the late Neoproterozoic, as part of West Gondwana amalgamation (DARDENNE, 2000; FUCK et al., 2017; HEILBRON et al., 2017) (Figure 2.1 and Figure 2.2).

The Brasília Orogen borders the western margin of the São Francisco Craton and is part of the Tocantins Tectonic Province (ALMEIDA, 1977; ALMEIDA et al., 1981) and its formation took place over a long period of time (900 – 600 Ma) involving subduction, magmatism and terrain accretion, as a result of the consumption of the Goiás oceanic lithosphere (PIMENTEL, 2016). The Pirineus Syntaxis divides the Brasília Orogen in northern and southern segments (ARAÚJO FILHO, 1980; ARAÚJO FILHO, 1992; ARAÚJO FILHO, 2000). The Southern Brasília Orogen is essentially composed of metasedimentary rocks that registers a complete Wilson Cycle, that underwent metamorphism and deformation with metamorphic peak at ca. 650 – 630 Ma, starting with the development of a passive margin and Goainides ocean (Tonian) and finishing with subduction of distal units (Ediacaran-Cambian) (VALERIANO, 2017; TROUW et al., 2000; VALERIANO et al., 2008; FUCK et al., 2017).

According to Dardenne (2000) the deformation and metamorphism in the Brasília Orogen increases progressively towards the west. The metamorphic grade varies from non metamorphosed sediments in the cratonic area (São Francisco Craton) to high-temperature amphibolite to granulite facies rocks (COSTA; ANGEIRAIS, 1971; DARDENNE, 1978; FUCK et al., 1994), including ultra-high-temperature conditions in the metamorphic core in the western part of the Brasília Orogen (MORAES et al., 2002; MORAES et al., 2015).

The Southern Brasilia Orogen is tectonic divided from the base to the top (or from east to west) into: (i) the cratonic zone; (ii) the external metamorphic fold-thrust belt; (iii) the upper nappe complex or internal domain (FUCK et al., 1994; VALERIANO et al., 2000; VALERIANO et al., 2004; DARDENNE, 2000; VALERIANO, 2017). The cratonic zone, according to the same authors, occurs in the eastern extremity of Southern Brasília Orogen (Figure 2.1 b) where the Neoproterozoic cover is virtually undeformed and unmetamorphosed. The external metamorphic fold-thrust belt is composed of metasedimentary rocks, from base to top, the Paranoá, Canastra and Ibiá groups that are metamorphosed in greenschist facies (VALERIANO, 2017). The upper nappe complex (Figure 2.3) is much more pervasively deformed than the underlying units and is mainly

Figure 2.1 – Regional maps showing the location of the study area in the Gondwana and in the Southern Brasília Orogen. a) Tectonic map of Southern Brasília orogen and adjoining southwestern margin of the São Francisco craton. Key: 1- São Francisco craton basement; 2- Paranoá Group; 3- Bambuí group cratonic cover; 4—Vazante Group; 5-Basement; 6- Canastra Group and Carrancas Group; 7- Ibiá Group; 8- Araxá Group and Andrelândia Nappe System; 9-Araxá/Andrelândia Group metamorphosed under granulite facies conditions; 10- Anápolis-Itauçu Complex; 11-Magmatic arc complexes; 12- Cretaceous alkaline massifs; 13- Phanerozoic cover (Paraná Basin) modified from Valeriano (2017), Campos Neto et al. (2010). b) Gondwana map (ca. 500 Ma) showing the location of the São Francisco Craton and the Gondwana orogens (red rectangle). Extracted from Spencer et al. (2013).

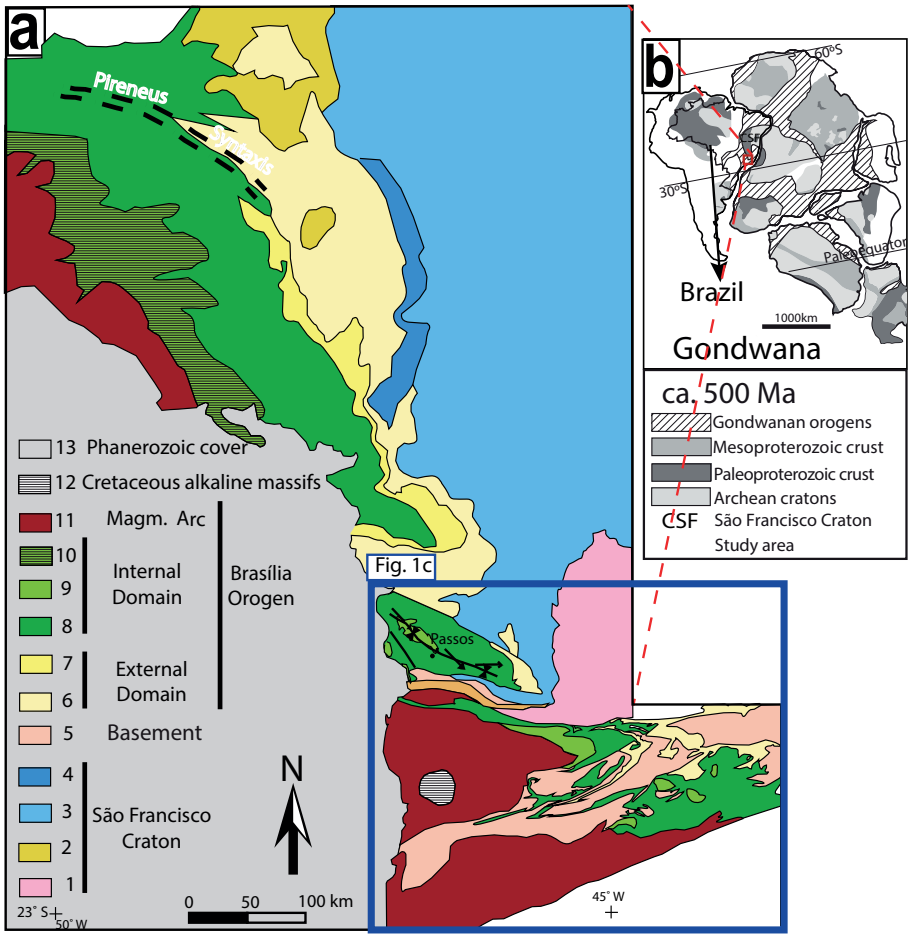

composed of metapelitic schist, paragneiss, quartzite with minor occurrences of metabasic, ultrabasic and calc-silicate rocks of the Araxá Group (SEER; DARDENNE, 2000; SEER et al., 2001; STRDEDER; NILSON, 1992; VALERIANO et al., 2004; VALERIANO et al., 2004a; VALERIANO, 2017). The Passos Nappe and Luminárias Nappe belong to the upper nappe complex.

According to Campos Neto et al. (2010) the metasedimentary rocks from the southernmost Brasília Orogen are organized in a stack of syn-metamorphic thick-skinned nappes (Figure 2.4 and Figure 2.3 c). From the structurally highest levels, in the west, to the structurally lowest levels, in the east, the following sequence of nappes can be recognized: (1) the Socorro-Guaxupé Nappe, that represents middle and lower crust root of the magmatic arc association; (2) the Andrelândia Nappe System that is composed of the

Figure 2.2 – Tectonic map from the Southern Brasília Orogen with the location of the Passos Nappe and Luminárias Nappe. Caption: 1- Phanerozoic sedimentary basin; 2- Upper Cretaceous/Cenozoic alkaline plutons; 3- Basement of São Francisco Craton; 4- Bambuí Group; 5- Mesoproterozoic and Neoproterozoic authochthonous succession form the São Francisco Craton; 6: Andrelândia Nappe System (ANS); 7- Socorro (S)-Guaxupé (G) Nappe; 8- Embu (E)- Paraíba do Sul (PS) Terrane; 9- Apiaí Terrane; 10- External domain from the Ribeira Orogen; 11: Juiz de Fora domain; 12- Rio Negro Arc; 13- Oriental Terrane and 14: Cabo Frio Terrane extracted from Caputo Neto et al. (2018).

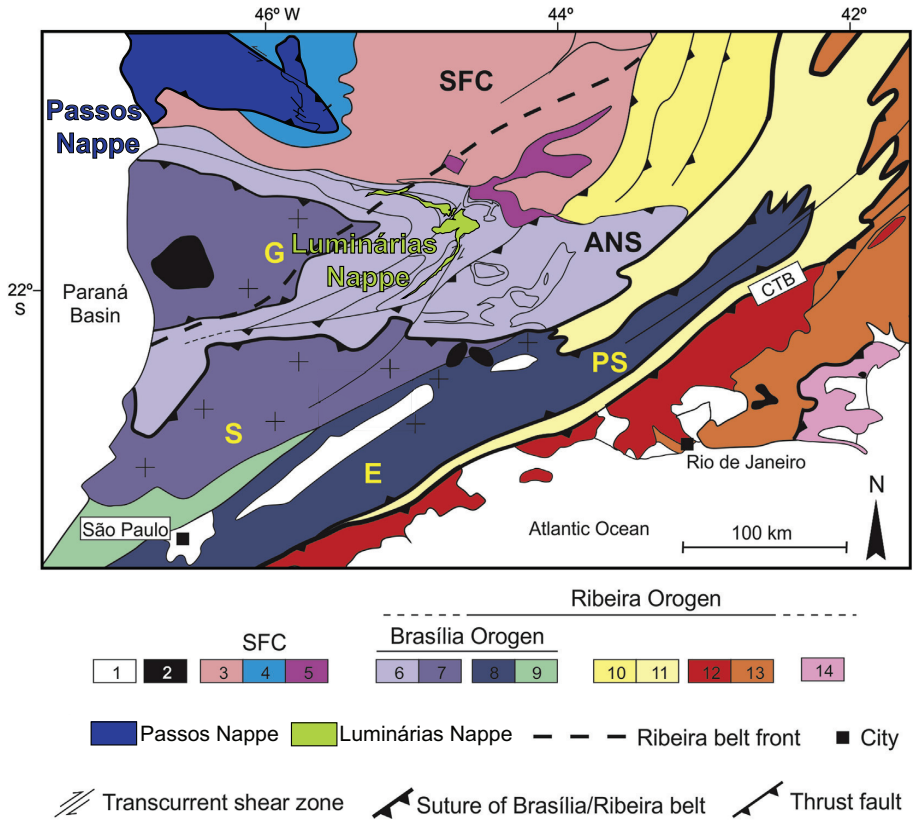

Três Pontas-Varginha Nappe and associated klippen, and the Liberdade and Andrelândia Nappes (CAMPOS NETO et al., 2010); and (3) the Carrancas Nappe System and the Lima Duarte Nappe (CAMPOS NETO et al., 2004; CAMPOS NETO et al., 2007; CAMPOS NETO et al., 2010; WESTIN; CAMPOS NETO, 2013; WESTIN et al., 2016), also known as Lower Nappe System (Figure 2.4). Windows composed of basement rocks from the Pouso Alegre Complex (Paleoproterozoic migmatitic orthogneisses) outcrop between the two domains of the Socorro-Guaxupé Nappe (CIOFFI et al., 2016).

Figure 2.3 – Geological sections through the Passos Nappe and Luminárias Nappe and adjacent areas. a) Tectonic map with the delimitation of the tectonic units in the area of the geological sections, modified from Valeriano (2017) (see Figure 2.1 b from a more detailed map). b) Geological section through the Passos Nappe and adjacent area, extracted from Valeriano (2017). c) Geological section through the Luminárias Nappe and adjacent area, extracted from Trouw et al. (2000).

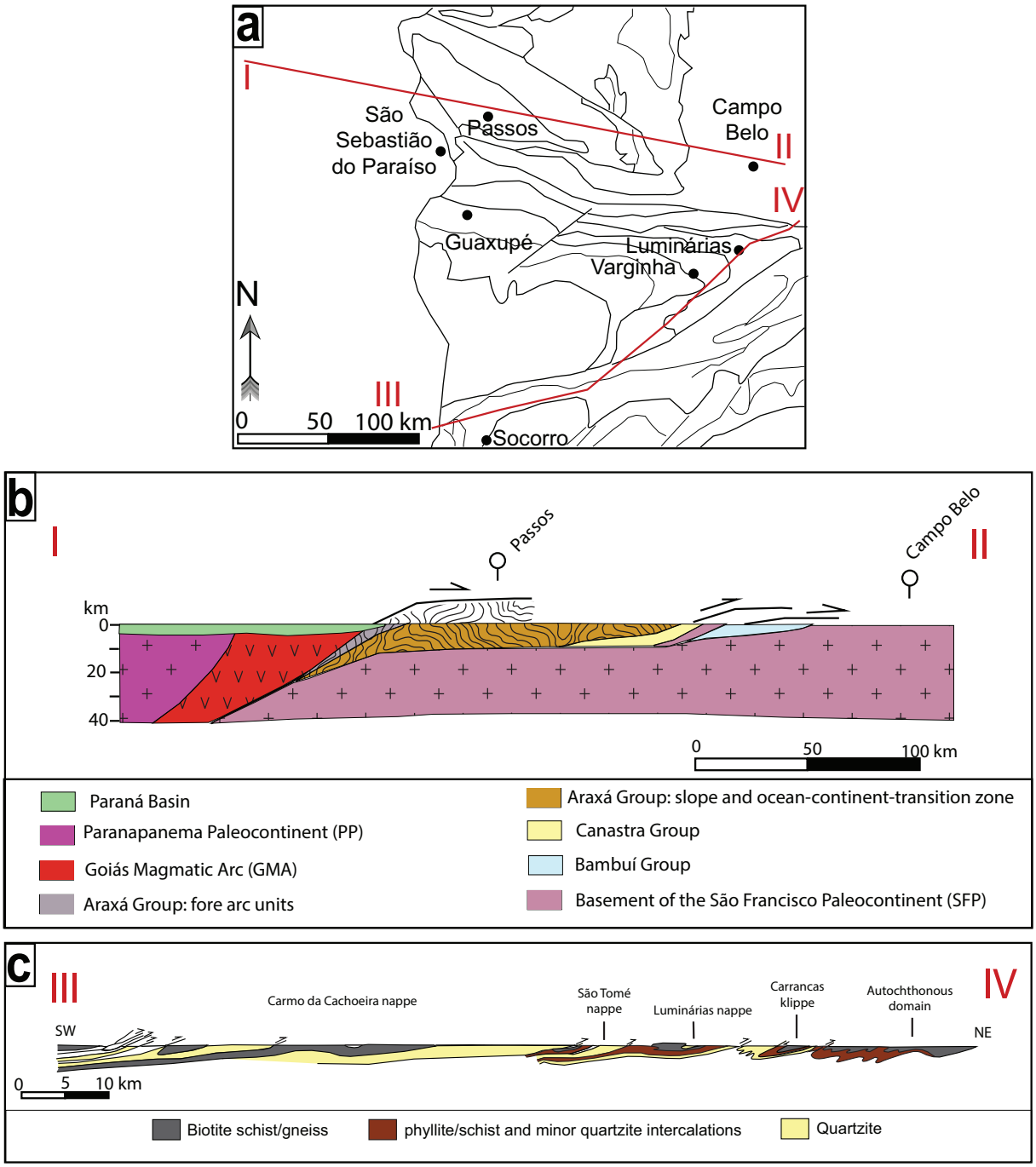

Figure 2.4 – a) Gondwana map (ca. 500 Ma) showing the location of the São Francisco Craton and the Gondwana orogens (red rectangle). Extracted from Spencer et al. (2013). b) Geological map of the southernmost portion of the Southern Brasília Orogen showing the localization of the Luminárias Nappe, extracted from the Westin e Campos Neto (2013).

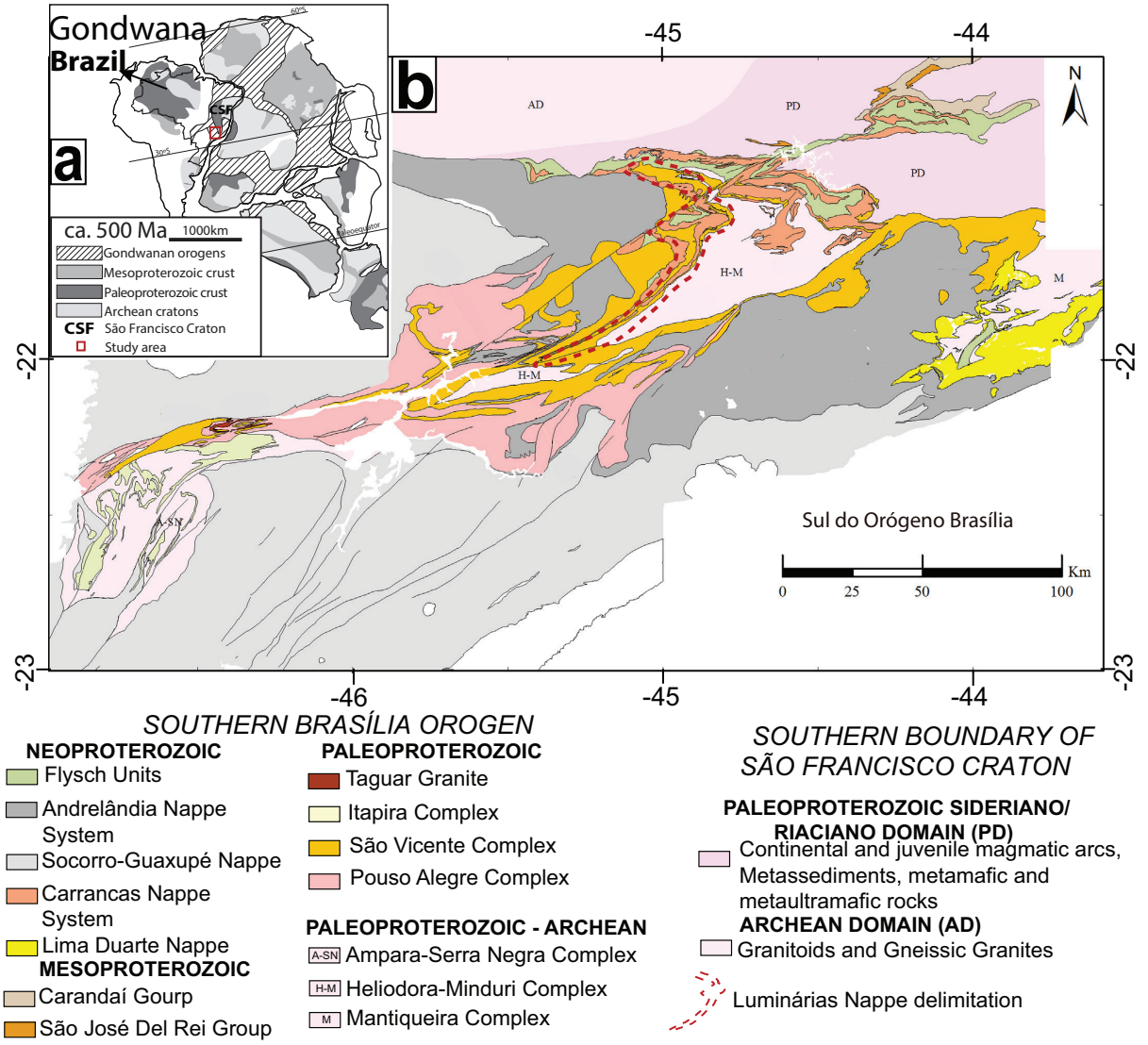

The Passos Nappe is not included in the division of the Southernmost Brasília Orogen presented above, since this nappe occurs northward of the area studied by Campos Neto et al. (2010). Nevertheless the metassedimentary rocks from the Passos Nappe are correlated with the southern units (the Andrelândia Nappe System and the Carrancas Nappe system), since they have similar depositional and metamorphic/deformation history (Figure 2.1, Figure 2.2 and Figure 2.3). According to Trouw, Paciullo e Heilbron (1984), Valeriano et al. (2004a), Reno et al. (2012) the Araxá and Andrelândia Groups are correlated as they have similar lithologies and metamorphic and deformation characteristics.

In this work, the tectonic division follows the classification of Fuck et al. (1994) and the rocks from the Passos Nappe are included into the Araxá Group unit. Furthermore, the subdivision of the southernmost portion of the Southern Brasilia Orogen, in the Luminárias Nappe region, follows the proposal of Campos Neto et al. (2010).

The Brasília Orogen is in contact with the Neoproterozoic Ribeira Orogen on its southeastern border, which includes the Luminárias Nappe (HASUI; CARNEIRO; COIMBRA, 1975; TROUW et al., 2000; HEILBRON et al., 2000; HEILBRON et al., 2004; HEILBRON et al., 2008; HEILBRON; CORDANI; ALKMIM, 2017). Contrasting interpretations about this region are presented in literature. The contact is either described as an interference zone between the Brasília and Ribeira Orogens, due to superposition of structures and metamorphism related to collision in both orogens (PETERNEL et al., 2005; TROUW et al., 2000; TROUW et al., 2013; HEILBRON et al., 2008; HEILBRON; CORDANI; ALKMIM, 2017; COELHO et al., 2017), or it is considered to be formed exclusively due to metamorphism and deformation associated with the Brasília Orogen (CAMPOS NETO, 2000; CAMPOS NETO et al., 2004; CAMPOS NETO et al., 2007; CAMPOS NETO et al., 2011; WESTIN et al., 2016; WESTIN et al., 2019). The discussion about these two interpretations of the contact between the Brasília and Ribeira Orogens is still open in the literature.

2.1 Passos Nappe

The rocks from the Passos Nappe were described as belonging to the Araxá Group by Teixeira e Danni (1978) and the group itself was defined by Barbosa (1955). Heilbron et al. (1987) have included the rocks from Passos Nappe into the Araxá-Canastra Group. This term Araxá-Canastra Group has was also been used in others works (*e. g.* Valeriano, Simões e Godoy (1989), Simões e Valeriano (1990), Schrank et al. (1990), Morales (1991), Zanardo (1992), Valeriano (1993), Zanardo, Del Lama e Morales (1990)). However, Simões (1995) proposes the use of Araxá Group for the rocks of the Passos Nappe and this term has been used in the literature since then.

According to Simões (1995), Valeriano et al. (2004) the Araxá Group in the Passos Nappe is compose of nine lithofacies units, namely: Unit A - metapelite, marble and minor quartzite; Unit B - quartzite; Unit C - metapelite and minor quartzite; Unit D - paragneiss and quartzite; Unit E - metapelitic schist, paragneisses and minor quartzite; Unit F - paragneiss; Unit G - metapelitic schists with minor quartzite; and, Unit H - paragneiss, minor schist and quartzite and I - metapelitic schist, quartzite and minor gneiss (Figure 2.5 and Figure 2.6). These lithofacies are divided in two depositional cycles, the lower depositional cycle (Unit A to C) and the upper depositional cycle (D to H) (SIMÕES, 1995).

Deformational structures in the Passos Nappe are divided in four deformational phases (D_1, D_2, D_3 and D_4) (SIMÕES; VALERIANO, 1990; HEILBRON et al., 1987; SIMÕES, 1995) and, according to the these authors, the D_1 is characterized by the the foliation S_1, which is parallel to the depositional bedding and is observed in hinge zones

Figure 2.5 – Lithostratigraphic column of the Passos Nappe, according to Simões (1995) and redesigned by Valeriano et al. (2004).

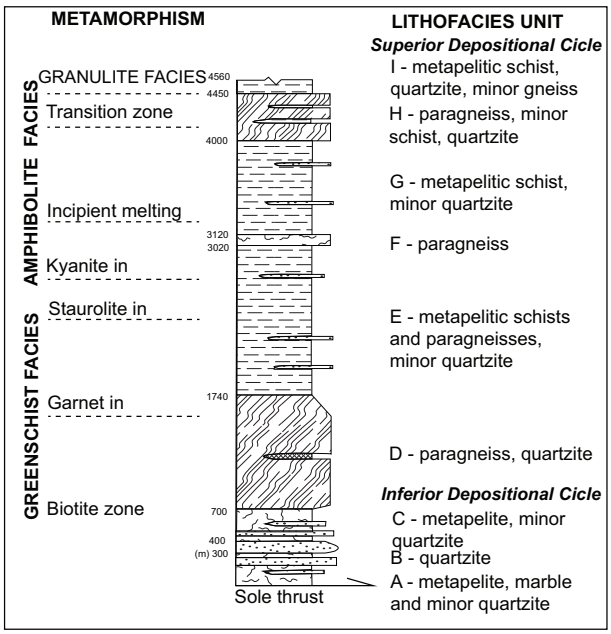

of D_2 folds. D_2 is associated with the main foliation (S_2), that may be a schistosity or a crenulation cleavage, and by folds and mineral lineation. The metamorphic peak and the nappe emplacement took place during early stage of the D_2 deformational phase, while the retrograde stage is related with late stages of D_2 (SIMÕES, 1995). Deformational phase D_3 is related with gentle to open folds (NW vertical axial surface and fold axis slight plunged to NW or SE). The D_4 is also associated with gentle to open folds, however with vertical axial surfaces and fold axis oriented to N and NNE with slight plunge to SSW or NNE (SIMÕES, 1995).

Fleischer e Schmidt (1978), Simões et al. (1988), Simões (1995) describe an inverted metamorphic gradient for the rocks from the Passos Nappe. According to Simões (1995) the metamorphic gradient ranges from the greenschist facies in the base (Unit A – biotite-muscovite schist) to upper amphibolite facies with anatexis textures in the top with pressure conditions higher than a typical barrovian gradient (SIMÕES, 1995; ZANARDO, 1992). Granulite facies rocks are mapped in the center of the structure by Valeriano et al. (2004), Valeriano (2017) and correspond to the Units H and I of Simões (1995).

Luvizotto (2003) studied the southern portion of Passos Nappe, nearby São Sebastião do Paraíso, and confirmed the inverted a metamorphic gradient ranging from 450 °C and 0.6 GPa in the base, to 750 °C and 1.1 GPa in the top unit of the of the nappe. The author also describes that some thermobarometric data point to granulite facies and pressure higher than 1.4 GPa, noticing the presence of retroeclogite in some top units. The metamorphic rocks from the southern Passos Nappe show a clockwise metamorphic path, according to Luvizotto (2003).

Figure 2.6 – Geological map of the Passos Nappe according to Hartung (2018).

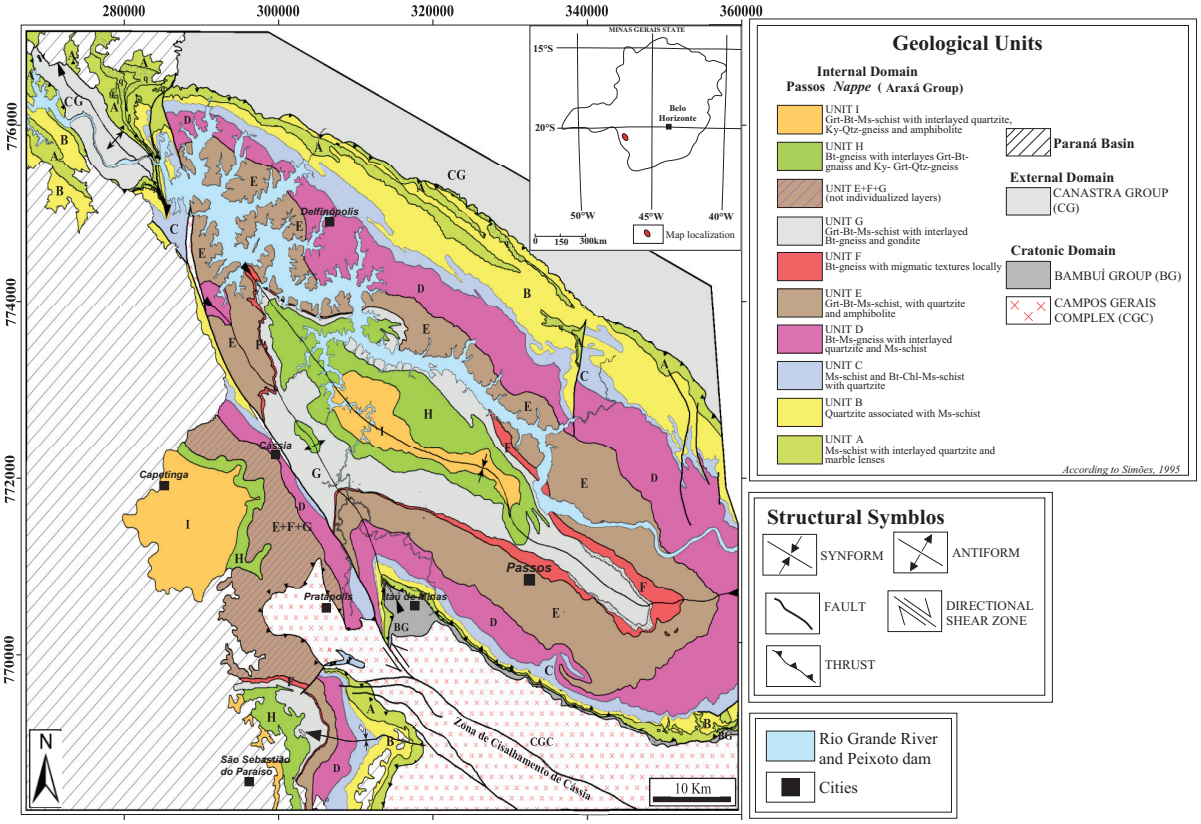

According to Luvizotto et al. (2017) the rocks of the top of Passos Nappe (Unit H) reached the (high-pressure) granulite facies, with peak metamorphic conditions of ∼850-870 °C and 1.4 GPa to 1.8 GPa. The pressure obtained in this more recent study is substantially higher than the calculated by Simões (1995), which is ∼0.8 GPa to 1.0 GPa to the Unit H.

High-pressure granulites are also observed in Andrelândia Nappe System, in the southern portion of the Brasília Orogen (CAMPOS NETO; CABY, 1999; CIOFFI et al., 2012; RENO et al., 2009; CAMPOS NETO, 2000; MOTTA; MORAES, 2017). Ultra-high temperature rocks occur further north along the orogen, in the Anápolis–Itauçu Complex (PIUZANA et al., 2003a; PIMENTEL, 2016; MORAES et al., 2002) and to the south of the studied area, in the Socorro-Guaxupé Nappe (ROCHA et al., 2018; ROCHA et al., 2017; TEDESCHI et al., 2017) (Figure 2.7).

High-pressure granulitic rocks occur in the Andrelândia Nappe System, at the Carvalhos and Serra da Natureza Klippen and the Três-Pontas Varginha Nappe (Figure 2.7). In rocks from the Carvalhos Klippe the peak mineral assemblage is Rt+Ky+Grt+Kfs±Bt (850-900 °C and 1.6 GPa). A channel flow model, which involves exhumation along the continuous movement and extrusion of the nappe stack is proposed in the literature (CAMPOS NETO et al., 2010; CIOFFI et al., 2012). However, Motta e Moraes (2017) propose a exhumation process similar to the numerical model developed for the western

portion of the Grenville Orogen, for the Andrelândia System rocks. The metamorphic peak conditions in the Três-Pontas Varginha Nappe, are ∼785-860 °C according to Reno et al. (2009) and monazite ages range from 678 ± 29 to and 647 ± 11 Ma. However, according to Campos Neto (2000) the metamorphic peak conditions in this nappe are 700-750 °C and 1.5 GPa at 630 Ma, while retrograde conditions took place at 600 Ma. In the Serra da Natureza Klippen peak conditions are 800 °C and 1.3 GPa and occurred at 604.5 ± 6.1 Ma (MOTTA; MORAES, 2017).

According to Pimentel (2016) the Araxá group has dominant Neoproterozoic detrital zircon populations, as young as 650 Ma, suggesting derivation from the Goiás Magmatic Arc. Piuzana et al. (2003a) presents geochronological data on the Araxá Group near Anápolis (central part of the Brasília Orogen), with peak ages of ca. 650 Ma and minor Paleoproterozoic ages, that allows for the interpretation that the Araxá Group was deposited in an arc-related or syn-orogenic basin within the Brasília Orogen. However, Falci et al. (2018) shows different ages pattern (peaks between 790 Ma and 2.5 Ga) from Araxá Group in the Araxá Nappe (north of Passos Nappe) with strong cratonic provenance zircons, corresponding to a distal passive margin of the western São Francisco paleocontinent.

Geochronological data (U-Pb zircon) in the basal units from Passos Nappe (Unit A, B and C) show major Rhyacian sources (ca. 2.1 Ga) and minor cluster with ages ranging from ca. 1.60 to 1.76 Ga source ages, indicating that the sedimentary sources are Paleoproterozoic terranes (Mineiro belt) of southwest margin of the São Francisco Craton (SILVA, 2018; SILVA; SIMÕES; DUFRANE, 2019).

2.2 Luminárias Nappe

The study of the geology of the southern portion of the Minas Gerais State started in the 1950s. Heinz Ebert was the pioneer, studying in detail the rocks near São João del Rei. In his works, he describes an increase of metamorphic conditions from the north to the south (EBERT, 1955; EBERT, 1956; EBERT, 1957; EBERT, 1958; EBERT, 1968; EBERT, 1971; EBERT, 1984).

The metasedimentary rocks in the south of São Francisco Craton were originally grouped into the São João del Rei and Andrelândia Groups (EBERT, 1956). Trouw, Ribeiro e Paciullo (1980) described the metasedimentary rocks near Luminárias Nappe as the Carrancas Group, with similar characteristics of both the São João del Rei and Andrelândia Groups, in a study between Lavras and Minduri cities. According to Trouw, Ribeiro e Paciullo (1980), Trouw, Ribeiro e Paciullo (1983) the Carrancas Group is divided into São Tomé das Letras Formation, that is composed of quartzite, and in the Campestre Formation, composed of metapelite and quartzite.

Figure 2.7 – Regional maps showing the location of granulite rocks in the Southern Brasília Orogen. a) Tectonic map of Southern Brasília orogen and adjoining southwestern margin of the São Francisco craton. Key: 1- São Francisco craton basement; 2- Paranoá Group; 3- Bambuí group cratonic cover; 4—Vazante Group; 5-Basement; 6- Canastra Group and Carrancas Group; 7- Ibiá Group; 8- Araxá Group and Andrelândia Nappe System; 9-Araxá/Andrelândia Group metamorphosed under granulite facies conditions; 10- Anápolis-Itauçu Complex; 11-Magmatic arc complexes; 12- Cretaceous alkaline massifs; 13- Phanerozoic cover (Paraná Basin) modified from Valeriano (2017), Campos Neto et al. (2010). [1]Campos Neto (2000), [2]Reno et al. (2009), [3]Motta e Moraes (2017), [4]Campos Neto et al. (2010), [5]Cioffi et al. (2012), [6]Cioffi et al. (2019), [7]Frugis, Neto e Lima (2018), [8]Coelho et al. (2017), [9]Tedeschi et al. (2018), [10]Rocha et al. (2018), [11]Rocha et al. (2017), [12]Del Lama et al. (1998), [13]Del Lama et al., (2000), [14]Luvizotto et al. (2017), [15]Valeriano et al. (2004), [16]Simões (1995), [17]Luvizotto (2003), [18]Baldwin e Brown (2008), [19]Moraes et al. (2002), [20]Baldwin et al. (2005), [21]Piuzana et al. (2003a), [22]Piuzana et al. (2003b), [23]Pimentel (2016), [24]Piuzana et al. (2003a), [25]Giustina et al. (2011), [26]Tedeschi et al., 2017 and [27]Coelho et al., 2017.

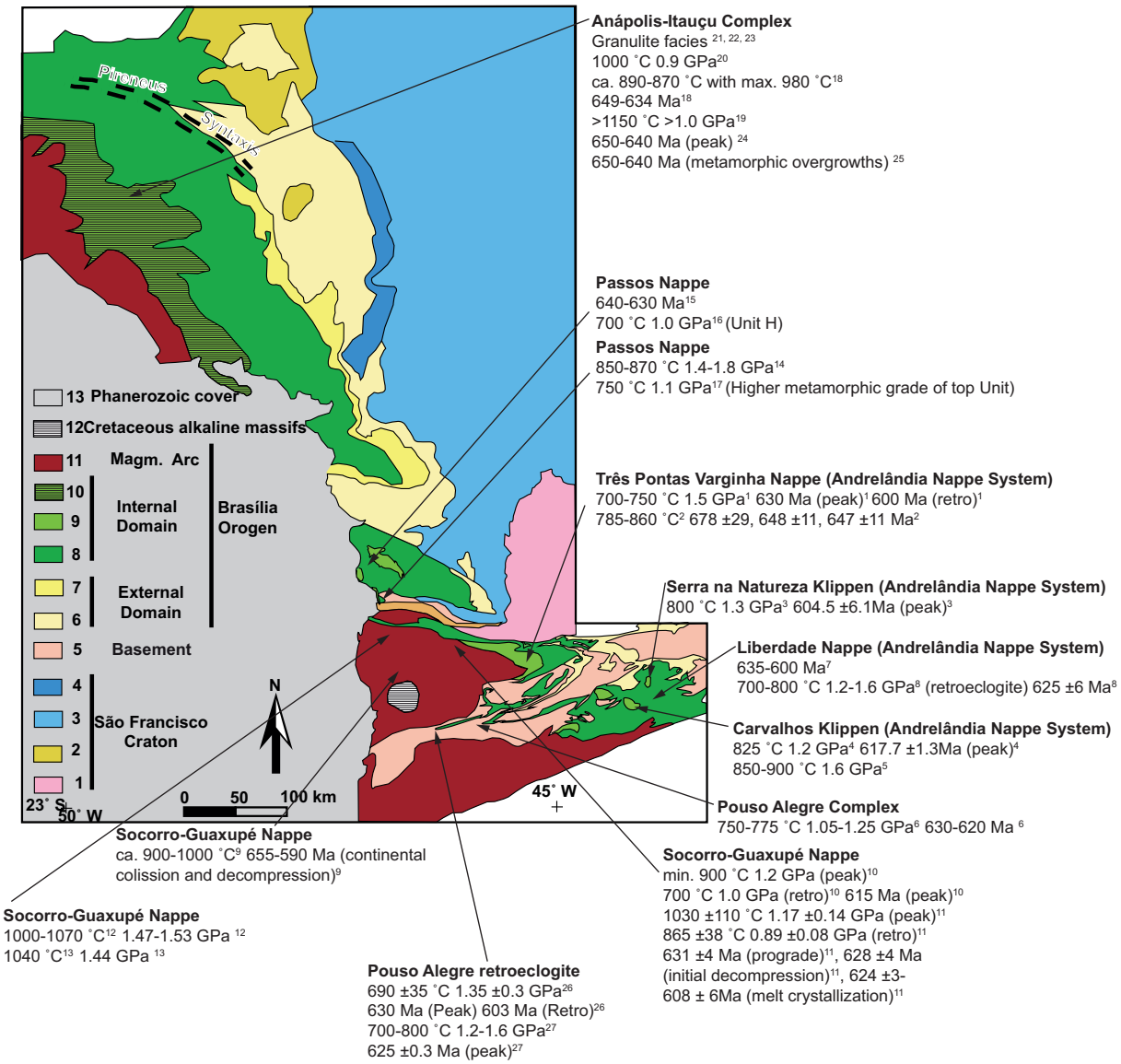

Paciullo, Ribeiro e Trouw (2003), Paciullo et al. (2000) grouped the Andrelândia Group and the Carrancas Group into the Andrelândia Mega-sequence, that is divided into six lithofacies, grouped in two depositional sequences, formed in a transition between a rift to passive margin succession (Figure 2.8 a):

- A_1: biotite gneiss and amphibolite, interpreted as a interlayered sequence of feldspathic sandstone and pelitic rocks from the rift stage of the basin, in the beginning of the Andrelândia Basin evolution;
- A_2: paragneiss interlayed with quartzite, schist, calcsilicatic rocks, marble, gondite and amphibolite, interpreted as retrograde parasequence formed during a transgressive system in a proto-oceanic phase;
- A_3: micaceous quartzite interlayered with schist, formed in a transgressive system tract in a continental stable margin;
- A_4: phyllite/schist interlayered with quartzite, deposited in a transgressive system tract in the maximum flooding surface (previous Campestre Formation);
- A_5: dark colored feldspathic biotite schist, with gneiss that are interpreted as deposited in transgressive and regressive system tract related with glacial and post-glacial events;
- A_6: feldspathic biotite schist and paragneiss interlayered with calcsilicatic rocks, metachert and amphibolite. This unit is interpreted as deposited on pelagic, epipelagic and turbidites in distal environments.

Figure 2.8 – Lithostratigraphic columns presented in the literature for the metasedimentary rocks from Luminárias Nappe. a) Composed lithostratigraphic column from the units of the Andrelândia basin which composed the Andrelândia Mega-sequence, according to Paciullo et al. (2000) and redesigned by Heilbron, Cordani e Alkmim (2017). Hs- highstand system; Ls- lowstand system; Tst- transgressive system tract; MxFs- maximum flooding surface; Mfs- maximum flooding surface. b) Lithostratigraphic column of the Carrancas group and probability age plots of the provenience of the units, extracted from Westin et al. (2019).

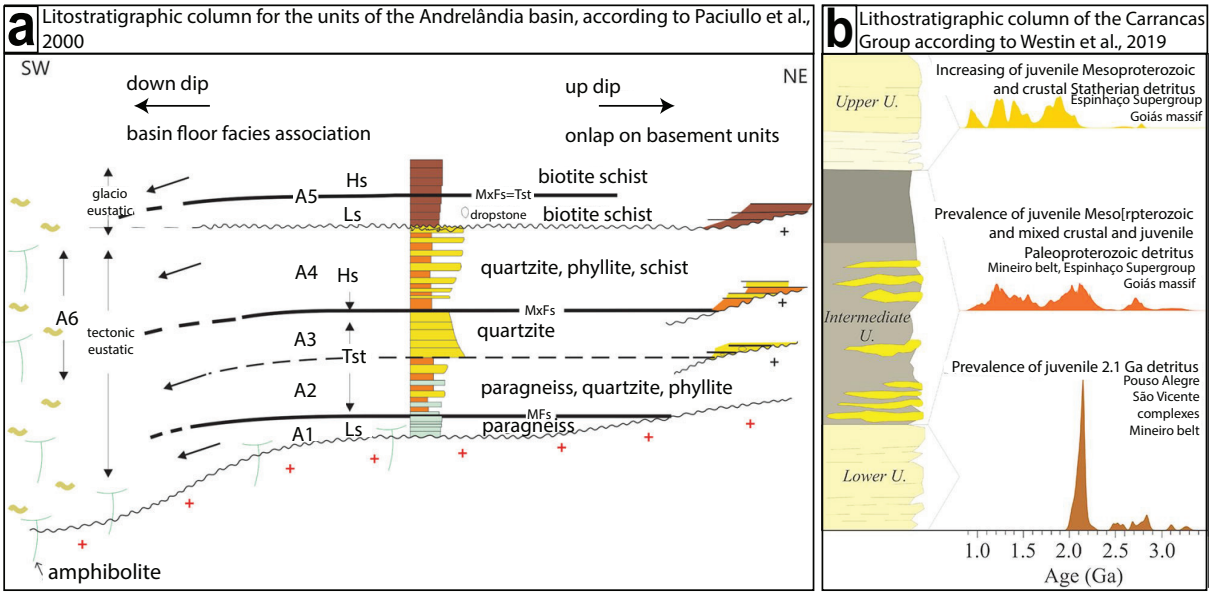

According to the geological maps from Almeida (1992), Trouw et al. (2003), Quéméneur et al. (2003), Peternel, Trouw e Castro (2008), the Luminárias Nappe is mostly

composed of Na_{1+2}, Na_3, Na_4 units in the northern portion, of the Na_{1+2}, Na_3, of Na_4 e Na_5 units in the center-north portion, of Na_{1+2}, Na_3 e Na_4 units in the center and south portion.

The Andrelândia Mega-sequence is interpreted to have formed along the southern margin of the São Francisco paleocontinent during the Neoproterozoic (RIBEIRO et al., 1995; PACIULLO et al., 2000; HEILBRON; CORDANI; ALKMIM, 2017). An alternative interpretation for the provenance of the basal lithofacies (Na_1 and Na_2 -biotite gneiss interbedded with schist and quartzite; from Andrelândia Mega-sequence) is that these rocks belong to the Paleoproterozoic and have affinity with fore arc basin and trench deposits (WESTIN et al., 2016; WESTIN et al., 2019). According to Westin et al. (2016), Westin et al. (2019), the Na_1 and Na_2 lithofacies are called São Vicente Complex and are not related neither to the Carrancas Group nor Andrelândia Mega-sequence.

Westin et al. (2019) proposed an alternative lithostratigraphy for the Carrancas Group in Carrancas Klippe (north of Luminárias Nappe) and defined three major units (Figure 2.8 b):

- i) Lower Unit: is a psammitic unit with prevalence of juvenile 2.1 Ga and subordinate crustal Archean zircons in the source of detrital;
- ii) Intermediate Unit: this unit is composed of interbedded psamo-pelites that presents source of detrital dominated by juvenile 2.3-1.8 Ga and 1.6-1.1 Ga zircons;
- iii) Upper Unit: is a psammitic unit with prevalence of crustal 1.9 and 1.7 Ga juvenile detritus. These authors interpreted that the deposition of the Carrancas Group began after 0.92 Ga and lasted until the Brasiliano collision events in 0.67 Ga, whose zircons correspond to different sources from the São Francisco Craton.

Recent work from Marimon et al. (2021) describes that the Carrancas Successions (Na_3 and Na_4) were the metamorphosed passive margin sequences with maximum depositional age of ∼900 Ma and the a main source of sediments is in the São Francisco paleocontinent. According to these authors the metagreywacke from Santo Antônio Unit (Na_5) is syn-collisional unit with maximum depositional age at ∼650 Ma.

Early studies from Ebert (1971) near São Tomé das Letras city describe greenschist facies conditions in the metasedimentary rocks from the region, with metamorphic conditions increasing southwest. According to Trouw, Ribeiro e Paciullo (1980), Ribeiro e Heilbron (1982) the peak metamorphic condition in the Carrancas Group rocks from the Luminárias Nappe, took place at greenschist facies (lower grade) in the northernmost portion (minerals assemblages: Ms+Ctd+Qtz+Chl; Ms+Ctd+Qtz+Grt; Ms+Qtz; Qtz+Ms+Ky and Bt+Ms+Qtz+Chl+Pl+Grt), at amphibolite facies in the southern portion (minerals assemblages: Ms+Grt+St+Qtz+Ky; Ms+Qtz e Qtz+Ms+Ky) both with intermediary

pressure. Retrograde reactions are observed in some parts of the Luminárias Nappe as post-peak chloritoid replacing the staurolite and garnet porphyroblasts (TROUW; RIBEIRO; PACIULLO, 1980; RIBEIRO; HEILBRON, 1982). At the southernmost portion of the Nappe, sillimanite is observed, interpreted as the influence of the Ribeira Orogen metamorphism (RIBEIRO; HEILBRON, 1982).

Metamorphic maps from Ribeiro e Heilbron (1982), Trouw, Paciullo e Heilbron (1984) (Figure 2.9 a) show that in the Luminárias Nappe, the distribution of the major metamorphic minerals, from north to south is: Grt, Grt+St, Grt+St+Ky e Grt+St+Ky+Sill. The isograds confirm the increase of metamorphic conditions from north to south which is oblique to the geological contacts. Recent studies that present metamorphic maps from the Southern Brasília Orogen confirm the previous findings, with greenschist facies conditions at the north and amphibolite facies in the center and south of the Luminárias Nappe (Figure 2.9 b, c and d) (TROUW et al., 2013; PETERNEL et al., 2005; RENO et al., 2012; HEILBRON; CORDANI; ALKMIM, 2017).

According to Campos Neto e Caby (1999), the metamorphic conditions of Carrancas Group rocks (correlated with the study rocks / Luminárias Nappe) took place at high-pressure and low temperature, with metamorphic assemblage garnet-kyanite-chloritoid.

Silva (2010) described, in the Carrancas Klippe, a metamorphic gradient that increases to the southeast, from lower amphibolite facies (staurolite-garnet-chlorite-chloritoid-muscovite-quartz at 10.0 ± 1.7 kbar and 577 ± 8°C) to high-pressure amphibolite facies in the transition to eclogite facies (kyanite-staurolite-garnet-quartz at 12.9 ± 1.0 kbar and 608.5 ± 19.5°C). According to Carvalho et al. (2020) the emplacement of the Carrancas klippe, occurred at upper greenschist facies conditions with relatively high pressures (470 ± 45 ±C and 12.3 ± 1 kbar), followed by a change in the direction of tectonic transport to north, under greenschist facies conditions in the northwest and medium pressure amphibolite facies conditions in the southeast (580 ± 35 ±C and 8.4 ± 1.4 kbar) at 562 ± 24 Ma.

Recent studies (FUMES, 2017; FUMES et al., 2017) on the metamorphism of metapelitic rocks and quartzite from the Luminárias Nappe confirms a metamorphic gradient with conditions increasing from north to south. In the northern portion the paragenesis is Cld + Chl + Ky + Rt + Qtz + Ms at 560 °C and 10 kbar, in the center-north portion the peak mineral assemblage is St + Grt + Rt + Qtz + Ms at 610 °C and 12.5 kbar and in the southern portion the paragenesis is Grt + Ky + St + Qtz + Rt + Ms at 630 °C and 15 kbar (FUMES, 2017; FUMES et al., 2017). These conditions are similar to those observed in the Carrancas Klippe (SILVA, 2010; CARVALHO et al., 2020).

Several studies describe the structural features of the Carrancas Group, dividing the formation of the structures into three deformational phases (TROUW; RIBEIRO; PACIULLO, 1980; TROUW et al., 1982; TROUW; RIBEIRO; PACIULLO, 1983; TROUW;

PACIULLO; HEILBRON, 1984; TROUW et al., 2000; RIBEIRO et al., 1990; PACIULLO, 1980; HEILBRON, 1984; VALERIANO, 1985):

- D_1 deformation phase: associated with the nappe emplacement and the formations of a slaty cleavage S_1;
- D_2 deformation phase: responsible for the generation of the most penetrative foliation (S_2) and the mineral or stretching lineation (L_2);
- D_3 deformation phase: this phase is observed in millimetric to kilometric folds with axial surface oriented to SE and NW which fold the S_2 foliation.

In respect to the relationship between metamorphism and deformational phases, D_1 is interpreted to be associated to the early stages of metamorphism, D_2 phase is related with the metamorphic peak and the D_3 phase with the retrograde metamorphism (TROUW; RIBEIRO; PACIULLO, 1980; TROUW; RIBEIRO; PACIULLO, 1983; RIBEIRO; HEILBRON, 1982; RIBEIRO et al., 1995). According to Trouw, Paciullo e Ribeiro (1994), Trouw et al. (2000), Ribeiro et al. (1995), Peternel et al. (2005) the D_1 e D_2 deformational phase are related to the Brasília Orogen and the D_3 are interpreted as result of the Ribeira Orogen.

Neoproterozoic ages of metamorphism (peak and retrograde) from whole southern Brasília Orogen vary, from 670 to 590 Ma (VLACH; GUALDA, 2000; CAMPOS NETO et al., 2004; VALERIANO et al., 2004; CAMPOS NETO et al., 2007; CAMPOS NETO et al., 2010; CAMPOS NETO et al., 2011; TROUW; TAVARES; ROBYR, 2008; RENO; BROWN; PICCOLI, 2010; RENO et al., 2012; WESTIN et al., 2016; COELHO et al., 2017; ROCHA et al., 2017; ROCHA et al., 2018; TEDESCHI et al., 2017; TEDESCHI et al., 2018). Monazite ages obtained with laser ablation–inductively coupled plasma–mass spectrometry (LA-ICP-MS) from the Carrancas Klippe rocks (northeast of the Luminárias Nappe) are ca. 590-575 Ma (VALERIANO et al., 2004; CAMPOS NETO et al., 2010). According to (CAMPOS NETO et al., 2010; CAMPOS NETO et al., 2011), the ages of ca. 590 Ma determined for the Carrancas rocks represent the propagation and migration of the deformation and metamorphism through the pile of nappes, from the upper to the lower nappes, in which Luminárias Nappe is included. Alternatively, the younger ages can be interpreted as an effect of the Ribeira Orogen overprint, according to the interference zone interpretation.

According to Westin et al. (2021) in the Luminárias Nappe the metamorphic peak (related with the syn-collisional event) occurred around 630 Ma, younger monazite ages record the continuous exhumation/cooling path from 620 to 611 Ma to until 605-590 Ma and $^{40}Ar/^{39}Ar$ muscovite ages indicate a slow cooling for these allochthons, reaching ∼350 °C around 540 Ma.

Figure 2.9 – Metamorphic maps from the Southern Brasília Orogen. a) Metamorphic map from the Carrancas and Andrelândia Group, showing the distribution of the major metamorphic minerals and the isograd traces, extracted from Ribeiro e Heilbron (1982). b) Map to show the metamorphic zones in the southern sector of the Southern Brasília Orogen (PETERNEL et al., 2005). c) Simplified metamorphic map on the southern Brasília Orogen. 1- Pre-1.8 Ga basement; 2- greenschist facies; 3- kyanite; 4- kyanite and sillimanite; 5- sillimanite, in amphibolite facies; 6- high pressure granulite (kyanite + K-feldspar); 7- retro-eclogite; Directions of tectonic transport related to 8- Brasília Orogen; 9- Ribeira Orogen; 10- Location with relation to São Francisco Craton, extract from Trouw et al. (2000). d) Metamorphic map of the Southern Brasília Orogen. 1- greenschist facies without biotite; 2- greenschist facies + biotite ± garnet (cover and basement); 3- amphibolites facies staurolite + kyanite; 4- amphibolite facies + kyanite + sillimanite; 5- amphibolite/granulite facies + sillimanite (without kyanite) + K-feldspar ± orthopyroxene; 6- granulite facies + kyanite + K-feldspar ± sillimanite (high P); 7- granulite facies + orthopyroxene (medium P); 8- granulite facies + sillimanite + K-feldspar ± cordierite (medium/low P); 9- amphibolite facies (without kyanite, medium P); 10- greenschist facies (medium/low P); 11- unmetamorphosed rocks; yellow star: retroeclogite, extracted from Trouw et al. (2013).

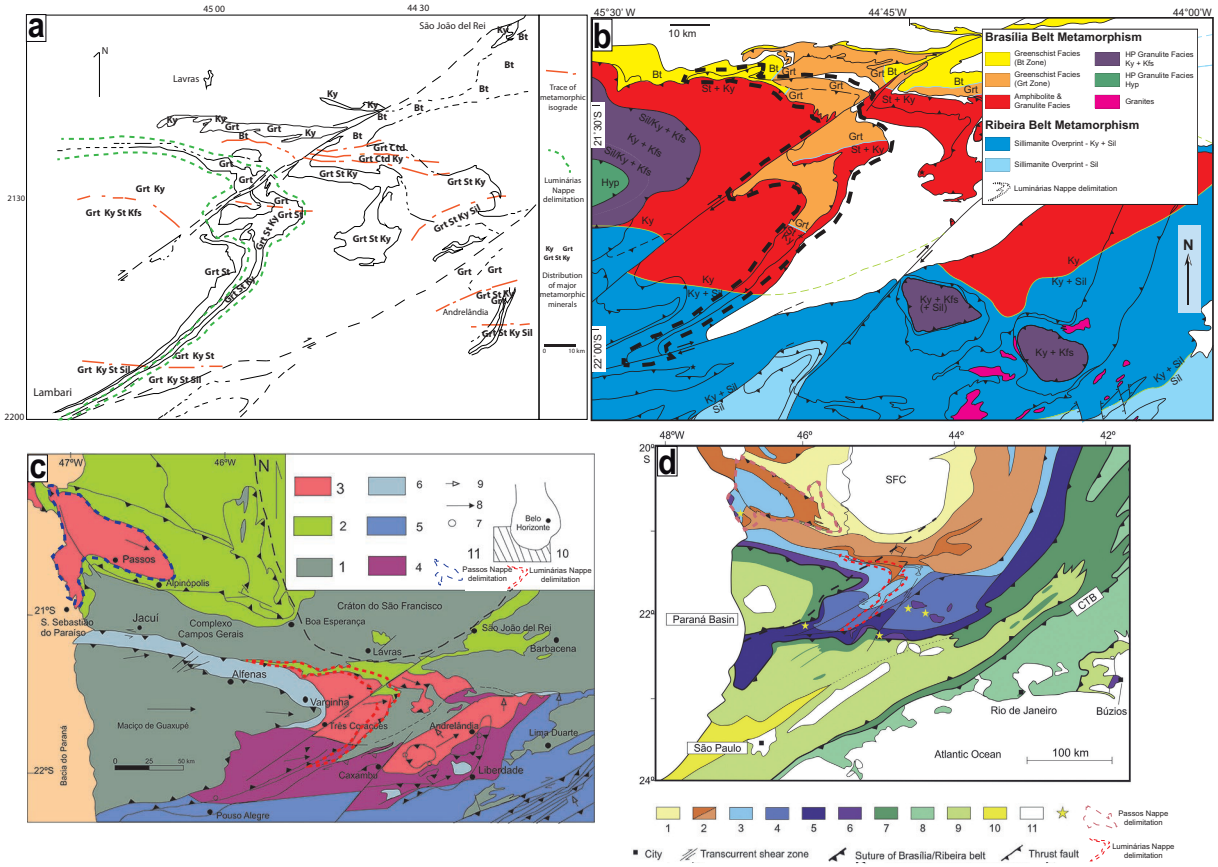

Reference

ALMEIDA, F. F. M. O Cratón do São Francisco. *Revista Brasileira de Geociências*, v. 7, p. 349–364, 1977.

ALMEIDA, F. F. M. et al. Brazilian Structural Provinces: An Introduction. *Earth Science Reviews*, v. 17, p. 1–29, 1981.

ALMEIDA, J. C. *Mapeamento geológico na Folha Luminárias (MG) 1:50.000 com ênfase na análise estrutural dos metassedimentos do Ciclo Deposicional Andrelândia.* Dissertação (Mestrado) — Universidade Federal do Rio de Janeiro, 1992.

ARAÚJO FILHO, J. O. The geology of the Pirineus Megainflection, Goiás, Central Brasil. *Geowissenschaftliches Lateinamerika Kolloquium*, v. 7, n. 9-11, 1980.

ARAÚJO FILHO, J. O. The Pireneus mega-inflection in Central Brazil: an example of poly-deformed Brasiliano fold-thrust belt. *Geowissenschaftliches Lateinamerika Kolloquium*, n. 129, 1992.

ARAÚJO FILHO, J. O. The Pirineus Syntaxis: An example of the intersection of two Brasiliano fold-thrust belts in central Brazil and its implications for the tectonic evolution of western Gondwana. *Revista Brasileira de Geociências*, v. 30, n. 1, p. 144–148, 2000.

BALDWIN, J. et al. Modelling of mineral equilibria in ultrahigh-temperature metamorphic rocks from the Anápolis–Itauçu Complex, central Brazil. *Journal of Metamorphic Geology*, Wiley Online Library, v. 23, n. 7, p. 511–531, 2005.

BALDWIN, J. A.; BROWN, M. Age and duration of ultrahigh-temperature metamorphism in the Anápolis-Itauçu Complex, Southern Brasília Belt, central Brazil - Constraints from U-Pb geochronology, mineral rare earth element chemistry and trace-element thermometry. *Journal of Metamorphic Geology*, v. 26, n. 2, p. 213–233, 2008. ISSN 02634929.

BARBOSA, O. Guia das excursões. In: SBG (Ed.). *Congresso Brasileiro de Geologia, 9.* [S.l.: s.n.], 1955. Noticiário 3, p. 3–5.

BERMAN, R. G. Internally-consistent thermodynamic data for minerals in the system Na_2O-K_2O-CaO-MgO-FeO-Fe_2O_3-Al_2O_3-SiO_2-TiO_2-H_2O-CO_2. *Journal of petrology*, Oxford University Press, v. 29, n. 2, p. 445–522, 1988.

BRITO NEVES, B. B. de; CAMPOS NETO, M. D. C.; FUCK, R. A. From Rodinia to Western Gondwana: as Aproach to the Brasiliano-Pan African Cycle and orogenic collage. *Episodes-Newsmagazine of International Union of Geological Science*, v. 22, n. 155-166, 1999.

BROWN, M. Metamorphic conditions in orogenic belts: a record of secular change. *International Geology Review*, Taylor & Francis, v. 49, n. 3, p. 193–234, 2007.

BROWN, M.; JOHNSON, T. Secular change in metamorphism and the onset of global plate tectonics. *American Mineralogist*, v. 103, n. 2, p. 181–196, 2018. ISSN 19453027.

BUCHER, K.; GRAPES, R. *Petrogenesis of metamorphic rocks.* [S.l.]: Springer Science & Business Media, 2011.

CAMPOS NETO, M. D. C. Orogenic Systems from Southwestern Gondwana: An Approach to Brasiliano-Pan African Cycle and Orogenic Collage in Southeastern Brazil. In: CORDANI, U. G. et al. (Ed.). *Tectonic Evolution of South America*. 1. ed. Rio de Janeiro: COMPANHIA DE PESQUISA DE RECURSOS MINERAIS, 2000. p. 335–365.

CAMPOS NETO, M. D. C. et al. Migração de Orógenos e Superposição de Orogêneses: Um Esboço da Colagem Brasiliana no Sul do Cráton do São Francisco, SE - Brasil. *Geologia USP - Serie Cientifica*, v. 4, n. 1, p. 13–40, 2004.

CAMPOS NETO, M. D. C. et al. Orogen migration and tectonic setting of the Andrelândia Nappe system: An Ediacaran western Gondwana collage, south of São Francisco craton. *Journal of South American Earth Sciences*, Elsevier Ltd, v. 32, n. 4, p. 393–406, 2011. ISSN 08959811. Avaible form internet: <http://dx.doi.org/10.1016/j.jsames.2011.02.006>.

CAMPOS NETO, M. D. C.; CABY, R. Neoproterozoic high-pressure metamorphism and tectonic constraint from the nappe system south of the Sao Francisco Craton, southeast Brazil. *Precambrian Research*, v. 97, n. 1-2, p. 3–26, 1999. ISSN 03019268.

CAMPOS NETO, M. D. C.; CABY, R. Lower crust extrusion and terrane accretion in the Neoproterozoic nappes of southeast Brazil. *Tectonics*, v. 19, n. 4, p. 669–687, 2000.

CAMPOS NETO, M. D. C. et al. Structural and metamorphic control on the exhumation of high-P granulites: The Carvalhos Klippe example, from the oriental Andrelândia Nappe System, southern portion of the Brasília Orogen, Brazil. *Precambrian Research*, v. 180, n. 3-4, p. 125–142, 2010. ISSN 03019268.

CAMPOS NETO, M. D. C. et al. Sistema de nappes andrelândia, setor oriental: litoestratigrafia e posição estratigráfica. *Revista Brasileira de Geociências*, v. 37, n. 4-Sup., p. 47–60, 2007.

CAMPOS NETO, M. D. C. et al. Sistema de nappes Andrelândia, setor oriental : litoestratigrafia e posição estratigráfica. *Revista Brasileira de Geociências*, v. 37, n. 4-suplemento, p. 47–60, 2007.

CAPUTO NETO, V. et al. The Pico do Itapeva Formation: A record of gravitational flow deposits in an Ediacaran intracontinental basin, southern Brasília Orogen, SE Brazil. *Journal of South American Earth Sciences*, Elsevier Ltd, v. 84, p. 34–47, 2018. ISSN 08959811. Avaible form internet: <https://doi.org/10.1016/j.jsames.2018.03.006>.

CARVALHO, B. R. et al. Microstructural and metamorphic evolution of the Carrancas Klippe, interference zone of the Neoproterozoic southern Brasilia and Ribeira orogens, SE brazil. *Journal of South American Earth Sciences*, Elsevier, v. 103, p. 102744, 2020.

CHAKRABORTY, S. et al. Channel flow and localized fault bounded slice tectonics (lfbst): Insights from petrological, structural, geochronological and geospeedometric studies in the sikkim himalaya, ne india. *Lithos*, v. 282, n. 464-482, 2017.

CHERNIAK, D.; MANCHESTER, J.; WATSON, E. Zr and Hf diffusion in rutile. *Earth and Planetary Science Letters*, Elsevier, v. 261, n. 1, p. 267–279, 2007.

CIOFFI, C. R. et al. Geochemical signatures of metasedimentary rocks of high-pressure granulite facies and their relation with partial melting: Carvalhos Klippe, Southern Brasília Belt, Brazil. *Journal of South American Earth Sciences*, v. 40, p. 63–76, 2012. ISSN 08959811.

CIOFFI, C. R. et al. Paleoproterozoic continental crust generation events at 2.15 and 2.08 ga in the basement of the southern brasília orogen, se brazil. *Precambrian Research*, Elsevier, v. 275, p. 176–196, 2016.

CIOFFI, C. R. et al. Titanite petrochronology of the southern Brasília Orogen basement: Effects of retrograde net-transfer reactions on titanite trace element compositions. *Lithos*, Elsevier, v. 344, p. 393–408, 2019.

COELHO, M. B. et al. Constraining timing and P-T conditions of continental collision and late overprinting in the Southern Brasília Orogen (SE-Brazil): U-Pb zircon ages and geothermobarometry of the Andrelândia Nappe System. *Precambrian Research*, Elsevier B.V., v. 292, p. 194–215, 2017. ISSN 03019268. Avaible form internet: <http://linkinghub.elsevier.com/retrieve/pii/S0301926816305496>.

COSTA, L. A. M.; ANGEIRAIS, A. G. Geosynclinal evolution in the epi-baikalian plataform of central brazil. *Geologische Rundschau*, v. 60, n. 2, p. 1024–1050, 1971.

CRUZ-URIBE, A. M. et al. Assessing trace element (dis)equilibrium and the application of single element thermometers in metamorphic rocks. *Lithos*, Elsevier B.V., v. 314-315, p. 1–15, 2018. ISSN 18726143. Avaible form internet: <https://doi.org/10.1016/j.lithos.2018.05.007>.

DARDENNE, M. A. Geologia da região de Morro Agudo (MG). In: SBG (Ed.). *Bol. Núcle Centro-Oeste*. [S.l.: s.n.], 1978. v. 7-8, p. 68–94.

DARDENNE, M. A. The Brasilia Fold Belt. In: *Tectonic Evolution of South Ameria*. [S.l.]: 31 Intern. Geol. Congr. Rio de Janeiro, 2000. p. 231–264.

De Capitani, C.; BROWN, T. H. The computation of chemical equilibrium in complex systems containing non-ideal solutions. *Geochimica et Cosmochimica Acta*, v. 51, n. 10, p. 2639–2652, 1987.

De Capitani, C.; PETRAKAKIS, K. The computation of equilibrium assemblage diagrams with Theriak/Domino software. *American Mineralogist*, v. 95, n. 7, p. 1006–1016, 2010. ISSN 0003004X.

DEL LAMA, E. A. *Terrenos granulíticos de Guaxupé : evolução petrológica de um segmento da crosta inferior*. Tese (Doutorado) — São Paulo State University, 1998.

DEL LAMA, E. A. et al. Exhumation of high-pressure granulites of the Guaxupé Complex, Southeastern Brazil. *Geological Journal*, v. 35, p. 231–249, 2000.

EBERT, H. *Pesquisas na parte Sudeste de Minas Gerais e no Nordeste. In: Relatório Anual do Diretor*. Rio de Janeiro, 1955. 79–89 p.

EBERT, H. *Relatório de atividades. In: Relatório Anual do Diretor da Div. Geol. Min.* Rio de Janeiro, 1956. 62–107 p.

EBERT, H. Beitrag sur Gliederung des Praakambriums in Minas Gerais. *Geol. Rundschau*, v. 45, p. 471–521, 1957.

EBERT, H. *Discordâncias pré- cambrianas em Carandaí, Minas Gerais. In: DGM/DNPM*. Rio de Janeiro: [s.n.], 1958. bol.183, 48 p.

EBERT, H. Ocorrências de fácies granulítica no sul de Minas Gerais e em áreas adjacentes, em dependência da estrutura orogênica; hipóteses sobre sua origem. *Anais da Academia Brasileira de Ciências*, v. 40, p. 215–229, 1968.

EBERT, H. Os Paraibides entre São João del Rei, Minas Gerais e Itapira, São Paulo, e a Bifurcação entre Paraibides e Araxaides. In: *XXV Congresso Brasileiro de Geologia*. [S.l.: s.n.], 1971. p. 1777–1778.

EBERT, H. *Aspectos da Geologia da Região de São João del Rei e a bifurcação entre Paraibíades e Araxaíades*. São Paulo, SP: SBG-SP, 1984. 114 p.

ENGI, M. Petrochronology Based on REE-Minerals: Monazite, Allanite, Xenotime, Apatite. *Reviews in Mineralogy and Geochemistry*, v. 83, n. 1, p. 365 LP – 418, 2017. Avaible form internet: <http://rimg.geoscienceworld.org/content/83/1/365.abstract>.

EWING, T. A.; HERMANN, J.; RUBATTO, D. The robustness of the Zr-in-rutile and Ti-in-zircon thermometers during high-temperature metamorphism (Ivrea-Verbano Zone, northern Italy). *Contributions to Mineralogy and Petrology*, v. 165, n. 4, p. 757–779, 2013. ISSN 00107999.

FALCI, A. et al. Provenance shift from a continental margin to a syn-orogenic basin in the neoproterozoic araxá nappe system, southern brasília belt, brazil. *Precambrian Research*, v. 306, p. 209 – 219, 2018. ISSN 0301-9268. Avaible form internet: <http://www.sciencedirect.com/science/article/pii/S030192681730520X>.

FLEISCHER, R.; SCHMIDT, W. Estilo estrutural do Precambriano no Sudeste de Minas Gerais. In: *Anais do XXX Congresso Brasileiro de Geologia*. [S.l.: s.n.], 1978. p. 55–56.

FRUGIS, G. L.; NETO, M. d. C. C.; LIMA, R. B. Eastern Paranapanema and southern São Francisco orogenic margins: Records of enduring Neoproterozoic oceanic convergence and collision in the southern Brasília Orogen. *Precambrian Research*, Elsevier, v. 308, p. 35–57, 2018.

FUCK, R. et al. Compartimentação tectônica da porção oriental da Província Tocantins. In: *SBG, Congresso Brasileiro de Geologia*. [S.l.: s.n.], 1994. v. 38, n. 1, p. 215–216.

FUCK, R. A. et al. The Northern Brasília Belt. In: HEILBRON, M.; CORDANI, U. G.; ALKMIM, F. F. (Ed.). *São Francisco Craton, Eastern Brazil Tectonic Genealogy of a Miniature Continent*. [S.l.]: Springer Berlin Heidelberg, 2017. p. 205–220.

FUMES, R. A. *Modelagem metamórfica e geotermobarometria de elementos traço em metapelitos e quartzitos: exemplo da Nappe de Luminárias-MG*. Dissertação (Mestrado) — São Paulo State University, January 2017.

FUMES, R. A. et al. Petrografia, química mineral e geotermobarometria de metapelito do grupo carrancas na Nappe de Luminárias (MG). *Geociências*, v. 36, n. 4, p. 639–639, 2017.

FUMES, R. A. et al. Metamorphic modeling and petrochronology of metapelitic rocks from the Luminárias Nappe, southern Brasília belt (SE Brazil). *Brazilian Journal of Geology*, v. 49, n. 2, 2019.

GIUSTINA, M. E. S. D. et al. Dating coeval mafic magmatism and ultrahigh temperature metamorphism in the anápolis–itauçu complex, central brazil. *Lithos*, Elsevier, v. 124, n. 1-2, p. 82–102, 2011.

HART, E. et al. A window into the lower crust: Trace element systematics and the occurrence of inclusions/intergrowths in granulite-facies rutile. *Gondwana Research*, The Authors, v. 59, p. 76–86, 2018. ISSN 1342937X. Avaible form internet: <http://linkinghub.elsevier.com/retrieve/pii/S1342937X18300856>.

HARTUNG, R. F. *Estudo de megaporfiroblastos de granada da Nappe de Passos*. Dissertação (Mestrado) — UNIVERSIDADE ESTADUAL PAULISTA “Júlio de Mesquita Filho”, 2018.

HASUI, Y.; CARNEIRO, C. D. R.; COIMBRA, A. The Ribeira folded belt. *Revista Brasileira de Geociências*, v. 5, n. 4, p. 275–266, 1975.

HEILBRON, M. *Evolução metamórfo-estrutural na área entre Itutinga e Madre de Deus de Minas, MG*. 151 p. Tese (Dissertação de Mestrado) — UFRJ, 1984.

HEILBRON, M.; CORDANI, U. G.; ALKMIM, F. F. *São Francisco Craton, Eastern Brazil: Tectonic Genealogy of a Miniature Continent*. [S.l.: s.n.], 2017. 331 p. ISBN 9783319017143.

HEILBRON, M. et al. From Collision to extension: the roots of the south-eastern continental margin of Brazil. In: TALWANI, M.; MOHRIAK, W. (Ed.). *Atlantic Rifts and Continental Margins of Brazil*. 115. ed. [S.l.]: American Geophysical Union, Geophysical Monographs, 2000. p. 1–34.

HEILBRON, M. et al. Província Mantiqueira. In: *Geologia do Continente sul-americano: evolução da obra de Fernando Flávio Marques de Almeida*. [S.l.: s.n.], 2004. p. 203–235.

HEILBRON, M. et al. The Ribeira Belt. In: HEILBRON, M.; CORDANI, U. G.; ALKMIM, F. F. (Ed.). *São Francisco Craton, Eastern Brazil. Regional Geology Reviews*. [S.l.: s.n.], 2017. p. 277–304.

HEILBRON, M. et al. Correlation of Neoproterozoic terrane between te Ribeira Belt, SE Brazil and its African countepart: comparative tectonic evolution and open questions. *Geological Society, London, Special Publications*, v. 294, p. 211–237, 2008.

HEILBRON, M. et al. O contato basal do Grupo Canastra entre Itaú de Minas e Carmo do Rio Claro, MG. In: *Anais do simpósio de geologia de Minas Gerais 4*. [S.l.: s.n.], 1987. p. 179–198.

KENDRICK, J.; INDARES, A. The Ti Record of Quartz in Anatectic Aluminous Granulites. *Journal of Petrology*, n. July, p. 1–23, 2018. ISSN 0022-3530.

KOHN, M. J.; PENNISTON-DORLAND, S. C.; FERREIRA, J. C. Implications of near-rim compositional zoning in rutile for geothermometry, geospeedometry, and trace element equilibration. *Contributions to Mineralogy and Petrology*, Springer, v. 171, n. 10, p. 78, 2016.

KOOIJMAN, E.; MEZGER, K.; BERNDT, J. Constraints on the U–Pb systematics of metamorphic rutile from in situ LA-ICP-MS analysis. *Earth and Planetary Science Letters*, Elsevier, v. 293, n. 3-4, p. 321–330, 2010.

KOOIJMAN, E. et al. Trace element systematics in granulite facies rutile: implications for Zr geothermometry and provenance studies. *Journal of Metamorphic Geology*, Wiley Online Library, v. 30, n. 4, p. 397–412, 2012.

KRETZ, R. Symbols for rock-forming minerals. *American Mineralogist*, v. 68, p. 277–279, 1983.

LANARI, P.; DUESTERHOEFT, E. Modeling Metamorphic Rocks Using Equilibrium Thermodynamics and Internally Consistent Databases: Past Achievements, Problems and Perspectives. *Journal of Petrology*, v. 60, n. 1, p. 19–56, 2019. ISSN 14602415.

LANARI, P.; ENGI, M.; BERN, C. Local Bulk Composition Effects on Metamorphic Mineral Assemblages. *Reviews in Mineralogy and Geochemistry*, v. 83, p. 55–93, 2017.

LANARI, P. et al. Xmaptools: A matlab©-based program for electron microprobe x-ray image processing and geothermobarometry. *Computers & Geosciences*, Elsevier, v. 62, p. 227–240, 2014.

LUVIZOTTO, G. *Caracterização metamórfica das rochas do Grupo Araxá na região de São Sebastião do Paraíso, sudoeste de Minas Gerais*. Dissertação (Mestrado) — Instituto de Geociências e Ciências Exatas da Universidade Estadual Paulista, 2003.

LUVIZOTTO, G. et al. P-T constraints on high-pressure granulites from southern Brasilian Belt: Ti-quartz and Zr-in-Rutile thermometry. In: *Goldschmitd2017 Abstract*. [s.n.], 2017. Avaible form internet: <https://goldschmidt.info/2017/abstracts/abstractView?id=2017004505>.

LUVIZOTTO, G. L. et al. Rutile occurrence and trace element behavior in medium-grade metasedimentary rocks: Example from the Erzgebirge, Germany. *Mineralogy and Petrology*, v. 97, n. 3-4, p. 233–249, 2009. ISSN 09300708.

MACHADO, N. et al. Ages of detrical zircon from Archean-Paleoproterozoic sequences: implication for greenstone belt setting and evolution of Transamazonian foreland basin in Quadrilátero Ferrífero, southeast Brazil. *Earth and Planetary Science Letters*, v. 141, p. 259–276, 1996.

MARIMON, R. S. et al. Provenance of passive-margin and syn-collisional units: Implications for the geodynamic evolution of the southern brasília orogen, west gondwana. *Sedimentary Geology*, Elsevier, v. 413, p. 105823, 2021.

MORA, C. A. S.; NETO, M. d. C. C.; BASEI, M. A. S. Syn-collisional lower continental crust anatexis in the Neoproterozoic Socorro-Guaxupé Nappe System, southern Brasília Orogen, Brazil: Constraints from zircon U–Pb dating, Sr–Nd–Hf signatures and whole-rock geochemistry. *Precambrian Research*, Elsevier, v. 255, p. 847–864, 2014.

MORAES, R. et al. Characterization and P-T Evolution of Melt-bearing Ultrahigh-temperature Granulites: an Example from the Anapolis-Itauçu Complex of the Brasília Fold Belt. *Journal of Petrology*, v. 43, p. 1673–1705, 2002.

MORAES, R. et al. Applications and limitations of thermobarometry in migmatites and granulites using as an example rocks of the Araçuaí Orogen in southern Bahia, including a discussion on the tectonic meaning of the current results. *Brazilian Journal of Geology*, v. 45, p. 517–539, 2015.

MORALES, N. *Evolução tectônica do cinturão de Cisalhamento Campo do Meio na sua porção ocidental*. Tese (Doutorado) — IGCE-UNESP, Rio Claro, 1991.

MOTTA, R. G.; MORAES, R. Pseudo- and real-inverted metamorphism caused by the superposition and extrusion of a stack of nappes: a case study of the Southern Brasília Orogen, Brazil. *International Journal of Earth Sciences*, 2017. ISSN 1437-3254. Avaible form internet: <http://link.springer.com/10.1007/s00531-016-1436-7>.

NACHLAS, W.; HIRTH, G. Experimental constraints on the role of dynamic recrystallization on resetting the Ti-in-quartz thermobarometer. *Journal of Geophysical Research: Solid Earth*, Wiley Online Library, v. 120, n. 12, p. 8120–8137, 2015.

NUNES, R.; TROUW, R. A. J.; CASTRO, E. *Mapa Gelógico - Folha Varginha – escala 1:100.000, Programa Geologia do Brasil*. [S.l.], 2008.

O'BRIEN, P. J.; RÖTZLER, J. R. High-pressure granulites: formation, recovery of peak conditions and implications for tectonics. *Journal of Metamorphic Geology*, v. 21, n. 3-20, 2003.

PACIULLO, F. V. P. Mapeamento geológico-estrutural da área de Minduri, MG. In: *Anais do II Simpósio de Geologia de Minas Gerais-Geologia do Pré-Cambriano*. [S.l.: s.n.], 1980. p. 440–448.

PACIULLO, F. V. P.; RIBEIRO, A. Mapa Geológico-Folha Nepumoceno. In: *CONTRATO - CPRM - UFRJ 067/P2/2005*. [S.l.: s.n.], 2008.

PACIULLO, F. V. P. et al. The Andrelândia Basin, a Neoproterozoic Intraplate Continental Margin, Southern Brasília Belt, Brazil. *Revista Brasileira de Geociências*, v. 30, n. 1, p. 200–202, 2000.

PACIULLO, F. V. P.; RIBEIRO, A.; TROUW, R. a. J. Geologia da Folha Andrelândia 1:100.000. *Geologia e recursos minerais do sudeste mineiro Projeto Sul de Minas - Etapa I*, p. 84–119, 2003.

PAULY, J. et al. Prolonged Ediacaran–Cambrian metamorphic history and short-lived high-pressure granulite-facies metamorphism in the HU Sverdrupfjella, Dronning Maud Land (East Antarctica): evidence for continental collision during Gondwana assembly. *Journal of Petrology*, Oxford University Press, v. 57, n. 1, p. 185–228, 2016.

PETERNEL, R. et al. Interferência Entre Duas Faixas Móveis Neoproterozóicas : O Caso Das Faixas Brasília E Ribeira No Sudeste Do Brasil. v. 35, n. 3, p. 297–310, 2005. ISSN 2317-4692.

PETERNEL, R.; TROUW, R. A. J.; CASTRO, E. O. *Mapa Gelógico - Folha Varginha*. [S.l.]: Serviço Geológico do Brasil, 2008. 1:100.000 p.

PIMENTEL, M. M. The tectonic evolution of the Neoproterozoic Brasília Belt, central Brazil: The tectonic evolutuion of the Neoproterozoic Brasília Bet, central Brasil: a geochronological and isotopic approach. *Brazilian Journal of Geology*, v. 46, n. Suppl 1, p. 67–82, 2016.

PIUZANA, D. et al. Neoproterozoic granulite facies metamorphism and coeval granitic magmatism in the Brasilia Belt, Central Brazil: regional implications of new SHRIMP U–Pb and Sm–Nd data. *Precambrian Research*, Elsevier, v. 125, n. 3-4, p. 245–273, 2003.

PIUZANA, D. et al. SHRIMP U–Pb and Sm–Nd data for the Araxá Group and associated magmatic rocks: constraints for the age of sedimentation and geodynamic context of the southern Brasılia Belt, central Brazil. *Precambrian Research*, Elsevier, v. 125, n. 1-2, p. 139–160, 2003.

POWELL, R.; HOLLAND, T. J. B. On thermobarometry. *Journal of Metamorphic Geology*, v. 26, n. 2, p. 155–179, 2008. ISSN 02634929.

QUÉMÉNEUR, J. J. G. et al. Mapa Geológico-Folha Lavras. In: *Geologia e Recursos Minerais do Sudeste Mineiro*. [S.l.: s.n.], 2003. p. 1:100.000.

RENO, B. L. et al. Eclogite–high-pressure granulite metamorphism records early collision in West Gondwana: new data from the Southern Brasília Belt, Brazil. *Journal of the Geological Society*, Geological Society of London, v. 166, n. 6, p. 1013–1032, 2009.

RENO, B. L.; BROWN, M.; PICCOLI, P. M. $^{40}Ar/^{39}Ar$ thermochronology of high-pressure granulite nappes in the southern Brasília Belt, Brazil: Implications for Nappe Exhumation. *American Journal of Science*, American Journal of Science, v. 310, n. 10, p. 1294–1332, 2010.

RENO, B. L. et al. In situ monazite (U-Th)-Pb ages from the Southern Brasília Belt, Brazil: Constraints on the high-temperature retrograde evolution of HP granulites. *Journal of Metamorphic Geology*, v. 30, n. 1, p. 81–112, 2012. ISSN 02634929.

RIBEIRO, A.; HEILBRON, M. Estratigrafia e Metamorfismo dos Grupos Carrancas e Adrelândia, Sul de Minas Gerais. In: *Anais do XXXII Congresso Brasileiro de Geologia*. [S.l.: s.n.], 1982. p. 177–186.

RIBEIRO, A. et al. Evolução Policíclica Proterozóica no Sul do Cráton de São Francisco: Análise da Região de São João del Rei e Andrelândia, MG. In: *Anais do XXXVI Congresso Brasileiro de Geologia*. [S.l.: s.n.], 1990. p. 2605–2614.

RIBEIRO, A. et al. Evolução das Bacias Proterozóicas e o Termo-Tectonismo Brasiliano na Margem Sul do Cráton do São Francisco. *Revista Brasileira de Geociências*, v. 25, n. 4, p. 235–248, 1995.

ROCHA, B. C. et al. Timing of anatexis and melt crystallization in the Socorro – Guaxupé Nappe , SE Brazil : Insights from trace element composition of zircon , monazite and garnet coupled to U — Pb geochronology. v. 277, p. 337–355, 2017.

ROCHA, B. C. et al. Magmatic inheritance vs. UHT metamorphism: Zircon petrochronology of granulites and petrogenesis of charnockitic leucosomes of the Socorro–Guaxupé nappe, SE Brazil. *Lithos*, v. 314-315, p. 16–39, 2018. ISSN 18726143.

SANTOS, T. Bento dos et al. Thermochronological evidence for long-term elevated geothermal gradients in Ribeira Belt, SE Brazil. In: *Goldschmidt Conference 2007*. [S.l.: s.n.], 2007.

SCHRANK, A. et al. Determinação dos vetores de transporte tectônico na borda sudoeste do Cráton do São Francisco. In: SBG (Ed.). *XXXVI Congresso Brasileiro de Geologia*. [S.l.: s.n.], 1990. v. 5, p. 2276–2283.

SEER, H. J. et al. Grupo Araxá em sua área tipo: Um fragmento de crosta oceânica neoproterozóica na faixa de dobramentos Brasília. *Revista Brasileira de Geociências*, v. 31, n. 3, p. 385–396, 2001.

SEER, H. J.; DARDENNE, M. A. Tectonostratigraphic terrane analysis on neoproterozoic times: the case study of Araxá Synform, Minas Gerais state, Brazil: Implications to the final collage of the Gondwanaland. *Revista Brasileira de Geociências*, v. 30, n. 1, p. 78–81, 2000.

SILVA, A. J. C. A. *Evolução Estrutural e Idades U-Pb das Unidades Litoestratigráficas da Nappe de Passos e do Grupo Canastra, Sudoeste de Minas Gerais*. Tese (Doutorado) — Universidade Estadual Paulista, 2018.

SILVA, A. J. C. A.; SIMÕES, L. S. A.; DUFRANE, S. A. Tectonic implications of U-Pb ages of detrital zircon grains in metasedimentary rocks of the northwestern sector of the Passos Nappe, southern Brasília Belt, Brazil. *Journal of South American Earth Sciences*, Elsevier, n. 95, p. 1–24, 2019.

SILVA, M. P. *Modelamento Metamórfico de Rocas das Fácies Xisto-Verde e Anfibolito com o Uso de Pseudosseções: Exemplo das Rochas da Klippe Carrancas, Sul de Minas Gerais*. Tese (Dissertação de mestrado) — Universidade de São Paulo, 2010.

SIMÕES, L. *Evolução tectono-metamórfica da nappe de Passos, sudoeste de Minas Gerais*. Tese (Doutorado) — IG-Universidade de São Paulo, 1995.

SIMÕES, L. S. A.; VALERIANO, C. M. Porção meridional da faixa de dobramentos brasilia: Estágio atual do conhecimento e problemas de correlação tectono-estratigráfica. In: *Anais do XXXVI Congresso Brasileiro de Geologia*. [S.l.: s.n.], 1990. v. 6, n. 1, p. 2564–2575.

SIMÕES, L. S. A. et al. Zonação metamórfica inversa do Grupo Araxá-Canastra na região de São Sebasião do Paraíso-Alpinópolis. In: SBG (Ed.). *Anais do XXXV Congresso Brasleiro de Geologia*. [S.l.: s.n.], 1988. v. 3, p. 1203–1215.

SIZOVA, E.; GERYA, T.; BROWN, M. Contrasting styles of Phanerozoic and Precambrian continental collision. *Gondwana Research*, Elsevier, v. 25, n. 2, p. 522–545, 2014.

SPENCER, C. J. et al. Not all supercontinents are created equal: Gondwana-rodinia case study. *Geology*, Geological Society of America, v. 41, n. 7, p. 795–798, 2013.

STRDEDER, A. J.; NILSON, A. A. Melange ofiolítica nos metassedimentos Araxá de Abadiância (GO) e implicações tectônicas regionais. *Revista Brasileira de Geociências*, v. 22, n. 2, p. 204–215, 1992.

TAYLOR-JONES, K.; POWELL, R. Interpreting zirconium-in-rutile thermometric results. *Journal of Metamorphic Geology*, v. 33, n. 2007, p. 115–122, 2015.

TEDESCHI, M. et al. Reconstruction of multiple PTt stages from retrogressed mafic rocks: Subduction versus collision in the Southern Brasília orogen (SE Brazil). *Lithos*, Elsevier, v. 294, p. 283–303, 2017.

TEDESCHI, M. et al. Protracted zircon geochronological record of UHT garnet-free granulites in the Southern Brasília orogen (SE Brazil): Petrochronological constraints on magmatism and metamorphism. *Precambrian Research*, Elsevier, v. 316, n. August, p. 103–126, 2018. ISSN 03019268. Avaible form internet: <https://doi.org/10.1016/j.precamres.2018.07.023>.

TEIXEIRA, N. A.; DANNI, J. Contribuição à Estratigrafia do Grupo Araxá na região de Passos (MG). In: *Anais do XXX Congresso Brasileiro de Geologia*. [S.l.: s.n.], 1978. p. 126.

THOMAS, J. B. et al. TitaniQ recrystallized: experimental confirmation of the original Ti-in-quartz calibrations. *Contributions to Mineralogy and Petrology*, v. 169, n. 3, 2015. ISSN 0010-7999. Avaible form internet: <http://link.springer.com/10.1007/s00410-015-1120-0>.

TOMKINS, H. S.; POWELL, R.; ELLIS, D. J. The pressure dependence of the zirconium-in-rutile thermometer. *Journal of Metamorphic Geology*, v. 25, n. 6, p. 703–713, 2007. ISSN 02634929.

TRIEBOLD, S. et al. Deducing source rock lithology from detrital rutile geochemistry: An example from the Erzgebirge, Germany. *Chemical Geology*, v. 244, n. 3-4, p. 421–436, 2007. ISSN 00092541.

TRIEBOLD, S.; EYNATTEN, H. von; ZACK, T. A recipe for the use of rutile in sedimentary provenance analysis. *Sedimentary Geology*, Elsevier B.V., v. 282, p. 268–275, 2012. ISSN 00370738. Avaible form internet: <http://dx.doi.org/10.1016/j.sedgeo.2012.09.008>.

TROUW, R. A. J. et al. The Central Segment of the Ribeira Belt. In: CORDANI, U. G. et al. (Ed.). *Tectonic Evolution of South America*. 1. ed. [S.l.]: COMPANHIA DE PESQUISA DE RECURSOS MINERAIS, 2000. p. 287–310.

TROUW, R. A. J. et al. Análise de Deformação numa Área a SE de Lavras Minas Gerais. In: *Anais do XXXII Congresso Brasileiro de Geologia*. Salvador, Bahia: [s.n.], 1982. p. 187–198.

TROUW, R. A. J.; PACIULLO, F. V. P.; HEILBRON, M. Os Grupos São João Del Rei, Carrancas e Andrelândia Interpretados como a Continuição dos Grupos Araxá e Canastra. In: *Anais do XXXIII Congresso Brasileiro de Geologia*. Rio de Janeiro, RJ: [s.n.], 1984. p. 177–178.

TROUW, R. A. J.; PACIULLO, F. V. P.; RIBEIRO, A. A Faixa Alto Rio Grande Reinterpretada como Zona de Interferência entre a Faixa Brasília e a Faixa Ribeira. In: *XXXVIII Congresso Brasileiro de Geologia*. [S.l.]: SBG, 1994. p. 234–235.

TROUW, R. A. J. et al. Mapa Geológico-Folha Caxambu. In: CODEMIG (Ed.). *Geologia e Recursos Minerais do Sudeste Mineiro*. [S.l.: s.n.], 2003. p. 1:100.000.

TROUW, R. A. J. et al. *Mapa Geológico-Folha Caxambu. Projeto Sul de Minas - etapa 1, escala 1:100.000*. [S.l.], 2013.

TROUW, R. A. J. et al. A new interpretation for the interference zone between the southern Brasília belt and the central Ribeira belt, SE Brazil. *Journal of South American Earth Sciences*, v. 48, p. 43–57, 2013. ISSN 08959811.

TROUW, R. A. J.; RIBEIRO, A.; PACIULLO, F. V. P. Evolução Estrutural e Metamórfica de uma àrea a SE de Lavras - Minas Gerias. In: *Anais do XXXI Congresso Brasieliro de Geologia, Balneário de Camboriú, Santa Catarina*. Balneário de Camburiú: [s.n.], 1980.

TROUW, R. A. J.; RIBEIRO, A.; PACIULLO, F. V. P. Geologia Estrutural do Grupos São João del Rei, Carrancas e Andrelândia, Sul de Minas Gerais. *Anais da Academia brasileira de Ciências*, v. 55, n. 1, p. 71–87, 1983.

TROUW, R. A. J.; TAVARES, F. M.; ROBYR, M. Rotated garnets: a mechanism to explain the high frequency of inclusion trail curvature angles around 90^o and 180^o. *Journal of Structural Geology*, v. 30, n. 8, p. 1024–1033, 2008. ISSN 01918141.

VALERIANO, C. M. *Geologia Estrutural e Estratigrafia do Grupo São João del Rei, MG*. Tese (Master Thesis) — Universidade Federal do Rio de Janeiro, 1985.

VALERIANO, C. M. *Evolução tectônica da extremidade meridional da Faixa Brasília, Região da represa de Furnas Sudoeste de Minas Gerais*. Tese (Doutorado) — IG-USP, 1993.

VALERIANO, C. M. The Southern Brasília Belt. In: HEILBRON, M.; CORDANI, U. G.; ALKMIM, F. (Ed.). *São Francisco Craton, Eastern Brazil. Regional Geology Reviews*. Switzerland: Springer International Publishing, 2017. cap. The Southe, p. 189–203. ISBN 9783319017150.

VALERIANO, C. M. et al. A evolução tectônica da faixa brasília. In: _____. *Geologia do Continente sul-americano: evolução da obra de Fernando Flávio Marques de Almeida.* [S.l.]: Beca, 2004. p. 575–592.

VALERIANO, C. M. et al. U-Pb Geochronology of Southern Brasília Belt (SE Brazil): sedumentary provenance, Neoproterozoic orogeny and assembly of Western Gondwana. *Precambrian Research*, v. 130, p. 7–11, 2004.

VALERIANO, C. M. et al. Tectonic evolution of the Brasília Belt, Central Brazil, and early assembly of Gondwana. In: PANKHURST, R. J. et al. (Ed.). *West Gondwana: Pre-Cenozoic Correlations Across the South Atlantic Region.* Geological. London: [s.n.], 2008. p. 197–210.

VALERIANO, C. M.; SIMÕES, L. S. A.; GODOY, A. M. Compartimentação Tectônica da porção meridional das Faixas Uruaçu e Brasília, SW de Minas Gerais: Dados Preliminares. In: *Anais do 5 Simpósio Geologia de MInas Gerais*. [S.l.: s.n.], 1989. v. 238-247.

VALERIANO, C. M. et al. Southern brasilia belt (se brazil): tectonic discontinuities, k-ar data and evolution during the neoproterozoic brasiliano orogeny. *Revista Brasileira de Geociências*, v. 30, n. 1, p. 195–199, 2000.

VLACH, S.; GUALDA, G. A. R. Microprobe monazite dating and the ages of some granitic and metamorphic rocks from southeastern Brazil. *Revista Brasileira de Geociências*, v. 30, n. 1, p. 214–218, 2000.

WELLER, O.; ST-ONGE, M. Record of modern-style plate tectonics in the Palaeoproterozoic Trans-Hudson orogen. *Nature Geoscience*, Nature Publishing Group, v. 10, n. 4, p. 305, 2017.

WESTIN, A.; CAMPOS NETO, M. D. C. Provenance and tectonic setting of the external nappe of the Southern Brasília Orogen. *Journal of South American Earth Sciences*, Elsevier Ltd, v. 48, p. 220–239, 2013. ISSN 08959811. Avaible form internet: <http://dx.doi.org/10.1016/j.jsames.2013.08.006>.

WESTIN, A. et al. The Neoproterozoic southern passive margin of the São Francisco craton: Insights on the pre-amalgamation of West Gondwana from U-Pb and Hf-Nd isotopes. *Precambrian Research*, p. 454–471, 2019.

WESTIN, A. et al. A paleoproterozoic intra-arc basin associated with a juvenile source in the Southern Brasilia Orogen: Application of U–Pb and Hf–Nd isotopic analyses to provenance studies of complex areas. *Precambrian Research*, v. 276, p. 178–193, 2016.

WESTIN, A. et al. The fast exhumation pattern of a neoproterozoic nappe system built during west gondwana amalgamation: Insights from thermochronology. *Precambrian Research*, Elsevier, v. 355, p. 106115, 2021.

YAKYMCHUK, C.; BROWN, M. Divergent behaviour of Th and U during anatexis: Implications for the thermal evolution of orogenic crust. *Journal of Metamorphic Geology*, v. 37, n. 899-916, 2019.

YAKYMCHUK, C.; GODIN, L. Coupled role of deformation and metamorphism in the construction of inverted metamorphic sequences: an example from far-northwest nepal. *Journal of Metamorphic Geology*, Wiley Online Library, v. 30, n. 5, p. 513–535, 2012.

ZACK, T.; MORAES, R.; KRONZ, A. Temperature dependence of Zr in rutile: Empirical calibration of a rutile thermometer. *Contributions to Mineralogy and Petrology*, v. 148, n. 4, p. 471–488, 2004. ISSN 00107999.

ZANARDO, A. *Análise petrográfica, estratigráfica e microestrutural da região de Guaxupé-Passos-Delfinópolis (MG)*. Tese (Doutorado) — Universidade Estadual Paulista, São Paulo, Brazil, 1992.

ZANARDO, A.; DEL LAMA, E. A.; MORALES, N. Análise microestrutural do grupo araxá-canastra nas proximidades de alpinópolis. In: SBG (Ed.). *Anais do XXXVI Congresso Brasileiro de Geologia*. [S.l.: s.n.], 1990. v. 5, p. 2167–2174.

3 Petrochronology of high-pressure granulite facies rocks from Southern Brasília Orogen, SE Brazil: combining quantitative compositional mapping, single-element thermometry and geochronology

Regiane Andrade Fumes[1*]; George Luiz Luvizotto[1]; Renato Moraes[2]; Pierre Lanari[3], Claudio de Morisson Valeriano[4], Thomas Zack[5], Mark J. Caddick[6], Luiz Sergio Amarante Simões[1]

[1]Department of Petrology and Metallogeny, São Paulo State University, Av. 24A, 1515, 13506- 900, Rio Claro, Brazil *Corresponding author e-mail: regiane.fumes@unesp.br

[2]Department of Mineralogy and Geotectonics, University of São Paulo, Rua do Lago, 562, 05508-080, São Paulo, Brazil

[3]Institute of Geological Sciences, University of Bern, Baltzerstrasse 1 + 3, Bern 3012, Switzerland

[4]TEKTOS Research Group, Geology Institute, Rio de Janeiro State University, Rua São Francisco Xavier 524/4030-A, Maracanã, Rio de Janeiro 20550-900, Brazil

[5]Department of Earth Sciences University of Gothenburg PO Box 460 41430 Gothenburg Sweden [6]Virginia Tech, Department of Geosciences, 926 West Campus Dr., Blacksburg, VA, USA

Abstract

We use a combination of several in situ techniques to assess the P-T-t path of high-pressure granulites from the Passos Nappe in the Southern Brasília Orogen (SE - Brazil). Quantitative element mapping and single-element thermometers (Zr-in-rutile and Ti-in-quartz) are coupled with P–T pseudosections and monazite and rutile dating. Compositional and temperature maps, based on cathodoluminescence mapping and in situ analyses of Ti in quartz, are presented as a novel approach to evaluate crystallization temperature. The studied rocks have a pelitic protolith and record a peak pressure assemblage of garnet + kyanite + rutile + K-feldspar + quartz + melt ± plagioclase that formed at ∼830 °C and 1.2 GPa. Retrograde conditions of ∼560 °C and 0.6 GPa are determined based on the grossular content of garnet, and the crystallization of biotite and ilmenite. Metamorphic peak conditions occurred ca. 635 Ma, according to monazite dating,

with a younger date of ca. 615 Ma associated with later kyanite crystallization. Rutile ages of ca. 590 Ma are linked to the late retrograde stage (at ∼600 °C). Results show that the distribution of Ti in quartz is heterogeneous, decreasing in abundance towards the rim of crystals, though the higher temperatures constrained with Ti-in-quartz thermometry are broadly consistent with peak conditions. The peak pressure conditions are consistent with the continental collision setting in the Southern Brasília Orogen and were followed by an early cooling/decompression stage and then by a slow cooling during exhumation and transport to shallower crustal levels.

Keywords: Cathodoluminescence, phase equilibrium modelling (THERMOCALC), P–T–t path, single element thermometers, Western Gondwana, XMapTools.

3.1 Introduction

High-pressure granulites are key markers of geodynamic processes in overthickened or subducted continental crust (O'BRIEN, 2008), recording extreme pressure (P) and temperature (T) conditions of crustal metamorphism. They enable us to access information about the roots of orogenic belts, where continental crust could be deeply subducted, and are frequently exposed in deeply eroded Precambrian orogens, such as the Brasília Orogen (SE – Brazil).

The reconstruction of P–T–t paths of high-pressure granulites contributes significantly to our understanding of the evolution of collisional orogenic belts. The metamorphic evolution of such rocks is often complex and should not generally be viewed as the result of a single phase of equilibration under granulite facies conditions (O'BRIEN; RÖTZLER, 2003). Many factors are involved in their genesis and control their evolution, including burial and exhumation rates, crustal heat budgets, contrasting intra- and inter-crystalline diffusion rates of the range of conditions involved, and the role of melt and fluids in metamorphic equilibration and deformation. Each of these parameters can be reflected in the results of geochronology and mineral thermobarometry, though the metamorphic record of each process is often difficult to read.

Trace element geothermometers are especially useful for high-pressure granulites because, in general, garnet is the only Fe-Mg phase in rocks with pelitic protoliths, so conventional exchange thermometry is not possible. In recent decades, single element geothermometers, such as Ti-in-quartz and Zr-in-rutile, have become important tools for calculating crystallization T in metamorphic rocks (e. g. Ashley e Law (2015), Cruz-Uribe et al. (2018), Kendrick e Indares (2018), Pape, Mezger e Robyr (2016), Pauly et al. (2016), Taylor-Jones e Powell (2015), Thomas et al. (2010), Thomas et al. (2015) since they are also generally considered less prone to post-peak resetting than, for example, Fe-Mg thermometers. Ti-in-quartz and Zr-in-rutile equilibria are also affected by pressure, so that

if quartz and rutile are in equilibrium, it is possible to extract both P and T information (THOMAS et al., 2010). Trace element thermometers are, therefore, useful for interpreting P-T-t paths, and are complementary to other approaches.

In high-grade rocks such as high-pressure granulites, Ti-in-quartz and Zr-in-rutile contents often show a large spread (e.g. Kendrick e Indares (2018), Pape, Mezger e Robyr (2016), Taylor-Jones e Powell (2015)). Cathodoluminescence (CL) mapping is a valuable tool to study the Ti distribution in quartz and its correlation with rock texture since CL emission in quartz (captured using a blue filter) has been shown to be proportional to its Ti content (LEEMAN et al., 2012; KENDRICK; INDARES, 2018). The ability to produce standardized maps (i.e., quantitative maps, e.g. (LANARI; DUESTERHOEFT, 2019) by co-processing qualitative CL maps and quantitative analyses raises the possibility of recovering detailed records of T conditions using the Ti-in-quartz thermometry, though this is still an emerging line of research.

Besides the importance of constraining the P-T evolution of high-grade rocks, it is also necessary to determine constraints on the relationship between the P-T conditions and age of this metamorphism and use geochronology to help place rocks within an appropriate regional tectonic context. The application of U-Pb(Th) geochronology techniques to assess accurate and precise ages of accessory minerals such as monazite and rutile has become particularly useful for deciphering the tectonic history of orogenic belts (ARMSTRONG, 1991; DICKIN, 1995; GEBAUER; GRÜNENFELDER, 1979), and detailed petro chronologyis becoming widespread in the many cases where multiple stages of the P-T-t path are be recorded (Engi, 2017; Foster et al., 2004). The ages of prograde heating, thermal peak conditions, and retrograde stages of metamorphism can be recorded in monazite (e.g. Prent et al. (2019), Reno et al. (2012), Rocha et al. (2017), Tiwari e Biswal (2019)), whereas rutile is potentially the most suitable mineral for studying the influence of intra- and intergrain ion diffusion during cooling (ZACK; KOOIJMAN, 2017). Combining ages from coexisting minerals is a powerful tool for uncovering complex metamorphic histories and constraining the cooling rates and thermal evolution of high-grade rocks.

The aim of this work is to present P-T data and ages on high-pressure granulites from the Passos Nappe, showing how a combination of tools, namely, mineral analysis, element mapping, thermodynamic modelling, single element thermometry and in situ dating, can be used to assess a detailed P-T-t path of these rocks. Furthermore, we discuss tectonic settings of the Passos Nappe and discuss possible correlation between the high-pressure granulite and similar rocks that occur further south in the Andrelândia Nappe System.

3.2 Geological Setting

3.2.1 Regional Setting

The Neoproterozoic Brasília Orogen (Figure 3.1) is located in central / southeastern Brazil, where it borders the western and southern margin of the São Francisco Craton. Its development is related to the early assembly of West Gondwana (DARDENNE, 2000; VALERIANO et al., 2004; VALERIANO et al., 2008; VALERIANO, 2017) Figure 3.1a). The Southern Brasília Orogen, that is, the portion of the orogen that occurs to the south of the Pirineus Syntaxis (Figure 3.1b) (ARAÚJO FILHO, 2000), is divided (FUCK et al., 1994), based on rock types and their tectonic setting, into four tectonic domains. From east to west and from bottom to structural top these are: (i) the Cratonic Zone and its sedimentary cover; (ii) the External (foreland) Zone that represents the low-grade metamorphic fold-and-thrust belt of the orogen; (iii) the Internal Zone, comprising the tectonically overlying nappes of high-grade metamorphic rocks; (iv) and the Goiás magmatic arc zone. This division is broadly accepted in the literature (DARDENNE, 2000; PIMENTEL, 2016; VALERIANO et al., 2004a; VALERIANO et al., 2008; VALERIANO, 2017). The rocks from the Brasília Orogen record a complete Wilson Cycle, starting in the Tonian (ca. 0.9 Ga) with rifting and the development of a passive margin and opening of the Goianides ocean, followed by subduction of distal continental margin units (ca. 0.63 Ga) and ending with nappe stacking and exhumation between ca. 610 and 580 Ma in a continental collision setting (FUCK et al., 2017; VALERIANO et al., 2000; VALERIANO et al., 2008; VALERIANO, 2017; TEDESCHI et al., 2018).

Most of the rocks of the Internal Zone belong to the Araxá Group (BARBOSA, 1955; SEER; DARDENNE, 2000; SEER et al., 2001; VALERIANO et al., 2004; VALERIANO et al., 2004a; VALERIANO, 2017), exposed in a series of nappes, such as the Passos Nappe, from where the studied samples derive. The rocks of Araxá Group in the southernmost portion of the Southern Brasília Orogen have been compared by Trouw, Paciullo e Heilbron (1984) to those of the Andrelândia Group, which occur further south and have similar lithology and metamorphic conditions.

3.2.2 Lithostratigraphy and tectonic setting

The Passos Nappe is predominantly composed of metasedimentary rocks (Figure 3.1c), traditionally included in the Araxá Group (SIMÕES, 1995; VALERIANO et al., 2004), with minor lenses of tholeiitic metabasic rocks. The basal units of the nappe contain biotite-muscovite schists, marble, and minor muscovite quartzite. These rocks are overlain by a thick package of muscovite-rich quartzites followed by fine grained muscovite-biotite gneiss, garnet-biotite-muscovite schist (that may contain kyanite), and minor muscovite-bearing quartzite lenses. Scarce lenses of amphibolite are also locally

Figure 3.1 – Geological setting of the study area. a) Gondwana map (ca. 500 Ma) showing the location of the study area (green rectangle), after Spencer et al. (2013). b) Tectonic map of the Southern Brasília Orogen and adjoining southwestern margin of the São Francisco craton modified from Valeriano (2017), Campos Neto et al. (2010). TPVN: Três Pontas-Varginha Nappe, SNK: Serra da Natureza Klippe, CK: Carvalhos Klippe, PAN: Pouso Alegre Nappe and AK: Aiuruoca Klippe. c) Geological map of the Passos Nappe (updated from Valeriano et al. (2004). d) Detail of the map in the southwest of the Passos Nappe with sample location.

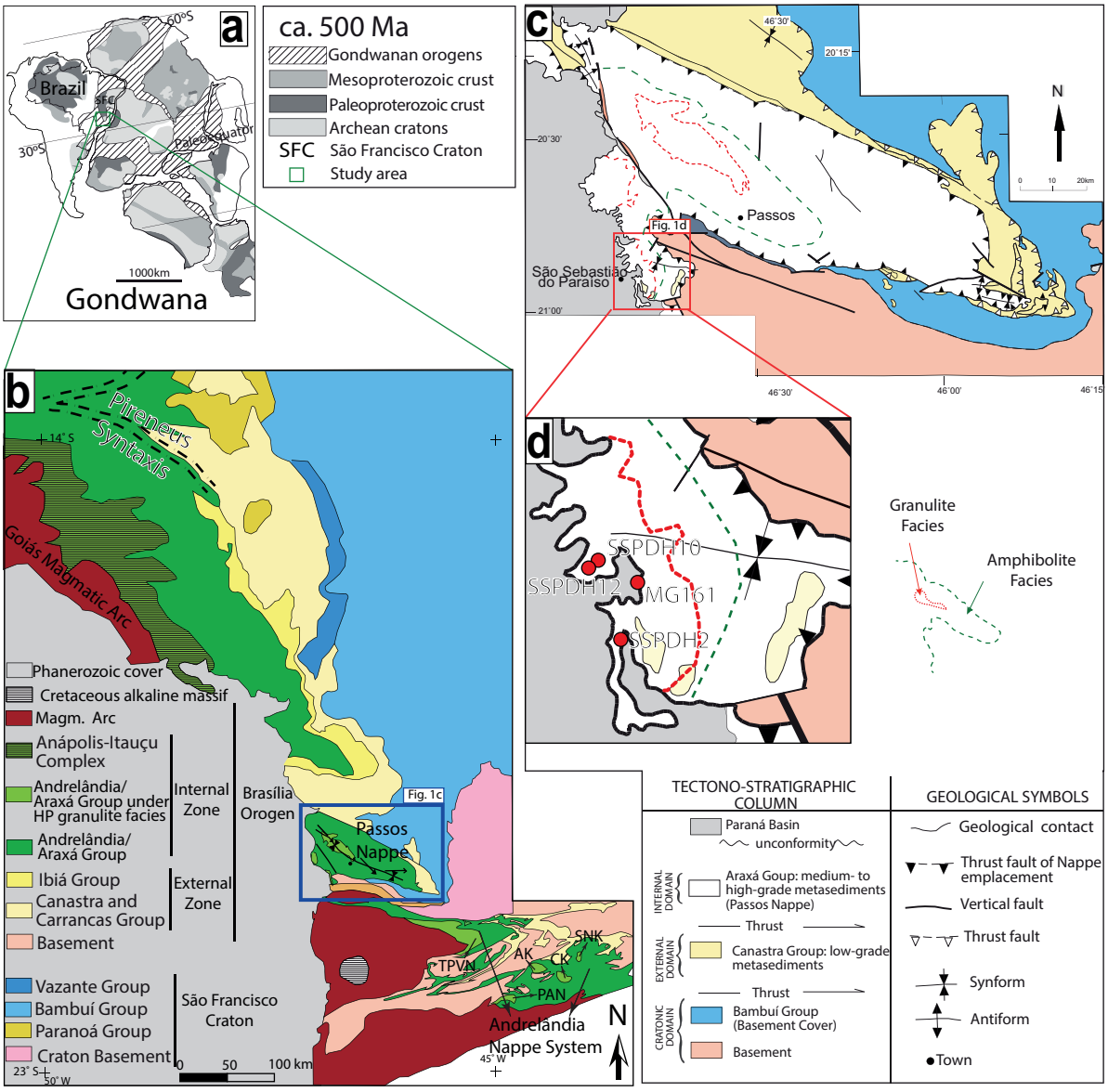

present. The upper units show partial melting features, locally, and are mainly composed of garnet-biotite-muscovite schists, that often have kyanite-bearing, with intercalations of garnet-biotite(±kyanite) paragneiss, high-pressure granulite (with rutile, kyanite, garnet and K-feldspar) and garnet amphibolite (SIMÕES, 1995; VALERIANO et al., 2004). Based on this lithological succession, the metasedimentary pile of the Passos Nappe is interpreted as having evolved broadly from platform to pelagic settings. The metabasic rocks are classified as high- and low-TiO_2 tholeiities and have crystallization ages of ca. 0.9 Ga (VALERIANO; SIMÕES, 1997). The predominance of the low-TiO_2 tholeiites towards the

top of the Passos Nappe, along with the transition from psammitic to pelitic-dominated sedimentation, was interpreted by Valeriano e Simões (1997) as reflecting progressive thinning of the continental lithosphere during the evolution of the Neoproterozoic passive margin.

3.2.3 Metamorphic record

Rocks from the Passos Nappe record an inverted metamorphic gradient (LUVIZOTTO, 2003; SIMÕES, 1995), ranging from greenschist-grade at the base (biotite-muscovite schist), to high-pressure granulite facies conditions at the top (kyanite-garnet gneiss with partial melting features). No precise *P-T* conditions are currently available for these rocks.

To the north of the Passos Nappe (Figure 3.1b), rocks from the Araxá group reached granulite facies in the Anápolis-Itauçu Complex (PIMENTEL, 2016; PIUZANA et al., 2003a; PIUZANA et al., 2003b), where ultra-high-temperature mineral assemblages are recognized (BALDWIN et al., 2005; MORAES et al., 2002), but not at particularly high-pressure conditions ($\sim$ 0.9 GPa). High-pressure granulite facies metamorphism is only recognized in rocks from the top of the Andrelãndia Nappe System, occurring further south than the Passos Nappe. Within the Andrelândia Nappe System, high-pressure granulites are recognized in the Três Pontas-Varginha and Pouso Alegre Nappes, and in the Carvalhos, Aiuruoca and Serra da Natureza Klippen (Figure 3.1b). *P–T* conditions of these rocks have been calculated at 800–850 °C and 1.2–1.4 GPa (CAMPOS NETO; CABY, 1999; CAMPOS NETO et al., 2007; CAMPOS NETO et al., 2010; CIOFFI et al., 2012; COELHO et al., 2017; MOTTA; MORAES, 2017; RENO et al., 2009; TROUW, 1992) or for higher pressure conditions, between 1.5 and 1.8 GPa (MARTINEZ, 2015).

3.2.4 Ages

The age of peak metamorphism in the Passos Nappe, based on TIMS U-Pb zircon data from syn-tectonic leucosome veins is 631 $\pm$4 Ma (VALERIANO et al., 2004). Monazite crystals collected from the leucosomes of migmatites, garnet biotite schists and muscovite quartzite from the upper portion of the Passos Nappe, indicate younger ages of ca. 605 Ma (VALERIANO et al., 2004). These monazite ages are interpreted to be associated with the exhumation and cooling of the nappe and are consistent, within uncertainties, with a rutile age of ca. 594 Ma (VALERIANO et al., 2004). Final cooling stages of the Passos Nappe are recorded by the youngest muscovite K-Ar ages near the studied area of ca. 570-580 Ma (VALERIANO et al., 2000).

The high-pressure granulite from the Andrelândia Nappe System (Três Pontas-Varginha Nappe and Serra da Natureza Klippe, Carvalhos Klippe, Pouso Alegre Nappe

and Aiuruoca Klippe, Figure 3.1b) is composed of rutile, kyanite, K-feldspar, garnet and quartz, with a quartz-feldspathic leucosome (CAMPOS NETO et al., 2010), very similar to the rocks studied here. A monazite age of 617.7 ±1.3 Ma, obtained by Campos Neto et al. (2010), was interpreted as the age of the metamorphic peak of the Carvalhos Klippe. For the Serra da Natureza klippe, (MOTTA; MORAES, 2017) obtained an age of matrix monazite of 604.5 ±6.1 Ma, which was also interpreted as dating the metamorphic peak. Reno et al. (2009), Reno et al. (2012) presented an older interval for the Três Pontas-Varginha Nappe rocks, indicating peak conditions at ca. 670–650 Ma (based on monazite from the matrix and inclusions in garnet). Younger ages of ca. 640–588 Ma, obtained from monazite crystals from the matrix, are interpreted by Reno et al. (2009), Reno et al. (2012) to be related to the retrograde path in the Três Pontas-Varginha Nappe, Carmo da Cachoeira Nappe and Carvalhos Klippe.

Lenses of high-pressure metabasic rocks in the Andrelândia Nappe System contain inherited zircon grains with rims dated at ca. 630 and 605 Ma the first of which was interpreted as dating the pressure peak of eclogite facies metamorphism (COELHO et al., 2017; FRUGIS; NETO; LIMA, 2018; TEDESCHI et al., 2017).

3.3 Methods

A multi-approach method was applied to assess the *P-T-t* path of high-pressure granulites of the Passos Nappe. Thermodynamic modelling using constraints from mineral compositions and zoning were combined with Ti-in-quartz and Zr-in-rutile thermometry to constrain a detailed *P-T-t* path. In situ dating of monazite and rutile yields information about the timing of two stages within this metamorphic evolution.

3.3.1 Optical and electron microscopy

Four representative samples (SSPDH10, SSPDH12, MG161 and SSPDH2, see location in Figure 3.1d) were prepared as standard polished thin sections and were studied with an optical polarizing microscope and using a JEOL JSM 6010LA scanning electron microscope (SEM) at the Department of Geology of São Paulo State University, Brazil (Unesp). A column accelerating voltage of 15 kV was used to obtain backscattered electron (BSE) images that were used to guide further analyses. The sample current used to obtain the images cannot be specified, since the equipment is not equipped with a probe current detector. The mineral proportions were estimated based on the optical polarizing microscope visual counts, field observations and the proportions in the mineral distribution maps.

Table 3.1 – Electron microprobe conditions applied for the rutile trace elements analysis.

20 kV / 80 nA	Si	Al	Cr	Ta	Fe	Ti	Nb	Zr
Crystal	TAP	TAP	PETJ	LIFL	LIFL	PETJ	PETJ	PETJ
Line	Kα	Kα	Kα	Lα	Kα	Kβ	Lα	Lα
Peak sec[a]	300	300	150	150	150	30	300	300
Bkg sec[b]	150	150	50	50	50	15	150	150
DL[c]	25	20	50	85	40	55	40	45

[a] Count time on peak position in seconds. [b] Count time on background position in seconds.
[c] 2 σ detection limit, based on repeated measurement of variation on background, values in μg/g

3.3.2 Electron Probe Micro Analyzer

Quantitative analyses of mineral compositions, compositional maps, and trace element analyses of rutile and Ti-in-quartz, were carried out using a JEOL JXA-8230 Electron Microprobe Analyzer (EPMA) equipped with five wavelength dispersive spectrometry (WDS) detectors at the Department of Geology of Unesp. WDS quantitative analyses of garnet, plagioclase, K-feldspar and biotite were conducted using a of 5 μm diameter electron beam, with a 15 kV voltage of and a 20 nA beam current. The counting times were set to 20 s for major element analysis and 30 s for minor element analysis, equally distributed on peak and background positions. Well-characterized natural and synthetic standards were used. Compositional mapping was carried out to: i) produce mineral distribution maps, ii) to identify compositional variation within these minerals, and iii) to calculate local bulk compositions used for the metamorphic modelling. Mapping was conducted at 15 kV and 100 nA, with step sizes ranging from 10 μm to 20 μm and dwell times from 60 ms to 200 ms, depending on the size of the map. The data were processed using the XMapTools 2.5.1 software (LANARI et al., 2014; LANARI; DUESTERHOEFT, 2019) to produce quantitative maps and extract local bulk compositions. Quantitative point analyses within the map area were used to calibrate X-ray maps.

Trace elements analyses in rutile followed the method outlined by Luvizotto et al. (2009) and were carried out under a focused beam, using an accelerating voltage of 20 kV and a current of 80 nA. Long counting times were used to reduce relative uncertainties and to improve detection limits (Table 3.1). The following elements were analyzed: Si, Al, Cr, Fe, Ta, Nb, Zr. Concentrations of Si were used as quality control to detect and avoid zircon inclusions and contamination from secondary fluorescence of neighboring silicates (all analyses with Si content above 300 μg/g were discarded). The R10 and Sy rutile reference materials (LUVIZOTTO et al., 2009) were used as secondary standards to ensure the quality and reproducibility of analyses. Rutile thermometry calculations followed the calibration of (TOMKINS; POWELL; ELLIS, 2007).

Analyses of Ti in quartz were performed using a 15 keV voltage and a beam current of 200 nA, using the Sy rutile (LUVIZOTTO et al., 2009) as an analytical standard for Ti. Peak (400 s) and background (200 s) Ti measurements were carried out simultaneously on

three WDS (PET crystals) spectrometers to improve counting statistics. With this setup, the minimum detection limit for Ti was 14 μg/g, considering background measurements and ZAF matrix correction factors. Ti-in-quartz temperatures were calculated following the calibration of Thomas et al. (2010).

Cathodoluminescence (CL) maps were produced to image the distribution of Ti in quartz and to investigate its textural relationships with other minerals. CL maps were acquired simultaneously with the compositional mapping, using a Hamamatsu H8259 CL system coupled to the JEOL JXA 8230 EPMA. An Astronomik L-RGB Type 2C blue filter (380 nm to 520 nm) was used for evaluating the Ti content in quartz (MÜLLER; LENNOX; TRZEBSKI, 2002; LEEMAN et al., 2012; KENDRICK; INDARES, 2018a; KIDDER; AVOUAC; CHAN, 2013). The XMapTools 2.5.1 software (LANARI et al., 2014; LANARI; DUESTERHOEFT, 2019) was used to generate quantitative maps (Ti content in quartz based on the blue CL emission), with calibration using WDS quantitative point analyses within the map area.

EPMA monazite dating (U-Th-Pb_T) followed the recommendations of Williams et al. (2006). Full thin section X-ray mapping of Ce and P was done using a voltage of 15 kV, a beam current of 200 nA, dwell times of 20–50 ms, an electron beam size of 30 μm and a step size of 30 μm. These maps were used to identify monazite crystals and examine their textural relationships with other phases. For the selected monazite crystals, high-resolution compositional X-ray maps were collected for Y, Al, Th, U, Pb, Si, Ca, Fe, La, and Ce, with conditions of 15 kV, 100 nA, 100 ms dwell time and 10 μm electron beam size and step. In order to compare concentration levels and zoning characteristics from crystal to crystal, X-ray maps collected for all crystals from the same sample were processed using the same color scale and same minimum and maximum intensity values. The maps were then used to target distinctive domains for spot analyses and age calculations. Unlike the procedure discussed by Williams et al. (2006), background measurements were performed for all analyses. Point analyses followed the method outlined by Vlach (2010), and the analytical conditions are presented in Table 3.2. The specimen current varied from 80 to 100 nA and was constantly monitored to evaluate and avoid beam damage. Every 10 to 20 analyses were bracketed by three analyses of Moacir monazite secondary standard (GONÇALVES et al., 2016). Spectral interference corrections were performed offline and considered matrix correction factors. Interference corrections and age calculations were performed using the Age_Cor program (VLACH, 2010). Uncertainties were calculated based on the relative standard error of each analysis, using the weighted average method in the Isoplot software (LUDWIG, 2003). Systematic uncertainties were not propagated.

Table 3.2 – Electron microprobe conditions used for the monazite trace element analysis.

Element	X-ray line	Crystal	CH	Acc. V	Peak Pos.	BG_L Pos.	BG_U Pos.	Peak (s)	BG (s)	High Volt.	Base Line	Window	Standard	Conc. Std. (%)	Curr. (A)	D.L. (ppm)
Y	La	TAP	1	15	70.048	1.25	1	100	50	1635	3.5	3.2 (V)	Y_2O_3 P&H	11.80	1.00E-07	110
Si	Ka	TAP	2	15	77.314	1.65	1.05	40	20	1630	2.2	4.1 (V)	Wollastonite P&H	50.96	2.00E-08	60
Al	Ka	TAP	2	15	90.577	2.47	1.72	40	20	1630	2.2	4.1 (V)	Al_2O_3 P&H	99.99	2.00E-08	50
Th	Ma	PETJ	3	15	132.571	2	1.95	140	70	1670	3.7	3.9 (V)	Th Glass MAC	5.90	1.00E-07	160
Ca	Ka	LIF	3	15	233.493	0.7	1.1	10	5	1628	0.9	3.0 (V)	Apatita	54.02	2.00E-08	240
La	La	LIF	3	15	185.373	1.45	1.65	10	5	1628	2.4	2.0 (V)	La_2O_3 P&H	11.50	2.00E-08	1200
Ce	La	LIF	3	15	178.132	1.45	1.65	10	5	1628	2.3	2.0 (V)	CeO_2 P&H	11.90	2.00E-08	1200
Pr	Lb	LIF	3	15	157.127	0.75	0.85	10	5	1628	2.7	2.0 (V)	Pr_6O_{11} P&H	12.20	2.00E-08	1600
Nd	Lb	LIF	3	15	150.713	0.9	1	10	5	1628	2.3	2.0 (V)	Nd_2O_2 P&H	11.80	2.00E-08	1900
Sm	Lb	LIF	3	15	139.059	0.55	0.55	10	5	1628	3.2	1.8 (V)	Sm_2O_3 P&H	11.20	2.00E-08	1800
Fe	Ka	LIF	3	15	134.693	0.75	0.65	10	5	1628	2.4	3.1 (V)	Ilmenite PMCS	35.03	2.00E-08	400
Gd	Lb	LIF	3	15	128.512	1	1	10	5	1628	3.5	2.1 (V)	Gd_2O_3 P&H	12.10	2.00E-08	1800
Er	La	LIF	3	15	124.195	0.75	0	10	5	1628	3.3	2.3 (V)	Er_2O_3 P&H	11.90	2.00E-08	1130
Tb	Lb	LIF	3	15	123.669	0.45	0	10	5	1628	3.7	2.0 (V)	Tb_4O_7 P&H	11.90	2.00E-08	2200
Dy	Lb	LIF	3	15	119.035	0.65	0.55	10	5	1628	3.7	2.3 (V)	Dy_2O_3 P&H	12.00	2.00E-08	1960
Yb	La	LIF	3	15	116.35	1.5	1.45	10	5	1628	3	2.0 (V)	Yb_2O_3 P&H	12.00	2.00E-08	1430
U	Mb	PETL	4	15	118.932	3.98	3.98	300	150	1670	3	2.7 (V)	UO_2 MAC	99.80	1.00E-07	65
S	Ka	PETL	4	15	172.02	-	2	10	5	1670	3	2.5 (V)	PbS P&H	33.46	2.00E-07	160
P	Ka	PETH	5	15	197.105	2.1	2.65	10	5	1686	1.7	3.0 (V)	Apatita	40.78	2.00E-08	150
Pb	Ma	PETH	5	15	169.251	3.65	4.2	300	150	1686	1.8	3.0 (V)	PbS P&H	93.29	2.00E-07	40

Acc. V: Acceleration voltage
Peak Pos.: Peak position in mm
BG_L Pos.: Lower background position in mm from the peak
BG_U Pos.: Upper background position in mm from the peak
Peak (s): counting time on peak position in s
BG (s): Counting time on each background (upper and lower) position in s
Conc. Stds (%): Concentration of the element in the standard
Curr. A: Current of standard analyses in A
D.L.: Minimum detection limit (3 sigma) for the unknowns

3.3.2.1 LA-ICP-MS analyses

U-Pb rutile dating and trace element analyses in rutile and quartz used the Laser Ablation Inductively Coupled Plasma Mass Spectrometry (LA-ICP-MS) at the Microgeochemistry Laboratory of the Department of Earth Sciences, University of Gothenburg, Sweden.

Rutile analyses were conducted using a New Wave NWR213 laser ablation system that was coupled to an Agilent 7500a quadrupole ICP-MS. Trace elements were analyzed with a 10 μm laser beam, surface energy of 4 J/cm2 and a repetition rate of 10 Hz. The following isotopes were analyzed: ^{27}Al, ^{51}V, ^{53}Cr, ^{56}Fe, ^{90}Zr, ^{93}Nb, ^{95}Mo, ^{128}Sn, ^{121}Sb, ^{178}Hf, ^{181}Ta, ^{184}W, ^{208}Pb, ^{232}Th and ^{238}U. For U-Pb rutile dating, analyses of trace elements in several crystals were initially performed, with high-U rutile crystals then selected for further analysis, following the recommendations of Zack et al. (2011). Isotopes were measured in time-resolved mode, with dwell times for each isotope for each mass scan of 10 ms for ^{90}Zr, ^{232}Th and ^{238}U, 30 ms for ^{206}Pb, and 50 ms for ^{207}Pb and ^{208}Pb. These analyses used a 50 μm diameter laser beam, at a laser energy of 5.6 J/cm^2 and a repetition rate of 10 Hz.

LA-ICP-MS analyses in quartz used a New Wave NWR213 laser ablation system coupled to an Agilent 8800 triple quadrupole. These analyses used a 10 μm diameter laser beam, with an energy of 6.7 J/cm2 and repetition rate of 4 Hz. He was flushed through the ablation cup at the rate of 1 ml/min. The following isotopes were analyzed: ^{2}Li, ^{27}Al, ^{29}Si, ^{48}Ti, ^{49}Ti, ^{57}Fe and ^{72}Ge. ^{49}Ti was used for calculations in order to avoid isobaric interference from ^{48}Ca, which is present in most well-characterized reference glasses containing ^{48}Ti.

In all LA-ICP-MS analyses, the signals were recorded over 60 s for each spot. The first 20 s were used to measure the background, the next 30 s for acquiring the analysis

signal and the last 10 s for system wash out. A He-Ar mixture was used as the carrier gas. The He was mixed with an Ar carrier and N, in order to enhance sensitivity. Each block of 10 unknown measurements was separated by 2–3 analyses of reference materials, using the R10 standard for rutile (LUVIZOTTO et al., 2009) and quartz reference materials NIST SRM 610 and from Audetat (AUDÉTAT et al., 2015).

3.3.3 Whole rock X-Ray fluorescence

Bulk-rock compositions were obtained by X-ray fluorescence (XRF) at the Department of Geology of Unesp. Representative sample powders were mixed with lithium tetraborate to obtain fused disks that were analyzed with a Philips PW 2400. Loss on ignition (LOI) was determined by the conventional gravimetric method. XRF results were used for bulk-rock compositions comparison between the samples.

3.3.4 Phase equilibria modelling

Phase diagrams were calculated in the Na_2O–CaO–K_2O–FeO–MgO–Al_2O_3–SiO_2 –H_2O–TiO_2–O_2 (NCKFMASHTO) chemical system using version 3.40 of THERMOCALC (POWELL; HOLLAND; WORLEY, 1998; POWELL; HOLLAND, 1988), the ds6.2 internally consistent data set of (HOLLAND; POWELL, 2011), updated in February 2012, and the activity-composition models of White et al. (2014). The whole-rock compositions used in the phase equilibria modelling were based on the quantitative maps. A low extra oxygen content of 0.01 mol% O_2 was used in all pseudosections, since studied samples are ilmenite- and rutile-bearing and hematite-free. Contours of mineral compositions and isomodes were generated using TCInvestigator 1.0 (PEARCE; WHITE; GAZLEY, 2015).

3.4 Results

3.4.1 Petrography

The investigated unit is a para-derived rutile-kyanite-garnet-K-feldspar granulite with a stromatic structure in which banding is parallel to the main foliation (Figure 2). The rock is coarse-grained and the studied samples (SSPDH10, SSPDH12, MG161 and SSPDH2) show only slight differences in modal proportions and in textural and structural characteristics (Figure 2).

Samples SSPDH10, SSPDH12 and MG161 contain porphyroblasts of garnet (up to 12 mm; ∼30 vol%) and kyanite (up to 10 mm, ∼5 vol%) (Figure 3.2 a-f). The melanosome and leucosomes contain quartz (∼35 vol%), K-feldspar (∼20 vol%), and plagioclase (less than 5 vol%), the distribution of these phases defining a foliation. Biotite only occurs in the melanosome (trace to less than 5 vol%). Minor phases include apatite, rutile, zircon,

ilmenite and monazite. Sample SSPDH2 also contains large, elongate garnet (up to 30 mm, ∼15 vol%) and kyanite (up to 50 mm, ∼20 vol%) porphyroblasts. Its melanosome and leucosomes consist of quartz (∼30 vol%) and K-feldspar (∼30 vol%). Biotite (∼5%) occurs in the matrix. Rutile, ilmenite, monazite and zircon are minor phases. Plagioclase is absent in sample SSPDH2, which also has a better defined foliation than the other samples. The peak mineral assemblage of all samples is interpreted to be quartz + garnet + kyanite + K-feldspar + rutile + melt ± plagioclase.

3.4.1.1 Garnet

In samples SSPDH10, SSPDH12, and MG161, garnet is sub-rounded (Figure 3.2a, b, c and d), poikiloblastic and usually shows resorbed rims. The abundance of inclusions varies from sample to sample. In samples SSPDH10, MG161 and SSPDH12, inclusions of rutile, quartz, plagioclase, apatite, monazite, kyanite and zircon are predominantly in garnet cores and inner rims (Figure 3.2b and c). Fewer inclusions of the same minerals occur in outer rims, where polymineralic inclusions of plagioclase, quartz and K-feldspar are also present (Figure 3.2f, g, h and i). Garnet crystals in sample SSPDH2 are usually elongated and contain inclusions of lobate quartz (Figure 3.2e), K-feldspar, rutile and kyanite. In all samples, garnet is in sharp contact with the kyanite porphyroblasts and biotite is frequently found in the garnet core. The presence of inclusions in garnet of rutile, quartz, K-feldspar (only in garnet rims), kyanite and apatite suggest their coexistence along the prograde path, prior to or during garnet growth.

3.4.1.2 Kyanite

Kyanite occurs mainly in the melanosome and rarely as small inclusions in garnet. In all samples, based on textural evidence, it is possible to distinguish two types of kyanite. The first type consists of deformed crystals with small, rare inclusions of quartz, plagioclase,

Figure 3.2 *(following page)* – Images of the studied samples. a) Photograph of sample SSPDH10. b) Garnet porphyroblast with quartz and rutile inclusions. Garnet is zoned and inclusions are concentrated in the core and inner rim. Garnet is surrounded by biotite (sample SSPDH10, plane-polarized light). c) Elongated garnet porphyroblast with quartz, rutile and K-feldspar inclusions (sample SSPDH2, scanned image). d) Garnet porphyroblast with rutile and quartz inclusions and biotite in the garnet rim (sample MG161, plane-polarized light). e) Garnet porphyroblast with zoned quartz and rutile inclusions, surrounded by biotite (sample SSPDH12, plane-polarized light). f) Polymineralic inclusion in garnet, composed of plagioclase, quartz, monazite and biotite (sample SSPDH10, back-scattered electron image). g) Polymineralic inclusion in garnet, composed of quartz and K-feldspar (sample SSPDH10, back-scattered electron image). h) Polymineralic inclusion in garnet, composed of plagioclase, quartz and K-feldspar (sample MG161, back-scattered electron image). i) Polymineralic inclusion in garnet, composed of quartz and plagioclase (sample SSPDH12, back-scattered electron image). Mineral abbreviations after Kretz (1983).

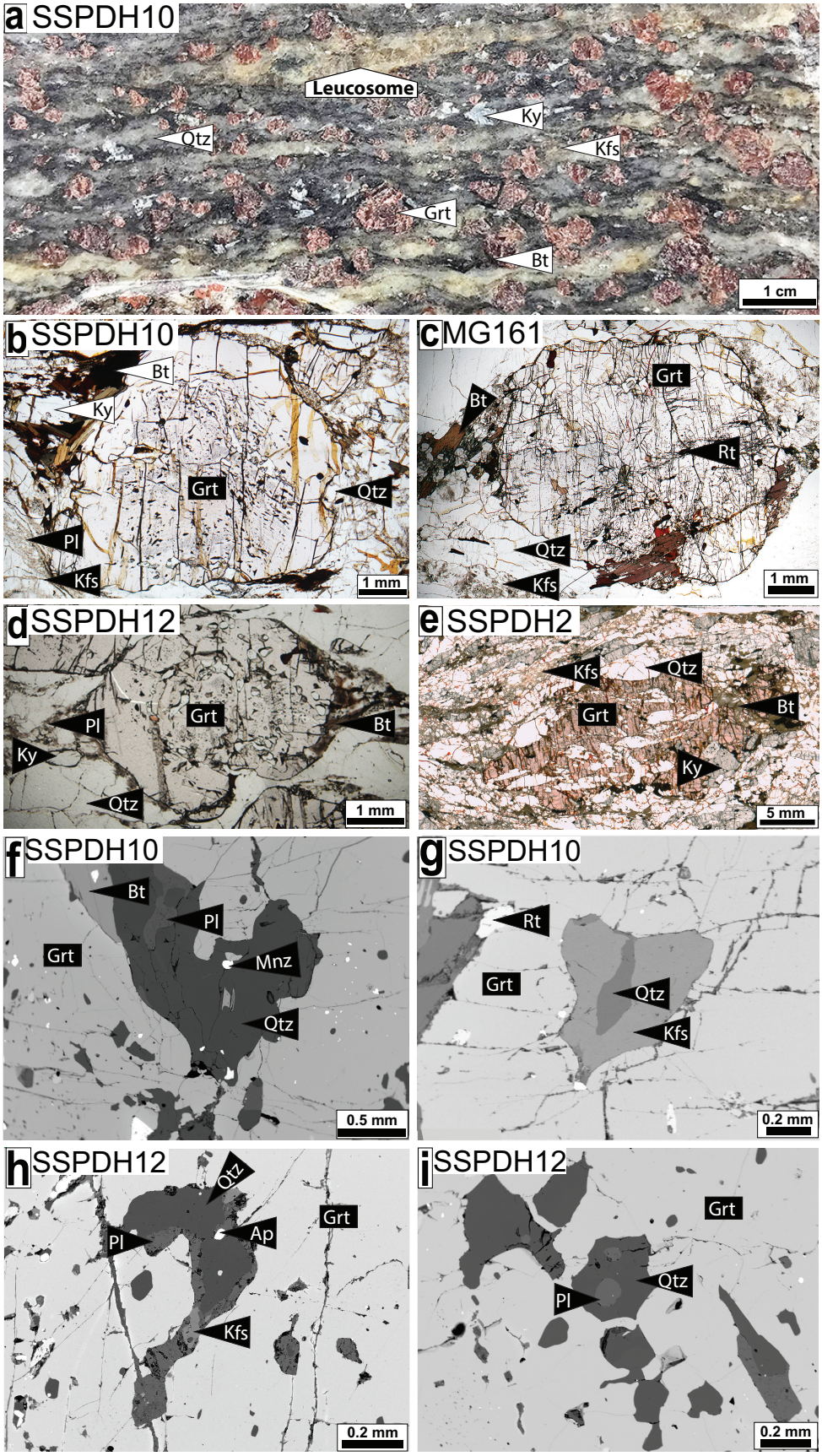
a SSPDH10
Leucosome
Ky
Qtz
Kfs
Grt
Bt
1 cm
b SSPDH10
Bt
Ky
Grt
Qtz
Pl
Kfs
1 mm
c MG161
Grt
Bt
Rt
Qtz
Kfs
1 mm
d SSPDH12
Pl
Grt
Bt
Ky
Qtz
1 mm
e SSPDH2
Kfs
Qtz
Grt
Bt
Ky
5 mm
f SSPDH10
Bt
Pl
Grt
Mnz
Qtz
0.5 mm
g SSPDH10
Rt
Grt
Qtz
Kfs
0.2 mm
h SSPDH12
Qtz
Grt
Pl
Ap
Kfs
0.2 mm
i SSPDH12
Grt
Qtz
Pl
0.2 mm

monazite and rutile (Figure 3.3a, c and d). The second type of kyanite lacks undulose extinction and contains more and larger inclusions (Figure 3.3b, c and d). These inclusions of rutile, quartz, plagioclase, K-feldspar, monazite, zircon and apatite are rounded in samples SSPDH10, SSPDH12 and MG161 and lobate in sample SSPDH2. Apatite only occurs as inclusion in the second type of kyanite. Based on these textural variations, it is interpreted that the more deformed type one kyanite crystallized earlier, at the prograde metamorphism in sample SSPDH2 and in the peak metamorphism in the sample SSPDH10, while the second type of kyanite is interpreted to have crystallized later, at the retrograde metamorphism in both samples.

3.4.1.3 Host Gneiss

In all samples, the quartz, K-feldspar and plagioclase (the latter absent in sample SSPDH2) in the melanosome are highly strained. These minerals present a bimodal size distribution, with aggregates of small, recrystallized grains of approximately uniform size (<500 μm) filling the spaces between larger grains that reach several millimeters (Figure 3.3e, f, g and h). Quartz, K-feldspar and plagioclase display undulose extinction. Textural features of quartz and plagioclase indicate dynamic recrystallization by grain boundary migration and subgrain rotation (Figure 3.3). K-feldspar is coarser grained than plagioclase. As the rocks are highly strained, textures recording crystallization of any trapped anatectic melt in the matrix are not preserved. However the lobate polymineralic inclusions (Figure 3.2f, g, h and i) of quartz, plagioclase and K-feldspar in garnet are interpreted as former melt inclusions and are locally found filling fractures in garnet (Figure 3.2h). It is interpreted that most of the K-feldspar, particularly the large crystals in the melanosome, the plagioclase and the garnet (Figure 3.3f and h) crystallized near the metamorphic peak, with minor additional growth of plagioclase and K-feldspar during melt crystallization on the retrograde path.

Figure 3.3 *(following page)* – Photomicrographs of the studied samples. a) Kyanite crystals with undulose extinction (sample SSPDH10, crossed-polarized light). b) Kyanite crystals with quartz and rutile inclusions (sample SSPDH10, crossed-polarized light). c and d) Kyanite crystals with undulose extinction (top of the image) and kyanite crystal with quartz, rutile and biotite inclusions (bottom of the image) (sample SSPDH2, plane-polarized light in c and crossed-polarized light with accessory gypsum plate in d). e) Melanosome composed of quartz and K-feldspar (sample SSPDH2, plane-polarized light). f) Melanosome composed of a large K-feldspar crystal and recrystallized quartz and plagioclase (sample SSPDH10, crossed-polarized light). g) Melanosome composed of K-feldspar, quartz and plagioclase (sample SSPDH10, crossed-polarized light). Quartz with K-feldspar and plagioclase is interpreted to have crystallized from a melt. h) Melanosome composed of quartz, plagioclase, K-feldspar and biotite (sample SSPDH12, plane-polarized light). Abbreviations after Kretz (1983).

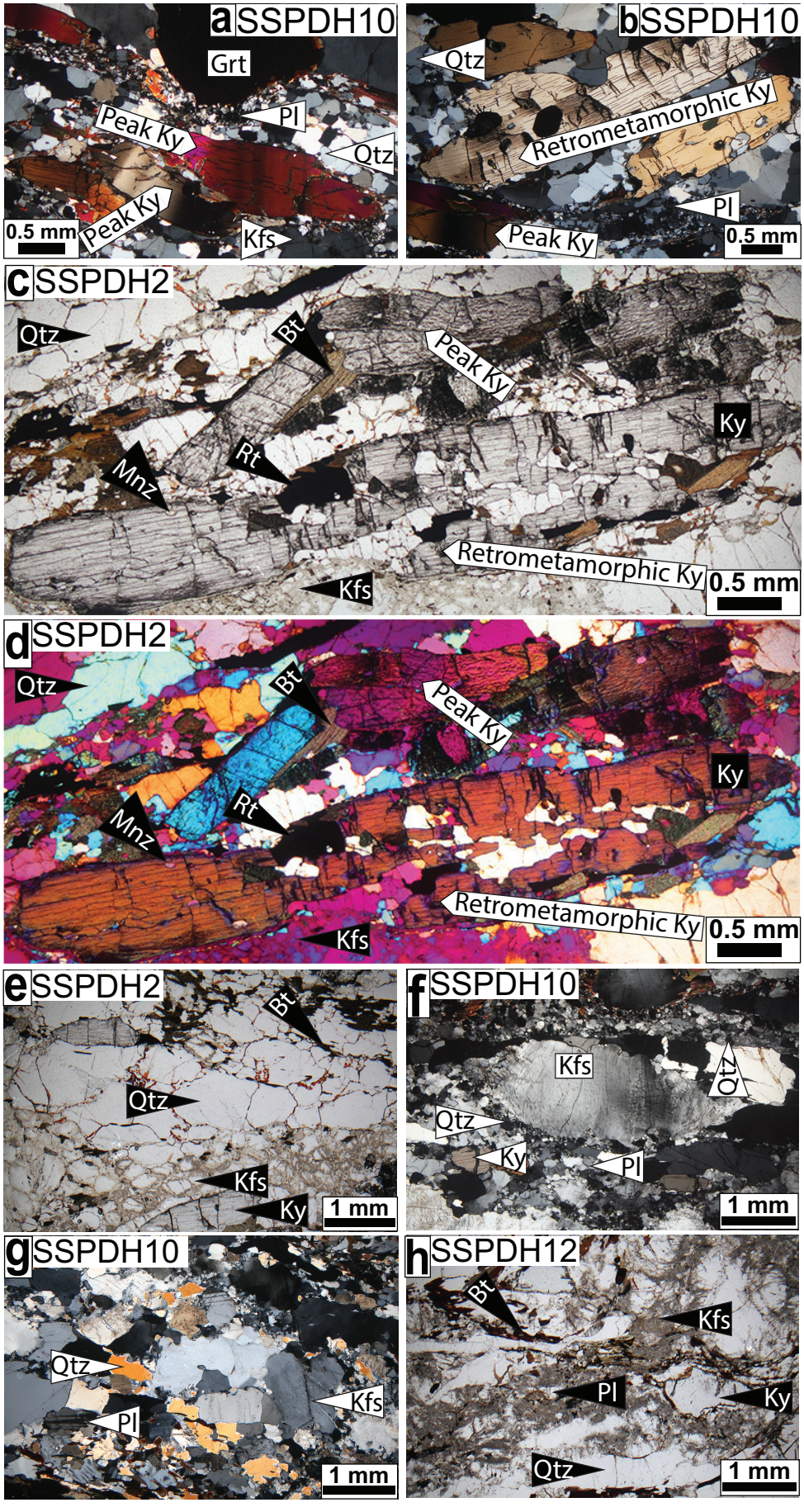
a SSPDH10
Grt
Peak Ky
Pl
Qtz
Peak Ky
Kfs
0.5 mm
b SSPDH10
Qtz
Retrometamorphic Ky
Pl
Peak Ky
0.5 mm
c SSPDH2
Qtz
Bt
Peak Ky
Ky
Rt
Mnz
Retrometamorphic Ky
Kfs
0.5 mm
d SSPDH2
Qtz
Bt
Peak Ky
Ky
Rt
Mnz
Retrometamorphic Ky
Kfs
0.5 mm
e SSPDH2
Bt
Qtz
Kfs
Ky
1 mm
f SSPDH10
Kfs
Qtz
Qtz
Ky
Pl
1 mm
g SSPDH10
Qtz
Kfs
Pl
1 mm
h SSPDH12
Bt
Kfs
Pl
Ky
Qtz
1 mm

3.4.1.4 Leucosome

In the field, millimeter size layers of quartz and feldspar, that occur parallel to the rock foliation, serve as clear evidence of melt (Figure 3.2a). However, textures related to leucosome crystallization were obliterated by later deformation and dynamic recrystallization, and are not preserved in thin section scale. The leucosome (∼10 vol%) is composed of quartz, K-feldspar and plagioclase. These are finer grained than in the matrix outside the leucosome. Clusters of quartz, plagioclase and K-feldspar also occur bordering the garnet and kyanite porphyroblasts. Quartz often occurs in K-feldspar and plagioclase aggregates, again indicative of its formation during melt crystallization. The garnet lobate polymineralic inclusions (Figure 3.2f, g, h and i) described above are interpreted as leucosome-forming melts trapped within the garnet.

3.4.1.5 Biotite and minor phases

Biotite crystals are anhedral and occur bordering garnet, mostly in strain shadows, and kyanite. Biotite also fills fractures in these minerals (Figure 3.2a, b, c, d and e) and is interpreted to be a retrograde phase. Rutile occurs in the melanosome or leucosome domain and as inclusions in garnet and kyanite in all studied samples. Ilmenite replaces and occurs as fine lamellae in rutile. Zircon crystals are euhedral to subhedral and occur in the mineral matrix, in the leucosome, and as inclusions in garnet and kyanite crystals. In all samples, monazite is found in the matrix and leucosome, and as inclusions in garnet and more rarely kyanite. Apatite occurs as small crystals in the matrix, in the leucosome, and as inclusions in garnet rims in samples SSPDH10, SSPDH12 and MG161.

3.4.2 Mineral Chemistry

3.4.2.1 Garnet

Garnet crystals display a complex chemical zoning (Figure 3.4b-e, j-m, Table 3.S1 and Figure 3.S1). The main grain pictured in Figure 4b-e, from sample SSPDH10, has a roughly centered core region. A rounded core is richer in spessartine (X_{Sps} core: 0.02-0.025, rim: 0.01-0.02) contrasts in shape and position with the core regions observed for almandine, pyrope and grossular (Figure 3.4b-e). This core is richer in grossular (X_{Grs} core: 0.11-0.16, rim: 0.05-0.10), while mantles and rims have higher almandine (X_{Alm} core: 0.57-0.59, rim: 0.595-0.63) and pyrope contents (X_{Prp} core: 0.22-0.28, rim: 0.28-0.34). Locally, an outer rim with the highest almandine proportion (0.63), intermediate pyrope (0.26) and higher spessartine proportion (0.025) is observed (Figure 3.4b-e). The high grossular inner core is rutile-free. Garnet X_{Fe} ranges from 0.67 in the core to 0.64 in the rim.

Garnet crystals in samples SSPDH12 (Figure S1) and MG161 (Table S1) have

similar compositional and zoning patterns to those in SSPDH10, but with off-centered core regions. These cores have relatively high grossular content (0.04-0.09) and low almandine (0.64-0.70) and pyrope contents (0.27-0.35) (Figure S1 and Table S1). Locally, an outer rim has higher spessartine and pyrope contents and lower almandine content. The spessartine content varies from 0.01 to 0.02. The X_{Fe} ranges from 0.63 (rim) to 0.70 (core).

Garnet compositions in sample SSPDH2 are substantially different from the other studied samples, but the general zoning patterns are similar. This sample is more highly strained, with distinctly elongated garnet grains. A subrounded, off-centered core with low almandine and high pyrope and grossular contents is observed. This core region is not apparent in the spessartine map. An outer rim with higher almandine, grossular and spessartine contents and lower pyrope content occurs locally. The almandine content ranges from 0.70 (core) to 0.71 (rim/mantle) and 0.77 (outer rim), coexisting with pyrope contents of 0.21 (core), 0.23 (rim/mantle) and 0.18 (outer rim) and grossular contents of 0.065 (core), 0.033 (rim/mantle) and 0.05 (outer rim). The spessartine content ranges from 0.13 (core/mantle/rim) and 0.022 (outer rim). In sample SSPDH2 the X_{Fe} ranges from 0.83 in the core to 0.93 in the rim.

3.4.2.2 Plagioclase

In all plagioclase bearing samples (SSPDH10, SSPDH12 and MG161), plagioclase is sodic (Figure 3.4f and Table S1), with X_{an} of 0.23-0.33 and no systematic zoning was observed in samples SSPDH10, SSPDH12 and MG161. Plagioclase adjacent to garnet has the same composition as grains from the leucosome layer (Figure 3.4f).

3.4.2.3 Biotite

In all samples, X_{Fe} and Ti in biotite increase with distance to garnet (Figure 4 g-h and Table S1), as observed in previous studies (LASALLE; INDARES, 2014; SPEAR; PARRISH, 1996). The Ti content ranges from 0.19 atoms per formula unit (a.p.f.u.) to 0.26 a.p.f.u. and the X_{Fe} from 0.37 to 0.58 in samples SSPDH10, SSPDH12 and MG161. In sample SSPDH2, the Ti content in biotite ranges from 0.15 to 0.25 a.p.f.u. and the X_{Fe} from 0.40 to 0.56 (Figure 3.4n-o).

3.4.3 Rutile thermometry

Rutile occurs in all studied samples, in the matrix and as inclusions in garnet and kyanite (Figure 3.5). We present the full rutile trace element dataset in Table 3.S2, Zr concentrations in Figure 3.6 and descriptive statistics of Zr contents in rutile in Table 3.3.

Figure 3.4 – Mineral compositional maps for samples SSPDH10 and SSPDH2. a) Mineral distribution map from sample SSPDH10. b-e) Almandine, pyrope, grossular and spessartine zoning in garnet, respectively (where X_{Alm}=Fe/(Fe+Ca+Mg+Mn), XPy=Mg/(Fe+Ca+Mg+Mn), X_{Grs}=Ca/(Fe+Ca+Mg+Mn) and X_{Sps}=Mn/(Fe+Ca+Mg+Mn)) for sample SSPDH10. f) Anorthite content of plagioclase for sample SSPDH2. g) Proportion of X_{Fe} in biotite (X_{Fe}=Fe/(Fe+ Mg)) from sample SSPDH10. h) Ti content in biotite from sample SSPDH10. i) Mineral distribution map for sample SSPDH2. j-m) Almandine, pyrope, grossular and spessartine zoning in garnet, respectively (where X_{Alm}=Fe/(Fe+Ca+Mg+Mn), X_{Prp}=Mg/(Fe+Ca+Mg+Mn), X_{Grs}=Ca/(Fe+Ca+Mg+Mn) and X_{Sps}=Mn/(Fe+Ca+Mg+Mn)) from sample SSPDH2. n) Proportion of X_{Fe} in biotite (X_{Fe}=Fe/(Fe+ Mg)) for sample SSPDH2. o) Ti content in biotite for Sample SSPDH2.

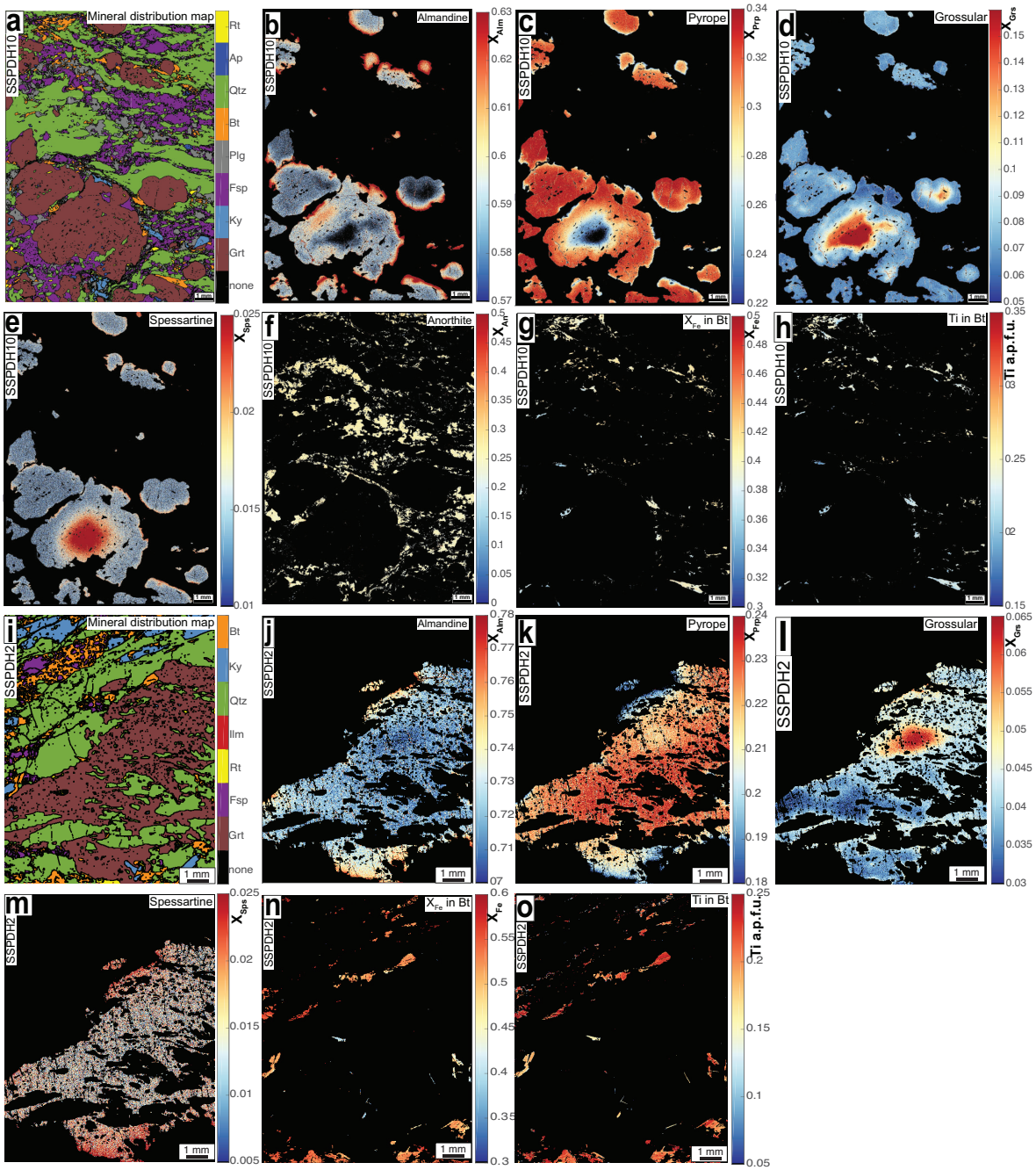

Sample SSPDH12 contains rutile included in garnet (Figure 3.5a) and in the matrix. These rutile crystals are subhedral, with an average size of 120 μm, reaching up to

Table 3.3 – Summary of Zr-in-rutile content in analyzed samples. Temperature calculated at 1.2 GPa. Min.: minimum, Max: maximum, Stdev 2s.: Standard derivation using 2 sigma, Incl: rutile crystals included in garnet or kyanite, Mtx: rutile crystals that occurs in the matrix.

		Number	Min	Max	1^{st} Quartile	Median	3^{rd} Quartile	Mean	Stdev 2s
SSPDH2C Incl	Zr (μg/g)	18	422	1503	620	1040	1308	975	723
	T (°C) @1.2 GPa	18	687	813	715	772	815	759	42
SSPDH2 Mtx	Zr (μg/g)	2	407	1510	683	959	1234	959	1560
	T (°C) @1.2 GPa	2	684	811	690	747	816	747	89
SSPDH12 Incl	Zr (μg/g)	8	912	1795	994	1316	1692	1340	748
	T (°C) @1.2 GPa	8	758	830	765	796	825	795	30
SSPDH12 Mtx	Zr (μg/g)	3	1511	1737	1561	1612	1674	1620	227
	T (°C) @1.2 GPa	3	811	827	815	818	824	818	8
MG161 Incl	Zr (μg/g)	12	767	1742	951	1046	1278	1141	626
	T (°C) @1.2 GPa	12	741	827	760	772	825	778	27
MG161 Mtx	Zr (μg/g)	9	856	1367	886	1010	1075	1027	333
	T (°C) @1.2 GPa	9	752	800	772	774	800	775	12
SSPDH10 Incl	Zr (μg/g)	30	585	1847	977	1096	1422	1171	648
	T (°C) @1.2 GPa	30	716	863	762	793	865	788	36
SSPDH10 Mtx	Zr (μg/g)	4	990	1282	1029	1091	1176	1114	257
	T (°C) @1.2 GPa	4	166	793	772	776	790	778	11

250 μm. Some rutile crystals contain ilmenite lamellae and rare rounded zircon inclusions. Zr contents in grains included in garnet vary between 912-1795 μg/g, with variation of 1511-1737 μg/g in grains in the matrix. Concentrations of Zr in rutile above the 90^{th} percentile ranges from 1793 to 1795 μg/g, corresponding to a calculated temperature of 830 °C (at 1.2 GPa).

Rutile crystals in sample MG161 are subhedral and occur either in the matrix or included in garnet and kyanite, averaging 200 μm in length and reaching up to 800 μm (Figure 3.5b and c). Ilmenite lamellae and zircon inclusions are present in almost half of the crystals. In rutile crystals included in garnet, Zr contents vary from 767 to 1742 μg/g. Those from the matrix contain 856 to 1367 μg/g Zr. Values above the 90^{th} percentile range from 1587 to 1742 μg/g, indicating temperatures of 816 to 827°C (at 1.2 GPa).

Sample SSPDH10 contains large rutile crystals as inclusions in garnet and in the matrix (Figure 3.5d). Rutile crystals are subhedral with an average of 200 μm length, occasionally reaching 500 μm. In this sample, tiny ilmenite lamellae occur in some crystals, and zircon inclusions in rutile are rare. Zr contents in rutile range from 585 to 1847 μg/g in grains included in garnet and from 990 to 1282 μg/g in those from the matrix (four LA-ICP-MS analyses). Zr contents above the 90^{th} percentile range from 1673 μg/g to 1847 μg/g, yielding temperatures of 822 to 837 °C (at 1.2 GPa).

Rutile crystals in sample SSPDH2 occur as inclusions in garnet and kyanite (Figure 3.5e, f and g) as well as in the matrix. The average size of rutile is around 200 μm, reaching up to 500 μm. The crystals are mainly anhedral, but some subhedral crystals are also present. Virtually all rutile crystals in sample SSPDH2 have ilmenite lamellae (Figure 5e, f and g), but zircon inclusions are rare. Zirconium contents in these rutile crystals show

Figure 3.5 – Back-scatter electron images of analyzed rutile crystals. Temperature calculations at 1.2 GPa. a) Rutile crystals Rt2.1 and Rt2.2 included in garnet from sample SSPDH12. b) Some of the analyzed rutile grains from sample MG161 included in the garnet. c) Some of the analyzed crystals from sample MG161. Rt2 and Rt5 are included in kyanite, and Rt1, Rt4 and Rt3 are in the matrix. d) Two rutile crystals (Rt1 and Rt2) analyzed from sample SSPDH10, R1 is included in the rim of garnet and the Rt2 is in the matrix. e) Analyzed rutile crystals included in garnet from sample SSPDH2. f) Rutile 2-3 included in kyanite and containing ilmenite lamellae, from sample SSPDH2. g) Rutile 9 included in garnet from sample SSPDH2. Note ilmenite in part of the rutile rim and faint ilmenite lamellae throughout.

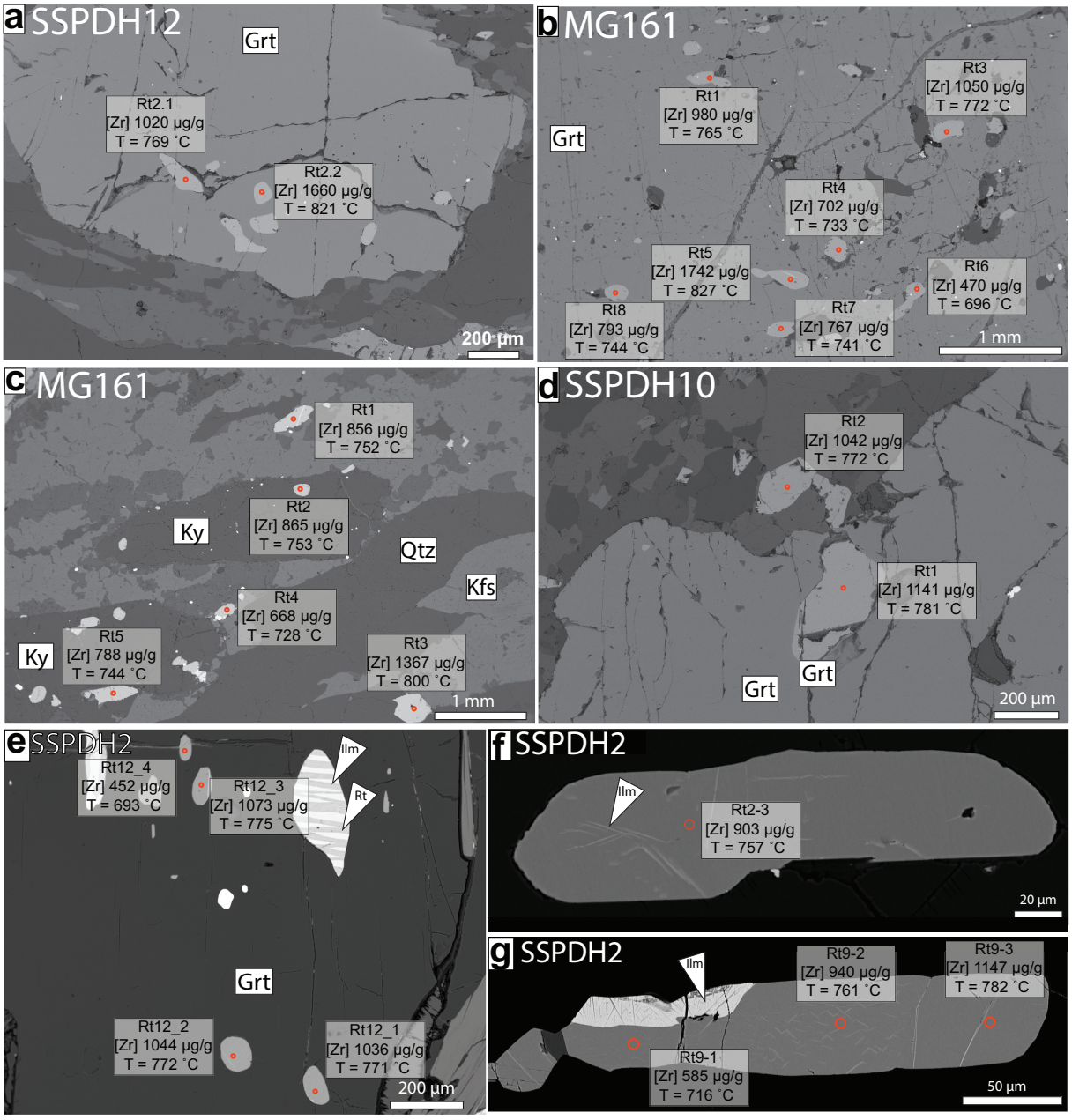

the largest variation of all analyzed samples: rutile in inclusions contains 423-1503 μg/g Zr and those in the matrix grains contain 408-1510 μg/g. Values above the 90th percentile range from 1489 to 1510 μg/g, corresponding to temperatures of 809 to 811 °C (at 1.2 GPa).

A summary of the Zr content of all analyzed rutile grains is presented in Figure

3.6c. In total, 9 values are above the 90^{th} percentile in all samples and the maximum Zr content is 1847 (sample SSPDH10). Considering only these values, the temperatures range from 821 to 834 °C (at 1.2 GPa).

Figure 3.6 – Box and whisker plots showing concentration (in μg/g) of Zr in rutile crystals (a), resultant Zr-in-rutile temperatures (at 1.2 Gpa) (b). Data from rutile included in garnet and kyanite crystals (Incl) are separated from matrix rutile (Mtx). Whiskers represent the 10th and 90^{th} percentile and boxes represent the second (bottom-25%) and third quartile (top-75%). For rutile grains with more than one spot, only one representative analysis is plotted. The minimum and maximum values are plotted as 'x', the small squares represent the median value, and the lines represent the mean value. The numbers at the top-right of each box represent the number of analyses for that sample. For samples in which less than three analyses are above detection limits, the values of each analysis are plotted as small squares. (d) Combined histogram of the Zr content of rutile in all analyses.

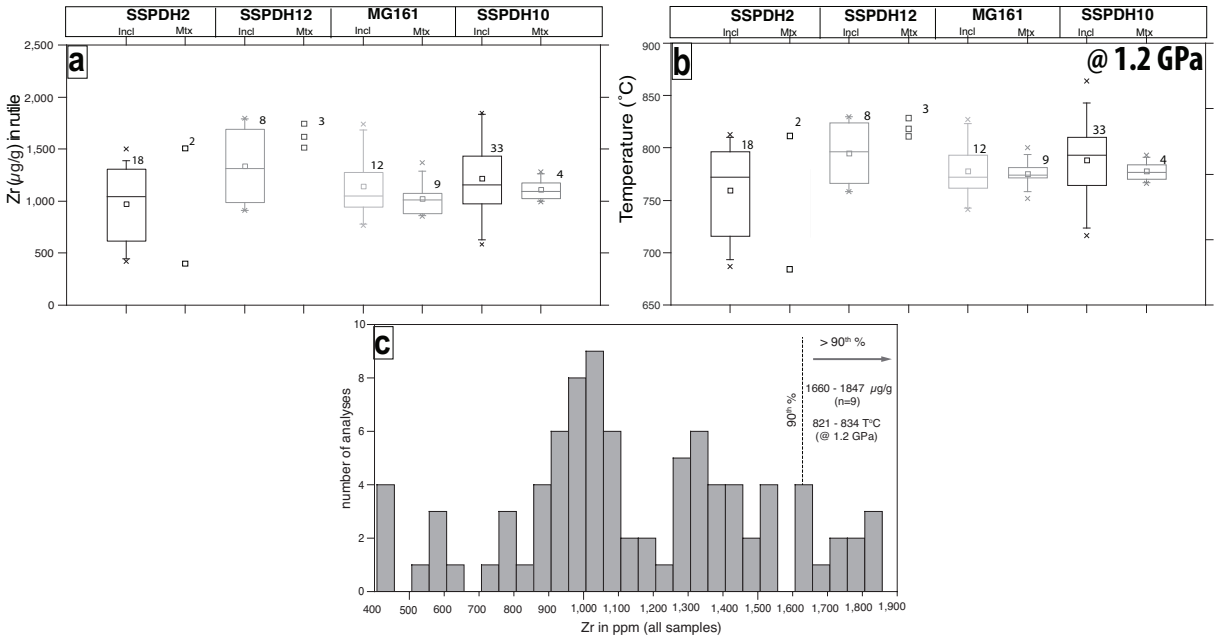

3.4.4 Quartz thermometry

The full dataset of Ti in quartz analyses is presented in Table 3.S3. A summary, with descriptive statistics, is presented in Table 3.4.

In samples SSPDH2 and SSPDH10, the Ti content of quartz ranges from 26 μg/g to 134 μg/g (n = 178 analyses and quantitative map) and 25 μg/g to 130 μg/g (n = 179 analyses and quantitative map), respectively (Figure 3.7, Figure 3.8 and Figure 3.9). CL maps of these two samples show that in most matrix crystals or crystals included in garnet the highest Ti values tend to occur in the core and decrease towards rims (Figure 3.8b and g and 3.9b), for both matrix and grains that are included in garnet. In some portions the high Ti domains in the quartz are rather patchy (Figure 3.9h). In samples MG161 and SSPDH12, Ti contents in quartz vary from 27 μg/g to 95 μg/g (n = 14) and from 23 μg/g to 99 μg/g (n = 21), respectively (Figure 3.7).

Figure 3.7 – Box and whisker plots showing concentration (in μg/g) of Ti in quartz (a) and the resultant Ti-in-quartz temperatures assuming 0.7 GPa (b), 1.2 GPa (c). Whiskers represent the 10th and 90th percentile. Boxes represent the second (bottom-25%) and third quartile (top-75%). The minimum and maximum values are plotted as 'x', the small squares represent the median value, and the lines represent the mean value. For rutile grains with more than one spot, only one representative analysis is plotted. The numbers at the top-right of each box represent the number of analyses for that sample.

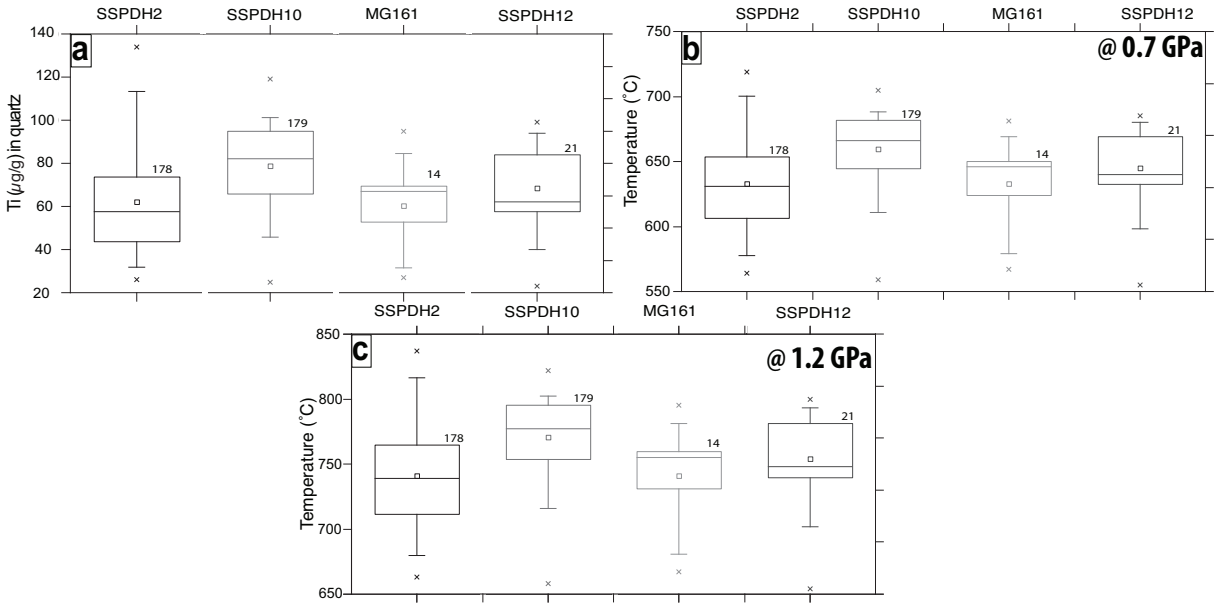

As a novel approach to further evaluate the Ti distribution, CL maps were converted into Ti content maps by referencing spot analyses in XMapTools and using the advanced calibration method Lanari e Duesterhoeft (2019). Figures 8 and 9 emphasize that the Ti content of quartz in the studied samples is extremely heterogeneous, with concentrations decreasing from core to rim. Few patches of Ti content higher than 115 μg/g are preserved.

Considering pressure conditions of 1.2 GPa the temperatures results range from ∼654 °C to 837 °C, while, at 0.7 GPa the results would range from ∼555 °C to 719 °C (Figure 8 and Figure 3.9 and Table 3.4).

Figure 3.8 *(following page)* – Quartz textures and compositions in sample SSPDH2. a) Mineral distribution map showing the occurrence of matrix quartz and quartz inclusions in garnet and kyanite. b) Ti in quartz map based on a CL map and quantitative point analyses. c) Apparent temperature map based on (b), assuming P = 0.7 GPa and $a\mathrm{TiO_2} = 1$. d) Apparent temperature map based on (b), assuming P = 1.2 GPa and $a\mathrm{TiO_2} = 1$. e) Mineral distribution map showing quartz in the matrix and included in kyanite. f) Ti in quartz map based on a CL map and quantitative point analyses. g) Temperature map assuming P = 0.7 GPa and $a\mathrm{TiO_2} = 1$. h) Temperature map assuming P = 1.2 GPa and $a\mathrm{TiO_2} = 1$.

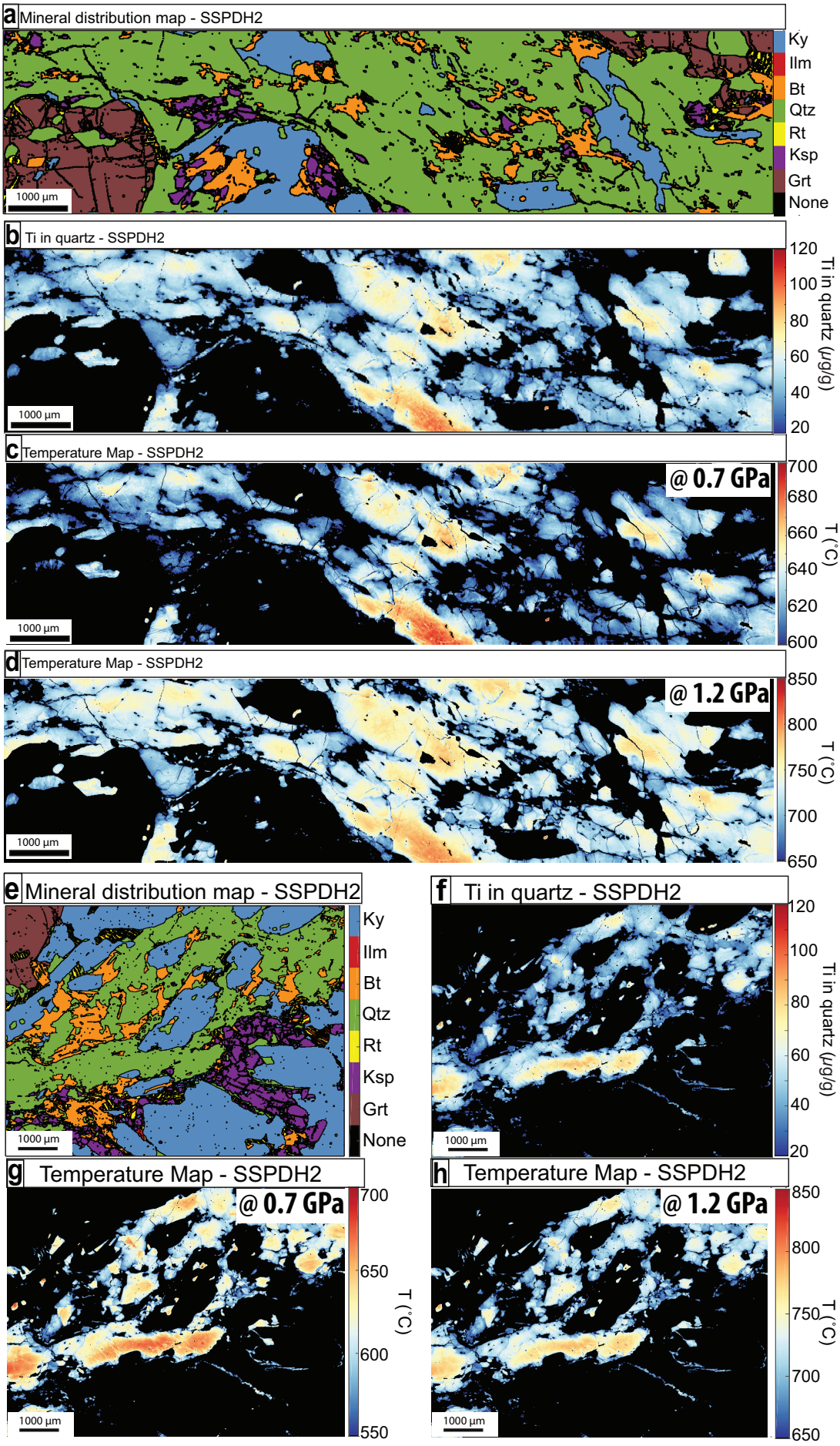
a Mineral distribution map - SSPDH2
Ky
Ilm
Bt
Qtz
Rt
Ksp
Grt
None
1000 µm
b Ti in quartz - SSPDH2
120
100
80
60
40
20
Ti in quartz (µg/g)
1000 µm
c Temperature Map - SSPDH2
@ 0.7 GPa
700
680
660
640
620
600
T (°C)
1000 µm
d Temperature Map - SSPDH2
@ 1.2 GPa
850
800
750
700
650
T (°C)
1000 µm
e Mineral distribution map - SSPDH2
Ky
Ilm
Bt
Qtz
Rt
Ksp
Grt
None
1000 µm
f Ti in quartz - SSPDH2
120
100
80
60
40
20
Ti in quartz (µg/g)
1000 µm
g Temperature Map - SSPDH2
@ 0.7 GPa
700
650
600
550
T (°C)
1000 µm
h Temperature Map - SSPDH2
@ 1.2 GPa
850
800
750
700
650
T (°C)
1000 µm

Figure 3.9 – Quartz textures and compositions in sample SSPDH10. a) Mineral distribution map showing the occurrence of quartz in the matrix and included in kyanite. b) Photomicrograph of mapped area, crossed-polarized light with accessory gypsum plate. c) Ti in quartz map based on a CL map and quantitative point analyses. d) Apparent temperature map based on (c), assuming P = 0.7 GPa and $a\mathrm{TiO_2} = 1$. e) Apparent temperature map based on (c), assuming P = 1.2 GPa and $a\mathrm{TiO_2} = 1$. f) Mineral distribution map showing quartz in the matrix. g) Photomicrograph of mapped area, crossed-polarized light with accessory gypsum plate. h) Ti in quartz map. i) Apparent temperature map based on (h), assuming P = 0.7 GPa and $a\mathrm{TiO_2} = 1$. j) Apparent temperature map based on (f), assuming P = 1.2 GPa and $a\mathrm{TiO_2} = 1$. Abbreviations according to Kretz (1983).

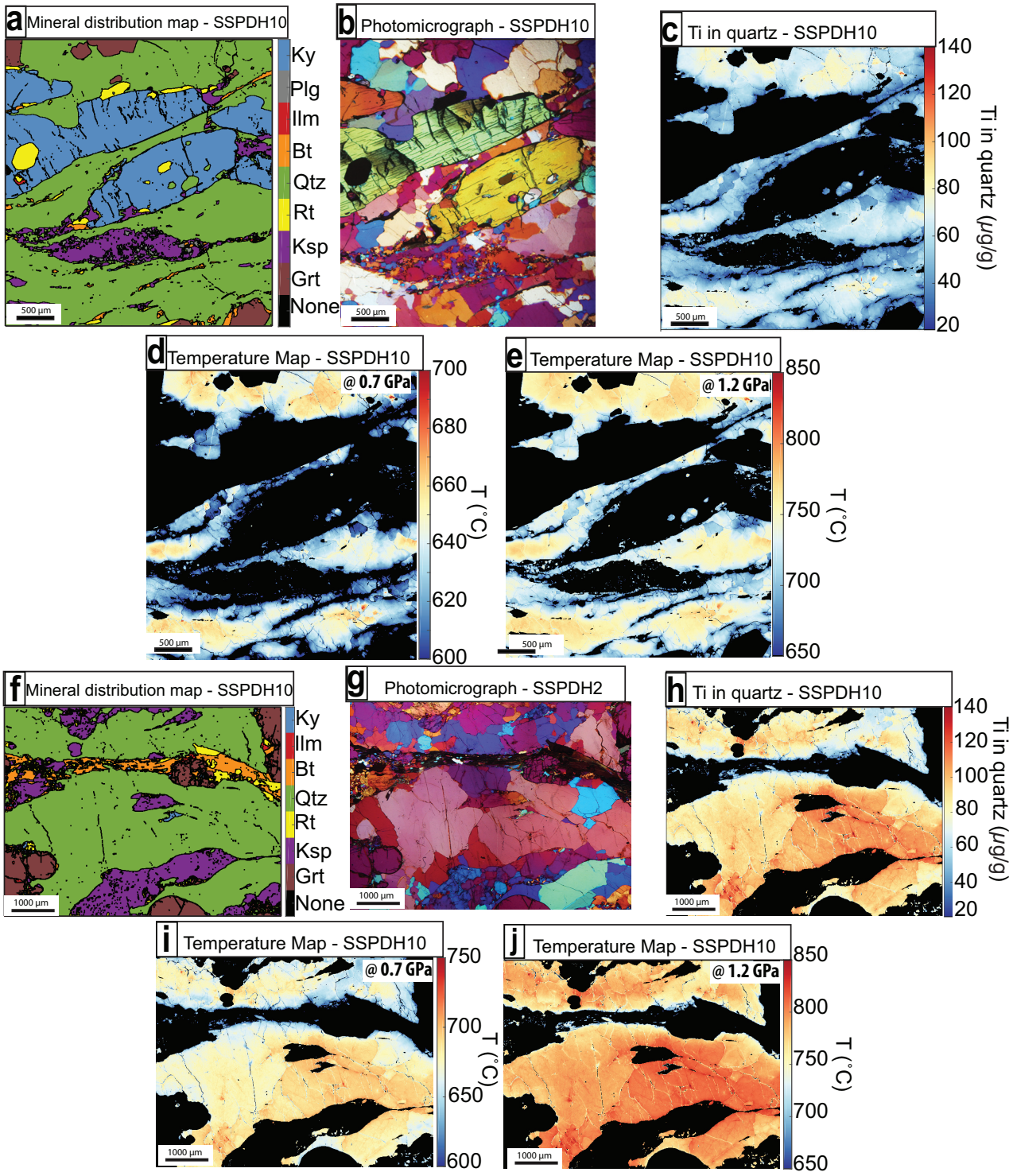

Table 3.4 – Summary of Ti-in-quartz content in analyzed samples. Min.: minimum, Max: maximum, Stdev 2s.: Standard derivation using 2 sigma. *T*.: temperature in °C.

	SSPDH2			SSPDH10		
	Ti (μg/g)	T @0.7 GPa	T @1.2 GPa	Ti (μg/g)	T @0.7 GPa	T @1.2 GPa
Number	178	178	178	179	179	179
Min	26	564	663	25	559	658
Max	134	719	837	119	705	822
1^{st} Quartile	44	610	710	66	635	755
Median	58	631	739	82	666	777
3^{rd} Quartile	74	653	760	95	670	795
Mean	62	633	741	79	659	770
Stdev 2s	48	35	39	37	26	29
	MG161			SSPDH12		
	Ti (μg/g)	T @0.7 GPa	T @1.2 GPa	Ti (μg/g)	T @0.7 GPa	T @1.2 GPa
Number	14	14	14	21	21	21
Min	27	567	667	23	555	654
Max	95	681	795	99	685	800
1^{st} Quartile	53	628	725	58	630	740
Median	67	646	755	62	640	748
3^{rd} Quartile	69	655	762	84	670	773
Mean	60	633	740	68	644	754
Stdev 2s	36	31	35	39	31	35

3.4.5 Phase Equilibria

Studied samples SSPDH10, SSPDH12, MG161 have similar modal proportions of minerals, mineral compositions, and bulk rock compositions (Table 3.S4). Thus, the pseudosections calculated for sample SSPDH10 (Figure 3.10) are assumed to be representative of these studied samples. Since sample SSPDH2 is plagioclase free and has slightly different bulk rock composition (Table 3.S4), a separate set of pseudosections were calculated for it. Two sets of phase equilibria were calculated. Firstly a pseudosection using the local bulk rock composition from the maps, but removing material from the garnet core was calculated (Figure 3.10a and c). Here, the bulk rock H_2O content was set to 1.00 mol% for sample SSPDH10 and 0.81 mol% for sample SSPDH2, which corresponds to the amount of water stored in the hydrous phases (biotite) observed in each sample. These pseudosections were used to infer the peak and retrograde conditions. Secondly, a set pseudosections were calculated to estimate the prograde conditions, in which melt and the garnet core composition was re-integrated into the bulk rock composition used to calculate the previous set (Figure 3.10b and e). Sufficient melt was re-integrated to bring the solidus down-T to H_2O saturated conditions (INDARES; WHITE; POWELL, 2008; LASALLE; INDARES, 2014). This corresponded to 16% reintegrated melt for sample SSPDH10 and 15% for SSPDH2; and iii) a set pseudosections used to estimate the prograde conditions, in which the garnet core composition was added back into the bulk rock composition and a set of diagrams to determine the peak *P*–*T* conditions, where

also the composition of melt was re-integrated into the bulk composition used previously (Figure 3.10). Sufficient melt was re-integrated to bring the solidus down-T to H_2O saturated conditions (INDARES; WHITE; POWELL, 2008; LASALLE; INDARES, 2014). This corresponded to 16% reintegrated melt for sample SSPDH10 and 15% for SSPDH2; in which the garnet core composition was added back into the bulk rock composition previously used to calculate peak P–T conditions (Figure 3.10c Figure 3.10b and fd). Garnet, quartz, K-feldspar, biotite, muscovite, rutile, kyanite, sillimanite and silicate melt are all stable in regions of the investigated P–T window and in all pseudosections. Plagioclase only occurs in the pseudosections for sample SSPDH10.

The inferred peak mineral assemblage of garnet + kyanite + K-feldspar + rutile + melt + quartz + plagioclase is predicted to be stable, in the 'peak-PT conditions' pseudosection calculated for sample SSPDH10 at T higher than 800 °C and P between 1.1 GPa and 1.65 GPa (Figure 3.10ab). Retrograde biotite is observed in the rock, with biotite stability only calculated at T lower than 820 °C (Figure 3.10a) in the kyanite stability field (sillimanite is absent in the rock and kyanite appears to have been the stable Al_2SiO_2 polymorph throughout). Ilmenite is only predicted to be stable at pressure below 0.52 GPa and temperatures below 575 °C, considering the kyanite stability (Figure 3.10a).

According to the peak condition pseudosection calculated for sample SSPDH2 (Figure 3.10c), the peak mineral assemblage of garnet + kyanite + K-feldspar + rutile + melt + quartz is stable above 790 °C and above 0.98 GPa. Retrograde biotite is also observed in this sample and occurs below 790 °C and 1.11 GPa (Figure 3.10c and d). Ilmenite is calculated to be stable below 705 °C and 0.8 GPa (Figure 3.10c), considering the kyanite stability fields.

Dehydration melting of muscovite occurs in the melt generation, as is common in high-pressure aluminous rocks (Figure 3.10c), according to the reaction:

$$Ms \pm Pl + Qtz = Ky + Ksp + Liq \tag{3.1}$$

In sample SSPDH2 the kyanite occurs in all fields pseudosections. On the other hand, in sample SSPDH10 the kyanite is absent throughout the prograde conditions (Figure 3.10b) and crystallizes in the peak assemblage field (Figure 3.10a), according to the muscovite-out reaction above.

The biotite forms in the early retrograde reaction at ∼800 °C in both pseudosection (Figure 3.10a and c), according to the reaction:

$$Grt + Kfs + Rt + Liq = Bt + Qtz \pm Pl + Ky \tag{3.2}$$

Compositional mineral contours can be used to further constrain the P–T conditions of the rock, with zoned porphyroblasts potentially preserving a detailed metamorphic

Figure 3.10 – Pressure-Temperature (P–T) pseudosections calculated in the NCKFMASHTO model chemical system. a) P–T pseudosection calculated by removing the garnet core area from the quantitative map for sample SSPDH10. b) Melt-reintegrated P–T pseudosection calculated by including the previously excluded garnet composition for sample SSPDH10. c) P–T pseudosection calculated by removing the garnet core area from the quantitative map for sample SSPDH2. d) Melt-reintegrated P–T pseudosection calculated by including the previously excluded garnet composition for sample SSPDH2. Quartz is also present in all fields. Compositions shown above diagrams in molar proportion.

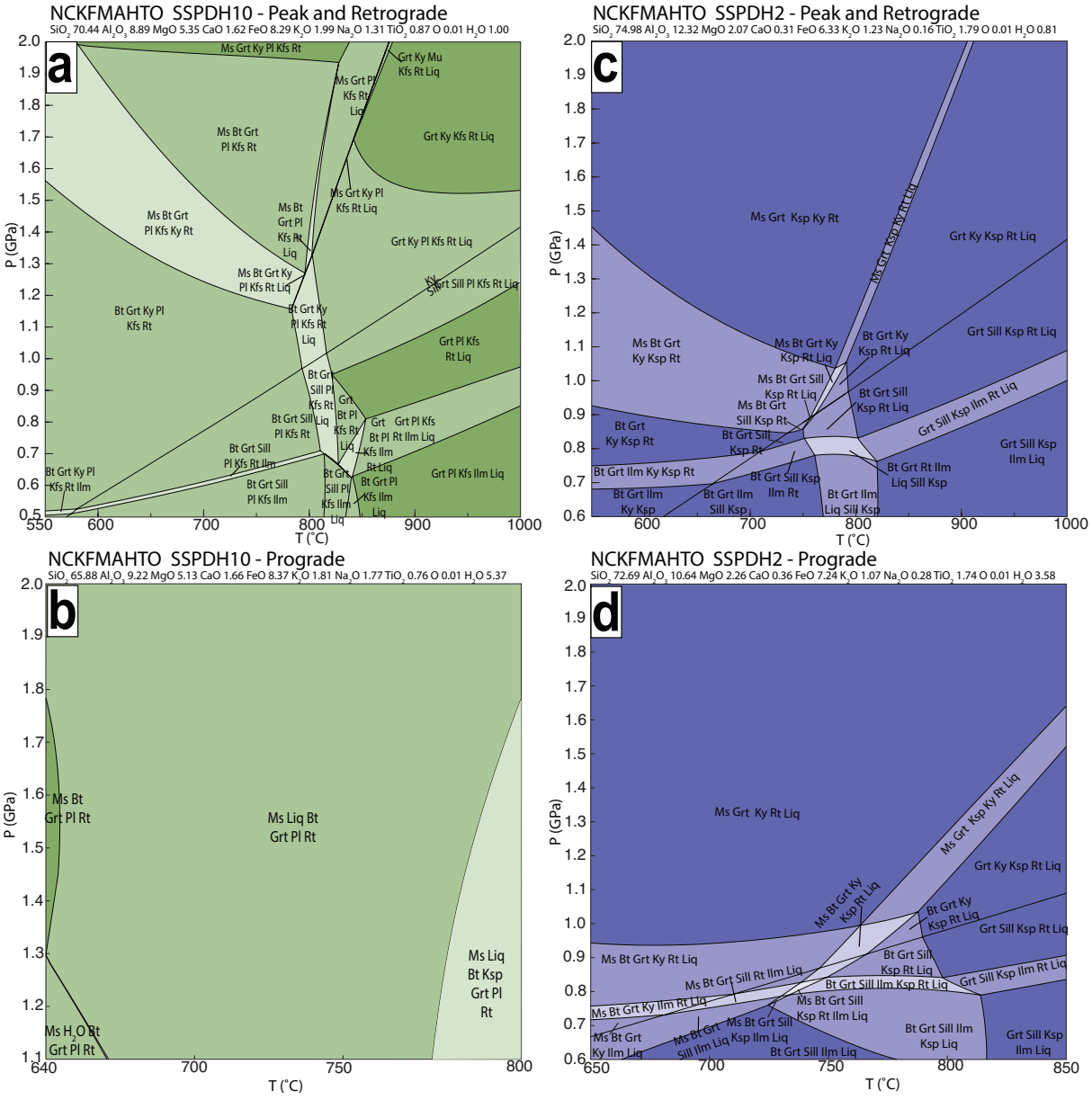

record, if that zoning has been relatively unmodified following initial equilibration.

Grossular content in garnet from SSPDH10 decreases from core to rim (from 0.16 to 0.05, Figure 3.4d), consistent with progressive growth over evolving P-T conditions (Figure 3.11a, and b and c). Initial growth of garnet at ~650 °C and 1.2 GPa (Figure 11a) would result in appropriate crystal core Ca contents, though we note that it is likely that core compositions have been partially modified subsequent to growth, particularly given the subsequent high peak temperature (CADDICK; KONOPÁSEK; THOMPSON, 2010).

The decrease of Ca content towards the garnet rim (XGrs down to 0.05) may indicate a post peak decompression of ∼0.6 GPa, from ∼1.2 to 0.6 GPa (Figure 3.11b and c).

Figure 3.11 – Isopleths of grossular content of garnet (Ca/Ca+Fe+Mg+Mn) and of anorthite content of plagioclase. a) Isopleths of grossular in the P–T pseudosection calculated by removing the garnet core area from the quantitative map for sample SSPDH10. b) Isopleths of grossular in the melt-reintegrated P–T pseudosection calculated by including the previously excluded garnet composition for sample SSPDH10. c) Isopleth of anorthite in the melt-reintegrated P–T pseudosection calculated by including the previously excluded garnet composition for sample SSPDH10. d) Isopleths of grossular in the P–T pseudosection calculated by removing the garnet core area from the quantitative map for sample SSPDH2. e) Isopleth of grossular in melt-reintegrated P–T pseudosection calculated by including the previously excluded garnet composition for sample SSPDH2. Calculated mineral compositions for samples SSPDH10 and SSPDH2 are shown on Figure 3.10.

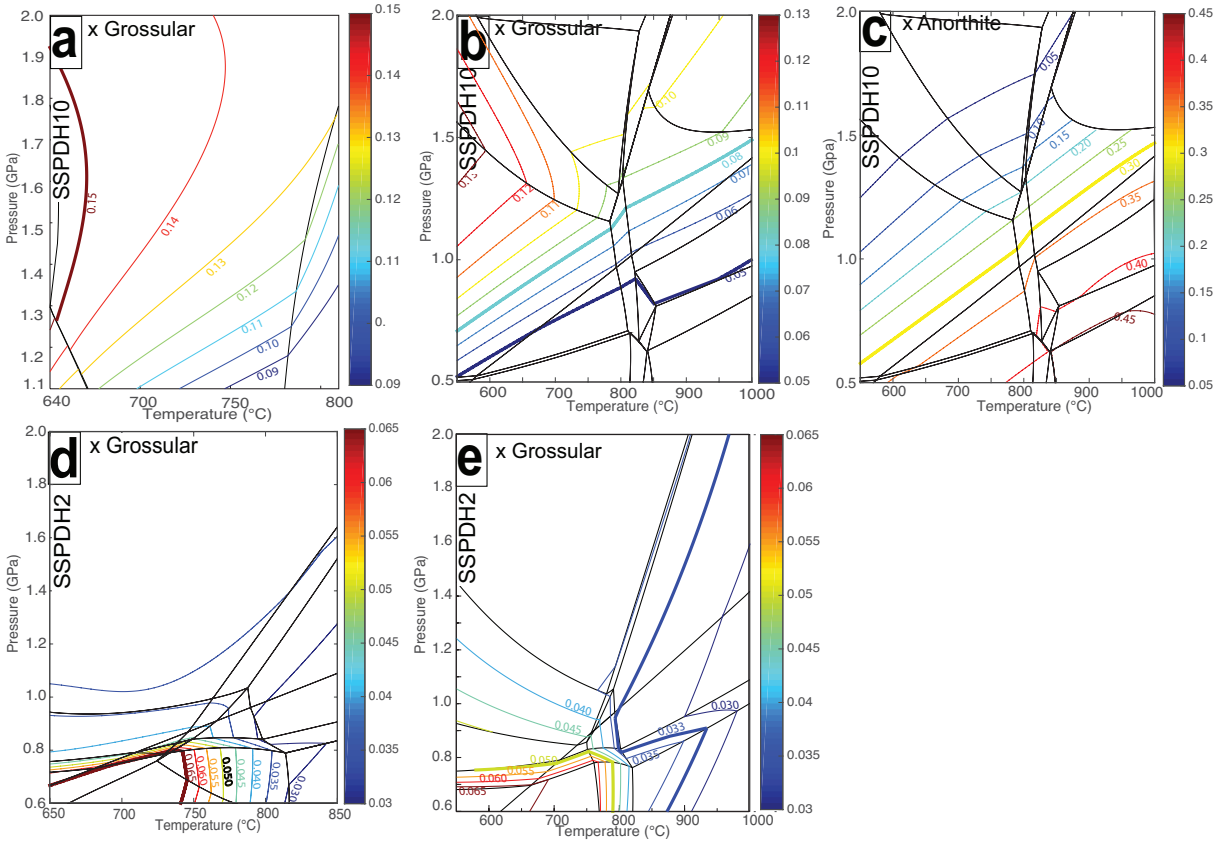

Grossular content in garnet from SSPDH2 also decreases from core to center-rim with a slight increase in the external rim (from 0.065 to 0.033 to 0.05 respectively, Figure 3.4l), despite the zoning not being perfectly concentric in the mapped garnet. The higher grossular content in the sample SSPDH2 is consistent with initial garnet growth at prograde conditions of ∼600 °C and 0.7 GPa (Figure 3.11d). The lower grossular content of 0.033 represents the peak conditions of 830 °C and 1.2 GPa (Figure 3.11e) and the external rim content of 0.05 is consistent with retrograde conditions of 650 °C and 0.75 GPa (Figure 3.11e), indicating a post peak decompression.

In the pseudosections, relative to the garnet abundance in the peak assemblage field a decrease in pressure and temperature would result in a decrease in garnet content

Table 3.5 – Summary of rutile and monazite dating data from samples SSPDH12, SSPDH2, MG161 and SSPDH10. 1s: 1 sigma error. rho: error correlation coefficient. Meas: measured, 2Sig: 2 sigma error. Values in μg/g

Sample	Mineral	Texture	Y_2O_3	SiO_2	ThO_2	CaO	La_2O_3	Ce_2O_3	Pr_2O_3	Nd_2O_3	Sm_2O_3	FeO	Gd_2O_3	Tb_2O_3	Dy_2O_3	UO_2	SO_3	P_2O_5	PbO	Total	Calc	2Sig
SSPDH12	Mnz	Incl Grt	0.39	0.16	4.61	0.96	14.29	31.97	3.17	13.22	1.94	0.10	1.21	BD	BD	0.27	BD	29.46	0.16	102.11	639	28
SSPDH12	Mnz	Mtx	BD	0.28	4.73	0.91	14.80	31.86	3.19	12.35	1.99	BD	0.72	BD	BD	0.74	BD	29.37	0.20	101.32	644	22
SSPDH12	Mnz	Mtx	BD	0.31	5.02	0.86	15.58	32.10	3.16	12.15	1.90	0.07	0.50	BD	BD	0.69	BD	29.14	0.20	101.46	631	22
SSPDH12	Mnz	Incl Grt	0.11	0.29	5.73	1.13	14.61	31.18	3.02	12.37	1.99	0.07	0.84	BD	BD	0.76	BD	29.76	0.19	102.01	669	27
SSPDH12	Mnz	Incl Grt	1.06	2.72	11.28	0.12	7.38	26.45	3.61	15.81	4.66	BD	2.30	BD	BD	0.98	BD	25.28	0.32	102.43	616	20
SSPDH12	Mnz	Incl Grt	0.76	1.39	7.73	0.39	14.11	30.77	3.34	11.35	2.45	BD	1.15	BD	BD	0.23	0.05	27.55	0.21	102.08	640	18
SSPDH12	Mnz	Mtx	0.71	0.04	4.24	1.08	14.14	30.89	3.06	12.04	2.24	BD	1.56	BD	BD	0.72	0.09	29.83	0.20	101.13	594	25
SSPDH12	Mnz	Mtx	2.17	0.07	2.28	0.52	14.08	30.81	3.01	12.89	2.38	BD	1.87	BD	0.65	0.53	BD	29.76	0.14	101.50	632	19
SSPDH2	Mnz	Mtx	1.27	0.06	3.93	0.92	15.17	30.96	3.15	12.32	2.01	BD	1.59	BD	0.64	0.34	BD	29.55	0.15	102.54	619	26
SSPDH2	Mnz	Mtx	0.20	0.19	4.72	1.23	14.73	31.67	3.10	12.01	1.96	BD	1.10	BD	BD	0.25	0.37	29.25	0.16	101.34	588	29
SSPDH2	Mnz	Incl Ky	0.75	0.04	3.71	0.89	13.49	30.85	3.12	13.05	2.56	BD	1.93	BD	BD	0.35	0.05	29.61	0.14	101.13	611	29
SSPDH2	Mnz	Incl Ky	0.75	0.04	3.18	0.82	13.25	30.50	3.09	13.40	2.99	BD	2.77	BD	0.48	0.22	0.05	29.58	0.11	101.06	637	29
SSPDH2	Mnz	Incl Ky	1.10	0.06	3.28	0.80	14.93	31.88	2.88	12.41	1.95	BD	1.69	BD	BD	0.29	0.06	29.57	0.13	101.73	605	28
SSPDH2	Mnz	Incl Ky	0.28	0.10	3.66	0.84	14.30	32.25	3.02	12.55	2.19	0.14	1.51	BD	BD	0.29	0.13	29.85	0.13	101.53	610	29
SSPDH2	Mnz	Incl Grt	0.30	BD	2.07	0.49	17.08	33.67	3.10	11.60	1.72	0.18	0.94	BD	BD	0.37	0.05	30.03	0.09	101.88	631	29
SSPDH2	Mnz	Incl Grt	0.26	0.16	4.35	1.00	14.39	31.68	2.79	12.51	2.36	0.39	1.49	BD	BD	0.25	0.12	29.51	0.15	101.63	637	26
SSPDH2	Mnz	Incl Grt	0.43	0.10	4.39	1.18	14.32	31.23	3.08	12.54	2.19	0.29	1.42	BD	BD	0.52	0.22	29.22	0.17	101.65	607	44
SSPDH2	Mnz	Incl Grt	1.10	0.04	3.91	1.02	13.95	30.91	2.88	11.90	2.07	0.05	1.67	BD	0.54	0.57	BD	29.45	0.17	100.46	634	21
SSPDH2	Mnz	Incl Bt	1.14	0.09	3.97	0.90	13.85	31.58	2.95	12.53	2.28	BD	1.71	BD	BD	0.76	0.04	29.31	0.15	101.85	622	27
SSPDH2	Mnz	Mtx	0.56	0.05	6.39	1.52	13.66	29.91	3.13	11.88	2.09	BD	1.21	BD	BD	0.67	0.11	29.14	0.26	100.76	656	18
SSPDH10	Mnz	Mtx	BD	0.26	6.14	1.32	14.45	32.47	3.23	12.48	1.78	BD	0.60	BD	BD	0.20	0.17	29.12	0.20	102.19	631	25
SSPDH10	Mnz	Incl Grt	0.18	0.17	4.63	1.08	14.66	31.72	3.32	12.78	1.89	BD	0.94	BD	BD	0.56	BD	28.97	0.19	101.03	634	24
SSPDH10	Mnz	Mtx	0.03	0.27	6.11	1.39	14.15	31.66	3.32	12.52	1.72	0.20	0.51	BD	BD	0.17	0.18	28.96	0.19	101.34	584	49
SSPDH10	Mnz	Mtx	0.15	0.48	6.26	1.26	15.51	31.13	2.83	11.49	1.62	BD	0.74	BD	BD	0.70	BD	26.05	0.25	98.34	664	27
SSPDH10	Mnz	Incl Grt	0.06	0.11	2.49	0.58	15.22	34.29	3.48	13.64	1.57	BD	0.59	BD	BD	0.16	0.13	29.18	0.08	101.44	637	23
SSPDH10	Mnz	Incl Grt	0.06	0.14	3.35	0.86	14.80	32.71	3.17	13.06	1.80	BD	0.59	BD	BD	0.16	0.13	28.36	0.11	99.26	651	21
SSPDH10	Mnz	Incl Grt	0.07	0.08	2.01	0.63	15.27	34.20	3.30	13.29	1.72	BD	0.75	BD	BD	0.18	0.18	29.15	0.07	101.05	626	25
SSPDH10	Mnz	Mtx	0.08	0.05	0.71	0.33	14.87	33.75	3.39	14.15	1.80	0.07	0.83	BD	BD	0.22	0.14	29.53	0.04	100.07	637	20
MG161	Mnz	Incl Grt	0.11	BD	2.40	0.46	18.26	35.50	2.95	10.98	0.97	BD	BD	BD	BD	0.07	BD	29.55	0.08	101.74	632	15
MG161	Mnz	Mtx	0.09	0.21	5.40	1.84	15.49	31.42	2.95	11.59	1.41	0.71	0.59	BD	BD	0.30	0.57	28.90	0.18	101.55	665	17
MG161	Mnz	Mtx	0.04	0.48	7.17	1.22	15.69	31.42	2.78	11.35	1.29	BD	0.52	BD	BD	1.17	BD	28.68	0.22	101.99	630	18
MG161	Mnz	Incl Grt	0.03	1.20	10.57	1.27	14.78	30.42	2.83	10.67	1.19	BD	0.46	BD	BD	0.22	BD	27.53	0.32	101.31	596	22
MG161	Mnz	Incl Grt	0.08	0.86	9.22	1.31	15.80	30.27	2.70	10.98	1.40	BD	BD	BD	BD	0.22	BD	28.23	0.28	101.89	632	18
MG161	Mnz	Incl Grt	0.75	1.37	7.70	0.42	14.09	31.02	3.18	11.43	2.32	BD	1.21	BD	BD	0.25	0.04	27.24	0.20	101.33	649	26
MG161	Mnz	Mtx	0.80	0.10	4.01	0.95	14.04	30.69	3.11	12.90	2.40	BD	1.84	BD	BD	0.52	BD	29.33	0.17	101.30	598	27
MG161	Mnz	Mtx	0.04	0.68	8.56	1.30	15.02	31.02	2.76	11.08	1.32	BD	BD	BD	BD	0.22	BD	28.51	0.26	101.30	631	24

					ratio		ratio		rho	ratio		age		age	
Sample	Mineral	U	Th	Th/U	207/235	1s	206/238	1s		207/206	1s	207/235	1s	206/238	1s
SSPDH12	Rt	34	<0.009	<0.00030	0.79	0.02	0.0963	0.0019	0.45	0.0594	0.0016	591	13	593	11
SSPDH12	Rt	24	<0.008	<0.00050	0.77	0.02	0.0972	0.0018	0.42	0.0575	0.0016	580	13	598	10
SSPDH12	Rt	27	0.033	0.0012	0.77	0.02	0.0946	0.0017	0.44	0.0594	0.0015	582	12	582	10
SSPDH1A	Rt	27	<0.010	<0.00050	0.76	0.02	0.0937	0.0015	0.41	0.0590	0.0015	575	12	577	9
MG-161	Rt	46	0.020	0.0004	0.80	0.02	0.0951	0.0017	0.47	0.0607	0.0014	594	11	586	10
MG-161	Rt	28	<0.012	<0.00039	0.80	0.02	0.0960	0.0016	0.36	0.0606	0.0017	598	14	591	9
MG-161	Rt	39	<0.011	<0.00021	0.77	0.02	0.0971	0.0016	0.43	0.0576	0.0014	580	12	597	10
MG-161	Rt	48	<0.012	<0.00023	0.76	0.02	0.0917	0.0017	0.52	0.0598	0.0013	572	10	566	10
SSPDH10	Rt	43	<0.009	<0.00026	0.79	0.02	0.0941	0.0019	0.46	0.0608	0.0015	590	12	579	11
SSPDH10	Rt	35	0.173	0.0049	0.76	0.02	0.0940	0.0017	0.41	0.0587	0.0014	575	11	579	10
SSPDH10	Rt	34	0.009	0.0003	0.80	0.02	0.0949	0.0018	0.48	0.0613	0.0013	598	10	584	11
SSPDH10	Rt	34	<0.009	<0.00028	0.82	0.02	0.0991	0.0020	0.45	0.0598	0.0016	607	13	609	12
SSPDH10	Rt	46	<0.009	<0.00021	0.78	0.02	0.0970	0.0018	0.42	0.0583	0.0014	586	11	597	11

whereas garnet content would be relatively constant with isobaric cooling (Figure 3.S3).

3.4.6 Monazite U-Th-Pb$_T$ dating

Monazite crystals from samples SSPDH10, SSPDH12, SSPDH2 and MG161 were analyzed (Table 3.S5, Table 3.5 and Figure 3.12). In samples SSPDH12 and SSPDH2, the ages of monazite that occurs as inclusions in garnet and kyanite overlap with matrix crystal ages within uncertainties, although the monazite in inclusions is systematically 9 to 10 myr older than the matrix grains (Figure 3.12a and b). The same pattern is observed in samples SSPDH10 and MG161, however with much smaller difference (< 5 Ma, Figure 3.12c and d). The monazite crystals are often zoned in Y, Pb, Ca and Th. This feature is concentric in some crystals and irregular in others. However, there is no clear correlation between the chemical zoning and dates.

In sample SSPDH12, 36 analyses in 8 crystals from the matrix yield a date of 630.9 $\pm$ 3.7 Ma, and 39 analyses in 7 crystals included in garnet yield a date of 638.9 $\pm$ 4.9 Ma (Figure 3.12a). In sample SSPDH2, a date of 623.2 $\pm$ 7.9 Ma is calculated from 4 analyzed crystals (28 single dates) in the matrix, and a date of 632.6 $\pm$ 5.6 Ma is obtained

Figure 3.12 – Error-weighted average of U–Th–Pb$_T$ EPMA ages of monazite. The diagrams are organized by sample and by monazite textural setting. Horizontal lines show the mean values. Data-point error symbols are all in 2 sigma. Wtd: weighted, conf.: confidence, rej.: rejected and MSWD: Mean Square of Weighted Derivates.

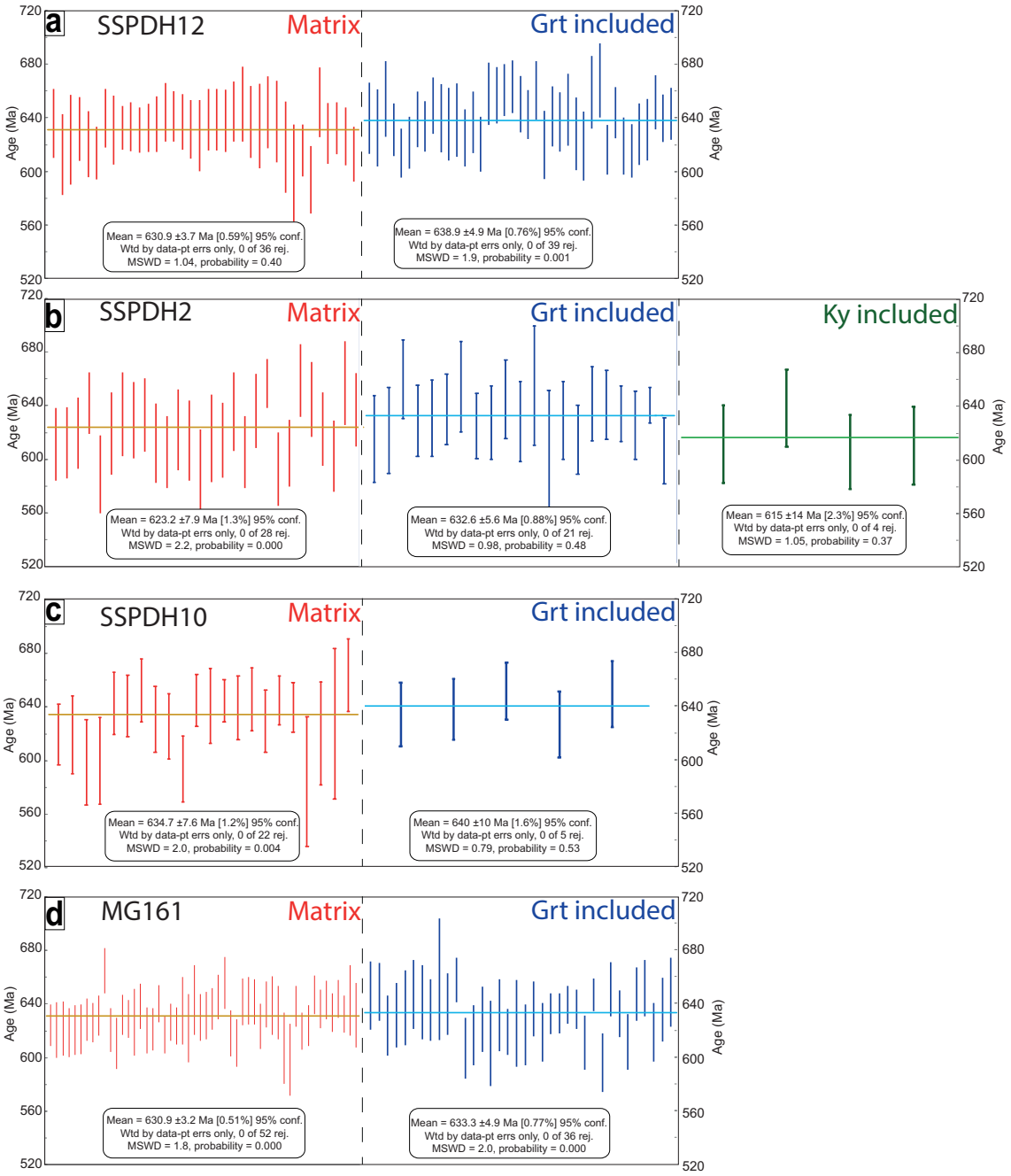

from monazite grains included in garnet (4 crystals and 21 spots). A younger date of 615 ±14 Ma was obtained for a monazite crystal included in kyanite (4 spots, Figure 3.12b). Monazite from the matrix of sample SSPDH10 yields a date of 634.7 ± 7.6 Ma (8 crystals and 22 analyses), with inclusions in garnet yielding a date of 640 ± 10 Ma (5 crystals and 5 analyses, Figure 12c). In sample MG161 monazite from the matrix yields a date of 630.9 ± 3.2 Ma (from 52 dates of 11 crystals), while crystals included in garnet yield a date of

633.3 ± 4.9 (36 analyses in 8 crystals, Figure 3.12d).

3.4.7 Rutile U-Pb dating

A total of 29 single-spot U-Pb analyses of 3 samples (SSPDH10, MG161 and SSPDH12) were carried out by LA-ICP-MS (Figure 3.13 d-I, Table 3.5 and Table S6). U-Pb rutile dates in all analyzed samples, in the matrix and as inclusions are similar and significantly younger than the U-Pb-Th$_T$ monazite dates. Concordia ages were calculated at 590.4 ±4.5 Ma in sample MG161 (MSWD = 0.40), 590.8 ±6.1 Ma in sample SSPDH10 (MSWD = 0.18) and 585.7 ±7.5 Ma in sample SSPDH12 (MSWD = 1.8, Figure 3.13a-c).

3.5 Discussion

3.5.1 Rutile thermometry interpretations

It has previously been shown that the Zr contents of populations of rutile crystals from granulite facies rocks often exhibit large spreads (e.g., Ewing, Hermann e Rubatto (2013), Hart et al. (2018), Kooijman et al. (2012), Luvizotto et al. (2009), Pauly et al. (2016)). This is also true for the data presented here, where Zr contents vary from 407 μg/g to 1847 μg/g. Although there is no consensus as to what grains and analyses should be used for calculating the temperature of the metamorphic peak, several works agree that part of the high-T assemblage is retained in high Zr content crystals (e.g., Clark et al. (2019), Ewing, Hermann e Rubatto (2013), Hart et al. (2018), Kohn, Penniston-Dorland e Ferreira (2016), Kooijman et al. (2012), Pape, Mezger e Robyr (2016), Pauly et al. (2016), Taylor-Jones e Powell (2015)). In an attempt to constrain the conditions of granulite facies metamorphism, and following the recommendation of Luvizotto et al. (2009) and Hart et al. (2018), we used Zr contents above the 90^{th} percentile to calculate temperature.

A summary of the Zr content of all analyzed rutile grains is presented in Figure 3.6c. In total, 9 values are above the 90^{th} percentile in all samples and the maximum Zr content is 1847 (sample SSPDH10). Considering only the values are above the 90^{th} percentile these values, the temperatures range from 821 to 834 °C, assuming pressure of 1.2 GPa as constrained by the peak assemblage (Figure 3.10). These are interpreted as the minimum peak temperature, since we cannot determine the extent to which rutile composition has been modified after its crystallization, but are consistent with the peak assemblage in the pseudosections calculated for samples SSPDH10 and SSPDH2 (Figure 3.14).

Zircon, rutile and quartz are present in all textural domains in the rock (i.e., in the matrix, in the leucosome and also in inclusions in garnet and kyanite). Therefore, it can be assumed that the Zr, Ti and Si system were buffered during the entire P–T–t path.

Figure 3.13 – U-Pb rutile dating. A-c) Concordia plot for LA-ICP-MS U-Pb rutile data from samples MG161 (a), SSPDH10 (b) and SSPDH12 (c). MSWD: Mean Square of Weighted Derivates. d-i) BSE images from the dated rutile with the $^{206}U/^{238}Pb$ age (*), $^{207}U/^{235}235Pb$ age (**), and the U and Zr content in the analyzed rutile crystals.

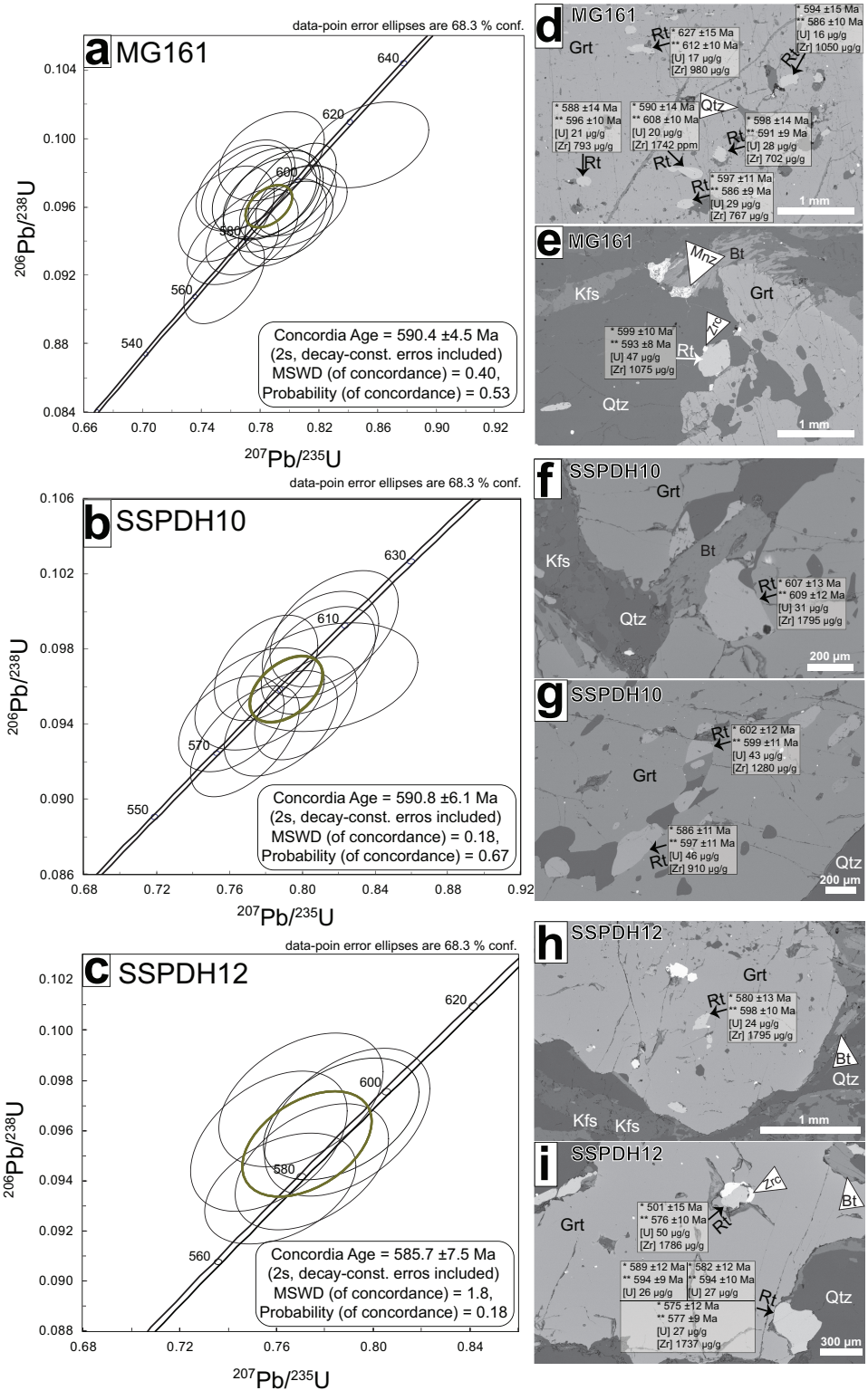

In order to give some constraint on rutile crystallization conditions, the modal proportions of rutile and biotite have been calculated for samples SSPDH10 and SSPDH2 (Figure 3.S5). We note that sample SSPDH2 is richer in Ti (1.23 wt% TiO2 – XRF

Figure 3.14 – Ti in quartz and Zr in rutile isopleths from sample SSPDH10 (a) and from sample SSPDH2 (b), calculated with the minimum concentrations of Zr in rutile above the 90^{th} percentile, and minimum and maximum Ti contents in quartz in this sample. The underlying phase diagram is from Figure 3.10.

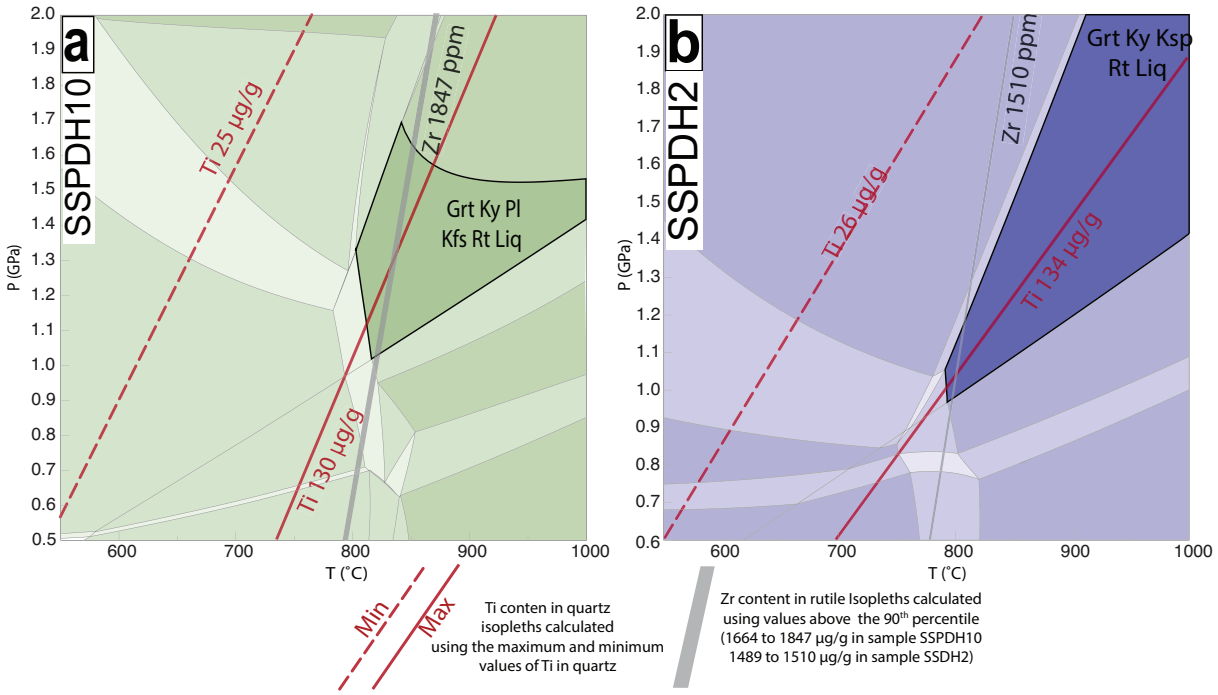

whole rock composition) than the other samples (0.91 – 0.96 wt% TiO_2, Table 3.S4) but that it contains less Mg (1.88 wt% MgO versus 2.12 – 3.94 wt% MgO, Table 3.S4). Therefore, modal proportions of biotite are higher in the calculated pseudosections (Figure 3.S5c, 3.S5b and f), for prograde and peak conditions, for sample SSPDH10 (up to 15vol%) than for sample SSPDH2 (up to 6 vol%). The opposite behavior is observed for rutile: calculated modal proportions (Figure 3.S5d and h) are lower for sample SSPDH10 (up to 0.078 vol%) than sample SSPDH2 (up to 1.54 vol%). In sample SSPDH2, ilmenite is stable in the pseudosections calculated for the prograde and peak stages (Figure 3.10a-c). Comparing the rutile and ilmenite modal proportions (Figure 3.S5l), it is apparent that rutile crystallizes at the expense of ilmenite in sample SSPDH2. We note that the ilmenite-out reaction is strongly pressure dependent (∼0.7 – 0.8 GPa in Figure 3.10f) and, according to our modelling, rutile crystallized within a narrow P window during the prograde path. The breakdown of biotite has practically no influence on the modal proportion of rutile for sample SSPDH2. Modal proportions calculated for sample SSPDH10 (Figure 3.S5f) indicate that rutile crystallizes at the expense of biotite in this sample. Furthermore, modal proportions of rutile rapidly increase with the increase of T within the field Ms+Liq+Bt+Ksp+Grt+Pl+Rt (Figures 3.S5f and 3.S5l), indicating prograde crystallization of rutile. We also note that the biotite-out reaction is strongly temperature dependent (∼810 °C at 1.2 GPa, Figure 3.10b), indicating that no rutile can be crystallized from biotite above this temperature. Since high temperatures are recorded by rutile thermometry in all studied samples (up to 837 °C), recrystallization may have

taken place, allowing for changes in the composition of rutile.

3.5.2 Quartz thermometry interpretations

The spread in Ti contents of quartz is large, with an overall variation from 23 to 134 μg/g (Figure 3.7, 3.8, 3.9 and 3.14). Therefore, a careful evaluation of the data combined with a detailed micro-textural study is required in order to extract meaningful temperatures with Ti-in-quartz thermometry. In this respect, detailed CL mapping is essential, as previously highlighted by Kendrick e Indares (2018). The quantificated Ti maps, based on the CL maps, as a novel approach to further evaluate the Ti distribution, CL maps were converted into Ti content maps by referencing spot analyses in XMapTools and using the advanced calibration method (Lanari et al. 2019). Figures 3.8 and 3.9 shows emphasize that the Ti content of quartz in the studied samples is extremely heterogeneous distribution of the Ti contents in quartz, with concentrations decreasing from core to rim. Few patches of Ti content higher than 115 μg/g are preserved.

The Ti-in-quartz geothermometer is strongly P dependent (THOMAS et al., 2010), so choosing an appropriate P is key. Furthermore, it has been shown that Ti incorporation in quartz is sensitive to post-peak P and T variations (e.g. Nachlas e Hirth (2015), Thomas et al. (2015)) and that dynamic recrystallization enhances the kinetics of Ti equilibration in quartz (GRUJIC; STIPP; WOODEN, 2011; KOHN; NORTHRUP, 2009; NACHLAS; HIRTH, 2015), favoring post crystallization modification of quartz compositions. According to Korchinski et al. (2012), the preservation of high Ti contents in quartz depends on cooling rates and recrystallization, where rapid cooling rates or slow recrystallization favor preservation of early high-Ti grains.

Textures observed in the studied samples indicate that large quartz crystals are interpreted as a peak phase because of the high Ti content and the occurrence in the core of the quartz. The temperature of this high Ti is coherent with the conditions of the peak in the pseudosection modeling and also the higher Zr in rutile content associated with K-feldspar and plagioclase in the leucossome and, therefore, likely crystallized from a melt (Figure 3.3e, f, g and h). In Figure 3.9g and h, large quartz grains tend to contain higher Ti contents than smaller grains. Furthermore, lower Ti contents are observed in the outer rim as well as in fractures along the crystals. Hence, the highest Ti contents are interpreted to represent the T of melt crystallization shortly after metamorphic peak conditions. Low Ti contents at the rim of large quartz crystals and in small grains are attributed to post crystallization changes associated with dynamic recrystallization, mostly by grain boundary migration and less frequently by bulging recrystallization. Figure 3.9b and c show that the lower Ti contents of quartz are strongly associated with recrystallized portions. This recrystallization is probably associated with the cooling and transport of the Passos Nappe to shallower depths during the later stages of the P–T–t path. Kendrick

e Indares (2018) also noted that two populations of quartz occur in aluminous granulites: i) recrystallized or resorbed quartz relics (Ti-rich cores), interpreted to have formed during prograde metamorphism; and, ii) quartz with Ti-poor rims, interpreted to have crystallized from melt. The textures and the variation in Ti content in quartz are similar to those in the present study, though we present an alternative interpretation.

In order to show the effect of P on the apparent temperature, and how an inappropriate P estimate would bias interpretations, T calculations were performed for a peak P of 1.2 GPa, based on pseudosection results for SSPDH10 and SSPDH2 (peak assemblage in Figure 3.10a and c), and for estimated retrograde conditions (grossular core compositions at 0.7 GPa, Figure 11Figure 10ab and e). For peak P, the results range from ∼654 °C to reach 837 °C, while, at 0.7 GPa the results would range from ∼555 °C to 719 °C (Figure 3.8 and Figure 3.9 and Table 3.4). The highest T calculated for 1.2 GPa is in good agreement with peak conditions constrained in the pseudosection (Figure 10). The lower contents of Ti in quartz are probably related to the retrograde conditions. This interpretation is consistent with the P–T conditions of the crystallization of ilmenite and biotite, as well as the grossular contents of garnet rims.

3.5.3 Petrochronology: monazite and rutile ages

Monazite is known to record multiple parts of P–T–t paths (ENGI, 2017; FOSTER et al., 2004; FOSTER et al., 2002; LANARI; ENGI; BERN, 2017; MONTEL, 2000; RUBATTO; CHAKRABORTY; DASGUPTA, 2013; WILLIAMS; JERCINOVIC; HETHERINGTON, 2007; WILLIAMS et al., 2017). The older dates found in our study are recorded by monazite crystals included in garnet (ca. 640 Ma in samples SSPDH12, and SSPDH10 and ca. 633 Ma in samples SSPDH12 and MG161). These dates are interpreted as reflecting prograde or near peak metamorphic conditions. Monazite from the matrix, usually present within the leucosome, yields slightly younger dates, 630 Ma in samples SSPDH12, SSPDH10 and MG161 and ca. 623 Ma in SSPDH2, which probably correlates with melt crystallization. The younger age of 615 Ma in a monazite crystal included in kyanite from sample SSPDH2 can be correlated with the growth of retrograde kyanite. Two kyanite textures are observed in the study (Figure 3.3a, b, c and d). Several generations of kyanite in high-pressure granulite were also observed by Kendrick e Indares (2018a). This younger age was obtained for monazite that is included in a kyanite that is interpreted as post-peak. Kyanite modal proportion increases with decreasing pressure and temperature in the calculated pseudosections (Figure 3.S4a and c). Sample SSPDH2 yields younger ages and has more retrograde features, including more biotite, and ilmenite needles in rutile, than other studied samples. These ages thus probably correlate with later processes associated with hydration upon exhumation and cooling to shallower crustal conditions. These ages are associated with biotite that is a hydrous phase and crystalized during the

early stages of the retrograde path.

The metamorphic peak age of 640-630 Ma is similar to previously presented data for the Passos Nappe (VALERIANO et al., 2004) and high-pressure mafic granulite lenses in the Andrelândia Nappe System (Coelho et al. (2017) - at 625 ± 6 Ma; Frugis, Neto e Lima (2018) - at 635-600 Ma; Tedeschi et al. (2017) at - ca. 630 Ma). However, our peak age is much older than the thermal peak monazite ages described in the high-pressure granulite in the Andrelândia Nappe System by Campos Neto et al. (2010), Motta e Moraes (2017), at 617.7 ± 1.3 Ma and 604.5 ± 6.1 Ma, respectively. It is noteworthy that the U-Pb ID-TIMS monazite concordia age of Campos Neto et al. (2010) was defined by dating seven euhedral up to millimeter-sized monazite crystals that are prevalent in the matrix of the granulite and are typically associated with retrogressed biotite. They can thus be interpreted as associated with cooling after decompression at 617.7 ±1.3 Ma (CAMPOS NETO et al., 2010) and not as peak ages. The range of monazite ages from Motta e Moraes (2017) is similar to the ages presented in this work, suggesting that the interpretation of peak metamorphism at 604.5 ± 6.1 Ma could be inappropriate. The interpretation of retrograde ages of ca. 618 Ma and 604 Ma are in agreement with our data in the Passos Nappe.

Even though rutile is a stable phase at high grade metamorphic conditions, the diffusion rates of trace elements, such as Zr, Pb, Nb, Hf, Nb and Ta, differ significantly at high P–T conditions (e.g. Cherniak (2000), Cherniak, Manchester e Watson (2007), Dohmen et al. (2018), Marschall, Dohmen e Ludwig (2013)). According to Cherniak (2000), the effective closure temperature of Pb in rutile is ∼600 °C for a 100 μm rutile grain, depending also on cooling rate. This implies that the U-Pb age will record cooling ages at lower crustal conditions, complementing earlier zircon and monazite ages in the same rock (ZACK; KOOIJMAN, 2017).

The U-Pb rutile ages obtained in the present study range from 590.8 ± 6.1 Ma (sample SSPDH10) 585.7 ± 7.5 Ma (sample SSPDH12) to 585.7 ± 7.5 Ma (sample SSPDH12) 590.8 ± 6.1 Ma (sample SSPDH10). These are identical within uncertainties to the TIMS rutile age of ca. 594 Ma obtained by Valeriano et al. (2004) for rutile in amphibolite from the Passos Nappe, and are also in agreement with a Rb–Sr isochron date of ca. 590 Ma presented by (RENO et al., 2009) in the Andrelândia Nappe System. The rutile ages record retrograde stages of the P–T path and indicate that the cooling and exhumation of the Passos Nappe to lower/middle crust conditions (∼600 °C, closure T of U-Pb system in rutile) occurred at ca. 590 Ma. Similar ages and interpretations are also presented for the Andrelândia Nappe System by (RENO et al., 2012; WESTIN et al., 2021).

3.5.4 *P–T–t* path

The data presented here indicate that the studied rocks followed a clockwise *P–T–t* path (Figure 3.15). The prograde stage is documented by the highest grossular content in garnet cores, up to 0.15 in the sample SSPDH10 and 0.065 in the sample SSPDH2 (Figure 11a and de). It is likely that initial growth compositions were even more calcic, and that intra-crystalline diffusion has subsequently modified the crystal core compositions (CADDICK; KONOPÁSEK; THOMPSON, 2010; BAXTER; CADDICK; DRAGOVIC, 2017). However, diffusion was not sufficiently intensive to completely eradicate zoning. Peak metamorphic conditions of ∼830 °C ± 30 °C and 1.30 GPa, are constrained by: i) the plagioclase composition in sample SSPDH10 (Figure 3.11c); ii) the grossular content in garnet inner rims (Figure 3.11b); iii) the Zr content in rutile (Figure 3.6 and Figure 3.14) and iv) the highest contents of Ti in quartz. Retrograde conditions involved a cooling path with a decompressional initial stage (to ∼0.5 GPa and 550°C in sample SSPDH10 and to ∼0.7 GPa and 650 °C in sample SSPDH2), recorded by: i) the decrease in grossular content of garnet to 0.05 in sample SSPDH10 and the increase to 0.65 in sample SSPDH2 (Figure 11a Figure 11b and e); ii) the crystallization of biotite; iii) replacement of rutile by ilmenite, and iv) lower contents of Ti in quartz rim, associated with recrystallization. The age of prograde-to-peak metamorphism is constrained by monazite crystals included in garnet at ∼640 – 633 Ma. Retrograde conditions of ∼680 °C and 0.9 GPa are constrained by the age of monazite included in retrograde kyanite at 615 Ma (Figure 3.15). Rutile ages of ca. 590 Ma indicate further cooling, down to ∼600 °C (U-Pb closure temperature).

Figure 3.15 – Pressure-Temperature-time *(P–T-t)* path for sample SSPDH10 (a) and SSPDH2 (b), based on constraints from the pseudosection, Zr-in-rutile content (concentrations above the 90th percentile), grossular values, anorthite values, Ti in quartz content, U-Pb-Th$_T$ dating in monazite and U-Pb dating in rutile. Depth (km) according to Bucher e Grapes (2011).

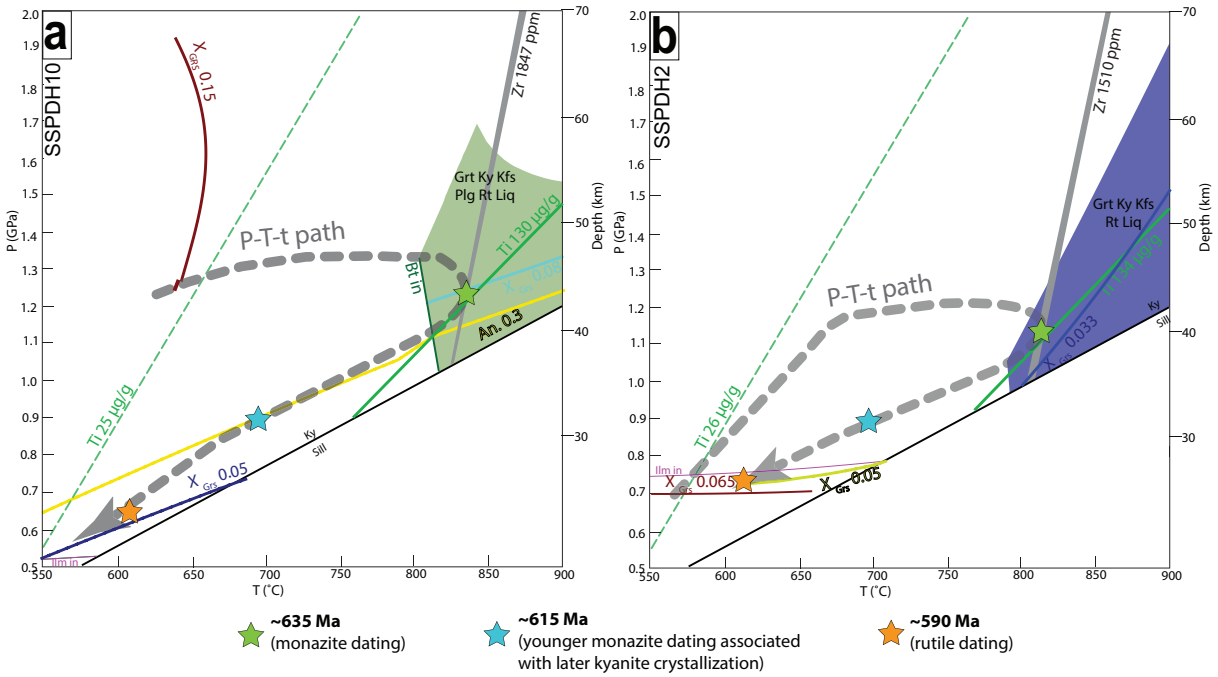

3.5.5 Tectonic setting and regional correlation

The clockwise *P–T–t* path indicates that the metamorphic peak occurred in the high-pressure granulite facies (Figure 3.15), under lower crust conditions, and was followed by stages of cooling and decompression (Figure 3.16). This *P–T–t* path reflects a sequence of events from initial subduction of the distal passive margin of the São Francisco paleocontinent, followed by crustal thickening and subsequent exhumation (Figure 3.16). Our data suggest an intermediate geothermal gradient of 18 °C/km or 690 °C/GPa, which is consistent with a continent-continent collisional setting (BROWN, 2007; BROWN; JOHNSON, 2018; SIZOVA; GERYA; BROWN, 2014). The studied rocks result from the metamorphism of continental margin sediments in the deep root of this Cryogenian-Ediacaran continent-continent collisional zone, at ca. 635 Ma, related with the early phases of West Gondwana formation (Figure 3.16a). The retrograde path (Figures 3.15 and 3.16) records exhumation to ∼600 °C at < 0.9 GPa at a relatively slow integrated cooling rate, of ∼6 °C/Ma.

Figure 3.16 – Simplified sketch of the tectonic evolution of the Southern Brasília Orogen at the latitude of the Passos Nappe interpreted in this study at 635 Ma (a), 615 Ma (a) and 590-570 Ma (c). The green star represents the position of the high-pressure granulite of the Passos Nappe.

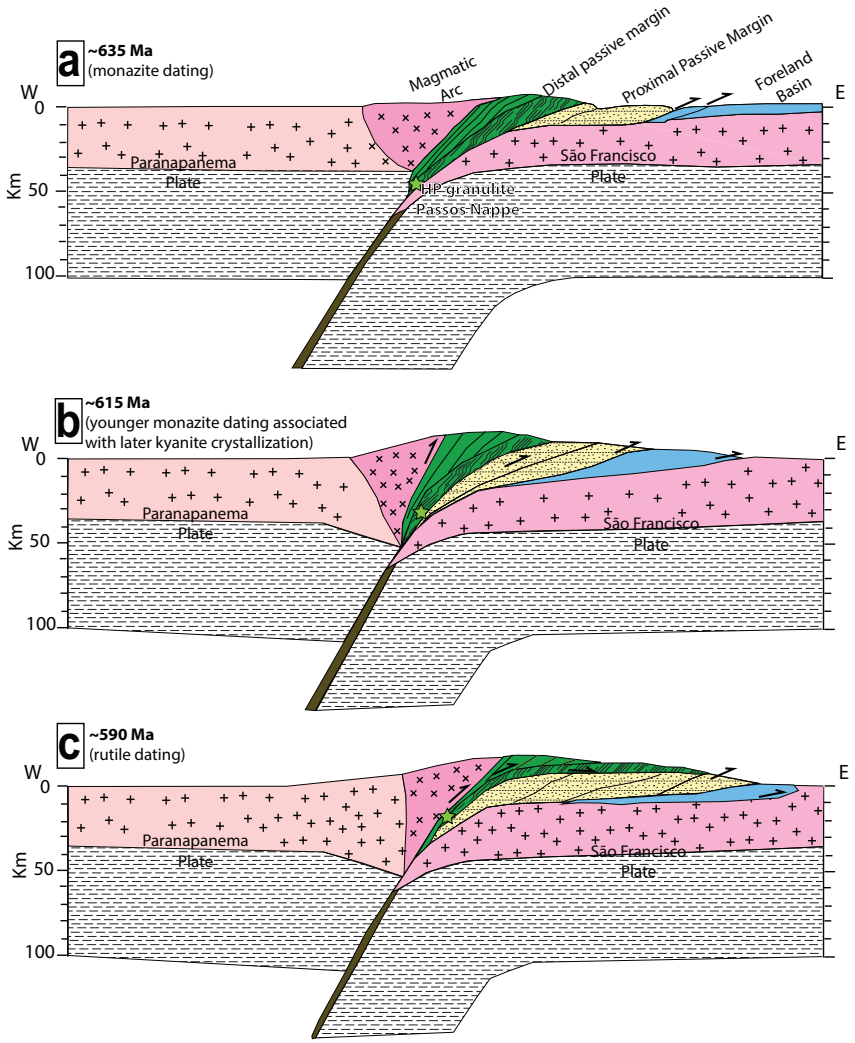

According to O'Brien e Rötzler (2003), high-pressure granulites are formed as a result of short-lived tectonic events that led to crustal thickening or subduction of the crust. They infer that the preservation of prograde zoning in minerals such as garnet is evidence of short durations at high-temperature conditions. Although our data indicate a relatively slow integrated cooling for the high-pressure granulite, garnet zoning is most likely preserved because the total time at or near the highest temperature was relatively short.

The slow cooling rates in the high-pressure granulite of the Passos Nappe corroborate previous descriptions of long-lived metamorphism and deformation, which lasted at least 30 my, in the Southern Brasília Orogen more to the south (CIOFFI et al., 2019; COELHO et al., 2017; ROCHA et al., 2017; TEDESCHI et al., 2018; TROUW et al., 2000). Muscovite K-Ar ages of ca. 570-580 Ma in the Passos Nappe are described by VALERIANO et al. (2000) and record the final cooling stages upon exhumation to the upper crust (∼300 °C). The cooling rate of this final stage of the retrograde *P–T–t* path is faster (∼15 °C/Ma) than calculated for the earlier phase. Similar exhumation/cooling $^{40}Ar/^{39}Ar$ biotite ages around 590-570 Ma are described in high-pressure granulite from Andrelândia Nappe System (WESTIN et al., 2021).

High-pressure granulites also occur in the southernmost portion of the Brasília Orogen, in the upper portion of the Andrelândia Nappe System, where rocks reached *P–T* conditions of ∼800-850 °C and 1.2 to 1.4 GPa (CAMPOS NETO, 2000; CAMPOS NETO et al., 2010; CIOFFI et al., 2012; CIOFFI et al., 2019; MOTTA; MORAES, 2017; RENO et al., 2009; RENO et al., 2012). The metamorphic peak conditions of the rocks from the Andrelândia Nappe System are very similar to those of the top of the Passos Nappe.

Although the present work is the first to systematically investigate the high-pressure granulite from Passos Nappe, a correlation of these rocks with the ones from the Andrelândia Nappe System has previously been previously presented in the literature (RENO et al., 2012; TROUW; PACIULLO; HEILBRON, 1984). Comparing Passos Nappe high pressure granulites with those from the Andrelândia Nappe System is possible on basis of similar mineral assemblages, similar *P-T* conditions, and similar ages of metamorphic peak and exhumation/coolling ages. In the Passos Nappe there is a gradual transition from low grade metamorphism in the lower part to high pressure granulite facies in the upper part, all within a single nappe in which the protoliths are interpreted to be derived from a passive margin sedimentary basin. In the Andrelândia Nappe System there are several nappes that are separated by basement slices and thrust faults. These nappes were originally defined, mapped (TROUW et al., 2000) and stacked based on these structures. Some authors (e. g. Campos Neto et al. (2010), Frugis, Neto e Lima (2018)) interpret these different nappes as derived from different sedimentary basins; the upper part of the stack would be derived from a fore arc basin related to the upper plate,

the active margin of the Paranapanema paleocontinent. However, other authors (e. g. Coelho et al. (2017), Trouw et al. (2013)) maintain the interpretation that the whole stack is derived from the passive margin of the São Francisco Paleocontinent, similar to the interpretation of the Passos Nappe presented here. It is, however, noteworthy that the retrograde replacement of kyanite by sillimanite, widely observed in the metasedimentary high-pressure Andrelândia Nappe rocks (CAMPOS NETO et al., 2010; CIOFFI et al., 2012; MOTTA; MORAES, 2017; RENO et al., 2012; TROUW et al., 2013), but sillimanite is absent in all studied high-pressure granulites from the Passos Nappe and other nappes to the north. The widespread occurrence of late metastable sillimanite in the Andrelândia Nappe System could be explained, at least in part, by the partial superposition of Ribeira Orogen metamorphism on the system (CARVALHO et al., 2020; COELHO et al., 2017; TROUW et al., 2013), or just by the following decompression, without the effect of this tectonic superposition (CAMPOS NETO et al., 2010; CIOFFI et al., 2012; MOTTA; MORAES, 2017). Exhumation of the Passos Nappe may have occurred at slightly higher pressure than the Andrelândia Nappe System, with rocks cooling inside the kyanite field.

3.6 Conclusions

The combination of petrological modelling, trace element geothermometry, and multi-phase geochronology allows the determination of the P–T–t path of high-pressure granulites from the upper Passos Nappe. Both Ti-in-quartz and Zr-in-rutile contents show a large spread, as expected. The highest contents of Zr in rutile and Ti in quartz record the metamorphic peak conditions. Lower Ti contents in quartz are consistent with retrograde conditions.

The studied samples record a clockwise P–T–t path with prograde conditions of ∼600 °C and 0.7 GPa, peak conditions of ∼830 °C and 1.2 GPa and retrograde conditions of ∼550 °C and 0.5 GPa. The prograde-to-peak metamorphism, inferred from monazite ages, occurred ca. 635 Ma. Rutile U-Pb dating indicates a cooling age to ∼600 °C at ca. 590 Ma. The metamorphic P–T path constrained in this work is consistent with a continental collision setting in the Southern Brasília Orogen and indicates a relatively slow cooling rate for rocks from the top of the Passos Nappe pile. Both the peak P–T conditions and metamorphic ages suggest that the high-pressure granulites from the Passos Nappe were involved in similar timing and conditions as the granulites from the Andrelândia Nappe System to the south.

Acknowledgements The authors thank Aphrodite Indares, Celine Martin and Rudolph Trouw for their constructive reviews that improved the presentation of this work. Julia Baldwin and Richard White are thanked for editorial handling of the manuscript. This research was funded by São Paulo Research Foundation (FAPESP), through grants

2015/05230-0 and 16/22627-3, and from the National Council for Scientific and Technological Development (CNPq, 486328/2013-9). R. RAF, GLL and RM acknowledge the National Council for Scientific and Technological Development (Conselho Nacional de Desenvolvimento Científico e Tecnológico, CNPq); RM and GLL are research fellows of the CNPq (grant 305720/2001-1 to RM and grant 311606/2019-9 to GGL) and RAF had PhD scholarship (141604/2018-2) R. A. Fumes thanks CNPq for PhD scholarship (141604/2018-2). GLL is supported by National Council for Scientific and Technological Development (CNPq, Brazil) (Grant Number 311606/2019-9). We gratefully acknowledge the assistance of Daniel Godoy in the EPMA lab. The authors would like to thank Mariana Diniz Silvestre and Daniel Marinzek de Souza for their work during undergraduate dissertation.

Reference

ARAÚJO FILHO, J. O. The Pirineus Syntaxis: An example of the intersection of two Brasiliano fold-thrust belts in central Brazil and its implications for the tectonic evolution of western Gondwana. *Revista Brasileira de Geociências*, v. 30, n. 1, p. 144–148, 2000.

ARMSTRONG, R. A brief history of geochronometry and radiogenic isotopic studies. *Applications of Radiogenic Isotope Systems to Problems in Geology: Short Course Handbook. Edited by L. Heaman and JN Ludden. Mineralogical Association of Canada, Nepean, Ontario*, p. 1–26, 1991.

ASHLEY, K. T.; LAW, R. D. Modeling prograde TiO2 activity and its significance for Ti-in-quartz thermobarometry of pelitic metamorphic rocks. *Contributions to Mineralogy and Petrology*, v. 169, n. 2, p. 1–7, 2015. ISSN 0010-7999. Avaible form internet: <http://link.springer.com/10.1007/s00410-015-1118-7>.

AUDÉTAT, A. et al. Characterisation of a natural quartz crystal as a reference material for microanalytical determination of ti, al, li, fe, mn, ga and ge. *Geostandards and Geoanalytical Research*, Wiley Online Library, v. 39, n. 2, p. 171–184, 2015.

BALDWIN, J. et al. Modelling of mineral equilibria in ultrahigh-temperature metamorphic rocks from the Anápolis–Itauçu Complex, central Brazil. *Journal of Metamorphic Geology*, Wiley Online Library, v. 23, n. 7, p. 511–531, 2005.

BARBOSA, O. Guia das excursões. In: SBG (Ed.). *Congresso Brasileiro de Geologia, 9*. [S.l.: s.n.], 1955. Noticiário 3, p. 3–5.

BAXTER, E.; CADDICK, M.; DRAGOVIC, B. Garnet: A Rock-Forming Mineral Petrochronometer. *Reviews in Mineralogy and Geochemistry*, v. 83, n. 1, p. 469–533, 2017. ISSN 1529-6466. Avaible form internet: <http://rimg.geoscienceworld.org/content/83/1/469>.

BROWN, M. Metamorphic conditions in orogenic belts: a record of secular change. *International Geology Review*, Taylor & Francis, v. 49, n. 3, p. 193–234, 2007.

BROWN, M.; JOHNSON, T. Secular change in metamorphism and the onset of global plate tectonics. *American Mineralogist*, v. 103, n. 2, p. 181–196, 2018. ISSN 19453027.

CADDICK, M. J.; KONOPÁSEK, J.; THOMPSON, A. B. Preservation of garnet growth zoning and the duration of prograde metamorphism. *Journal of Petrology*, Oxford University Press, v. 51, n. 11, p. 2327–2347, 2010.

CAMPOS NETO, M. D. C. Orogenic Systems from Southwestern Gondwana: An Approach to Brasiliano-Pan African Cycle and Orogenic Collage in Southeastern Brazil. In: CORDANI, U. G. et al. (Ed.). *Tectonic Evolution of South America*. 1. ed. Rio de Janeiro: COMPANHIA DE PESQUISA DE RECURSOS MINERAIS, 2000. p. 335–365.

CAMPOS NETO, M. D. C.; CABY, R. Neoproterozoic high-pressure metamorphism and tectonic constraint from the nappe system south of the Sao Francisco Craton, southeast Brazil. *Precambrian Research*, v. 97, n. 1-2, p. 3–26, 1999. ISSN 03019268.

CAMPOS NETO, M. D. C. et al. Structural and metamorphic control on the exhumation of high-P granulites: The Carvalhos Klippe example, from the oriental Andrelândia Nappe System, southern portion of the Brasília Orogen, Brazil. *Precambrian Research*, v. 180, n. 3-4, p. 125–142, 2010. ISSN 03019268.

CAMPOS NETO, M. D. C. et al. Sistema de nappes andrelândia, setor oriental: litoestratigrafia e posição estratigráfica. *Revista Brasileira de Geociências*, v. 37, n. 4-Sup., p. 47–60, 2007.

CARVALHO, B. R. et al. Microstructural and metamorphic evolution of the Carrancas Klippe, interference zone of the Neoproterozoic southern Brasilia and Ribeira orogens, SE brazil. *Journal of South American Earth Sciences*, Elsevier, v. 103, p. 102744, 2020.

CHERNIAK, D. Pb diffusion in rutile. *Contributions to Mineralogy and Petrology*, Springer, v. 139, n. 2, p. 198–207, 2000.

CHERNIAK, D.; MANCHESTER, J.; WATSON, E. Zr and Hf diffusion in rutile. *Earth and Planetary Science Letters*, Elsevier, v. 261, n. 1, p. 267–279, 2007.

CIOFFI, C. R. et al. Geochemical signatures of metasedimentary rocks of high-pressure granulite facies and their relation with partial melting: Carvalhos Klippe, Southern Brasília Belt, Brazil. *Journal of South American Earth Sciences*, v. 40, p. 63–76, 2012. ISSN 08959811.

CIOFFI, C. R. et al. Titanite petrochronology of the southern Brasília Orogen basement: Effects of retrograde net-transfer reactions on titanite trace element compositions. *Lithos*, Elsevier, v. 344, p. 393–408, 2019.

CLARK, C. et al. Testing the fidelity of thermometers at ultrahigh temperatures. *Journal of Metamorphic Geology*, Wiley Online Library, v. 37, n. 7, p. 917–934, 2019.

COELHO, M. B. et al. Constraining timing and P-T conditions of continental collision and late overprinting in the Southern Brasília Orogen (SE-Brazil): U-Pb zircon ages and geothermobarometry of the Andrelândia Nappe System. *Precambrian Research*, Elsevier B.V., v. 292, p. 194–215, 2017. ISSN 03019268. Avaible form internet: <http://linkinghub.elsevier.com/retrieve/pii/S0301926816305496>.

CRUZ-URIBE, A. M. et al. Assessing trace element (dis)equilibrium and the application of single element thermometers in metamorphic rocks. *Lithos*, Elsevier B.V., v. 314-315, p. 1–15, 2018. ISSN 18726143. Avaible form internet: <https://doi.org/10.1016/j.lithos.2018.05.007>.

DARDENNE, M. A. The Brasilia Fold Belt. In: *Tectonic Evolution of South Ameria*. [S.l.]: 31 Intern. Geol. Congr. Rio de Janeiro, 2000. p. 231–264.

DICKIN, A. Isotope geochemistry of oceanic volcanics. *Radiogenic isotope geology*, Cambridge Univ. Press, 1995.

DOHMEN, R. et al. Diffusion of zr, hf, nb and ta in rutile: effects of temperature, oxygen fugacity, and doping level, and relation to rutile point defect chemistry. *Physics and Chemistry of Minerals*, Springer, v. 46, n. 3, p. 311–332, 2018.

ENGI, M. Petrochronology Based on REE-Minerals: Monazite, Allanite, Xenotime, Apatite. *Reviews in Mineralogy and Geochemistry*, v. 83, n. 1, p. 365 LP – 418, 2017. Avaible form internet: <http://rimg.geoscienceworld.org/content/83/1/365.abstract>.

EWING, T. A.; HERMANN, J.; RUBATTO, D. The robustness of the Zr-in-rutile and Ti-in-zircon thermometers during high-temperature metamorphism (Ivrea-Verbano Zone, northern Italy). *Contributions to Mineralogy and Petrology*, v. 165, n. 4, p. 757–779, 2013. ISSN 00107999.

FOSTER, G. et al. Textural, chemical and isotopic insights into the nature and behaviour of metamorphic monazite. *Chemical Geology*, Elsevier, v. 191, n. 1-3, p. 183–207, 2002.

FOSTER, G. et al. The generation of prograde p–t–t points and paths; a textural, compositional, and chronological study of metamorphic monazite. *Earth and Planetary Science Letters*, Elsevier, v. 228, n. 1-2, p. 125–142, 2004.

FRUGIS, G. L.; NETO, M. d. C. C.; LIMA, R. B. Eastern Paranapanema and southern São Francisco orogenic margins: Records of enduring Neoproterozoic oceanic convergence and collision in the southern Brasília Orogen. *Precambrian Research*, Elsevier, v. 308, p. 35–57, 2018.

FUCK, R. et al. Compartimentação tectônica da porção oriental da Província Tocantins. In: *SBG, Congresso Brasileiro de Geologia*. [S.l.: s.n.], 1994. v. 38, n. 1, p. 215–216.

FUCK, R. A. et al. The Northern Brasília Belt. In: HEILBRON, M.; CORDANI, U. G.; ALKMIM, F. F. (Ed.). *São Francisco Craton, Eastern Brazil Tectonic Genealogy of a Miniature Continent*. [S.l.]: Springer Berlin Heidelberg, 2017. p. 205–220.

GEBAUER, D.; GRÜNENFELDER, M. U—th—pb dating of minerals. In: *Lectures in isotope geology*. [S.l.]: Springer, 1979. p. 105–131.

GONÇALVES, G. O. et al. An assessment of monazite from the itambé pegmatite district for use as u–pb isotope reference material for microanalysis and implications for the origin of the "moacyr" monazite. *Chemical Geology*, Elsevier, v. 424, p. 30–50, 2016.

GRUJIC, D.; STIPP, M.; WOODEN, J. L. Thermometry of quartz mylonites: Importance of dynamic recrystallization on ti-in-quartz reequilibration. *Geochemistry, Geophysics, Geosystems*, Wiley Online Library, v. 12, n. 6, 2011.

HART, E. et al. A window into the lower crust: Trace element systematics and the occurrence of inclusions/intergrowths in granulite-facies rutile. *Gondwana Research*, The Authors, v. 59, p. 76–86, 2018. ISSN 1342937X. Avaible form internet: <http://linkinghub.elsevier.com/retrieve/pii/S1342937X18300856>.

HOLLAND, T. J. B.; POWELL, R. An improved and extended internally consistent thermodynamic dataset for phases of petrological interest, involving a new equation of state for solids. *Journal of Metamorphic Geology*, v. 29, n. 3, p. 333–383, 2011. ISSN 02634929.

INDARES, A.; WHITE, R.; POWELL, R. Phase equilibria modelling of kyanite-bearing anatectic paragneisses from the central grenville province. *Journal of Metamorphic Geology*, Wiley Online Library, v. 26, n. 8, p. 815–836, 2008.

KENDRICK, J.; INDARES, A. The reaction history of kyanite in high- P aluminous granulites. *Journal of Metamorphic Geology*, v. 36, p. 125–146, 2018.

KENDRICK, J.; INDARES, A. The Ti Record of Quartz in Anatectic Aluminous Granulites. *Journal of Petrology*, n. July, p. 1–23, 2018. ISSN 0022-3530.

KIDDER, S.; AVOUAC, J. P.; CHAN, Y. C. Application of titanium-in-quartz thermobarometry to greenschist facies veins and recrystallized quartzites in the Hsüehshan range, Taiwan. *Solid Earth*, v. 4, n. 1, p. 1–21, 2013.

KOHN, M. J.; NORTHRUP, C. J. Taking mylonites' temperatures. *Geology*, Geological Society of America, v. 37, n. 1, p. 47–50, 2009.

KOHN, M. J.; PENNISTON-DORLAND, S. C.; FERREIRA, J. C. Implications of near-rim compositional zoning in rutile for geothermometry, geospeedometry, and trace element equilibration. *Contributions to Mineralogy and Petrology*, Springer, v. 171, n. 10, p. 78, 2016.

KOOIJMAN, E. et al. Trace element systematics in granulite facies rutile: implications for Zr geothermometry and provenance studies. *Journal of Metamorphic Geology*, Wiley Online Library, v. 30, n. 4, p. 397–412, 2012.

KORCHINSKI, M. et al. Variation of ti-in-quartz in gneiss domes exposing the world's youngest ultrahigh-pressure rocks, d'entrecasteaux islands, papua new guinea. *Geochemistry, Geophysics, Geosystems*, Wiley Online Library, v. 13, n. 10, 2012.

KRETZ, R. Symbols for rock-forming minerals. *American Mineralogist*, v. 68, p. 277–279, 1983.

LANARI, P.; DUESTERHOEFT, E. Modeling Metamorphic Rocks Using Equilibrium Thermodynamics and Internally Consistent Databases: Past Achievements, Problems and Perspectives. *Journal of Petrology*, v. 60, n. 1, p. 19–56, 2019. ISSN 14602415.

LANARI, P.; ENGI, M.; BERN, C. Local Bulk Composition Effects on Metamorphic Mineral Assemblages. *Reviews in Mineralogy and Geochemistry*, v. 83, p. 55–93, 2017.

LANARI, P. et al. Xmaptools: A matlab©-based program for electron microprobe x-ray image processing and geothermobarometry. *Computers & Geosciences*, Elsevier, v. 62, p. 227–240, 2014.

LASALLE, S.; INDARES, A. Anatectic record and contrasting p–t paths of aluminous gneisses from the central grenville province. *Journal of Metamorphic Geology*, Wiley Online Library, v. 32, n. 6, p. 627–646, 2014.

LEEMAN, W. P. et al. A study of cathodoluminescence and trace element compositional zoning in natural quartz from volcanic rocks: Mapping titanium content in quartz. *Microscopy and Microanalysis*, Cambridge University Press, v. 18, n. 6, p. 1322–1341, 2012.

LUDWIG, K. R. Isoplot 3.00: A geochronological toolkit for microsoft excel. *Berkeley Geochronology Center Special Publication*, v. 4, p. 70, 2003.

LUVIZOTTO, G. *Caracterização metamórfica das rochas do Grupo Araxá na região de São Sebastião do Paraíso, sudoeste de Minas Gerais*. Dissertação (Mestrado) — Instituto de Geociências e Ciências Exatas da Universidade Estadual Paulista, 2003.

LUVIZOTTO, G. L. et al. Rutile occurrence and trace element behavior in medium-grade metasedimentary rocks: Example from the Erzgebirge, Germany. *Mineralogy and Petrology*, v. 97, n. 3-4, p. 233–249, 2009. ISSN 09300708.

MARSCHALL, H. R.; DOHMEN, R.; LUDWIG, T. Diffusion-induced fractionation of niobium and tantalum during continental crust formation. *Earth and Planetary Science Letters*, Elsevier, v. 375, p. 361–371, 2013.

MARTINEZ, R. B. *Avaliação de métodos para cálculo e inferência de condições PT em rochas da fácies Granulito: investigação das rochas das nappes Três Pontas-Varginha e Socorro-Graxupé*. Tese (Doutorado) — Universidade de São Paulo, 2015.

MONTEL, J. Preservation of old u-th-pb ages in shielded monazite; example from the beni bousera hercynian kinzigites (morocco). *J. metamorphic Geol.*, v. 18, p. 335–342, 2000.

MORAES, R. et al. Characterization and P-T Evolution of Melt-bearing Ultrahigh-temperature Granulites: an Example from the Anapolis-Itauçu Complex of the Brasília Fold Belt. *Journal of Petrology*, v. 43, p. 1673–1705, 2002.

MOTTA, R. G.; MORAES, R. Pseudo- and real-inverted metamorphism caused by the superposition and extrusion of a stack of nappes: a case study of the Southern Brasília Orogen, Brazil. *International Journal of Earth Sciences*, 2017. ISSN 1437-3254. Avaible form internet: <http://link.springer.com/10.1007/s00531-016-1436-7>.

MÜLLER, A.; LENNOX, P.; TRZEBSKI, R. Cathodoluminescence and micro-structural evidence for crystallisation and deformation processes of granites in the eastern lachlan fold belt (se australia). *Contributions to Mineralogy and Petrology*, Springer, v. 143, n. 4, p. 510–524, 2002.

NACHLAS, W.; HIRTH, G. Experimental constraints on the role of dynamic recrystallization on resetting the Ti-in-quartz thermobarometer. *Journal of Geophysical Research: Solid Earth*, Wiley Online Library, v. 120, n. 12, p. 8120–8137, 2015.

O'BRIEN, P. Challenges in high-pressure granulite metamorphism in the era of pseudosections: reaction textures, compositional zoning and tectonic interpretation with examples from the bohemian massif. *Journal of Metamorphic Geology*, Wiley Online Library, v. 26, n. 2, p. 235–251, 2008.

O'BRIEN, P. J.; RÖTZLER, J. R. High-pressure granulites: formation, recovery of peak conditions and implications for tectonics. *Journal of Metamorphic Geology*, v. 21, n. 3-20, 2003.

PAPE, J.; MEZGER, K.; ROBYR, M. A systematic evaluation of the zr-in-rutile thermometer in ultra-high temperature (uht) rocks. *Contributions to Mineralogy and Petrology*, Springer, v. 171, n. 5, p. 44, 2016.

PAULY, J. et al. Prolonged Ediacaran–Cambrian metamorphic history and short-lived high-pressure granulite-facies metamorphism in the HU Sverdrupfjella, Dronning Maud Land (East Antarctica): evidence for continental collision during Gondwana assembly. *Journal of Petrology*, Oxford University Press, v. 57, n. 1, p. 185–228, 2016.

PEARCE, M. A.; WHITE, A. J. R.; GAZLEY, M. F. TCInvestigator: Automated calculation of mineral mode and composition contours for thermocalc pseudosections. *Journal of Metamorphic Geology*, v. 33, n. 4, p. 413–425, 2015. ISSN 15251314.

PIMENTEL, M. M. The tectonic evolution of the Neoproterozoic Brasília Belt, central Brazil: The tectonic evolutuion of the Neoproterozoic Brasília Bet, central Brasil: a geochronological and isotopic approach. *Brazilian Journal of Geology*, v. 46, n. Suppl 1, p. 67–82, 2016.

PIUZANA, D. et al. Neoproterozoic granulite facies metamorphism and coeval granitic magmatism in the Brasilia Belt, Central Brazil: regional implications of new SHRIMP U–Pb and Sm–Nd data. *Precambrian Research*, Elsevier, v. 125, n. 3-4, p. 245–273, 2003.

PIUZANA, D. et al. SHRIMP U–Pb and Sm–Nd data for the Araxá Group and associated magmatic rocks: constraints for the age of sedimentation and geodynamic context of the southern Brasılia Belt, central Brazil. *Precambrian Research*, Elsevier, v. 125, n. 1-2, p. 139–160, 2003.

POWELL, R.; HOLLAND, T.; WORLEY, B. Calculating phase diagrams involving solid solutions via non-linear equations, with examples using THERMOCALC. *Journal of Metamorphic Geology*, v. 16, p. 577–588, 1998. ISSN 02634929 (ISSN).

POWELL, R.; HOLLAND, T. J. B. An internally consistent dataset with uncertainties and correlations: 3. Applications to geobarometry, worked examples and a computer program. *Journal of metamorphic Geology*, v. 6, n. 2, p. 173–204, 1988.

PRENT, A. M. et al. Monazite as a monitor for melt-rock interaction during cooling and exhumation. *Journal of Metamorphic Geology*, Wiley Online Library, v. 37, n. 3, p. 415–438, 2019.

RENO, B. L. et al. Eclogite–high-pressure granulite metamorphism records early collision in West Gondwana: new data from the Southern Brasília Belt, Brazil. *Journal of the Geological Society*, Geological Society of London, v. 166, n. 6, p. 1013–1032, 2009.

RENO, B. L. et al. In situ monazite (U-Th)-Pb ages from the Southern Brasília Belt, Brazil: Constraints on the high-temperature retrograde evolution of HP granulites. *Journal of Metamorphic Geology*, v. 30, n. 1, p. 81–112, 2012. ISSN 02634929.

ROCHA, B. C. et al. Timing of anatexis and melt crystallization in the Socorro – Guaxupé Nappe , SE Brazil : Insights from trace element composition of zircon , monazite and garnet coupled to U — Pb geochronology. v. 277, p. 337–355, 2017.

RUBATTO, D.; CHAKRABORTY, S.; DASGUPTA, S. Timescales of crustal melting in the higher himalayan crystallines (sikkim, eastern himalaya) inferred from trace element-constrained monazite and zircon chronology. *Contributions to Mineralogy and Petrology*, Springer, v. 165, n. 2, p. 349–372, 2013.

SEER, H. J. et al. Grupo Araxá em sua área tipo: Um fragmento de crosta oceânica neoproterozóica na faixa de dobramentos Brasília. *Revista Brasileira de Geociências*, v. 31, n. 3, p. 385–396, 2001.

SEER, H. J.; DARDENNE, M. A. Tectonostratigraphic terrane analysis on neoproterozoic times: the case study of Araxá Synform, Minas Gerais state, Brazil: Implications to the final collage of the Gondwanaland. *Revista Brasileira de Geociências*, v. 30, n. 1, p. 78–81, 2000.

SIMÕES, L. *Evolução tectono-metamórfica da nappe de Passos, sudoeste de Minas Gerais*. Tese (Doutorado) — IG-Universidade de São Paulo, 1995.

SIZOVA, E.; GERYA, T.; BROWN, M. Contrasting styles of Phanerozoic and Precambrian continental collision. *Gondwana Research*, Elsevier, v. 25, n. 2, p. 522–545, 2014.

SPEAR, F.; PARRISH, R. Petrology and petrologic cooling rates of the valhalla complex. *British Columbia, Canada. J Petrol*, v. 37, p. 733–765, 1996.

SPENCER, C. J. et al. Not all supercontinents are created equal: Gondwana-rodinia case study. *Geology*, Geological Society of America, v. 41, n. 7, p. 795–798, 2013.

TAYLOR-JONES, K.; POWELL, R. Interpreting zirconium-in-rutile thermometric results. *Journal of Metamorphic Geology*, v. 33, n. 2007, p. 115–122, 2015.

TEDESCHI, M. et al. Reconstruction of multiple PTt stages from retrogressed mafic rocks: Subduction versus collision in the Southern Brasília orogen (SE Brazil). *Lithos*, Elsevier, v. 294, p. 283–303, 2017.

TEDESCHI, M. et al. Protracted zircon geochronological record of UHT garnet-free granulites in the Southern Brasília orogen (SE Brazil): Petrochronological constraints on magmatism and metamorphism. *Precambrian Research*, Elsevier, v. 316, n. August, p. 103–126, 2018. ISSN 03019268. Avaible form internet: <https://doi.org/10.1016/j.precamres.2018.07.023>.

THOMAS, J. B. et al. TitaniQ under pressure: The effect of pressure and temperature on the solubility of Ti in quartz. *Contributions to Mineralogy and Petrology*, v. 160, n. 5, p. 743–759, 2010. ISSN 00107999.

THOMAS, J. B. et al. TitaniQ recrystallized: experimental confirmation of the original Ti-in-quartz calibrations. *Contributions to Mineralogy and Petrology*, v. 169, n. 3, 2015. ISSN 0010-7999. Avaible form internet: <http://link.springer.com/10.1007/s00410-015-1120-0>.

TIWARI, S. K.; BISWAL, T. K. Dynamics, epma th-u-total pb monazite geochronology and tectonic implications of deformational fabric in the lower-middle crustal rocks: A case study of ambaji granulite, nw india. *Tectonics*, Wiley Online Library, v. 38, n. 7, p. 2232–2254, 2019.

TOMKINS, H. S.; POWELL, R.; ELLIS, D. J. The pressure dependence of the zirconium-in-rutile thermometer. *Journal of Metamorphic Geology*, v. 25, n. 6, p. 703–713, 2007. ISSN 02634929.

TROUW, R. A. J. et al. The Central Segment of the Ribeira Belt. In: CORDANI, U. G. et al. (Ed.). *Tectonic Evolution of South America*. 1. ed. [S.l.]: COMPANHIA DE PESQUISA DE RECURSOS MINERAIS, 2000. p. 287–310.

TROUW, R. A. J. Evolução Tectônica ao Sul do Cráton de São Francisco, Baseada na Análise Metamórfica. In: *Boletim de Resumos Expandidos do XXXVII Congresso Brasileiro de Geologia*. [S.l.: s.n.], 1992. p. 327.

TROUW, R. A. J.; PACIULLO, F. V. P.; HEILBRON, M. Os Grupos São João Del Rei, Carrancas e Andrelândia Interpretados como a Continuição dos Grupos Araxá e Canastra. In: *Anais do XXXIII Congresso Brasileiro de Geologia*. Rio de Janeiro, RJ: [s.n.], 1984. p. 177–178.

TROUW, R. A. J. et al. A new interpretation for the interference zone between the southern Brasília belt and the central Ribeira belt, SE Brazil. *Journal of South American Earth Sciences*, v. 48, p. 43–57, 2013. ISSN 08959811.

VALERIANO, C. D. M.; SIMÕES, L. S. A. Geochemistry of proterozoic mafic rocks from the passos nappe (minas gerais, brazil): tectonic implications to the evolution of the southern brasilia belt. *Brazilian Journal of Geology*, v. 27, n. 1, p. 99–110, 1997.

VALERIANO, C. M. The Southern Brasília Belt. In: HEILBRON, M.; CORDANI, U. G.; ALKMIM, F. (Ed.). *São Francisco Craton, Eastern Brazil. Regional Geology Reviews*. Switzerland: Springer International Publishing, 2017. cap. The Southe, p. 189–203. ISBN 9783319017150.

VALERIANO, C. M. et al. A evolução tectônica da faixa brasília. In: _____. *Geologia do Continente sul-americano: evolução da obra de Fernando Flávio Marques de Almeida*. [S.l.]: Beca, 2004. p. 575–592.

VALERIANO, C. M. et al. U-Pb Geochronology of Southern Brasília Belt (SE Brazil): sedumentary provenance, Neoproterozoic orogeny and assembly of Western Gondwana. *Precambrian Research*, v. 130, p. 7–11, 2004.

VALERIANO, C. M. et al. Tectonic evolution of the Brasília Belt, Central Brazil, and early assembly of Gondwana. In: PANKHURST, R. J. et al. (Ed.). *West Gondwana: Pre-Cenozoic Correlations Across the South Atlantic Region*. Geological. London: [s.n.], 2008. p. 197–210.

VALERIANO, C. M. et al. Southern brasilia belt (se brazil): tectonic discontinuities, k-ar data and evolution during the neoproterozoic brasiliano orogeny. *Revista Brasileira de Geociências*, v. 30, n. 1, p. 195–199, 2000.

VLACH, S. R. F. Th-u-pbt dating by electron probe microanalysis, part i. monazite: analytical procedures and data treatment. *Geologia USP: Série Científica*, v. 10, n. 1, p. 61–85, 2010.

WESTIN, A. et al. The fast exhumation pattern of a neoproterozoic nappe system built during west gondwana amalgamation: Insights from thermochronology. *Precambrian Research*, Elsevier, v. 355, p. 106115, 2021.

WILLIAMS, M. et al. Format and philosophy for collecting, compiling, and reporting microprobe monazite ages. *Chemical Geology*, Elsevier, v. 225, n. 1-2, p. 1–15, 2006.

WILLIAMS, M. L.; JERCINOVIC, M. J.; HETHERINGTON, C. J. Microprobe monazite geochronology: understanding geologic processes by integrating composition and chronology. *Annu. Rev. Earth Planet. Sci.*, Annual Reviews, v. 35, p. 137–175, 2007.

WILLIAMS, M. L. et al. Electron Microprobe Petrochronology. *Reviews in Mineralogy and Geochemistry*, v. 83, n. 1, p. 153 LP – 182, 2017. Avaible form internet: <http://rimg.geoscienceworld.org/content/83/1/153.abstract>.

YAKYMCHUK, C.; BROWN, M. Divergent behaviour of Th and U during anatexis: Implications for the thermal evolution of orogenic crust. *Journal of Metamorphic Geology*, v. 37, n. 899-916, 2019.

ZACK, T.; KOOIJMAN, E. Petrology and geochronology of rutile. *Reviews in Mineralogy and Geochemistry*, Mineralogical Society of America, v. 83, n. 1, p. 443–467, 2017.

4 Metamorphic modeling and petrochronology of metapelitic rocks from the Luminárias Nappe, southern Brasília belt (SE Brazil)

Regiane Andrade Fumes[1*]; George Luiz Luvizotto[1]; Renato Moraes[2]; Monica Heilbron[3], Silvio Roberto Farias Vlach[2]

[1]Department of Petrology and Metallogeny, São Paulo State University, Av. 24A, 1515, 13506- 900, Rio Claro, Brazil *Corresponding author e-mail: regiane.fumes@unesp.br

[2]Department of Mineralogy and Geotectonics, University of São Paulo, Rua do Lago, 562, 05508-080, São Paulo, Brazil

[3]TEKTOS Research Group, Geology Institute, Rio de Janeiro State University, Rua São Francisco Xavier 524/4030-A, Maracanã, Rio de Janeiro 20550-900, Brazil

Abstract

Luminárias Nappe was formed in the agglutination of West Gondwana. A high-pressure metamorphic gradient, oblique to the geological contacts, is recorded in metapelitic rocks from the this Nappe. In the northern portion the metamorphic peak conditions are in high-pressure lower-amphibolite-facies at 580 ±4 °C and ∼0.9GPa (Chl+Ky+St+Ms+Qtz+Rt); in the central portion are in high-pressure amphibolite-facies at 600 ±15 °C and 1.1 ±0.3GPa (St+Bt+Grt+Ms+Qtz+Rt) and in the southern portion the metamorphic conditions reach the eclogite facies at 630 ±13 °C and 1.4 ±0.6 GPa (St+Ky+Grt+Ms+Qtz+Rt). Clockwise metamorphic P-T-t paths are registered in the studied rocks, with the increase of temperature and pressure followed by a strong decompression with retrograde phases as chloritoid (northern portion), chlorite and ilmenite (central portion) and biotite, chlorite and ilmenite (southern portion). U-Th-Pb $_T$ monazite ages range from 632 ±4Ma (southern portion) to 600 ±8Ma (northern portion-included crystals in garnet and staurolite). The metamorphic age, the high-pressure conditions calculated in this work and the clockwise metamorphic path indicate that the tectonic evolution of the Luminárias Nappe rocks is tightly related to the subduction and collision processes of the southern Brasília belt. The overprint of the younger Ribeira belt is interpreted to be responsible for tilting of the rock pile, producing the oblique metamorphic

gradient.

Keywords: West Gondwana, Monazite dating, THERMOCALC, single element geothermometer, pseudosection.

4.1 Introduction

Pressure-temperature-time (P-T-t) paths of high-pressure rocks are key to understand the evolution of an orogen. High-pressure rocks are the main record of deep portions of continental crust formed in convergent plate boundaries. Furthermore, they give insight into geodynamic processes that transform the rocks from the crust and lithospheric mantle into metamorphic and igneous rocks (MÖLLER et al., 2018). The root of precambrian eroded orogens, such as the Brasilia belt, Brazil, are crucial places to study high-pressure rocks. In eroded orogens a variety of high-pressure metamorphic rocks are exposed for hundreds of kilometers, giving the opportunity to study processes that take place in convergent plate boundaries.

In this sense, linking portions of the P-T path to ages, textures and equilibrium mineral assemblages is a key issue, since a well-defined P-T-t path can provide reliable information about metamorphic and tectonic processes. The concept of petrochronology has recently been introduced (FRASER; ELLIS; EGGINS, 1997) and deals with the fact that rocks face a complex history of heating, cooling and exhumation, and so, do not record just a single age. This concept is especially useful in areas where orogenic processes are overprinted.

The Luminárias Nappe comprises a set of quartzite and metapelitic rocks that represents part of the passive margin sequence of the São Francisco Craton, e.g. Paciullo et al. (2000). This passive margin was metamorphosed during the Ediacaran-Cambrian orogenesis that led to the agglutination of West Gondwana (DARDENNE, 2000; FUCK et al., 2017; HEILBRON; CORDANI; ALKMIM, 2017). There are controversial interpretations about the tectonic evolution of the Luminárias Nappe, that is, either in a single tectonic episode related to the formation of the southern Brasília belt (CAMPOS NETO, 2000; CAMPOS NETO et al., 2004; CAMPOS NETO et al., 2007; CAMPOS NETO et al., 2011; WESTIN et al., 2016) or as part of the interference zone between the southern Brasília and Central Ribeira belts (PETERNEL et al., 2005; TROUW et al., 2000; TROUW et al., 2013; HEILBRON et al., 2008; COELHO et al., 2017).

Previous regional studies in the southern Brasília belt and central Ribeira belt describe a regional metamorphic gradient with conditions increasing from north to south and from east to west, from greenschist to granulite facies conditions Trouw, Ribeiro e Paciullo (1980), Ribeiro e Heilbron (1982), Peternel et al. (2005), Reno et al. (2012), Trouw et al. (2000), Trouw et al. (2013) (with a regional metamorphic map)). Although

numerous studies describe the regional metamorphic gradient, they are mostly based on petrography and mineral assemblage of the rocks. Here, we present a more accurate and up to date approach to characterize the metamorphic conditions using pseudosection modeling, Zr-in-rutile and Ti-in-quartz thermometry and in-situ U-Th-Pb_T monazite EPMA dating. This work aims to define metamorphic conditions, *P-T-t* paths and age of metamorphism of metapelitic rocks from Luminárias Nappe, and with this, contribute to the understanding of the tectonic framework of the southern Brasília and Ribeira belts.

4.2 Geological Setting

The Brasília belt borders the western margin of São Francisco Craton (Fig. 4.1) in central and southwestern Brazil. It extends for more than 1100 km roughly in N-S direction and is the record of the convergence and collision that took place during the Brasiliano orogeny in the late Neoproterozoic, as part of West Gondwana amalgamation (DARDENNE, 2000; FUCK et al., 2017; HEILBRON; CORDANI; ALKMIM, 2017).

The Brasília belt is usually subdivided in northern and southern Brasília belts by the Pirineus Syntaxis (ARAÚJO FILHO, 2000). The southern portion of the Brasilia belt is dominated by metasedimentary rocks that underwent metamorphism and deformation during the Brasiliano orogeny, with metamorphic peak of ca. 650 – 630 Ma (VALERIANO, 2017). Most of these metasedimentary rocks represent sections of the stratigraphy of one of the former neoproterozoic passive margins developed around the São Francisco paleocontinent (VALERIANO, 2017).

The metasedimentary rocks south of São Francisco Craton were originally grouped into the São João del Rei and Andrelândia Groups (EBERT, 1956). Trouw, Ribeiro e Paciullo (1980) describe the metasedimentary rocks near Luminárias Nappe as the Carrancas Group, with intermediary characteristics between São João del Rei and Andrelândia Groups. The Carrancas Group is divided into the São Tomé das Letras Formation that is composed of quartzite and in the Campestre Formation that is composed of metapelites and quartzites (TROUW; RIBEIRO; PACIULLO, 1980; TROUW; RIBEIRO; PACIULLO, 1983) (Fig. 4.1). (ALMEIDA, 1992) did a detailed description of the geology, mapping the Luminárias region at scale 1:50.000. Further works (PACIULLO et al., 2000; PACIULLO; RIBEIRO; TROUW, 2003), interpret the Carrancas Group as two formations within the Andrelândia Megasequence, that is divided into six lithofacies (A1, A2, A3, A4 A5 and A6). The Campestre Formation from Luminárias Nappe corresponds (Fig. 4.1) to the A4 lithofacies (PACIULLO et al., 2000; PACIULLO; RIBEIRO; TROUW, 2003). The Megasequence is interpreted to be formed in a transition between a rift to passive margin succession, developed along the southern margin of the São Francisco paleocontinent during the Neoproterozoic (RIBEIRO et al., 1995; PACIULLO et al., 2000). An alternative

Figure 4.1 – Geological setting of the study area. (A) Gondwana map (ca. 500 Ma) showing the location of the study area (red rectangle). Extracted from Spencer et al. (2013). (B) Tectonic framework of the Ribeira and Southern Brasília belts extract from Heilbron et al. (2017). 1. Phanerozoic cover; 2. Upper Cretaceous alkaline plutons; 3 and 4 east verging units of the Brasília Belt, including the Guaxupé nappe and lower nappes; 5-7 Units of the São Francisco craton: 5. Paleoproterozoic Archean basement, 6. Neoproterozoic cratonic cover, Bambuí Group, 7. Mesoproterozoic to Neoproterozoic metasediments of autochthonous domains; 7-16 Terranes and structural domains of the Ribeira Belt: 8. Andrelândia and 9. Juiz de Fora domains of Occidental terrane, 10. Socorro Nappe; 11. Apiaí terrane; 12. Embú terrane; 13. Paraíba do Sul terrane; 14. Cambuci terrane; 15. Cryogenean to Ediacaran magmatic arc, 16. Neoproterozoic metasedimentary sucessions and 13. Tonian magmatic arc of the Oriental terrane; 12. Cabo Frio terrane. (C) Simplified geological map of the Luminárias Nappe. Modified after Quéméneur et al. (2003), Nunes, Trouw e Castro (2008), Paciullo e Ribeiro (2008), Trouw et al. (2013a). The geological map of Luminarias sheet is based on (ALMEIDA, 1992) and mapping of undergraduate courses in the 80ths of Federal University of Rio de Janeiro. The circles (white and black) show the localization of the studied metapelite samples. The arrows in the legend of the biotite gneiss interlayered with schists and quartzite is due the different interpretations presented in the literature of the age of this unit, according Ribeiro et al. (1995), Paciullo et al. (2000) this unit is Neoproterozoic (A1 and A2), however according Westin et al. (2016) this is a Paleoproterozoic unit (São Vicente Complex). Geographical coordinates of analyzed samples are present in Table 4.1.

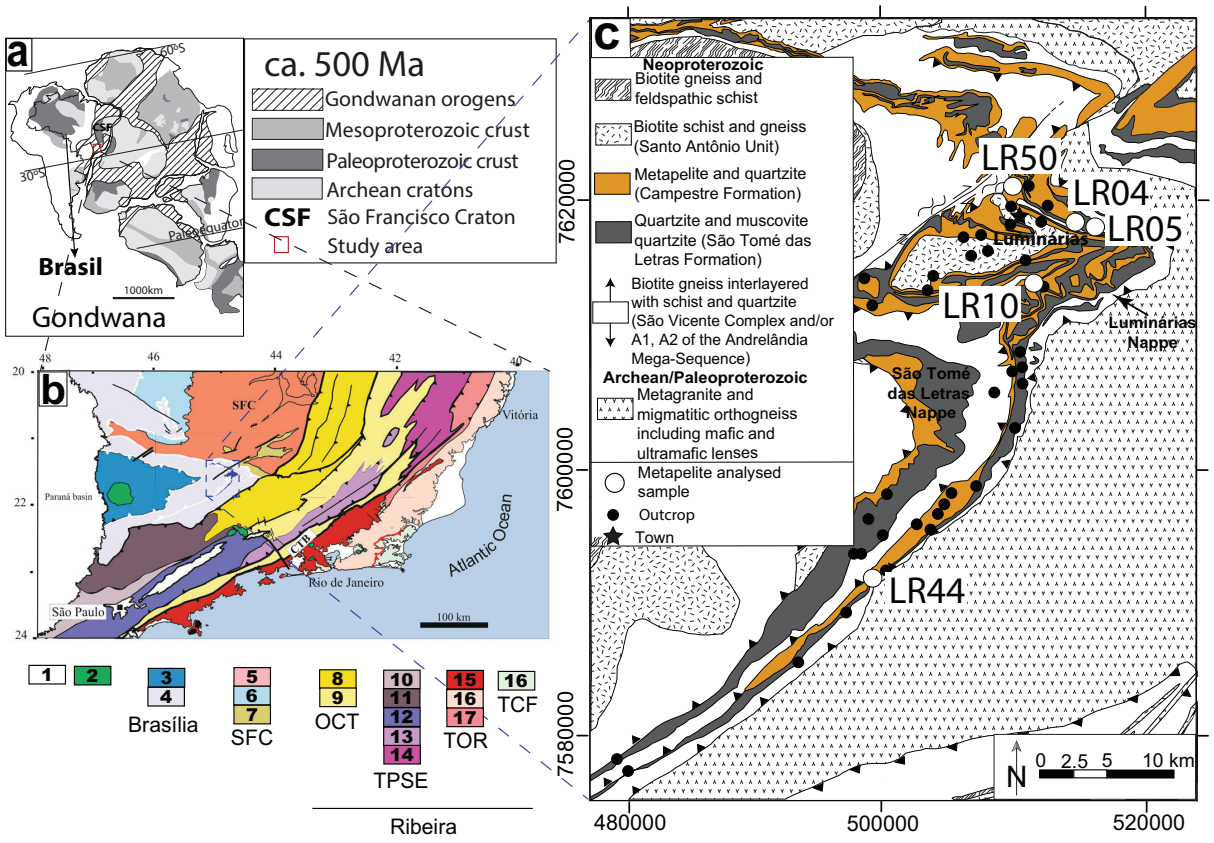

interpretation for the provenance of the basal lithofacies (A1 and A2 - biotite gneiss interlayered with schist and quartzite (Fig. 4.1) from Andrelândia Megasequence) is that these rocks belong to the Paleoproterozoic and have affinity with fore arc basin and trench deposits (WESTIN et al., 2016; WESTIN et al., 2019). According to Westin et al. (2016), Westin et al. (2019) the lithofacies A1 and A2 are called São Vicente Complex and are not

related either to the Carrancas Group or Andrelândia Megasequence.

The metasedimentary rocks from the southern Brasília belt are organized in a stack of syn-metamorphic thick-skinned nappes. From the structurally highest levels, in the west, to the structurally lowest levels, in the east, the following sequence of nappes can be recognized: (1) the Socorro-Guaxupé Nappe, that represents the middle and lower crust; (2) the Andrelândia Nappe System that is composed of the Três Pontas-Varginha Nappe and associated klippen, and the Liberdade and Andrelândia nappes (CAMPOS NETO et al., 2010); and (3) the Carrancas Nappe System and the Lima Duarte Nappe (CAMPOS NETO et al., 2004; CAMPOS NETO et al., 2007; CAMPOS NETO et al., 2010; WESTIN; CAMPOS NETO, 2013; WESTIN et al., 2016), also known as Lower Nappe System (Fig. 4.1). The Carrancas Nappe system is the farthest east and the deepest in the pile, containing deformed rocks of the former passive continental margin, located at the margin of São Francisco paleocontinent (CAMPOS NETO et al., 2010). This Nappe system is composed of rocks from Carrancas Group (TROUW; RIBEIRO; PACIULLO, 1980; TROUW; RIBEIRO; PACIULLO, 1983), associated with slices of basement, and is divided from structural top to bottom in the São Tomé das Letras Nappe, Luminárias Nappe, Carrancas-Itumirim Klippe, Serra da Bandeira allochthon and Madre de Deus allochthon (CAMPOS NETO et al., 2004).

The Brasília belt is in contact with the neoproterozoic Ribeira belt on its southeastern border (HASUI; CARNEIRO; COIMBRA, 1975; TROUW et al., 2000; HEILBRON et al., 2000; HEILBRON et al., 2004; HEILBRON et al., 2008; HEILBRON; CORDANI; ALKMIM, 2017). Contrasting interpretations of this region were presented in the literature, as this region is either described as an interference zone between the Brasília and Ribeira belts due to superposition of structures and metamorphism related to collision in both belts (PETERNEL et al., 2005; TROUW et al., 2000; TROUW et al., 2013; HEILBRON et al., 2008; HEILBRON; CORDANI; ALKMIM, 2017; COELHO et al., 2017) or it is considered as formed exclusively due to metamorphism and deformation related to the Brasília Orogeny (CAMPOS NETO, 2000; CAMPOS NETO et al., 2004; CAMPOS NETO et al., 2007; CAMPOS NETO et al., 2011; WESTIN et al., 2016).

Metamorphic conditions of Brasília belt rocks increase westwards from non-metamorphic and low-greenschist facies rocks, at the cratonic border in the east, to high-temperature amphibolite to granulite facies rocks, up to ultrahigh-temperature conditions at the metamorphic core (MORAES et al., 2002; MORAES et al., 2015), and decreases again westwards to amphibolite and greenschist facies towards the Goiás Magmatic Arc (FUCK et al., 2017). Previous metamorphic studies in the Carrancas Group rocks from the Luminárias Nappe show a metamorphic gradient increasing from greenschist facies, in the north, to amphibolite facies, in the south (TROUW; RIBEIRO; PACIULLO, 1980; RIBEIRO; HEILBRON, 1982; PETERNEL et al., 2005; RENO et al., 2012; TROUW et al., 2000; TROUW

et al., 2013). According to Campos Neto e Caby (1999), the metamorphic conditions of the Carrancas Group rocks (correlated to the study rocks) are high-pressure and low temperature, with metamorphic assemblage garnet-kyanite-chloritoid. Silva (2010) described in the Carrancas Klippe, also composed of rocks from Carrancas Group, a metamorphic gradient that increases to the southeast, from upper greenschist facies to high-pressure amphibolite facies in the transition to eclogite facies. A recent study in the metapelitic rocks of the Luminárias Nappe using average PT mode of THERMOCALC indicates the presence of a metamorphic gradient with conditions increasing from greenschist/amphibolite facies, in the northern and center-north portion, to amphibolite/eclogite facies in the southern portion (FUMES, 2017).

Neoproterozoic ages of metamorphism, peak and retrograde, from whole southern Brasília belt vary from 670 to 590 Ma (VLACH; GUALDA, 2000; CAMPOS NETO et al., 2004; VALERIANO et al., 2004; CAMPOS NETO et al., 2007; CAMPOS NETO et al., 2010; CAMPOS NETO et al., 2011; TROUW; TAVARES; ROBYR, 2008; RENO; BROWN; PICCOLI, 2010; RENO et al., 2012; WESTIN et al., 2016; COELHO et al., 2017; ROCHA et al., 2017; ROCHA et al., 2018; TEDESCHI et al., 2017; TEDESCHI et al., 2018). Monazite ages obtained with LA-ICP-MS from the Carrancas Klippe rocks (northeast of the Luminárias Nappe) are ca. 590-575 Ma (VALERIANO et al., 2004; CAMPOS NETO et al., 2010). According to (CAMPOS NETO et al., 2010; CAMPOS NETO et al., 2011) the younger ages of ca. 590 Ma determined for the Carrancas rocks are interpreted to represent the propagation and migration of the deformation and the metamorphism through the pile of nappes, from the upper to the lower nappes, where Luminárias Nappe is included. Alternatively, the younger ages can be interpreted as an effect of the Ribeira belt overprint.

4.3 Local Geology

The Luminárias Nappe croups out in a ∼80 km long N-S elongated nappe, near Luminárias town in Minas Gerais, in southeastern Brazil. In the northern portion of the study area (Fig. 4.1c), rocks from Luminárias Nappe present an irregular exposure pattern due to low-dipping folded layers exposed on a steep topography. Observed outcrops and collected samples cover the whole extend of the Luminárias Nappe (Fig. 4.1, Table 4.6 and Table 4.S1).

The Luminárias Nappe was thrusted over the basement rocks, which are composed of metagranite and migmatitic orthogneiss with lenses of mafic and ultramafic rocks. The basement is overthrusted by biotite gneiss interlayered with schist and quartzite from the São Vicente Complex and/or the basal formation of Andrelândia Group. At the top of the biotite gneiss, a group of quartzite and muscovite quartzite occurs (São Tomé das Letras

Formation). At its top the Campestre Formation crops out, composed of metapelitc rocks, the focus of this work, and quartzite. The uppermost unit of the Luminárias Nappe is composed of biotite schist and gneiss from Santo Antônio Unit.

Deformational structures in Luminárias Nappe region are grouped into three successive deformational phases (D_1, D_2 and D_3). Deformational phases D_1 and D_2 are related and responsible for the main flat lying composite foliation $S_1//S_2$ (CAMPOS NETO; CABY, 1999; CAMPOS NETO, 2000; TROUW et al., 2000; TROUW; TAVARES; ROBYR, 2008). Locally it is possible to distinguish these two phases using interference structures, such as fold and foliation overprint. Therefore, D_1 and D_2 are interpreted as representing a single progressive deformation related to later stages of subduction and continental collision (TROUW; TAVARES; ROBYR, 2008). As proposed by (TROUW; TAVARES; ROBYR, 2008) the main foliation observed in the rocks is the result of D_1 and D_2 deformation phases and is labeled here as $S_{1/2}$. Classification of foliations and kinematic interpretations of porphyroblasts presented here are according (PASSCHIER; TROUW, 2005). The $S_{1/2}$ foliation often occurs as a continuous foliation and occurs as a slaty cleavage in the northern portion and as schistosity in the southern portion of the Luminárias Nappe (Fig. 4.2). Sometimes $S_{1/2}$ occurs as a crenulation cleavage, where it is possible to identify the older, S_1 foliation preserved in the microlithons. Depending on the location of the rocks along the Luminárias Nappe, the main foliation $S_{1/2}$ is marked by different minerals, reflecting the metamorphic gradient. The relationship between the porphyroblasts and the main foliation changes as well. For example, in the northern portion the chloritoid porphyroblasts do not present strain shadows and deflection of external foliation around the porphyroblasts (Fig 4.2b), in different situation from the garnet porphyroblasts in southern portion which present strain shadows and deflection of external foliation around them (Fig. 4.2g).

4.4 Materials and Methods

The analytical work was done at the laboratories of the Department of Petrology and Metallogeny of São Paulo State University, Brazil, except for the LA-ICP-MS analysis, carried out at the Microgeochemistry Laboratory of the Department of Earth Sciences at the University of Gothenburg, Sweden. Petrography was carried out in polished thin sections (see locations in the Fig. 4.1 and Table 4.1) using optical and scanning electron microscopes. A JEOL JSM 6010LA SEM was used under a column accelerating voltage of 15 kV and varied beam currents to obtain backscattered electron images (BSE).

Table 4.1 – Location and metamorphic conditions of the studied quartzite samples. Coordinates are in UTM (Zone 23K, WGS84).

Analysed sample	UTM E	UTM S
LR04	516069	7620512
LR05	516522	7619845
LR10	513194	7615681
LR44	501284	7593736
LR50	510651	7604100

4.4.1 Whole-rock chemistry and pseudosection

Whole-rock chemical compositions for eleven samples were obtained by X-ray fluorescence. Representative sample powders were mixed with lithium tetraborate to obtain fused disks, that were analyzed with a Philips PW 2400 equipment. Loss on ignition (LOI) was determined by the conventional gravimetric method. Two P-T pseudosections were calculated for samples LR10C and LR44C, using the THERMOCALC (Powell and Holland 1988; Powell et al. 1998), version 3.40 and the internally consistent thermodynamic dataset

Figure 4.2 *(following page)* – Representative transmitted light photomicrographs and schematic representations from thin section of studied metapelite. a) Photomicrograph of staurolite and kyanite-bearing chlorite-chloritoid schist with showing an anhedral staurolite crystal in chlorite matrix from the northern portion (plane polarized light) (Sample LR05). b-I) Photomicrograph of chloritoid and kyanite-bearing muscovite schist showing the muscovite matrix and porphyroblasts of chloritoid (post-tectonic) from the northern portion (crossed polarized light) (Sample LR04). b-II) Schematic representation of photomicrograph b, showing the slaty cleavage / fine grained schistosity $S_1//S_2$ and the internal foliation in the post-tectonic chloritoid. c) Photomicrograph of muscovite schist with chloritoid and kyanite showing in detail the kyanite from the northern portion (plane polarized light) (Sample LR04). d) Photomicrograph of staurolite and biotite-bearing garnet schist showing a porphyroblast of garnet and porphyroblasts of staurolite in a matrix of muscovite, biotite and quartz and a biotite included in staurolite from the central portion (plane polarized light) (Sample LR10C). e-I) Photomicrograph of a staurolite-bearing garnet schist band showing a porphyroblast of garnet and porphyroblasts of staurolite in a matrix of muscovite, biotite and quartz from the central portion (plane polarized light) (Sample LR10E). e-II) Schematic representation of microphotograph e-I showing the schistosity, the inclusion pattern in the garnet and staurolite and the random orientation of chlorite. f) Photomicrograph of a staurolite and chloritoid-bearing garnet schist band showing a porphyroblast of chloritoid associated with staurolite from the central portion (plane polarized light) (Sample LR10E). g-I) Photomicrograph of kyanite-bearing garnet-staurolite schist showing a porphyroblast of garnet and staurolite and kyanite in the matrix. Sample from the southern portion (plane polarized light) (Sample LR44C). g-II) Schematic representation of photomicrograph g-I showing the continuous schistosity slightly deviated around garnet porphyroblast and the inclusions pattern in the garnet. h) Photomicrograph of kyanite-bearing garnet-staurolite schist showing a porphyroblast of garnet surrounded by biotite and chlorite with random orientation. Sample from the southern portion (plane polarized light) (Sample LR44C). Abbreviations according to Kretz (1983). HP=high-pressure.

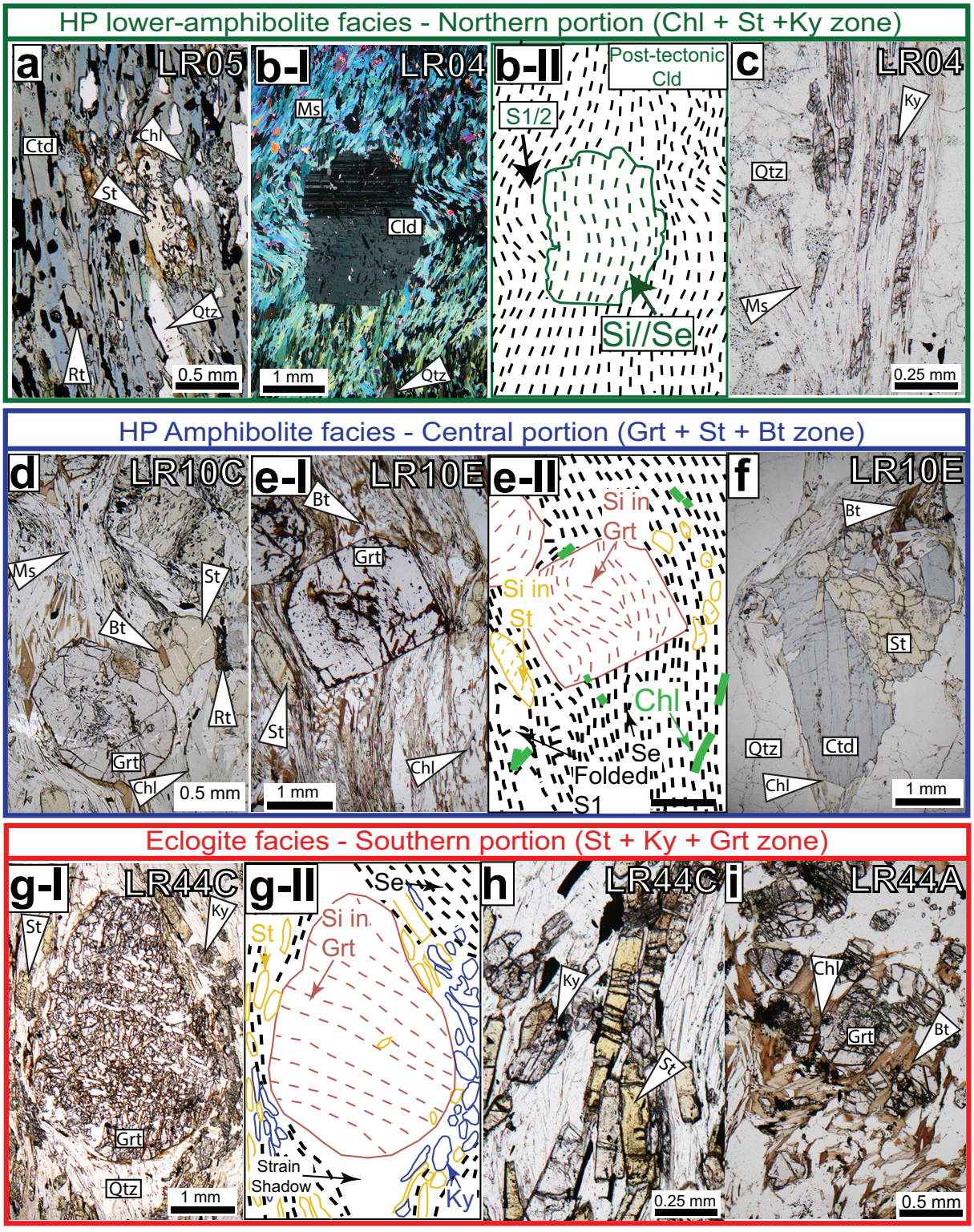
HP lower-amphibolite facies - Northern portion (Chl + St +Ky zone)
a
LR05
Ctd
Chl
St
Qtz
Rt
0.5 mm
b-I
LR04
Ms
Cld
1 mm
Qtz
b-II
Post-tectonic Cld
S1/2
Si//Se
c
LR04
Ky
Qtz
Ms
0.25 mm
HP Amphibolite facies - Central portion (Grt + St + Bt zone)
d
LR10C
Ms
St
Bt
Rt
Grt
Chl
0.5 mm
e-I
LR10E
Bt
Grt
St
Chl
1 mm
e-II
Si in Grt
Si in St
Chl
Se
Folded S1
f
LR10E
Bt
St
Qtz
Ctd
Chl
1 mm
Eclogite facies - Southern portion (St + Ky + Grt zone)
g-I
LR44C
St
Ky
Grt
Qtz
1 mm
g-II
Se
Si in Grt
St
Strain Shadow
Ky
h
LR44C
Ky
St
0.25 mm
i
LR44A
Chl
Grt
Bt
0.5 mm

tc-ds62 of Holland and Powell (2011), updated in February 2012. All calculations were based on the chemical model system K_2O-FeO-MgO-Al_2O_3-SiO_2-H_2O-TiO_2-O_2 (KFMASHTO), which represents a pelitic composition with the addition of TiO_2 and O_2 in order to evaluate rutile and ilmenite stability. As all samples lack plagioclase and present very low CaO (LR10C = 0.51 wt.%, LR44C = 0.15 wt.%) and Na2O (LR10C = 0.35 wt.%, LR44C = 0.28 wt.%) contents, these oxides were not considered in the investigated model system. Oxygen (O_2) contents were estimated as suggested by (WHITE et al., 2000) and, since the studied samples are ilmenite and rutile bearing free of hematite, a low O (0.11 mol.%) value was used.

4.4.2 Electron Microprobe Analysis (EPMA)

Chemical mineral analysis was carried out trough wavelength dispersive spectrometry (WDS) using a JEOL JXA-8230 Electron Microprobe equipped with 5 WDS detectors. Matrix correction was carried out online by the software provided by JEOL, using the ZAF method.

Garnet, chlorite, chloritoid, staurolite, biotite, and muscovite were analyzed under a focused beam with 15 kV and 20 nA for the column accelerating voltage and beam current, respectively. Point analyses were carried out in the core and rim of the minerals, as well as core-rim profiles, considering total counting times of 20s and 30s for major and minor elements, respectively, equally distributed on peak and background positions. Minerals and synthetic oxides, as referenced on the laboratory, were used as standards. Mineral formulae were computed with the AX software (HOLLAND, 2009).

Analyses of trace elements in rutile were made using a focused beam at 20 kV and 80 nA, following the method outlined by (LUVIZOTTO et al., 2009). Si, Al, Cr, Fe, Ta, Nb and Zr were measured and Si concentrations were used as a quality control to detect and avoid zircon inclusions as well as contamination. Following the recommendation of (ZACK; MORAES; KRONZ, 2004), measurements with Si concentrations higher than 300 ppm and with high Zr content were excluded from the dataset. R10 and Sy were used as secondary standards to ensure the quality and reproducibility of the analyses (LUVIZOTTO et al., 2009). Zr-in-rutile temperatures were calculated with the calibration of Tomkins, Powell e Ellis (2007).

Monazite dating (U-Th-Pb_T) has been carried out in samples LR10E and LR44C and followed the recommendations of Williams et al. (2006). A full thin section x-ray map (15 kV, 200 nA, 20-50 s dwell time and 30 μm electron beam size and step) was carried out for Ce and P to identify all monazite crystals and examine their textural relationships with other mineral phases. On selected monazite crystals high resolution compositional x-ray maps were carried out for Y, Al, Th, U, Pb, Si, Ca, Fe, La and Ce (15 kV, 100 nA, 100 s dwell time and 10 μm electron beam size and step). X-ray maps collected for

Table 4.2 – EPMA conditions applied for the monazite trace element analysis.

Element	X-ray line	Crystal	CH	Acc.v	Peak Pos.	BG_L Pos.	BG_U Pos.	Peak (s)	BG (s)	High Volt.	Base Line	Window	Standard	Conc. Std. (%)	Curr. (A)	D.L. (ppm)
Y	La	TAP	1	15	70.048	1.25	1	100	50	1635	3.5	3.2 (V)	Y2O3 P&H	11.80	1.00E-07	110
Si	Ka	TAP	2	15	77.314	1.65	1.05	40	20	1630	2.2	4.1 (V)	Wollastonite P&H	50.96	2.00E-08	60
Al	Ka	TAP	2	15	90.577	2.47	1.72	40	20	1630	2.2	4.1 (V)	Al2O3 P&H	99.99	2.00E-08	50
Th	Ma	PETJ	3	15	132.571	2	1.95	140	70	1670	3.7	3.9 (V)	Th Glass MAC	5.90	1.00E-07	160
Ca	Ka	LIF	3	15	233.493	0.7	1.1	10	5	1628	0.9	3.0 (V)	Apatite	54.02	2.00E-08	240
La	La	LIF	3	15	185.373	1.45	1.65	10	5	1628	2.4	2.0 (V)	La2O3 P&H	11.50	2.00E-08	1200
Ce	La	LIF	3	15	178.132	1.45	1.65	10	5	1628	2.3	2.0 (V)	CeO2 P&H	11.90	2.00E-08	1200
Pr	Lb	LIF	3	15	157.127	0.75	0.85	10	5	1628	2.7	2.0 (V)	Pr6O11 P&H	12.20	2.00E-08	1600
Nd	Lb	LIF	3	15	150.713	0.9	1	10	5	1628	2.3	2.0 (V)	Nd2O3 P&H	11.80	2.00E-08	1900
Sm	Lb	LIF	3	15	139.059	0.55	0.55	10	5	1628	3.2	1.8 (V)	Sm2O3 P&H	11.20	2.00E-08	1800
Fe	Ka	LIF	3	15	134.693	0.75	0.65	10	5	1628	2.4	3.1 (V)	Ilmenite MCS	35.03	2.00E-08	400
Gd	Lb	LIF	3	15	128.512	1	1	10	5	1628	3.5	2.1 (V)	Gd2O3 P&H	12.10	2.00E-08	1800
Er	La	LIF	3	15	124.195	0.75	0	10	5	1628	3.3	2.3 (V)	Er2O3 P&H	11.90	2.00E-08	1130
Tb	Lb	LIF	3	15	123.669	0.45	0	10	5	1628	3.7	2.0 (V)	Tb2O3 P&H	11.90	2.00E-08	2200
Dy	Lb	LIF	3	15	119.035	0.65	0.55	10	5	1628	3.7	2.3 (V)	Dy2O3 P&H	12.00	2.00E-08	1960
Yb	La	LIF	3	15	116.35	1.5	1.45	10	5	1628	3	2.0 (V)	Yb2O3 P&H	12.00	2.00E-08	1430
U	Mb	PETL	4	15	118.932	3.98	3.98	300	150	1670	3	2.7 (V)	UO2 MAC	99.80	1.00E-07	65
S	Ka	PETL	4	15	172.02	-	2	10	5	1670	3	2.5 (V)	PbS P&H	33.46	2.00E-07	160
P	Ka	PETH	5	15	197.105	2.1	2.65	10	5	1686	1.7	3.0 (V)	Apatite	40.78	2.00E-08	150
Pb	Ma	PETH	5	15	169.251	3.65	4.2	300	150	1686	1.8	3.0 (V)	PbS P&H	93.29	2.00E-07	40

CH: Spectrometer Chanel; Acc. V: Acceleration voltage; Peak Pos.: Peak position in mm; BG_L Pos.: Lower backbround position in mm from the peak; BG_U Pos.: Upper background position in mm from the peak; Peak (s): counting time on peak positon in s; BG (s): Counting time on each background (upper and lower) position in s; Conc. Stds (%): Concentration of the element in the standard Curr. A: Current of standard analyses in A; D.L.: Minimum detection limit (3 sigma) for the unknowns; MAC: Micro-Analysis Consultants Ltd. P and H Developments Ltd. MCS

crystals form the same sample were processed together (i.e., using the same color table for all crystals). This way, concentration levels and zoning characteristics can be compared from crystal to crystal. The maps are then used to target distinctive domains for spot analyses and age calculations. Differently from the procedures highlighted by Williams et al. (2006), background measurements were performed for all analyses. Point analyses followed the method outlined by Vlach (2010), and the analytical conditions are presented in Table 4.2. Sample current values used for the analyses varied from 80 to 200 nA and were constantly monitored to evaluate and avoid beam damage. Every 10 to 20 analyses on the unknowns were bracketed by 3 analyses on the Moacir monazite secondary standard to evaluate the quality of the analyses. Spectral interference corrections (Th on U Mb and Th + Y on Pb Ma) were carried out offline and considered matrix correction factors. Interference corrections and age calculations were performed using the Age_Cor program (VLACH, 2010).

4.4.3 LA-ICP-MS

Trace elements analyses in quartz were carried out by a New Wave NWR213 laser ablation system coupled to an Agilent 8800 triple quadrupole ICP-MS. The carrier gas was a He-Ar mixture. Helium gas carries the laser ablated sample aerosol from the sample cell, the He gas is mixed with Ar carrier gas and N to enhance sensitivity that flows into the ICP-MS torch. He was flushed through the ablation cup at 1 ml/min. A laser beam with diameter of 10 μm at laser energy of 6.7 J/cm^2 and a repetition rate of 4 Hz is used to ablate the sample. The signals were recorded over 60 s for each spot. The first 20 s were used to measure the background, while the next 30 s for acquiring the analysis signal and the last 10 s were used for system wash out. The following isotopes were analyzed: ^{2}Li, ^{27}Al, ^{29}Si, ^{48}Ti, ^{49}Ti, ^{57}Fe and ^{72}Ge. Ti concentrations were calculated using ^{49}Ti to avoid the isobaric interference from ^{49}Ca (present in most well characterized reference glasses) on ^{48}Ti. The SRM 610 was used as the calibration standard. Ti-in-Quartz temperatures were calculated using the calibration of (THOMAS et al., 2010).

4.5 Sample descriptions: microstructures and mineral assemblages

In the following descriptions and throughout the text, the metapelitc rocks from Campestre Formation are grouped according to their geographical distribution and mineral assemblages. In all results and discussion, quartz and muscovite are omitted from mineral assemblages, as they are phases in excess. It is considered that a fluid rich in H_2O was also in excess and present during the metamorphism. A summary of mineral chemistry of the samples is presented below. A detailed description of the mineral chemistry of the studied rocks can be found in (FUMES, 2017).

4.5.1 High-pressure lower-amphibolite facies - Northern portion of the Luminárias Nappe (samples LR04, LR50 and LR05)

Staurolite and kyanite-bearing chlorite-chloritoid schist; and chloritoid and kyanite-bearing muscovite schist are the metapelitic rocks from the northern portion (Fumes 2017). In both rocks, the foliation $S_{1/2}$ is a slaty cleavage / fine-grained schistosity and texture is lepidoblastic.

The continuous schistosity of the staurolite and kyanite-bearing chlorite chloritoid schist (sample LR05) is defined by chloritoid, chlorite, quartz, muscovite, rutile, staurolite, kyanite, ilmenite, zircon and apatite (Fig. 4.2a). Staurolite only occurs as anhedral crystals with rims replaced by chlorite (Fig. 4.2a). Chlorite also occurs as anhedral crystals, always associated with the chloritoid crystals (Fig. 4.2a).

In the muscovite schist with chloritoid and kyanite (samples LR04 and LR50), the rock matrix is composed of muscovite, quartz, kyanite, ilmenite, rutile, zircon and chlorite (Fig. 2b and c). The foliation is slightly crenulated according to F_3 microfolds. Chloritoid occurs as porphyroblasts, with abundant inclusions of quartz, ilmenite and rutile, that is orientated parallel to main foliation $S_{1/2}$. Based on their microstructural relationship, overgrowing the main cleavage, and the absence of strain shadows, chloritoid porphyroblasts are interpreted to be post-tectonic to the main foliation $S_{1/2}$ (Fig. 2b). The average formula of the chloritoid porphyroblasts is $Fe^{+2}{}_{0.77}Mg_{0.16}Mn_{0.05}Al_{1.95}Fe^{+3}{}_{0.07}Si_{0.99}O_5(OH)_2$ with X_{Fe} (Fe/Fe+Mg) ratio between 0.81-0.87. Chlorite average formula is $Mg_{2.02}Fe^{+2}{}_{2.43}Mn_{0.05}Si_{2.51}Al_{2.94}Fe^{+3}{}_{0.02}Na_{0.01}O_{10}(OH)_{16}$ and X_{Fe} ranges between 0.51 and 0.59.

The peak metamorphic assemblage in the northern portion is represented by Chl+Ky+St+Rt, under high-pressure lower-amphibolite facies conditions. As chloritoid in sample LR04 is post-tectonic to $S_{1/2}$, (Fig. 2b), it is interpreted as a retrograde phase, not present in the peak metamorphic assemblage.

4.6 High-pressure amphibolite facies - Central portion of the Luminárias Nappe (samples LR10C and LR10E)

In the central portion the main rock type is a staurolite-biotite-garnet muscovite schist (sample LR10C, Fig. 2d), in which muscovite, biotite and quartz define the main and homogeneous schistosity ($S_{1/2}$). Ilmenite, zircon, monazite and rutile occur as accessory minerals and follow the fabric of the main foliation. Garnet porphyroblasts range from 1 to 5 mm in diameter, whereas staurolite varies from 1 to 2.5 mm in length. Both porphyroblasts contain abundant inclusions of quartz, monazite, ilmenite and tourmaline. Biotite crystals occur oriented along the $S_{1/2}$ foliation, in contact with garnet as well as included in staurolite. This texture indicates that biotite is in equilibrium with garnet and staurolite (Fig. 4.2d and e). Furthermore, garnet and staurolite are interpreted as syntectonic with relation to $D_{1/2}$ because their inclusion patterns are rotated and curved (Fig. 4.2d). Therefore, the peak metamorphic assemblage in the central portion is Bt+St+Grt+Rt, which is stable under amphibolite facies conditions. Chlorite occurs as a retrograde phase at garnet and staurolite rims as well as replacing biotite. Chlorite does not follow the main foliation (Fig. 4.2d).

Sample LR10E is from the same outcrop as sample LR10C, but this sample is banded with distinct mineral assemblages in each band. One band is composed of garnet, muscovite, staurolite and quartz (Fig. 4.2e), whereas the other of chloritoid, staurolite, quartz, muscovite and biotite (Fig. 4.2f). In both bands ilmenite, rutile, monazite and zircon are accessory minerals and chlorite occurs as a retrograde phase (Fig. 4.2e). Garnet, chloritoid and staurolite are porphyroblasts, with average diameter of 2.0, 1.5 and 1.0 mm, respectively. The foliation is defined by the preferred orientation of muscovite, biotite, staurolite and quartz and is classified as a fine-grained schistosity ($S_{1/2}$). Garnet and staurolite porphyroblasts have inclusions of ilmenite, quartz and tourmaline. Both staurolite and garnet porphyroblasts are interpreted as syntectonic to $S_{1/2}$ based on the inclusion pattern that indicates rotation and on the continuity of the internal foliation defined by inclusions (Si) and the external foliation (Se // $S_{1/2}$). Chloritoid porphyroblasts with corroded rims are associated with euhedral staurolite (Fig. 4.2f) and are interpreted as pre-tectonic to $S_{1/2}$. The compositional banding and the mineral assemblages described above indicate that equilibrium was only attained within the same compositional band. Although mineral phases from both compositional bands may have coexisted in different domains in the rock, they are not necessarily in equilibrium with each other. Since sample LR10C has a relatively homogeneous composition (i.e., it is not banded), it is taken as a representative sample of the central portion of the Luminárias Nappe.

In the central portion of Luminárias Nappe the garnet prophyroblasts are intensely zoned with higher contents of grossular and spessartine in the core, whereas almandine and

pyrope increase towards the rims. Garnet formula is $Fe^{+2}_{2.2-2.6}Mn_{0-0.2}Mg_{0.2-0.4}Ca_{0.2-0.5}Ti_{0-0.3}Fe^{+3}_{0-0.2}Al_{1.9-2}Si_{2.8-3}O_{12}$ and the medium X_{Fe} has almost no variation from core to rim, from 0.86 to 0.87. The average formula of the staurolite in this sample is $Fe^{+2}_{3.18}Mg_{0.55}Mn_{0.01}Ti_{0.12}Cr_{0.01}Al_{17.7}0Si_{7.72}\ O_{46.5}H_3$ with X_{Fe} medium of 0.85 (0.84-0.86) and Zn content varying from 0,05 to 0,13 a.p.f.u.. Biotite has 0.08 a.p.f.u. of Ti and X_{Fe} is 0.51. Muscovite has X_{Fe} 0.47.

Monazite is observed in all samples from the central portion. This mineral occurs in the matrix and included in garnet, staurolite and rutile. In sample LR10A, similar to LR10C, rounded crystals of allanite occur associated to anhedral monazite crystals (Fig. 4.3).

Figure 4.3 – Back-scattered electron (BSE) image from LR10A sample showing a monazite associated with circular allanite crystals in the rock matrix.

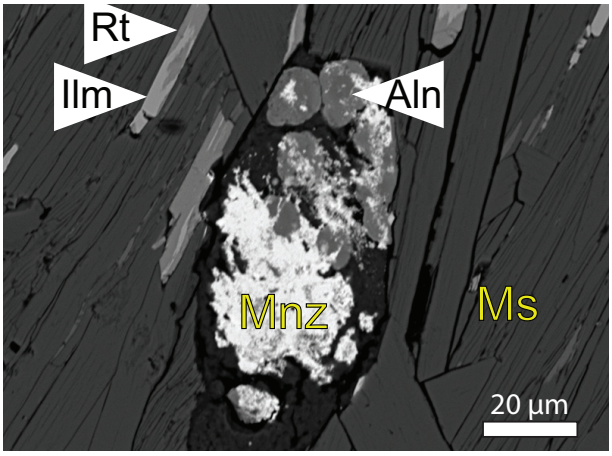

4.6.1 Eclogite facies - Southern portion of the Luminárias Nappe (Samples LR44C and LR44A)

Southern portion rocks are represented by sample LR44C, a garnet-staurolite schist where the matrix is composed of staurolite, muscovite, quartz, kyanite, rutile, ilmenite, zircon, monazite and garnet. The latter occurs as porphyroblasts with inclusions of quartz, staurolite, ilmenite, monazite and rutile (Fig. 4.2g). Oblique internal inclusions and strain shadows indicate that the garnet porphyroblasts are syntectonic to $S_{1/2}$. The continuous schistosity is defined by preferred orientation of staurolite, quartz and kyanite. Kyanite crystals are often observed associated with staurolite (Fig. 4.2h), indicating equilibrium between the two minerals. Therefore, textural relationships indicate that the metamorphic peak assemblage is St+Ky+Grt+Rt, a high-pressure, amphibolite to eclogite facies assemblage. Biotite and chlorite are interpreted as retrograde phases, since both minerals occur with random orientation in the matrix or at the garnet rims (Fig. 4.2i).

The garnet porphyroblasts from southern portion are also zoned with representative formula of $Fe^{+2}_{1.6-2.5}Mn_{0-0.6}Mg_{0.1-1.2}Ca_{0-0.5}Ti_{0-0.5}Fe^{+3}_{0-0.8}Al_{1.8-2}Si_{2.6-3}O_{12}$, in the

cores *XFe* is 0.90 and in rims it is 0.89. Garnet cores present higher contents of spessartite and lower almandine percentages, whereas pyrope and grossular maintain constant concentrations along sections through all the garnet crystals. Staurolite average composition is $Fe^{+2}{}_{3.18}Mg_{0.59}Mn_{0.03}Ti_{0.13}Cr_{0.01}Al_{17.59}0Si_{7.77}O_{46.5}H_3$ with X_{Fe} of 0.84 and Zn content varies from 0.01 and 0.03 a.p.f.u.. The X_{Fe} of the muscovite is 0.44.

4.7 *P-T* Pseudosection

P-T pseudosections calculated for samples LR10C (amphibolite facies, central portion) and LR44C (eclogite facies, southern portion) are presented in Fig 4.4. Whole rock chemical composition (in molar proportion) is presented in Fig. 4.4. The projection is in the system KFMASHTO and the minerals involved in the calculations are quartz, muscovite, garnet, chloritoid, staurolite, ilmenite, rutile, chlorite, kyanite, sillimanite, K-feldspar and water. Quartz and muscovite are ubiquitous in the studied rocks and metamorphism took place under sub-solidus *P-T* conditions. Therefore, quartz, muscovite and water were set to be in excess. The two *P-T* pseudosections (samples LR10C and LR44C) have a similar topology and were calculated between 0.4-1.8 GPa and 450-700 °C (Fig. 4.4a and b). In both diagrams, the chloritoid stability is exclusively controlled by temperature and the mineral is stable at temperatures below 590 °C. The occurrence of chlorite is also controlled by temperature. In the pseudosection calculated for sample LR10C, chlorite occurs along all the P range and in T lower than 615 °C. In the pseudosection calculated for sample LR44C, chlorite occurs under P conditions lower than 1.4 GPa and T lower than 580 °C. For both samples, staurolite occurs in T between 505 and 690 °C and P lower than 1.7 GPa. Garnet is stable in P higher than 0.8 GPa and T higher than 490 °C in the pseudosection of the LR10C sample and 555 °C in the pseudosection of sample LR44C. Biotite occurs at P lower than 1.1 GPa and at T higher than 480 °C in the pseudosection of sample LR10C and 530 °C in the pseudosection of sample LR44C. Kyanite and sillimanite are the aluminum silicates that appear in the pseudosections, within the investigated *P-T* range. Kyanite is stable at T higher than 580 °C and P higher than 0.8 GPa, whereas sillimanite is only stable at P lower than 0.8 GPa and T higher than 580 °C. Ilmenite and rutile are the Ti-bearing phases, the former is stable at P lower than 1.0 GPa and T lower than 500 °C and the latter is only stable in conditions of P higher than 1.0 GPa and T higher than 500 °C. Muscovite, quartz and water are stable and appear in all the fields except for T higher than 575 °C and P lower than 0.5 GPa were K-feldspar occurs instead of muscovite.

According to the calculated pseudosections (Fig. 4), the mineral peak assemblage of the central portion of the Luminárias Nappe (St+Bt+Grt+Rt) is stable from 590 to 685 °C and from 0.9 to 1.2 GPa. The mineral peak assemblage that represents the southern portion of the Luminárias Nappe (St+Ky+Grt+Rt) occurs in a tight diagonal field and is

Figure 4.4 – Pressure-Temperature (P-T) pseudosections for Luminárias Nappe from the bulk compositions (presented on top of the diagram in molar proportion) calculated for the KFMASHTO model chemical system. The arrow indicates the P-T-t paths. (a) P-T pseudosection for sample LR10C (central portion of the Luminárias Nappe). (b) P-T pseudosection for sample LR44C (southern portion of the Luminárias Nappe).

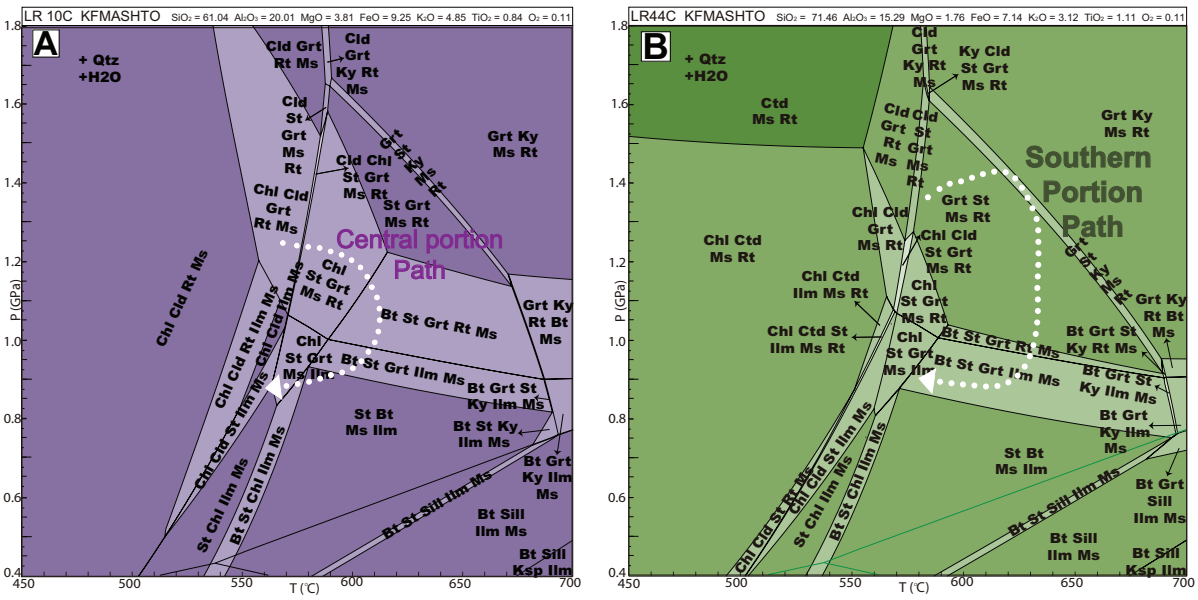

stable from 585 to 690 °C and from 0.9 to 1.65 GPa that corresponds to high-pressure amphibolite - eclogite facies transition.

4.8 Single Element thermobarometry

Single element thermobarometry is applied as an independent technique to constrain the metamorphic peak. The geothermometers applied in this study are the Zr-in-rutile and the Ti-in-quartz and both are suitable to be applied here since all rocks contain quartz, zircon and rutile in excess.

4.8.1 Trace Elements in Rutile and Quartz

Rutile crystals from five samples, LR04, LR05, LR10C, LR10E and LR44C, were analyzed. Trace elements rutile data obtained for all the studied samples are presented in Table 4.3 and Fig. 4.6.

In samples LR04 and LR05, from the northern portion of the Luminárias Nappe (high-pressure lower-amphibolite facies mineral assemblage, since the mineral peak assemblage is chlorite+kyanite+staurolite+muscovite+quartz+rutile), rutile is abundant and occurs as subhedral crystals in the matrix. Most rutile crystals contain ilmenite needles and zircon inclusions (Fig. 4.5a, b and c).

In samples LR10C and LR10E, from the central portion (high-pressure amphibolite facies mineral assemblage), rutile is rare, has an anhedral shape and is frequently associated

Table 4.3 – Trace element composition (in ppm) of analyzed rutile from LR04, LR05, LR10C and LR44C samples. DL: 2 sigma minimum detection limit (in ppm). RSE: Relative standard errors from counting statistics (2 sigma). T (Temperature) is calculate using equation of Tomkins et al. (2007). P (Pressure) estimate based on the pseudosection. *: data plotted in figure 5 (grains with more than 1 spot). T (°C) + and T (°C) - : errors in temperature calculated based on the RSE, BD: bellow detection limit.

	DL		25	20	40	50	85	45	40					RSE in ppm						
Sample	Spot	Texture	Si	Al	Fe	Cr	Ta	Zr	Nb	P (Gpa)	T (°C)	T (°C) +	T (°C) -	Si	Al	Fe	Cr	Ta	Zr	Nb
LR04	Rt1-1	Mtx	108	191	9662	1478	BD	BD	1573					3	3	19	8			9
LR04	Rt1-2*	Mtx	159	275	10649	1492	254	89	11345	0.9	557	5	6	3	3	20	8	14	8	16
LR04	Rt2	Mtx	93	228	10097	1752	328	104	12163	0.9	567	5	5	3	3	19	8	14	7	17
LR04	Rt3	Mtx	BD	90	12864	1444	180	96	11646	0.9	563	5	5		3	22	8	14	8	16
LR04	Rt4	Mtx	136	254	11683	1512	532	126	12904	0.9	581	4	4	3	3	21	8	14	8	17
LR04	Rt5	Mtx	215	619	8807	814	303	148	5746	0.9	592	4	4	3	3	18	7	14	8	13
LR04	Rt7	Mtx	276	365	9880	972	262	126	6585	0.9	581	4	4	3	3	20	7	14	8	13
LR04	Rt8	Mtx	238	614	9678	958	BD	89	7606	0.9	557	5	6	3	3	19	7		7	14
LR04	Rt9C	Mtx	266	714	9685	1019	BD	81	4530	0.9	552	6	6	3	3	19	7		8	12
LR04	Rt9D	Mtx	252	656	8714	931	98	104	4292	0.9	567	5	5	3	3	18	7	15	8	11
LR04	Rt9E	Mtx	299	794	8550	978	BD	111	4257	0.9	572	5	5	3	3	18	7		8	11
LR04	Rt11	Mtx	89	212	6475	445	BD	104	1482	0.9	567	5	5	3	3	16	6		7	9
LR04	Rt13	Mtx	178	524	5519	855	BD	133	2922	0.9	585	4	4	3	3	15	7		7	10
LR05	Rt1-1*	Mtx	192	418	8434	1505	BD	BD	10723	0.9		9	10	3	3	19	8			16
LR05	Rt1-2	Mtx	206	429	5395	1266	BD	BD	3083	0.9				3	3	15	8			10
LR05	Rt6	Mtx	252	656	5503	978	BD	BD	BD	0.9				3	3	15	7			
LR05	Rt7	Mtx	220	614	5348	BD	BD	BD	98	0.9		10	12	3	3					7
LR05	Rt8	Mtx	229	566	9079	828	106	BD	11408	0.9		10	12	3	3	19	7			16
LR05	Rt9	Mtx	187	572	5690	657	BD	BD	BD	0.9				3	3	15	7			
LR05	Rt10	Mtx	271	175	7921	1273	BD	52	5564	0.9	523	7	8	3	3	17	8		6	12
LR10C	Rt3	Mtx	210	217	2293	62	BD	141	1510	1.1	597	3	3	3	3	12	5		6	7
LR10C	Rt4	Mtx	266	307	2371	BD	131	104	881	1.1	575	4	4	3	3		4	12	6	6
LR10C	Rt10	Mtx	131	228	2130	BD	106	74	993	1.1	553	5	5	3	3		4	12	6	7
LR10E	Rt1-1*	Mtx	98	262	4229	BD	BD	149	912	1.1	601	13	15	12	11				28	36
LR10E	Rt1-2	Mtx	125	131	3893	BD	BD	99	1211	1.1	572	17	21	12	11				27	37
LR10E	Rt7	Mtx	227	327	1725	BD	BD	149	1180	1.1	601	13	15	12	11				28	37
LR44C	Rt68-1*	Mtx	159	206	1119	62	BD	BD	1342					11	8	29	17			32
LR44C	Rt68-2	Mtx	257	487	1422	89	BD	BD	1797					11	9	30	17			35
LR44C	Rt65-1*	Incl. Grt	28	450	7758	554	1679	192	12960	1.4	632	8	9	10	9	51	19	53	21	66
LR44C	Rt65-2	Incl. Grt	BD	413	7128	506	1032	163	11583	1.4	619	9	10		9	49	19	52	21	64
LR44C	4_Rt1_1*	Mtx	89	196	1158	62	BD	BD	762					10	8	29	18			30
LR44C	4_Rt1_2	Mtx	65	127	1998	BD	BD	BD	426					10	8		16			28
LR44C	4_Rt1_3	Mtx	28	79	941	BD	BD	BD	510					10	8		17			29
LR44C	5_Rt1_1*	Mtx	84	318	1283	62	BD	BD	643					10	9	30	16			29
LR44C	5_Rt1_2	Mtx	51	106	1026	BD	BD	BD	1070					10	8		16			31
LR44C	6_Rt1_1*	Mtx	BD	69	715	BD	BD	BD	419						8		19			28
LR44C	6_Rt1_2	Mtx	BD	58	490	BD	BD	BD	482						7		17			28
LR44C	6_Rt1_3	Mtx	BD	64	575	55	BD	BD	615						7	26	17			29
LR44C	7_Rt1_1	Incl. Grt	28	111	5099	335	BD	185	3230	1.4	629	8	9	11	8	43	18		21	40
LR44C	7_Rt2_1	Incl. Grt	70	228	8955	643	786	192	9863	1.4	632	8	9	10	8	54	20	51	21	59
LR44C	7B_Rt1_1*	Incl. Grt	28	238	6654	561	647	192	7494	1.4	632	8	9	9	8	48	19	51	21	53
LR44C	7B_Rt1_2	Incl. Grt	BD	222	6452	547	197	170	7361	1.4	623	9	10		8	47	19	50	21	53
LR44C	8_Rt1_1	Incl. Grt	BD	233	6459	554	213	178	7361	1.4	626	8	9		8	48	19	49	20	53
LR44C	3_Rt1_1	Mtx	28	48	466	BD	BD	BD	1685					11	7		17			34
LR44C	3_Rt1_2*	Mtx	BD	BD	513	BD	82	BD	1251								15	50		32
LR44C	Rt1(mount)	Incl. Grt	52	267	11124	493	BD	170	14362	1.4	622	11	13	12	11	60	37		28	80

with ilmenite in a texture that indicates that the latter replaces rutile (Fig. 4.5e). Rutile does not occur as inclusion in garnet and several crystals have zircon inclusions. Due to characteristics described above, only 6 out of 23 analyses of samples LR10C and LR10E passed adopted quality control, that is, Si content below 300 ppm.

In sample LR44C, from the southern portion (eclogite facies mineral assemblage), rutile crystals are mostly free of inclusions, although sometimes a few ilmenite needles and zircon inclusions are observed. Rutile crystals have subhedral shape and occur either in the matrix or as inclusion in garnet (Fig. 4.5d).

Rutile crystals from the northern portion samples (LR04 and LR05) have similar composition of trace elements and have the highest contents of Nb (several rutile crystals

Figure 4.5 – Back-scattered electron (BSE) images of representative rutile grains with concentrations of Zr (in ppm). A) Rutile (Rt7) from LR04 sample (northern portion). B) Rutile (Rt8) from the LR05 sample (northern portion). C) Rutile (Rt10) from the LR05 sample (northern portion) with ilmenite inclusion and ilmenite lamella. D) Rutile (Rt7) from LR44C sample (southern portion) included in garnet. Ilmenite lamella is observed in a grain. E) Rutiles (Rt3 and Rt4) from LR10C (northern portion) sample associate with ilmenite. Red circles indicate position of the analyzed spots. Grains are labelled according Table 4.2.

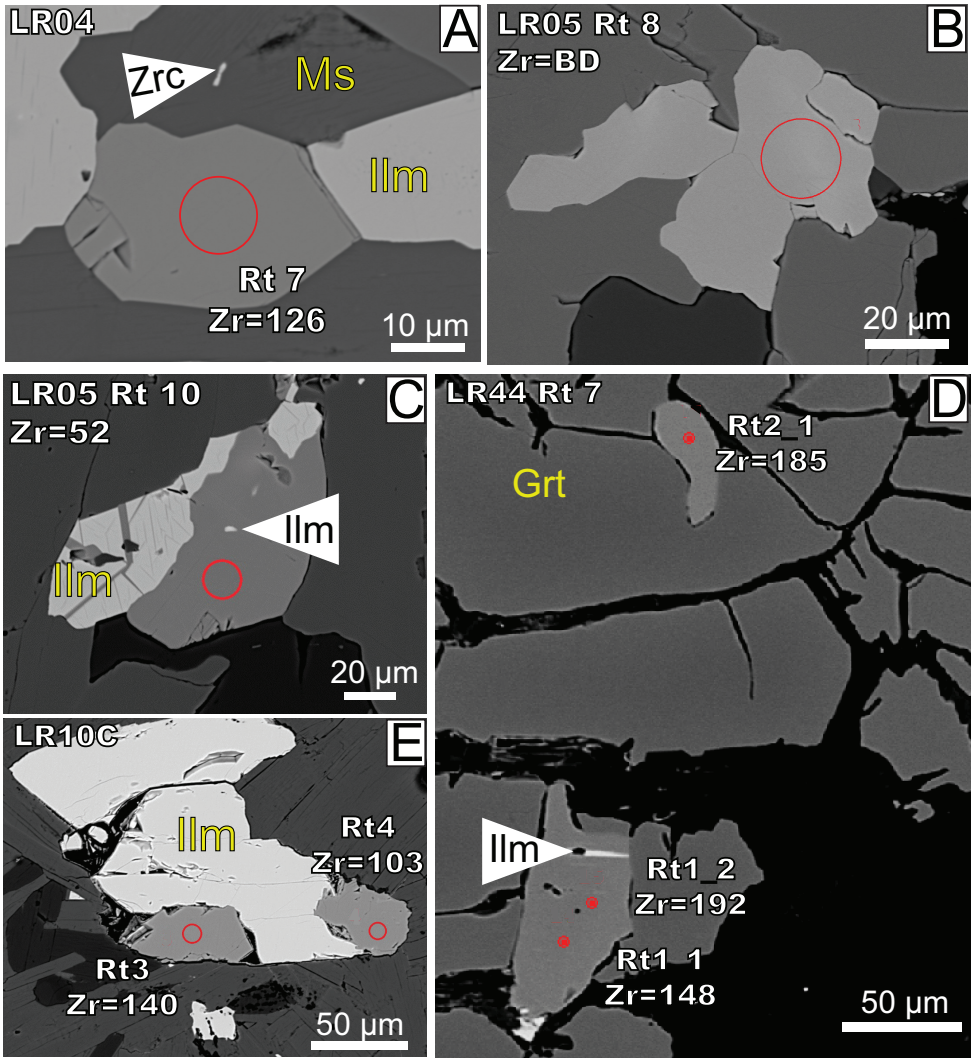

from sample LR44C also have high Nb content), Fe, Al and Cr among all the studied samples (table 4.3 and Fig. 4.6). The high values of Nb are not followed by Ta. The average Zr concentration is the lowest among the studied samples, although maximum (148 ppm, LR04) and minimum (52 ppm, LR05) values are similar to those of samples LR10C and LR10E. It has to be noted that Zr is below the EPMA detection limit (45 ppm) in one analysis of sample LR04 and 6 analyses of sample LR05. In the central portion samples (LR10C and LR10E), rutile crystals have the lowest contents of Nb, Fe, Cr and Ta among the studied samples (table 4.3 and Fig. 4.6). Al contents are similar to sample LR44C. As presented above, maximum (149 ppm, LR10E) and minimum (74 ppm, LR10C) Zr contents in rutile from samples LR10C and LR10E are similar to those of samples LR04 and LR05, although the average is higher.

Figure 4.6 – Boxplots showing concentration (in ppm) of the trace elements (Nb,Cr, Fe, Ta, Al and Zr) in rutile crystals from studied samples. In LR44C sample data from matrix rutile (Mtx) and included in garnet rutile crystals (Incl) are individualized. Whiskers represent the 5th and 95^{th} percentile. Boxes represent the second (bottom-25%) and third quartile (top-75%). The square and bar inside the boxes represent the average and the media, respectively. The numbers on top of each box represent the number of analyses that are showed in the graph. When the numbers of analyses above detection limits are equal or lower than three only the value of the analyzed spots are plotted (solid squares). Only analyses above the minimum detection limit are presented.

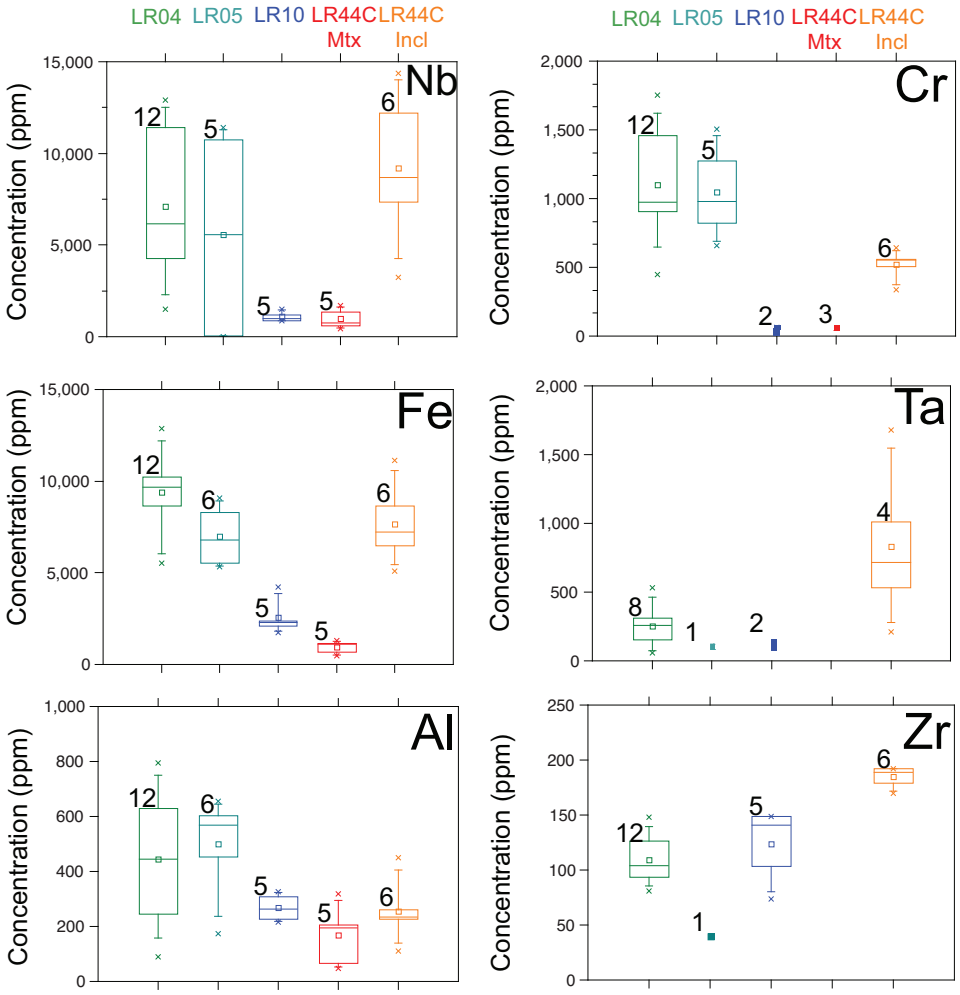

Differently from the other samples, rutile occurs as inclusion in garnet and in the matrix in sample LR44C (southern portion). Crystals from the two textural contexts have distinct trace elements composition. Those crystals that are included in garnet have the highest contents of all trace elements when compared to those from the matrix. All analyses of Ta and Zr are below the EPMA detection limit (85 and 45 ppm, respectively) for matrix rutile. Zr contents in included rutile crystals from sample LR44C are the highest among all analyzed samples, with average of 159 ppm and maximum concentration of 192 ppm.

Quartz trace element concentrations were measured by LA-ICP-MS from sample LR44C, southern portion (table 4.4). Only quartz of this sample was analyzed because Zr-in-rutile contents show a small spread and the sample is from the higher metamorphic

Table 4.4 – Trace element composition of analyzed quartz from LR44C sample. Concentrations are in ppm. Temperature calculations are after the calibration of Thomas et al. (2010), using 1.4 GPa. RSE: Relative Standard Errors from counting statistics (2 sigma) in ppm (only shown for analyses above the detection limit).

Spot #	Li	Al	Ti	Fe	Ge	T (°C)	T (°C) +	T (°C) -	RSE-Al	RSE-Ti	RSE-Fe
128	<12.64	75.20	11.30	<14.23	<1.59	631	22	29	2.53	3.51	
130	<12.07	27.11	6.61	<12.79	<1.56	590	26	37	1.80	2.70	
131	<12.72	46.39	10.75	51.0	<1.61	627	17	20	1.72	2.47	<19.19
132	<12.17	69.60	9.33	94.0	<1.40	616	19	23	1.92	2.48	<17.53
133	<15.62	24.61	6.84	<15.91	<2.00	593	27	40	1.99	2.99	

conditions of the Luminárias Nappe. Ti contents range from 6.6 to 11.3 ppm.

4.8.2 Temperature calculations

Isopleths for the Zr-in-rutile (TOMKINS; POWELL; ELLIS, 2007) and the Ti-in-quartz (calibration of Thomas et al. (2010) geothermometers are presented in Fig. 4.7. Since both geothermometers are pressure dependent, it is crucial to have a pressure estimate to calculate temperature. However, if both Zr-in-rutile and Ti-in-quartz geothermometers are applied for the same sample, equilibrium pressure and temperature conditions are given by the crossing of the isopleths in P-T space. According to Tomkins, Powell e Ellis (2007), a conservative estimate of temperature is given by the upper end of the box-plot box (third quartile). Temperatures presented here are calculated according to this recommendation.

Figure 4.7 – Minimum, average and maximum isopleths of Zr-in-rutile from LR04 (a), LR05 (a), LR10C (b) and LR44C (c) samples. And minimum, average and maximum isopleths of Ti-in-quartz for LR44C sample (c). Peak assemblage pseudosection fields are those of Fig. 4.3. Isopleths of Zr-in-rutile were calculated using the calibration of Tomkins, Powell e Ellis (2007) and Ti-in-quartz using the calibration of Thomas et al. (2010). Yellow star in c indicates the intersection of maximum values of Ti-in-quartz and Zr-in-rutile.

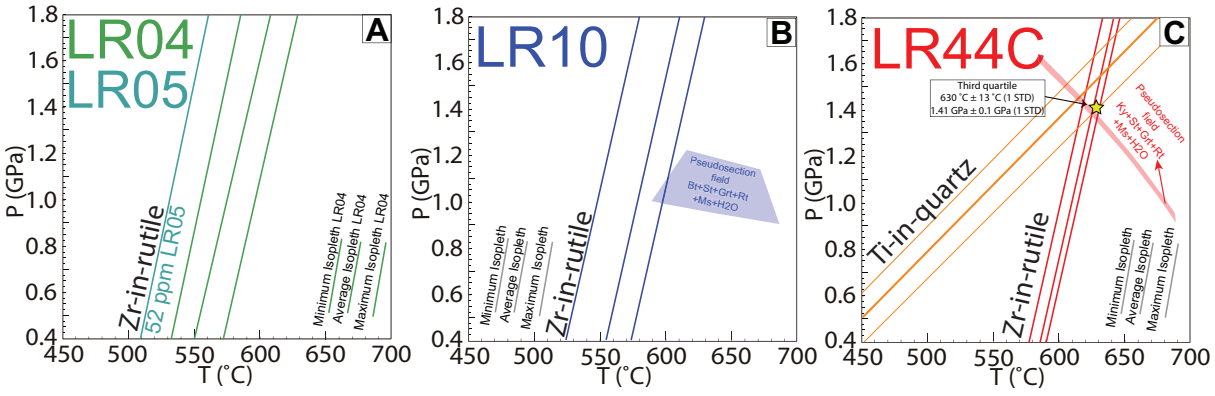

Taking into account the stability field for the peak assemblage (Bt+St+Grt+Rt) in samples LR10C and LR10E (Fig. 4.4) and the Zr-in-rutile isopleths (Fig. 4.7b), the results indicate that only the highest concentration of Zr plot in the stability field, defining a pressure range from 1.0 to 1.1 GPa. For this pressure range, temperatures calculated for the third quartile content (149 ppm) are 597±3 °C and 601±15 °C, respectively.

For sample LR44C the Zr-in-rutile and Ti-in-quartz isopleths intercept each other at ∼630±13 °C and 1.4 GPa (third quartile values for both elements). These results agree with the stability field for the peak assemblage of the rock (Grt+St+Ky+Rt - Fig. 4.7).

For the northern portion, high-pressure lower-amphibolite facies conditions are constrained by the peak mineral assemblage Chl+Ky+St+Rt. This assemblage occurs along a wide pressure window (see, e.g., KFMASH petrogenic grid in (WHITE et al., 2014). However, since results for LR10C/E and LR44C confirm that metamorphic conditions decrease to the north, an estimated pressure of 0.9 GPa was used to calculate Zr-in-rutile temperatures for the northern portion. For sample LR04 the calculated temperature is 580±4 °C (125 ppm – third quartile).

4.9 Monazite Geochronology

U-Th-Pb_T monazite dating was carried out in samples of the central portion (LR10E) and the southern portion (LR44C) and comprised crystals from the matrix of the rock as well as included in garnet, staurolite, kyanite and rutile. Major and trace elements analyses, as well as compositional maps of thirty-two crystals were carried out (Fig. 4.8 and Table 4.5).

Figure 4.8 – Representative compositional X-ray maps and back-scattered electron (BSE) imagens of analyzed monazite showing the compositional variance in different crystals. Circles (white or black) indicate the analyses localization. Annotations on the left hand side of the image indicate the sample, the monazite identification (as in Table 4.4) and the textural context of the crystal (e.g., LR10E Mnz23 St: monazite number 23, from LR10E sample, that is included in staurolite). Age is presented in Ma. Scale bars in all images measure 5 μm.

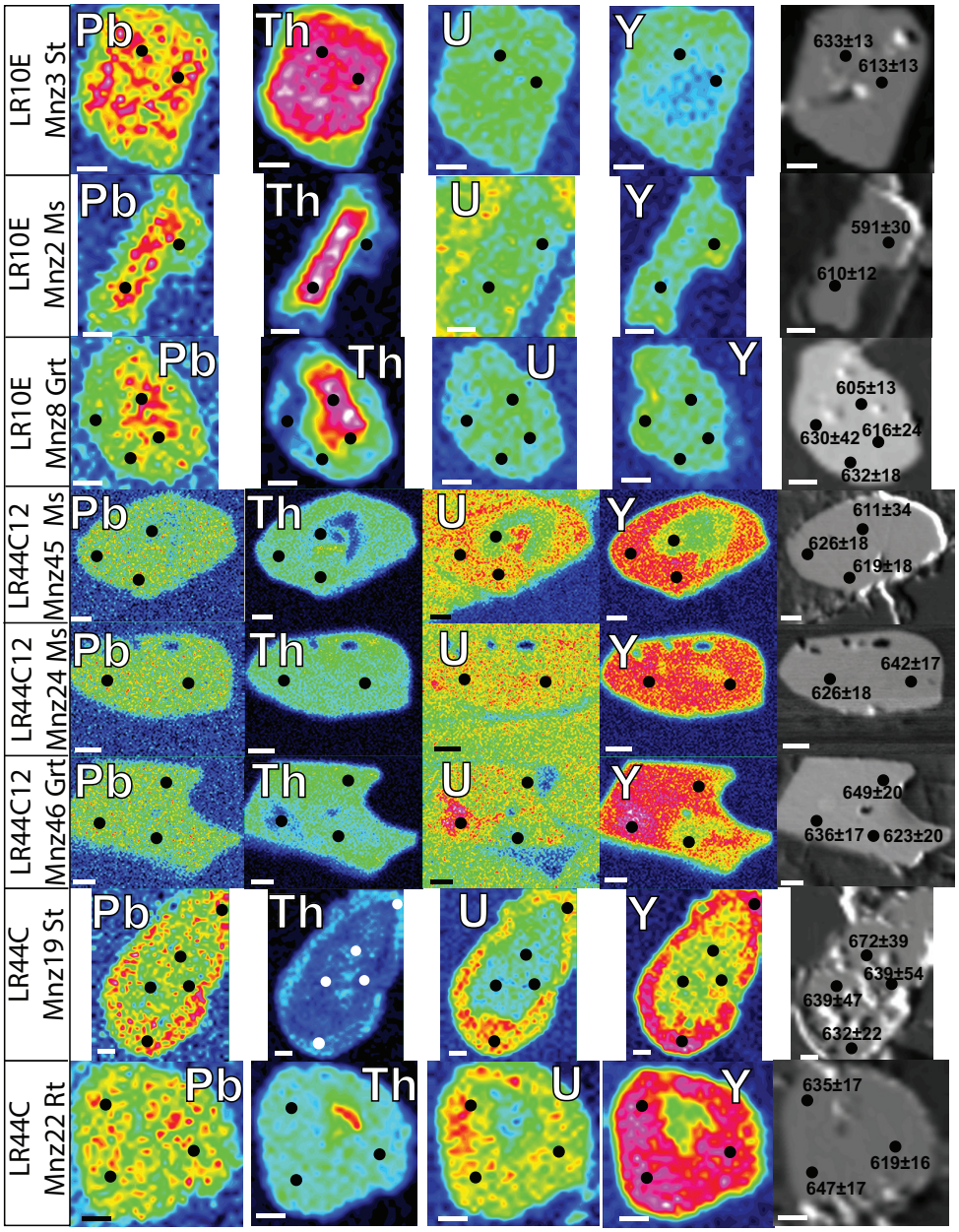

Table 4.5 – EPMA monazite major and trace element composition. Values are in element %wt. Detection limits are those presented in table 4.1. BD: bellow detection limit.

Sample	Spot #	Texture	Y	Si	Al	Th	Ca	La	Ce	Pr	Nd	Sm	Fe	Gd	Er	Tb	Dy	Yb	U	S	P	Pb
LR10E	Mnz12_1	Incl Grt	0.87	0.12	0.45	2.14	0.40	9.81	20.91	2.08	9.46	1.28	7.31	0.85	BD	BD	0.39	BD	0.22	0.03	11.06	0.09
LR10E	Mnz12_2	Incl Grt	0.42	0.12	0.11	2.43	0.46	11.34	23.46	2.42	10.24	1.50	1.38	0.97	BD	BD	BD	BD	0.29	BD	11.40	0.10
LR10E	Mnz4_1	Mtx	0.54	0.25	BD	7.87	1.11	9.37	20.07	2.08	9.60	1.50	0.20	1.40	BD	BD	0.38	BD	0.47	BD	12.04	0.27
LR10E	Mnz4_2	Mtx	0.80	0.36	0.31	3.44	0.57	10.52	22.24	2.26	10.04	1.60	0.27	1.35	BD	BD	0.44	BD	0.34	BD	12.24	0.13
LR10E	Mnz4_3	Mtx	0.16	2.85	3.17	3.06	0.45	10.20	20.72	1.98	9.89	1.68	0.42	1.07	BD	BD	BD	BD	0.32	BD	11.41	0.11
LR10E	Mnz3_1	Incl St	0.20	0.29	0.01	8.77	1.26	9.71	20.13	2.16	9.33	1.54	0.49	1.03	BD	BD	BD	BD	0.47	BD	11.84	0.29
LR10E	Mnz3_2	Incl St	0.41	0.30	0.01	8.74	1.16	9.27	20.26	2.06	9.58	1.56	0.48	1.52	BD	BD	0.30	BD	0.46	BD	11.90	0.30
LR10E	Mnz2_1	Mtx	0.40	0.37	0.01	9.65	1.25	9.17	18.95	1.96	9.08	1.70	0.46	1.48	BD	BD	0.29	BD	0.49	BD	11.96	0.32
LR10E	Mnz2_2	Mtx	0.59	0.08	0.01	2.62	0.40	11.29	22.87	2.30	10.78	1.60	0.38	1.43	BD	BD	0.43	BD	0.32	BD	12.40	0.11
LR10E	Mnz1_1	Mtx	0.43	0.38	BD	9.84	1.26	8.95	19.03	1.96	9.08	1.58	0.08	1.55	BD	BD	BD	BD	0.49	BD	11.68	0.32
LR10E	Mnz1_2	Mtx	0.46	0.29	BD	8.18	1.14	9.39	20.40	1.93	9.48	1.58	0.13	1.59	BD	0.23	0.31	BD	0.45	BD	11.90	0.27
LR10E	Mnz1_4	Mtx	0.12	0.13	0.05	2.70	0.45	11.01	23.07	2.50	10.84	1.92	0.14	1.32	BD	BD	BD	BD	0.31	BD	12.18	0.10
LR10E	Mnz8_1	Incl Grt	0.46	0.28	0.01	8.49	1.23	9.43	19.73	1.94	9.48	1.53	0.88	1.42	BD	0.22	0.22	BD	0.46	0.02	11.98	0.28
LR10E	Mnz8_2	Incl Grt	0.05	0.71	0.45	3.74	0.73	10.48	21.88	2.37	10.15	1.75	1.96	1.04	BD	BD	BD	BD	0.42	BD	11.90	0.14
LR10E	Mnz8_3	Incl Grt	0.49	0.14	0.01	5.37	0.86	10.42	21.28	2.36	10.08	1.64	0.86	1.41	BD	BD	0.29	BD	0.38	BD	12.23	0.20
LR10E	Mnz8_4	Incl Grt	0.47	0.15	0.08	1.82	0.34	11.70	23.10	2.30	10.40	1.62	1.31	1.20	BD	BD	0.37	BD	0.25	BD	12.34	0.08
LR10E	Mnz7_1	Incl Grt	0.42	0.34	BD	9.77	1.37	9.05	19.06	1.94	9.27	1.56	0.86	1.47	BD	BD	0.30	BD	0.49	BD	11.88	0.33
LR10E	Mnz7_2	Incl Grt	0.67	0.12	0.03	2.55	0.44	11.12	22.24	2.35	10.47	1.75	1.27	1.47	BD	BD	0.34	BD	0.28	BD	12.23	0.10
LR10E	Mnz7_3	Incl Grt	0.17	0.66	0.46	2.78	0.48	10.93	22.67	2.28	10.17	1.69	1.90	1.15	BD	BD	BD	BD	0.28	BD	12.01	0.11
LR10E	Mnz9_1	Mtx	0.33	0.10	BD	4.10	0.60	10.15	21.84	2.08	10.56	1.86	0.12	1.50	BD	BD	BD	BD	0.33	BD	12.19	0.15
LR10E	Mnz9_2	Mtx	0.50	0.05	0.01	1.68	0.28	10.99	22.79	2.22	11.20	1.90	0.26	1.65	BD	BD	0.27	BD	0.22	BD	12.34	0.07
LR10E	Mn15_1	Incl Grt	0.38	0.11	BD	4.15	0.66	10.40	21.62	2.56	10.15	1.70	0.24	1.76	BD	BD	0.32	BD	0.34	BD	12.27	0.15
LR10E	Mn15_2	Incl Grt	0.40	0.13	BD	4.88	0.74	9.89	21.48	2.36	9.63	2.07	0.31	1.95	BD	BD	0.30	BD	0.41	BD	12.20	0.18
LR10E	Mn15_3	Incl Grt	0.26	0.18	BD	6.07	0.90	10.43	21.07	2.29	9.91	1.52	0.97	1.36	BD	BD	0.21	BD	0.42	BD	12.11	0.21
LR10E	Mn15_4	Incl Grt	0.25	0.15	BD	5.32	0.84	10.57	21.34	2.47	10.31	1.64	0.52	1.28	BD	BD	BD	BD	0.39	BD	12.14	0.18
LR10E	Mn15_5	Incl Grt	0.34	0.17	0.03	4.39	0.72	10.33	21.78	2.10	10.09	1.74	0.89	1.71	0.11	0.24	0.33	BD	0.39	BD	12.18	0.16
LR44C	Mnz19_1	Incl St	0.83	0.05	0.02	1.46	0.25	12.03	24.42	2.28	9.41	1.38	0.24	0.99	BD	BD	0.34	BD	0.22	BD	12.29	0.07
LR44C	Mnz19_2	Incl St	0.96	0.10	0.05	1.50	0.32	11.30	25.01	2.30	9.91	1.36	0.28	1.12	0.13	BD	0.36	BD	0.35	BD	12.38	0.09
LR44C	Mnz19_3	Incl St	0.81	0.13	0.10	1.16	0.21	11.81	25.60	2.36	9.69	1.60	0.29	1.17	BD	BD	0.39	BD	0.21	BD	12.28	0.06
LR44C	Mnz19_4	Incl St	1.45	0.02	0.02	1.62	0.48	10.71	23.81	2.14	9.26	1.41	0.42	1.37	BD	0.28	0.54	BD	1.05	BD	12.33	0.16
LR44C	Mnz1_1	Incl St	1.45	0.01	BD	3.80	0.74	10.25	22.34	2.25	8.79	1.48	0.24	1.21	BD	BD	0.44	BD	0.93	BD	12.46	0.21
LR44C	Mnz22_1	Incl Rt	1.36	0.03	0.01	3.91	0.75	9.49	22.58	2.20	9.35	1.46	0.35	1.01	0.12	BD	0.52	BD	0.95	BD	12.38	0.21
LR44C	Mnz22_2	Incl Rt	1.49	0.01	BD	3.37	0.72	9.91	21.99	2.05	8.84	1.49	0.30	1.23	BD	BD	0.45	BD	0.96	BD	12.37	0.21
LR44C	Mnz22_3	Incl Rt	1.51	0.01	BD	3.21	0.75	10.07	22.74	1.99	8.72	1.27	0.43	1.17	BD	BD	0.54	BD	1.09	BD	12.45	0.21

Table 4.5 continued from previous page

Sample	Spot #	Texture	Y	Si	Al	Th	Ca	La	Ce	Pr	Nd	Sm	Fe	Gd	Er	Tb	Dy	Yb	U	S	P	Pb
LR44C	Mnz23_1	Mtx	1.58	0.03	0.02	3.42	0.80	9.98	22.16	2.11	9.00	1.54	0.08	1.30	BD	0.29	0.52	BD	1.11	BD	12.58	0.22
LR44C	Mnz23_2	Mtx	1.28	0.12	0.07	3.25	0.64	10.40	23.12	2.29	9.17	1.42	0.12	1.10	BD	BD	0.37	BD	0.75	BD	12.36	0.17
LR44C	Mnz23_3	Mtx	1.48	0.02	0.01	3.44	0.76	9.97	22.48	2.06	9.29	1.33	0.10	1.16	BD	BD	0.46	BD	0.97	BD	12.43	0.21
LR44C	Mnz26_3	Mtx	1.36	0.03	0.01	3.35	0.72	10.03	23.26	2.15	9.15	1.39	0.05	1.15	BD	BD	0.45	BD	1.02	BD	12.42	0.20
LR44C	Mnz20_1	Mtx	1.27	0.02	BD	3.98	0.75	9.92	22.17	2.05	9.68	1.59	0.10	1.13	BD	BD	0.46	BD	0.74	BD	12.46	0.20
LR44C	Mnz20_2	Mtx	1.43	0.01	0.01	3.39	0.74	10.42	22.62	2.12	9.04	1.31	0.11	1.08	0.14	BD	0.40	BD	0.95	BD	12.41	0.21
LR44C	Mnz21_2	Mtx	1.54	0.01	BD	3.82	0.85	9.90	21.99	2.07	9.22	1.46	0.05	1.25	0.11	BD	0.47	BD	1.16	BD	12.36	0.24
LR44C	Mnz24_1	Mtx	1.44	0.02	0.01	3.53	0.77	10.13	22.29	2.15	9.26	1.47	BD	1.06	BD	BD	0.45	BD	0.93	BD	12.43	0.20
LR44C	Mnz24_2	Mtx	1.47	0.03	0.01	3.54	0.78	10.08	22.01	2.11	9.51	1.26	BD	1.04	0.12	0.25	0.44	BD	0.95	BD	12.47	0.21
LR44C	Mnz22_1	Mtx	1.47	0.03	BD	3.54	0.71	10.12	22.65	2.16	9.25	1.38	0.24	1.26	BD	BD	0.49	BD	0.94	BD	12.49	0.20
LR44C	Mnz22_2	Mtx	0.71	0.06	0.04	2.84	0.54	8.53	18.68	1.78	7.65	1.18	0.08	0.77	BD	BD	0.33	BD	0.40	BD	10.98	0.13
LR44C	Mnz22_3	Mtx	1.44	0.01	BD	3.37	0.68	10.10	22.83	2.17	9.01	1.51	0.10	1.15	BD	BD	0.56	BD	0.94	BD	12.55	0.20
LR44C	Mnz5_1	Incl Grt	0.85	0.12	0.01	5.92	0.99	9.01	21.39	2.33	10.23	1.46	0.81	1.16	BD	BD	0.36	BD	0.40	BD	12.28	0.21
LR44C	Mnz4_1	Incl Grt	0.92	0.04	0.01	2.90	0.57	10.22	22.21	1.98	9.10	1.30	1.32	0.82	BD	BD	0.41	BD	0.47	BD	11.76	0.14
LR44C	Mnz4_2	Incl Grt	0.56	7.09	4.76	1.75	0.46	6.22	14.57	1.27	5.94	0.82	12.18	0.61	BD	BD	0.31	BD	0.36	BD	7.88	0.09
LR44C	Mnz45_1	Mtx	0.80	0.03	0.01	1.76	0.37	12.44	25.74	2.28	8.82	1.12	0.33	0.73	BD	BD	0.28	BD	0.43	BD	12.45	0.10
LR44C	Mnz45_2	Mtx	1.25	0.02	0.01	3.32	0.71	9.66	22.06	2.09	8.96	1.40	0.22	1.09	BD	BD	0.47	BD	0.89	BD	11.96	0.19
LR44C	Mnz45_3	Mtx	1.45	0.02	0.01	3.54	0.78	9.67	22.54	2.22	9.73	1.53	0.22	1.15	BD	BD	0.52	BD	0.93	BD	12.44	0.20
LR44C	Mnz11_1	Mtx	1.53	0.04	0.03	3.25	0.69	10.27	22.69	2.20	9.46	1.43	BD	1.17	BD	BD	0.47	BD	1.05	BD	12.46	0.21
LR44C	Mnz11_2	Mtx	1.20	0.07	0.02	3.16	0.62	10.72	23.36	2.20	9.56	1.34	BD	1.32	BD	BD	0.37	BD	0.67	BD	12.41	0.16
LR44C	Mnz46_1	Incl Grt	1.63	0.02	BD	2.60	0.66	10.04	22.48	2.17	9.67	1.45	0.05	1.25	BD	BD	0.49	BD	1.22	BD	12.44	0.21
LR44C	Mnz46_2	Incl Grt	1.42	0.03	0.01	3.58	0.78	10.02	22.05	1.98	9.02	1.56	0.07	1.22	BD	BD	0.54	BD	0.99	BD	12.40	0.22
LR44C	Mnz46_3	Incl Grt	0.99	0.04	0.01	3.32	0.67	10.82	22.89	2.16	9.42	1.37	BD	1.03	BD	BD	0.40	BD	0.73	BD	12.39	0.17
LR44C	Mnz32_1	Mtx	1.42	0.03	0.01	3.61	0.78	10.18	22.49	2.12	8.98	1.30	0.18	1.21	BD	BD	0.45	BD	0.94	BD	12.37	0.20
LR44C	Mnz32_2	Mtx	0.67	0.04	0.01	4.08	0.67	6.91	23.61	2.57	12.41	1.72	0.17	0.88	BD	BD	0.37	BD	0.40	BD	12.37	0.16
LR44C	Mnz33_1	Incl Ky	1.37	0.02	0.02	3.56	0.72	10.21	22.05	2.11	8.77	1.39	0.09	0.97	BD	0.24	0.54	BD	0.89	BD	12.57	0.20
LR44C	Mnz42_1	Mtx	1.40	0.01	0.01	3.45	0.72	10.14	22.26	2.35	9.78	1.61	0.20	1.25	BD	BD	0.59	BD	0.88	BD	12.53	0.20
LR44C	Mnz42_2	Mtx	1.39	0.01	0.01	3.84	0.78	10.19	22.54	2.04	9.31	1.50	0.19	1.22	BD	BD	0.44	BD	0.85	BD	12.49	0.20
LR44C	Mnz44_1	Mtx	1.42	0.01	BD	3.33	0.74	10.80	22.85	2.24	9.11	1.42	0.06	1.08	BD	BD	0.50	BD	0.96	BD	12.45	0.19
LR44C	Mnz44_2	Mtx	1.55	0.02	0.01	3.47	0.75	9.98	22.35	2.24	9.32	1.46	BD	1.44	0.15	BD	0.48	0.16	1.03	BD	12.45	0.21
LR44C	Mnz47_1	Mtx	1.23	0.10	0.01	3.82	0.65	10.43	22.97	2.11	8.91	1.45	0.11	1.08	BD	BD	0.39	BD	0.60	BD	12.31	0.18
LR44C	Mnz47_2	Mtx	1.30	0.12	0.02	3.76	0.69	10.34	22.83	2.04	9.18	1.35	0.25	1.21	BD	BD	0.55	BD	0.69	BD	12.24	0.18
LR44C	Mnz48_1	Mtx	1.34	0.01	BD	3.28	0.64	10.34	22.72	2.16	9.45	1.43	0.13	1.25	BD	BD	0.41	BD	0.86	BD	12.45	0.19
LR44C	Mnz48_2	Mtx	1.55	0.02	0.01	3.72	0.78	9.88	22.23	2.19	9.19	1.41	0.10	1.33	BD	BD	0.52	BD	0.97	BD	12.41	0.22
LR44C	Mn49_1	Mtx	1.48	0.03	0.01	3.53	0.75	10.04	22.50	2.17	9.05	1.37	0.11	1.31	BD	BD	0.56	BD	0.95	BD	12.48	0.21
LR44C	Mn49_3	Mtx	1.47	0.02	0.01	3.88	0.83	9.97	22.16	2.25	8.77	1.56	0.15	1.23	BD	BD	0.46	BD	0.94	BD	12.50	0.22

Table 4.5 continued from previous page

Sample	Spot #	Texture	Y	Si	Al	Th	Ca	La	Ce	Pr	Nd	Sm	Fe	Gd	Er	Tb	Dy	Yb	U	S	P	Pb
LR44C	Mn49_4	Mtx	1.47	0.01	0.01	3.28	0.72	9.93	22.91	2.22	9.18	1.57	0.16	1.30	BD	BD	0.33	BD	0.96	BD	12.47	0.20
LR44C	Mnz29_1	Incl St	0.76	0.07	0.01	4.03	0.68	9.24	23.54	2.27	10.89	1.48	0.43	0.99	BD	BD	BD	BD	0.45	BD	12.23	0.17
LR44C	Mnz29_2	Incl St	1.31	0.04	0.01	3.23	0.67	10.51	22.81	2.13	9.29	1.36	0.52	1.10	BD	BD	0.50	BD	0.88	BD	12.46	0.19

A compositional zoning of Y, Th, Pb and U is observed in several monazite crystals (Fig. 4.8), but it has no effect on the calculated ages. Systematic variations on the mean ages are linked to textural settings of monazite in sample LR10E, where monazite crystals included in garnet and staurolite present older ages (615±6 Ma) when compared to those in the matrix (600±8 Ma) (Fig. 4.9 and table 4.6). In sample LR44C, results obtained for matrix and included monazites crystals (inclusions in garnet, staurolite, kyanite and rutile) are indistinguishable and the mean age is 632±4 Ma. We note that monazite crystals from sample LR44C have the highest contents of Y among all analyzed samples (Fig. 4.10).

Figure 4.9 – Error-weighted average of U–Th–Pb_T EPMA ages of monazite. a) Data from all analyzed monazite from LR10E sample. b) Data from all analyzed monazite from LR44C sample. c) Data from included monazite in garnet and staurolite from LR10E sample. d) Data from included monazite in garnet, staurolite, kyanite and rutile from LR44C sample. e) Data from monazite in the matrix from LR10E sample. f) Data from monazite in the matrix from LR44C sample. Green lines show the mean values. Data-point error symbols are all 2 sigma. Wtd: weighted, conf.: confidence, rej.: rejected and MSWD: Mean Square of Weighted Derivates.

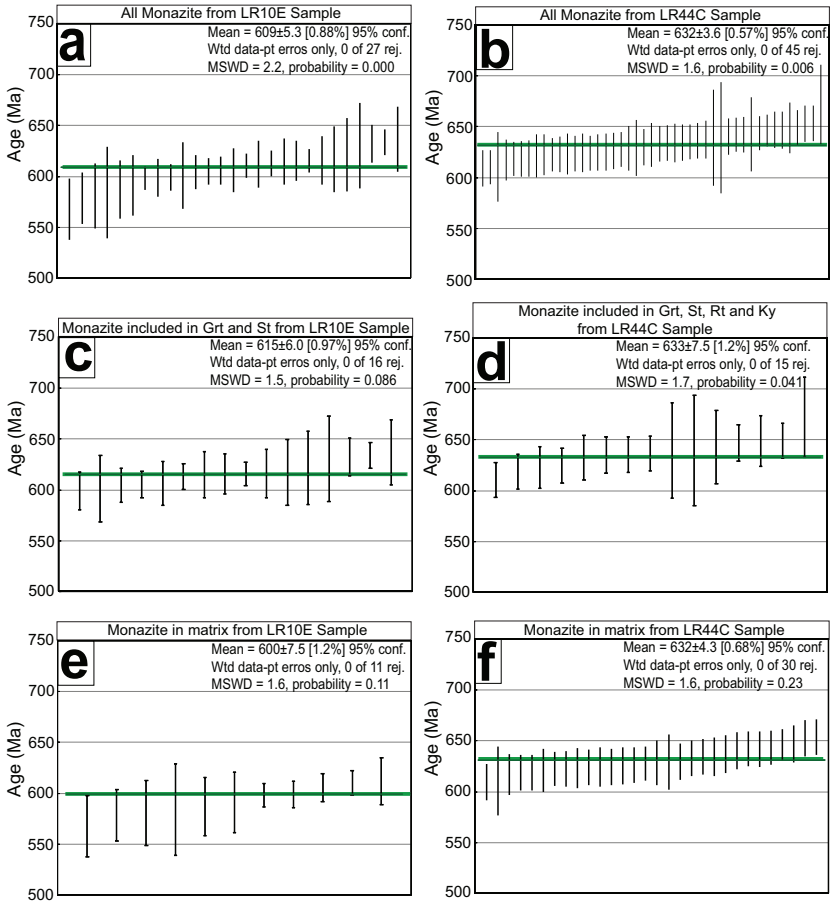

Figure 4.10 – Y (%wt) content variation among monazite textural varieties and between samples versus the age (Ma). Incl: included crystals. Mtx: cystals in the matrix.

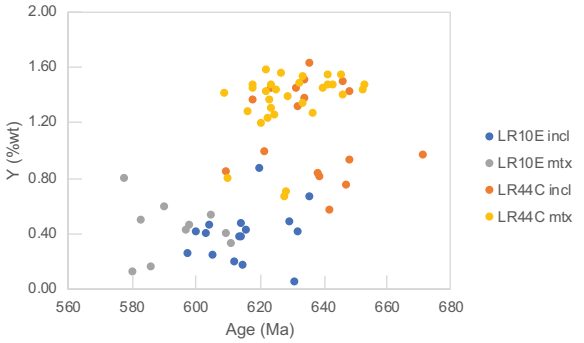

Table 4.6 – Corrected concentrations of Th, U and Pb (in ppm) and calculated ages (Ma) for the analyzed monazite. Meas: measured, 2Sig: 2 sigma error.

			Th		U		Pb		Age	
Sample	Spot #	Texture	Meas	2Sig	Meas	2Sig	Meas	2Sig	Calc	2Sig
LR10E	Mnz12_1	Incl Grt	21419	221	2080	68	791	48	621	36
LR10E	Mnz12_2	Incl Grt	24260	233	2776	72	903	51	601	32
LR10E	Mnz 5_2	Mtx	19522	217	4292	78	984	50	648	31
LR10E	Mnz4_1	Mtx	78653	378	4315	74	2533	60	606	14
LR10E	Mnz4_2	Mtx	34412	265	3242	74	1173	53	578	25
LR10E	Mnz4_3	Mtx	30645	254	3041	73	1074	55	587	29
LR10E	Mnz3_1	Incl St	87724	395	4288	73	2811	60	613	13
LR10E	Mnz3_2	Incl St	87416	393	4164	73	2886	60	633	13
LR10E	Mnz2_1	Mtx	96547	415	4490	75	3060	62	610	12
LR10E	Mnz2_2	Mtx	26234	239	3117	75	970	51	591	30
LR10E	Mnz1_1	Mtx	98405	413	4427	74	3042	61	598	11
LR10E	Mnz1_2	Mtx	81755	384	4099	73	2569	59	599	13
LR10E	Mnz1_4	Mtx	26962	240	2921	73	956	55	581	32
LR10E	Mnz8_1	Incl Grt	84877	390	4181	74	2687	60	605	13
LR10E	Mnz8_2	Incl Grt	37423	273	3984	76	1401	57	616	24
LR10E	Mnz8_3	Incl Grt	53717	317	3587	74	1866	57	632	18
LR10E	Mnz8_4	Incl Grt	18193	209	2381	73	740	52	630	42
LR10E	Mnz7_1	Incl Grt	97720	410	4472	74	3116	61	615	12
LR10E	Mnz7_2	Incl Grt	25452	237	2681	73	952	52	617	32
LR10E	Mnz7_3	Incl Grt	27750	244	2681	72	1050	54	637	32
LR10E	Mnz9_1	Mtx	41032	283	3152	73	1416	56	612	23
LR10E	Mnz9_2	Mtx	16834	204	2151	72	628	50	584	45
LR10E	Mn15_1	Incl Grt	41474	286	3195	73	1439	56	615	23
LR10E	Mn15_2	Incl Grt	48773	307	3902	75	1707	57	615	20

Table 4.6 continued from previous page

			Th		U		Pb		Age	
Sample	Spot #	Texture	Meas	2Sig	Meas	2Sig	Meas	2Sig	Calc	2Sig
LR10E	Mn15_3	Incl Grt	60663	334	3879	74	1998	58	604	17
LR10E	Mn15_4	Incl Grt	53184	319	3634	74	1755	57	599	19
LR10E	Mn15_5	Incl Grt	43940	294	3653	75	1528	56	606	21
LR44C	Mnz19_1	Incl St	14615	196	2111	72	622	48	639	47
LR44C	Mnz19_2	Incl St	15034	197	3407	76	797	49	672	39
LR44C	Mnz19_3	Incl St	11589	182	1999	72	524	47	640	55
LR44C	Mnz19_4	Incl St	16230	201	10422	93	1442	53	632	22
LR44C	Mnz1_1	Incl St	38008	277	9148	90	1918	56	625	17
LR44C	Mnz1_2	Incl St	35157	267	3207	73	1211	52	589	24
LR44C	Mnz22_1	Incl Rt	39057	277	9263	90	1939	56	619	17
LR44C	Mnz22_2	Incl Rt	33689	263	9439	91	1892	55	647	18
LR44C	Mnz22_3	Incl Rt	32089	257	10719	93	1931	56	635	17
LR44C	Mnz23_1	Mtx	34189	263	10974	94	1974	56	623	17
LR44C	Mnz23_2	Mtx	32531	260	7323	86	1575	54	617	20
LR44C	Mnz23_3	Mtx	34437	265	9530	91	1880	55	634	17
LR44C	Mnz26_1	Mtx	32763	259	12550	84	1818	55	547	16
LR44C	Mnz26_2	Mtx	36655	271	12487	84	1852	55	532	15
LR44C	Mnz26_3	Mtx	33546	262	10000	92	1870	56	624	17
LR44C	Mnz20_1	Mtx	39788	282	7198	85	1825	56	637	18
LR44C	Mnz20_2	Mtx	33872	264	9368	90	1909	56	653	18
LR44C	Mnz21_2	Mtx	38201	275	11398	95	2210	57	646	16
LR44C	Mnz24_1	Mtx	35328	268	9101	89	1844	55	626	18
LR44C	Mnz24_2	Mtx	35416	269	9334	91	1917	55	642	17
LR44C	Mnz22_1	Mtx	35380	269	9238	91	1835	55	619	18
LR44C	Mnz22_2	Mtx	28392	244	3816	74	1162	53	630	27
LR44C	Mnz22_3	Mtx	33700	263	9260	91	1855	55	641	18
LR44C	Mnz5_1	Incl Grt	59198	332	3761	74	1968	57	611	17
LR44C	Mnz5_2	Incl Grt	57832	330	4241	73	2207	58	681	17
LR44C	Mnz4_1	Incl Grt	28975	246	4599	77	1292	52	649	25
LR44C	Mnz4_2	Incl Grt	17543	207	3479	73	841	50	643	36
LR44C	Mnz45_1	Mtx	17583	207	4191	78	863	51	611	34
LR44C	Mnz45_2	Mtx	33203	262	8758	88	1749	54	626	18
LR44C	Mnz45_3	Mtx	35378	269	9110	89	1823	55	619	18
LR44C	Mnz11_1	Mtx	32545	260	10310	93	1903	55	634	17
LR44C	Mnz11_2	Mtx	31633	256	6577	84	1492	54	622	21
LR44C	Mnz46_1	Incl Grt	25968	239	12122	97	1892	55	636	17

Table 4.6 continued from previous page

			Th		U		Pb		Age	
Sample	Spot #	Texture	Meas	2Sig	Meas	2Sig	Meas	2Sig	Calc	2Sig
LR44C	Mnz46_2	Incl Grt	35790	268	9750	91	1990	56	649	17
LR44C	Mnz46_3	Incl Grt	33239	259	7182	85	1596	55	623	20
LR44C	Mnz32_1	Mtx	36118	271	9185	90	1863	55	623	17
LR44C	Mnz32_2	Mtx	40843	286	3781	75	1510	55	629	22
LR44C	Mnz33_1	Incl Ky	35621	271	8734	89	1843	55	635	18
LR44C	Mnz42_1	Mtx	34492	266	8602	89	1835	55	647	18
LR44C	Mnz42_2	Mtx	38443	277	8351	88	1873	56	630	18
LR44C	Mnz44_1	Mtx	33267	259	9438	91	1766	55	610	18
LR44C	Mnz44_2	Mtx	34651	267	10091	92	1922	55	628	17
LR44C	Mnz47_1	Mtx	38211	275	5830	81	1613	54	623	20
LR44C	Mnz47_2	Mtx	37648	275	6754	84	1686	54	625	19
LR44C	Mnz48_1	Mtx	32789	259	8399	88	1730	55	635	19
LR44C	Mnz48_2	Mtx	37191	271	9475	91	1982	55	642	17
LR44C	Mn49_1	Mtx	35292	268	9373	90	1953	55	654	17
LR44C	Mn49_2	Mtx	37360	273	9221	89	2034	56	665	17
LR44C	Mn49_3	Mtx	38760	279	9164	90	2002	56	644	17
LR44C	Mn49_4	Mtx	32823	259	9481	90	1803	55	625	18
LR44C	Mnz29_1	Incl St	40323	282	4339	77	1597	55	648	21
LR44C	Mnz29_2	Incl St	32339	259	8651	89	1736	55	633	19

We would also like to point out that allanite occurs associated with the monazite in sample LR10A (Fig. 4.3). All monazite analyses in this sample were discarded due to the low total (sum of all analyzed elements) and no coherent U-Th-Pb_T ages. Although the analyses are not used in further discussion, the presence of allanite replacing monazite is useful to establish the metamorphic *P-T* path that is discussed below.

4.10 Discussion

4.10.1 Metamorphic conditions and *P-T* paths

In the present study, the metamorphic gradient that has previously been described for the Luminárias Nappe region (TROUW; RIBEIRO; PACIULLO, 1980; RIBEIRO; HEILBRON, 1982; PETERNEL et al., 2005; TROUW et al., 2000; SILVA, 2010) is characterized based on peak metamorphic mineral assemblage, pseudosection modeling and trace elements geothermometry. It is the first attempt to quantify, by a multi-method approach, the peak metamorphic conditions of the studied rocks. Furthermore, based on

pre-peak, peak and post-peak mineral assemblages, P-T paths are presented (Fig. 4.11).

Figure 4.11 – Pressure-temperature-time (P-T-t) paths for the three portions of metapelites from Luminárias Nappe based on textural relationships, pseudosection modelling, Zr-in-rutile and Ti-in-quartz and geothermometry EPMA geochronology of monazite. a) (P-T-t) path from the northern portion. b) (P-T-t) path from the central portion (pseudosections fields from fig. 4.4a with quartz and H_2O in excess). c) (P-T-t) path from the southern portion (pseudosections fields from fig. 4.4b with quartz and H_2O in excess). Pressure-temperature fields of metamorphic facies according to Bucher e Grapes (2011).

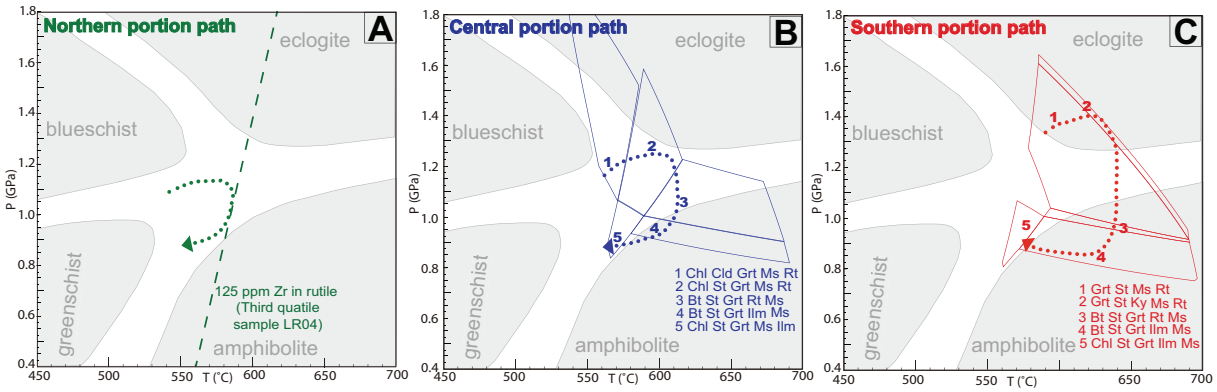

Peak mineral assemblages indicate that the metamorphic grade increases from high-pressure lower-amphibolite facies conditions in the north (Chl+Ky+St+Rt) to high-pressure amphibolite facies in the central portion (St+Bt+Grt+Rt), and, to eclogite facies in the southern portion (St+Ky+Grt+Rt). In all of the studied rocks, kyanite is the only stable Al-silicate, consistent with the high-pressure conditions of metamorphism these rocks underwent. It has to be stressed that, due to the lack of plagioclase, quantification of pressure conditions is problematic. Even when mineral composition isopleths are calculated and presented in the respective fields of the pseudosections, they form sub-parallel lines, and their crossing results in large uncertainties when pressure is calculated.

Post-tectonic chloritoid (to $S_{1/2}$) in sample LR04 (Fig. 4.2b) is interpreted as a retrograde phase in respect to peak condition attained under high-pressure lower-amphibolite facies (northern portion). In the high-pressure amphibolite facies rocks from the central portion (Fig. 4.2d), chlorite overgrows the main foliation and is interpreted as retrograde. Chloritoid porphyroblasts associated with staurolite are present in a specific compositional layer in sample LR10E (Fig. 4.2f). Two possible interpretations for this association are presented here. The first hypothesis is that chloritoid occurrence is controlled by the chemical composition of the layer. Another hypothesis is that the chloritoid is pre-tectonic and was preserved only in this band. Since staurolite has a subhedral shape, we interpret that staurolite is replacing chloritoid. We acknowledge that the metamorphic texture is complex and an opposite interpretation, where chloritoid is replacing staurolite, cannot be ruled out.

The metamorphic peak assemblage observed in samples from the southern portion of Luminárias Nappe is represented by St+Ky+Grt+Rt that indicate the highest temperature

and pressure condition observed in the region. According to the calculated pseudosection, this metamorphic peak assemblage is formed under eclogite facies conditions (Fig. 4.11). Staurolite occurs as inclusion in garnet porphyroblasts. Kyanite also occurs as inclusion in garnet, but only in the rim. Both staurolite and kyanite occur as oriented crystals in the matrix defining the foliation (Fig. 4.2g). Biotite and chlorite with no preferred orientation are observed in several samples from the southern portion and are interpreted as retrometamorphic.

Taking into consideration mineral assemblages, the textural relationships and the stability fields obtained in the pseudosection, clock-wise *P-T* paths can be defined for the studied samples (Fig. 4.11). No pseudosection has been calculated for northern portion samples (LR04 and LR05). Peak T condition (580±4 °C at ∼0.9 GPa) is given by the Zr content in rutile from sample LR04 and is compatible with the peak mineral assemblage Chl+Ky+St+Rt. The post-peak path is characterized by the crystallization of post-tectonic chloritoid (Fig. 4.2b). For the central portion (samples LR10C and LR10E), the *P-T* path starts in the stability field of the Chl+Cld+Grt+Rt assemblage (Fig. 4.11b). The replacement of chloritoid by staurolite (Fig. 4.2f) and the presence of biotite (Fig 4.2d) indicate that the *P-T* path crosses the Chl+St+Grt+Rt field, reaching the Bt+St+Grt+Rt field in peak metamorphic conditions. Post-peak metamorphism is evidenced by the crystallization of chlorite and ilmenite (Fig. 4.2e) in the Chl+St+Grt+Ilm field (Fig. 4.11b). For the southern portion (sample LR44C), the *P-T* path starts in the stability field of the St+Grt+Rt assemblage, reaches the metamorphic peak at the St+Ky+Grt+Rt assemblage field, crossing through Bt+St+Grt+Rt and Bt+St+Grt+Ilm fields, finishing in retrograde assemblage Chl+St+Grt+Ilm field (Fig. 4.4b and 4.10c).

Temperature of metamorphism of Luminárias Nappe rocks is close the equilibration temperature of rutile, at ∼of 550-650 °C (STENDAL et al., 2006; TRIEBOLD et al., 2007; KOHN; PENNISTON-DORLAND; FERREIRA, 2016; CRUZ-URIBE et al., 2018). Although the Zr content in rutile from sample LR04 gives consistent results, the registered temperature is lower than the expected re-equilibration temperature of rutile. It has to be noted that temperature of ∼580 °C obtained for this sample agrees with the peak mineral assemblage (KFMASH petrogenic grid in White et al. (2014). According to (CRUZ-URIBE et al., 2018) single element thermometers in temperatures lower than 600 °C only can be applied if trace element equilibrium can be demonstrated. That is the case of the studied samples, where quartz, rutile and zircon are present, buffering the equilibrium of the system SiO_2–TiO_2–ZrO_2.

In sample LR44C, only rutile crystals included in garnet have Zr contents above the EPMA detection limit, indicating that post-peak metamorphism may have changed the composition of rutile. We note that higher contents of Zr in rutile are often observed in crystals included in garnet and kyanite (ZACK; MORAES; KRONZ, 2004; LUVIZOTTO

et al., 2009; HART et al., 2018).

With the trace element data, it is possible to interpret a correlation between Nb content in rutile and the occurrence of biotite. Higher Nb content in rutile is correlated with the absence of biotite (rutile in samples LR04 and LR05 and rutile included in garnet in sample LR44C, where peak assemblage is biotite free). As pointed out before by Luvizotto et al. (2009), high Nb contents in rutile can be linked to rutile growth associated with biotite breakdown during prograde metamorphism, since rutile favors Nb over Ti, when compared to biotite. In samples LR10C and LR10E, rutile with lower Nb content occurs in the matrix where rutile coexists with biotite in the peak metamorphic assemblage. In sample LR44C biotite is retro-metamorphic and only occurs in the matrix where the rutile also presents lower Nb content. According to our data (Fig. 4.4b), retro-metamorphic crystallization of the biotite in the presence of rutile in sample LR44C, occurs in T conditions between 590 °C (lowest T stability in Fig. 4.4b) and 630 °C (peak T condition) and P conditions lower than 1.05 GPa (highest P stability in Fig. 4.4b).

Pressure conditions of the metamorphic peak are higher than the barrovian metamorphism. High-pressure conditions were also obtained by (SILVA, 2010) in the Carrancas Klippe, northeast of the Luminárias Nappe. The author calculated peak P-T conditions (1.0±0.17 GPa and 577±8 °C in the north and 1.29±0.1 GPa and 608.5±19.5 °C in the south) that are similar to those presented here, and somewhat higher in pressure than previously calculated for these units (CAMPOS NETO; CABY, 1999).

The basal unit gneiss from the São Vicente Complex and/or $Na_{1/2}$ (Fig. 1) has plagioclase. Lenses of amphibolite are common in this unit. Mineral assemblages in both rocks are incompatible with eclogite facies metamorphic conditions. This may suggest that either the high-pressure conditions calculated here are overestimated or that the Carrancas Group was thrusted over the São Vicente Complex after metamorphic peak conditions, and that they are, therefore, unrelated as suggested by recent data (WESTIN et al., 2016; WESTIN et al., 2019).

4.10.2 Age of metamorphism

Three distinct U-Th-Pb_T monazite ages (Fig. 4.9) have been obtained for the Luminárias Nappe rocks: 600±8 Ma for matrix monazite in sample LR10E (central portion); 615±6 Ma for monazite included in peak metamorphic minerals in sample LR10E; and, 632±4 Ma for matrix and included monazite in sample LR44C (southern portion).

The textural setting of monazite in sample LR44C has no influence on the results and the age (average of 632±4 Ma) is older than those obtained for sample LR10E. The results indicate, therefore, that a single monazite growth episode is registered in rocks from the southern portion. There are two possibilities to explain the older age. It may

represent the age of the metamorphic peak associated to the collision of the southern Brasília belt. According to Campos Neto et al. (2004), Campos Neto et al. (2010), Campos Neto et al. (2011), rocks from the Carrancas Nappe System are the youngest among all related nappes from the Southern Brasília belt, in a continuous migration of the orogen model. Rocks from the Carrancas Nappe System can be lithologically and stratigraphically correlated to the Luminárias Nappe rocks. The age (632±4 Ma) determined in this work for sample LR44C is, however, older when compared to those of the Carrancas Nappe System (590-575 Ma, U-Pb monazite ages, Valeriano et al. 2004; Campos Neto et al. 2011). Alternatively, the monazite crystals in sample LR44C may be interpreted as detrital, deriving from metamorphic units within the southern Brasília belt, for example, the Socorro-Guaxupé Nappes (ROCHA et al., 2017), Passos Nappe (VALERIANO et al., 2004), Carmo da Cachoeira Nappe e Três Pontas-Varginha Nappe (RENO; BROWN; PICCOLI, 2010; RENO et al., 2012). Reno et al. (2012) have presented a comprehensive set of monazite ages for the Southern Brasília belt. Oldest ages (662 – 665 Ma) are obtained for high-pressure granulite from the Três Pontas-Varginha Nappe and are interpreted to represent near-peak conditions. Ages of 640-631 Ma are obtained for high yttrium monazite from the same unit and are interpreted as monazite growth from local garnet breakdown. These ages are similar to those obtained for sample LR44C (632±8 Ma). We would like to notice that monazite crystals from sample LR44C have the highest yttrium contents among all analyzed grains (Fig. 4.10). Younger ages (616 – 613 Ma) are presented by (RENO et al., 2012) for the Carmo da Cachoeira Nappe and the Carvalhos Klippe. For these units, ages younger than 605 Ma are also obtained and are interpreted to be related to the orogenic loading associated with terrane accretion in the Ribeira Belt.

The age difference between included and matrix monazite in sample LR10E is quite significant (ca. 15 Myr) and may indicate changes in the tectonometamorphic conditions along the *P-T-t* path. Records of prograde steps of metamorphism in garnet porphyroblasts are confirmed by their chemical zoning, as documented by Fumes (2017). We interpret that the older age presented by the included monazite represents the time of garnet and staurolite porphyroblasts crystallization at metamorphic peak conditions. Younger ages are interpreted to represent post-peak crystallization of monazite in the matrix of the rock. A possible interpretation is that monazite grew during a single metamorphic event, during the retrograde part of the *P-T-t* path. An alternative interpretation is that the area faced two metamorphic events, an older one at ca. 632-615 Ma, related to the collision of the southern Brasília belt and a younger one at about 600 Ma related to collision of the Ribeira belt, as proposed in the literature (TROUW et al., 2013; COELHO et al., 2017; RENO et al., 2012; PETERNEL et al., 2005; VINAGRE et al., 2016).

Replacement of allanite by monazite is observed in sample LR10A (Fig. 4.3). Sample LR10A is from the central portion of Luminárias Nappe; it is similar to sample LR10C, a staurolite-biotite-garnet schist. The metamorphic peak assemblage is St+Bt+Grt+Rt and

corresponds to high-pressure-amphibolite facies. According to (GOSWAMI-BANERJEE; ROBYR, 2015) the monazite-forming reaction occurs at temperatures higher than 600 °C, in Barrovian terranes. Although the pressure conditions in Luminárias Nappe rocks are higher than Barrovian terranes, the temperature of 600 °C is near to the peak temperature observed *P-T-t* path of rocks in the northern portion of Luminárias Nappe. According to the calculated pseudosection (Fig. 4.4a), an invariant curve occurs at ∼600 °C, where chlorite becomes instable and biotite is crystalized, nearby this reaction probably the allanite also become instable and the monazite is crystalized.

4.10.3 Tectonic implications of *P-T-t* path and ages

Pressure conditions of peak metamorphism registered in Luminárias Nappe rocks indicate that equilibrium took place under conditions that are higher than those of typical barrovian-type metamorphism. It, therefore, points to a thick-skinned tectonic setting that is coherent with the continental collision, that may involve subduction of continental crust, proposed for the southern Brasília belt (DARDENNE, 2000; FUCK et al., 2017; HEILBRON; CORDANI; ALKMIM, 2017; TEDESCHI et al., 2017). The ages presented here (Fig. 4.9) for the Luminárias Nappe rocks (615±6 Ma – included crystals, 600±8 Ma – matrix crystals for sample LR10E and 632±4 Ma– matrix and included crystals for sample LR44C), are within the time interval of the events that led to the formation of both the southern Brasília belt (630-607 Ma is the age of metamorphic peak according to Rocha et al. (2017), Mora, Neto e Basei (2014), Coelho et al. (2017), Tedeschi et al. (2017), Tedeschi et al. (2018) and the Ribeira belt (620-520 Ma according to Machado et al. (1996), Santos et al. (2007), Heilbron, Cordani e Alkmim (2017). The oldest ages obtained in the present work are, therefore, in agreement with processes associated with the Brasília orogeny, while younger ages may be related to retrometamorphism or to processes associated with the Ribeira orogeny, extending the interference zone to the study area. According to the orogen migration model proposed by Campos Neto et al. (2004), Campos Neto et al. (2010), Campos Neto et al. (2011) for the southern Brasília belt, the Carrancas nappe system, that encompasses the studied rocks, corresponds to the last stage of the collision pile and has metamorphic monazite ages of ca. 590-575 Ma. The monazite ages presented in this work, especially those from the southern portion and from the included monazite crystals in the central portion, are considerably older than the ages presented by the authors and, therefore, are inconsistent with the model proposed by Campos Neto et al. (2011). However, a word of caution with respect to monazite ages seems appropriate since many reports on such ages show a wide range of results casting some doubt as to the precise meaning of an average monazite age (e.g. Reno et al. (2012), Campos Neto et al. (2011) and this paper).

We would like to note that recently published data (TEDESCHI et al., 2017) on

high-pressure amphibolite facies mafic rocks from Pouso Alegre (SW of Luminárias Nappe) indicate that these rocks were metamorphosed at peak *P-T* conditions of 690±35 °C and 1.35±0.30 GPa. The authors interpret that these rocks represent the deep root of the Ediacaran (630 Ma, U-Pb in zircon and monazite) continent-continent collision zone associated with the Brasília belt. The age and the metamorphic conditions presented here for the southern portion of the Luminárias Nappe agree with the data presented by Tedeschi et al. (2017) and may reflect the continental collision associated with the Brasilia Belt.

Based on metamorphic and geochronologic data of metamorphic and magmatic rocks from Andrelândia Nappe System (SE of Luminárias Nappe), Coelho et al. (2017) described an orogen-scale interference model for the area, with continental subduction at 625±6 Ma and nappe emplacement at 618±5 Ma both associated to the Southern Brasília Orogen and a second heat pulse associated to Central Ribeira Orogen at 586±9 Ma. Although more detailed geochronological studies need to be carried out, the ages obtained for the southern portion of the Luminárias Nappe (632±4 Ma), for the included monazite crystals (615±6 Ma) and for the matrix monazite crystals from the central portion (600±8 Ma) agree, respectively, with the steps of subduction, nappe emplacement and the heat pulse associated with the Central Ribeira Orogen proposed by Coelho et al. (2017).

It has to be noted that sillimanite replacement over kyanite is described in rocks from the southern portion of Luminárias Nappe (RIBEIRO; HEILBRON, 1982; TROUW et al., 2000; PETERNEL et al., 2005; RENO et al., 2012; TROUW et al., 2013) and is interpreted as a post-peak superposition of deformation and metamorphism associated with the Ribeira belt. Neto et al. (2018) have recently presented data on metasedimentary rocks that formed between the late collisional stage of the southern Brasília belt and the main collision in the central Ribeira belt (max. deposition at ca. 611 Ma, evolution range between 611 and 580 Ma). The data presented by the authors suggest that an important uplift by erosion took place in this interval. The decompression associated with the uplift, followed by heating associated with the main collision in the central Ribeira Belt may be responsible for the sillimanite replacement over kyanite. The fact that sillimanite does not occur in any of the studied samples may be related to the whole rock composition. As can be seen in Fig. 4.4, the lower limit of the peak stability fields for rocks from the central (Bt+St+Grt+Rt) and southern portions (Grt+St+Ky) is strongly controlled by P. A decompression to conditions of about 1.0 to 0.9 GPa would lead to the crystallization of ilmenite, in the St+Bt+Grt+Ilm stability field, where neither kyanite or sillimanite would be present. Ilmenite is indeed present in the studied rocks. An even greater decompression would destabilize garnet in the St+Bt+Ilm field but, still, no aluminum silicate would be present. According to our modeling, a further decompression to conditions of approximately 0.7 GPa, at temperatures between 630 and 680 °C, would be required for the crystallization

of sillimanite in the studied samples.

The regional metamorphic gradient that is described for the Southern Brasilia belt rocks, at the interference zone with the Ribeira belt, is oblique to the main geological contacts (TROUW; RIBEIRO; PACIULLO, 1980; RIBEIRO; HEILBRON, 1982; PETERNEL et al., 2005; RENO et al., 2012; TROUW et al., 2000). This observation is corroborated by our results, since *P-T* conditions increase from north to south along the Luminárias Nappe rocks.

One possible scenario to explain the high-pressure signature of the studied rocks, as well as the oblique position of the metamorphic gradient in respect to the geological contacts, would be a progressive event that starts with the deformation and metamorphism associated with the Brasilia belt and evolves until a collisional, or near collisional stage (older monazite ages). It is not clearly shown by our data if the overprint of the younger Ribeira belt occured before the rocks were exhumed to shallower settings or after uplift and erosion of the Brasilia Orogen. In any case, the overprint would be responsible for the oblique metamorphic gradient (tilting of the rock pile in respect to the isotherm and isobar) as well as the younger ages (monazite in the matrix).

It has to be stressed that the overprint of two distinct tectonic events is not undoubtedly confirmed by the data presented here. It is still possible that the evolution of the Luminárias Nappe rocks is associated to one single event, entirely related to the Brasília belt event.

4.11 Concluding remarks

- The metamorphic gradient described in the literature for the Luminárias Nappe rock is confirmed by the present work. In the northern portion the peak metamorphic condition is ∼580±4 °C and ∼0.9 GPa (high-pressure lower-amphibolite facies), in the central portion it is ∼600±15 °C and 1.1±0.3 GPa (high-pressure-amphibolite facies) and in the southern portion it is ∼630±113 °C and 1.4±0.6 GPa (eclogite facies);

- Petrographic data, combined with metamorphic modeling, thermobarometric calculations and U-Th-PbT monazite dating indicate that the Luminárias Nappe rocks followed a continuous, single step, clockwise *P-T-t* path;

- The peak metamorphic age from Luminárias Nappe is 615±6 Ma for the central portion of Luminárias (sample LR10E) and 632±4 Ma for the southern portion (sample LR44C) according to included monazite. The age of monazite crystallization in matrix in the central portion is ca. 15 Ma younger and there is no difference between included monazite and matrix monazite in the southern portion;

- The integrated approach used in this work, combining pseudosection modeling and single element thermometers (Zr-in-Rt and Ti-in-Qtz), is a useful tool to constrain the metamorphic conditions;

- According to the petrological textures, deformation features, metamorphic conditions and ages presented in this work, the tectonic evolution of the Luminárias Nappe rocks is tightly related to the east-verging orogenic processes of the southern Brasília belt. The effect of the superposition of the younger, northwest-verging, Ribeira belt is interpreted to have caused the tilting of the rock pile in respect to the isotherm and isobars, leading to the formation of the oblique metamorphic gradient. Since kyanite is the only stable Al-silicate, the studied rocks were deformed and metamorphosed under High-Pressure conditions, in agreement with the calculated values of 630 °C and 1.4 GPa for the highest-grade rocks.

Acknowledgements: The authors acknowledge support from São Paulo Research Foundation (FAPESP) thought grants 2015/07750-0, 2015/05230-0 and 2016/22627-3 and the National Council CNPq (PhD scholarship for RAF- 141604/2018-2). We would like to thank Thomas Zack for LA-ICP-MS analysis. The authors are grateful to Rudolph Trouw and the anonymous reviewer for the comments that improved the article quality. We would like to thank Carlos Grohmann for the attentive editorial handing.

Reference

ALMEIDA, J. C. *Mapeamento geológico na Folha Luminárias (MG) 1:50.000 com ênfase na análise estrutural dos metassedimentos do Ciclo Deposicional Andrelândia.* Dissertação (Mestrado) — Universidade Federal do Rio de Janeiro, 1992.

ARAÚJO FILHO, J. O. The Pirineus Syntaxis: An example of the intersection of two Brasiliano fold-thrust belts in central Brazil and its implications for the tectonic evolution of western Gondwana. *Revista Brasileira de Geociências*, v. 30, n. 1, p. 144–148, 2000.

BUCHER, K.; GRAPES, R. *Petrogenesis of metamorphic rocks.* [S.l.]: Springer Science & Business Media, 2011.

CAMPOS NETO, M. D. C. Orogenic Systems from Southwestern Gondwana: An Approach to Brasiliano-Pan African Cycle and Orogenic Collage in Southeastern Brazil. In: CORDANI, U. G. et al. (Ed.). *Tectonic Evolution of South America.* 1. ed. Rio de Janeiro: COMPANHIA DE PESQUISA DE RECURSOS MINERAIS, 2000. p. 335–365.

CAMPOS NETO, M. D. C. et al. Migração de Orógenos e Superposição de Orogêneses: Um Esboço da Colagem Brasiliana no Sul do Cráton do São Francisco, SE - Brasil. *Geologia USP - Serie Cientifica*, v. 4, n. 1, p. 13–40, 2004.

CAMPOS NETO, M. D. C. et al. Orogen migration and tectonic setting of the Andrelândia Nappe system: An Ediacaran western Gondwana collage, south of São Francisco craton. *Journal of South American Earth Sciences*, Elsevier Ltd, v. 32, n. 4, p. 393–406, 2011. ISSN 08959811. Avaible form internet: <http://dx.doi.org/10.1016/j.jsames.2011.02.006>.

CAMPOS NETO, M. D. C.; CABY, R. Neoproterozoic high-pressure metamorphism and tectonic constraint from the nappe system south of the Sao Francisco Craton, southeast Brazil. *Precambrian Research*, v. 97, n. 1-2, p. 3–26, 1999. ISSN 03019268.

CAMPOS NETO, M. D. C. et al. Structural and metamorphic control on the exhumation of high-P granulites: The Carvalhos Klippe example, from the oriental Andrelândia Nappe System, southern portion of the Brasília Orogen, Brazil. *Precambrian Research*, v. 180, n. 3-4, p. 125–142, 2010. ISSN 03019268.

CAMPOS NETO, M. D. C. et al. Sistema de nappes andrelândia, setor oriental: litoestratigrafia e posição estratigráfica. *Revista Brasileira de Geociências*, v. 37, n. 4-Sup., p. 47–60, 2007.

COELHO, M. B. et al. Constraining timing and P-T conditions of continental collision and late overprinting in the Southern Brasília Orogen (SE-Brazil): U-Pb zircon ages and geothermobarometry of the Andrelândia Nappe System. *Precambrian Research*, Elsevier B.V., v. 292, p. 194–215, 2017. ISSN 03019268. Avaible form internet: <http://linkinghub.elsevier.com/retrieve/pii/S0301926816305496>.

CRUZ-URIBE, A. M. et al. Assessing trace element (dis)equilibrium and the application of single element thermometers in metamorphic rocks. *Lithos*, Elsevier B.V., v. 314-315, p. 1–15, 2018. ISSN 18726143. Avaible form internet: <https://doi.org/10.1016/j.lithos.2018.05.007>.

DARDENNE, M. A. The Brasilia Fold Belt. In: *Tectonic Evolution of South Ameria.* [S.l.]: 31 Intern. Geol. Congr. Rio de Janeiro, 2000. p. 231–264.

EBERT, H. Pesquisas geológicas na parte sudoeste de Minas Gerais. *Relatório Anual do Diretos de Geologia e Minas*, p. 97–107, 1956.

FRASER, G.; ELLIS, D.; EGGINS, S. Zirconium abundance in granulite-facies minerals, with implications for zircon geochronology in high-grade rocks. *Geology*, Geological Society of America, v. 25, n. 7, p. 607–610, 1997.

FUCK, R. A. et al. The Northern Brasília Belt. In: HEILBRON, M.; CORDANI, U. G.; ALKMIM, F. F. (Ed.). *São Francisco Craton, Eastern Brazil Tectonic Genealogy of a Miniature Continent*. [S.l.]: Springer Berlin Heidelberg, 2017. p. 205–220.

FUMES, R. A. *Modelagem metamórfica e geotermobarometria de elementos traço em metapelitos e quartzitos: exemplo da Nappe de Luminárias-MG*. Dissertação (Mestrado) — São Paulo State University, January 2017.

GOSWAMI-BANERJEE, S.; ROBYR, M. Pressure and temperature conditions for crystallization of metamorphic allanite and monazite in metapelites: a case study from the miyar valley (high himalayan crystalline of zanskar, nw india). *Journal of Metamorphic Geology*, Wiley Online Library, v. 33, n. 5, p. 535–556, 2015.

HART, E. et al. A window into the lower crust: Trace element systematics and the occurrence of inclusions/intergrowths in granulite-facies rutile. *Gondwana Research*, The Authors, v. 59, p. 76–86, 2018. ISSN 1342937X. Avaible form internet: <http://linkinghub.elsevier.com/retrieve/pii/S1342937X18300856>.

HASUI, Y.; CARNEIRO, C. D. R.; COIMBRA, A. The Ribeira folded belt. *Revista Brasileira de Geociências*, v. 5, n. 4, p. 275–266, 1975.

HEILBRON, M.; CORDANI, U. G.; ALKMIM, F. F. *São Francisco Craton, Eastern Brazil: Tectonic Genealogy of a Miniature Continent*. [S.l.: s.n.], 2017. 331 p. ISBN 9783319017143.

HEILBRON, M. et al. From Collision to extension: the roots of the south-eastern continental margin of Brazil. In: TALWANI, M.; MOHRIAK, W. (Ed.). *Atlantic Rifts and Continental Margins of Brazil*. 115. ed. [S.l.]: American Geophysical Union, Geophysical Monographs, 2000. p. 1–34.

HEILBRON, M. et al. Província Mantiqueira. In: *Geologia do Continente sul-americano: evolução da obra de Fernando Flávio Marques de Almeida*. [S.l.: s.n.], 2004. p. 203–235.

HEILBRON, M. et al. Correlation of Neoproterozoic terrane between te Ribeira Belt, SE Brazil and its African countepart: comparative tectonic evolution and open questions. *Geological Society, London, Special Publications*, v. 294, p. 211–237, 2008.

HOLLAND, T. J. B. *AX: A program to calculate activities of mineral endmembers from chemical analyses (usually determined by electron microprobe);*. 2009. Avaible form internet: <http://ccp14.cryst.bbk.ac.uk/ccp/web-mirrors/crush/astaff/holland/ax.html>.

KOHN, M. J.; PENNISTON-DORLAND, S. C.; FERREIRA, J. C. Implications of near-rim compositional zoning in rutile for geothermometry, geospeedometry, and trace element equilibration. *Contributions to Mineralogy and Petrology*, Springer, v. 171, n. 10, p. 78, 2016.

KRETZ, R. Symbols for rock-forming minerals. *American Mineralogist*, v. 68, p. 277–279, 1983.

LUVIZOTTO, G. L. et al. Rutile occurrence and trace element behavior in medium-grade metasedimentary rocks: Example from the Erzgebirge, Germany. *Mineralogy and Petrology*, v. 97, n. 3-4, p. 233–249, 2009. ISSN 09300708.

MACHADO, N. et al. Ages of detrical zircon from Archean-Paleoproterozoic sequences: implication for greenstone belt setting and evolution of Transamazonian foreland basin in Quadrilátero Ferrífero, southeast Brazil. *Earth and Planetary Science Letters*, v. 141, p. 259–276, 1996.

MÖLLER, C. et al. High- and ultrahigh-pressure rocks—keys to lithosphere dynamics. *Journal of Metamorphic Geology*, v. 36, n. 5, p. 511–515, 2018. ISSN 15251314.

MORA, C. A. S.; NETO, M. d. C. C.; BASEI, M. A. S. Syn-collisional lower continental crust anatexis in the Neoproterozoic Socorro-Guaxupé Nappe System, southern Brasília Orogen, Brazil: Constraints from zircon U–Pb dating, Sr–Nd–Hf signatures and whole-rock geochemistry. *Precambrian Research*, Elsevier, v. 255, p. 847–864, 2014.

MORAES, R. et al. Characterization and P-T Evolution of Melt-bearing Ultrahigh-temperature Granulites: an Example from the Anapolis-Itauçu Complex of the Brasília Fold Belt. *Journal of Petrology*, v. 43, p. 1673–1705, 2002.

MORAES, R. et al. Applications and limitations of thermobarometry in migmatites and granulites using as an example rocks of the Araçuaí Orogen in southern Bahia, including a discussion on the tectonic meaning of the current results. *Brazilian Journal of Geology*, v. 45, p. 517–539, 2015.

NETO, V. C. et al. The pico do itapeva formation: A record of gravitational flow deposits in an ediacaran intracontinental basin, southern brasília orogen, se brazil. *Journal of South American Earth Sciences*, Elsevier, v. 84, p. 34–47, 2018.

NUNES, R.; TROUW, R. A. J.; CASTRO, E. *Mapa Gelógico - Folha Varginha – escala 1:100.000, Programa Geologia do Brasil*. [S.l.], 2008.

PACIULLO, F. V. P.; RIBEIRO, A. Mapa Geológico-Folha Nepumoceno. In: *CONTRATO - CPRM - UFRJ 067/P2/2005*. [S.l.: s.n.], 2008.

PACIULLO, F. V. P. et al. The Andrelândia Basin, a Neoproterozoic Intraplate Continental Margin, Southern Brasília Belt, Brazil. *Revista Brasileira de Geociências*, v. 30, n. 1, p. 200–202, 2000.

PACIULLO, F. V. P.; RIBEIRO, A.; TROUW, R. a. J. Geologia da Folha Andrelândia 1:100.000. *Geologia e recursos minerais do sudeste mineiro Projeto Sul de Minas - Etapa I*, p. 84–119, 2003.

PASSCHIER, C. W.; TROUW, R. A. *Microtectonics*. [S.l.]: Springer Science & Business Media, 2005.

PETERNEL, R. et al. Interferência Entre Duas Faixas Móveis Neoproterozóicas : O Caso Das Faixas Brasília E Ribeira No Sudeste Do Brasil. v. 35, n. 3, p. 297–310, 2005. ISSN 2317-4692.

QUÉMÉNEUR, J. J. G. et al. Mapa Geológico-Folha Lavras. In: *Geologia e Recursos Minerais do Sudeste Mineiro*. [S.l.: s.n.], 2003. p. 1:100.000.

RENO, B. L.; BROWN, M.; PICCOLI, P. M. $^{40}Ar/^{39}Ar$ thermochronology of high-pressure granulite nappes in the southern Brasília Belt, Brazil: Implications for Nappe Exhumation. *American Journal of Science*, American Journal of Science, v. 310, n. 10, p. 1294–1332, 2010.

RENO, B. L. et al. In situ monazite (U-Th)-Pb ages from the Southern Brasília Belt, Brazil: Constraints on the high-temperature retrograde evolution of HP granulites. *Journal of Metamorphic Geology*, v. 30, n. 1, p. 81–112, 2012. ISSN 02634929.

RIBEIRO, A.; HEILBRON, M. Estratigrafia e Metamorfismo dos Grupos Carrancas e Adrelândia, Sul de Minas Gerais. In: *Anais do XXXII Congresso Brasileiro de Geologia*. [S.l.: s.n.], 1982. p. 177–186.

RIBEIRO, A. et al. Evolução das Bacias Proterozóicas e o Termo-Tectonismo Brasiliano na Margem Sul do Cráton do São Francisco. *Revista Brasileira de Geociências*, v. 25, n. 4, p. 235–248, 1995.

ROCHA, B. C. et al. Timing of anatexis and melt crystallization in the Socorro – Guaxupé Nappe , SE Brazil : Insights from trace element composition of zircon , monazite and garnet coupled to U — Pb geochronology. v. 277, p. 337–355, 2017.

ROCHA, B. C. et al. Magmatic inheritance vs. UHT metamorphism: Zircon petrochronology of granulites and petrogenesis of charnockitic leucosomes of the Socorro–Guaxupé nappe, SE Brazil. *Lithos*, v. 314-315, p. 16–39, 2018. ISSN 18726143.

SANTOS, T. Bento dos et al. Thermochronological evidence for long-term elevated geothermal gradients in Ribeira Belt, SE Brazil. In: *Goldschmidt Conference 2007*. [S.l.: s.n.], 2007.

SILVA, M. P. *Modelamento Metamórfico de Rocas das Fácies Xisto-Verde e Anfibolito com o Uso de Pseudosseções: Exemplo das Rochas da Klippe Carrancas, Sul de Minas Gerais*. Tese (Dissertação de mestrado) — Universidade de São Paulo, 2010.

STENDAL, H. et al. Derivation of detrital rutile in the yaounde region from the neoproterozoic pan-african belt in southern cameroon (central africa). *Journal of African Earth Sciences*, Elsevier, v. 44, n. 4-5, p. 443–458, 2006.

TEDESCHI, M. et al. Reconstruction of multiple PTt stages from retrogressed mafic rocks: Subduction versus collision in the Southern Brasília orogen (SE Brazil). *Lithos*, Elsevier, v. 294, p. 283–303, 2017.

TEDESCHI, M. et al. Protracted zircon geochronological record of UHT garnet-free granulites in the Southern Brasília orogen (SE Brazil): Petrochronological constraints on magmatism and metamorphism. *Precambrian Research*, Elsevier, v. 316, n. August, p. 103–126, 2018. ISSN 03019268. Avaible form internet: <https://doi.org/10.1016/j.precamres.2018.07.023>.

THOMAS, J. B. et al. TitaniQ under pressure: The effect of pressure and temperature on the solubility of Ti in quartz. *Contributions to Mineralogy and Petrology*, v. 160, n. 5, p. 743–759, 2010. ISSN 00107999.

TOMKINS, H. S.; POWELL, R.; ELLIS, D. J. The pressure dependence of the zirconium-in-rutile thermometer. *Journal of Metamorphic Geology*, v. 25, n. 6, p. 703–713, 2007. ISSN 02634929.

TRIEBOLD, S. et al. Deducing source rock lithology from detrital rutile geochemistry: An example from the Erzgebirge, Germany. *Chemical Geology*, v. 244, n. 3-4, p. 421–436, 2007. ISSN 00092541.

TROUW, R. A. J. et al. The Central Segment of the Ribeira Belt. In: CORDANI, U. G. et al. (Ed.). *Tectonic Evolution of South America*. 1. ed. [S.l.]: COMPANHIA DE PESQUISA DE RECURSOS MINERAIS, 2000. p. 287–310.

TROUW, R. A. J. et al. *Mapa Geológico-Folha Caxambu. Projeto Sul de Minas - etapa 1, escala 1:100.000*. [S.l.], 2013.

TROUW, R. A. J. et al. A new interpretation for the interference zone between the southern Brasília belt and the central Ribeira belt, SE Brazil. *Journal of South American Earth Sciences*, v. 48, p. 43–57, 2013. ISSN 08959811.

TROUW, R. A. J.; RIBEIRO, A.; PACIULLO, F. V. P. Evolução Estrutural e Metamórfica de uma àrea a SE de Lavras - Minas Gerias. In: *Anais do XXXI Congresso Brasieliro de Geologia, Balneário de Camboriú, Santa Catarina*. Balneário de Camburiú: [s.n.], 1980.

TROUW, R. A. J.; RIBEIRO, A.; PACIULLO, F. V. P. Geologia Estrutural do Grupos São João del Rei, Carrancas e Andrelândia, Sul de Minas Gerais. *Anais da Academia brasileira de Ciências*, v. 55, n. 1, p. 71–87, 1983.

TROUW, R. A. J.; TAVARES, F. M.; ROBYR, M. Rotated garnets: a mechanism to explain the high frequency of inclusion trail curvature angles around 90^o and 180^o. *Journal of Structural Geology*, v. 30, n. 8, p. 1024–1033, 2008. ISSN 01918141.

VALERIANO, C. M. The Southern Brasília Belt. In: HEILBRON, M.; CORDANI, U. G.; ALKMIM, F. (Ed.). *São Francisco Craton, Eastern Brazil. Regional Geology Reviews*. Switzerland: Springer International Publishing, 2017. cap. The Southe, p. 189–203. ISBN 9783319017150.

VALERIANO, C. M. et al. U-Pb Geochronology of Southern Brasília Belt (SE Brazil): sedumentary provenance, Neoproterozoic orogeny and assembly of Western Gondwana. *Precambrian Research*, v. 130, p. 7–11, 2004.

VINAGRE, R. et al. Superposition of structures in the interference zone between the southern brasília belt and the central ribeira belt in the region sw of itajubá (mg), se brazil. *Brazilian Journal of Geology*, SciELO Brasil, v. 46, p. 547–566, 2016.

VLACH, S.; GUALDA, G. A. R. Microprobe monazite dating and the ages of some granitic and metamorphic rocks from southeastern Brazil. *Revista Brasileira de Geociências*, v. 30, n. 1, p. 214–218, 2000.

VLACH, S. R. F. Th-u-pbt dating by electron probe microanalysis, part i. monazite: analytical procedures and data treatment. *Geologia USP: Série Científica*, v. 10, n. 1, p. 61–85, 2010.

WESTIN, A.; CAMPOS NETO, M. D. C. Provenance and tectonic setting of the external nappe of the Southern Brasília Orogen. *Journal of South American Earth Sciences*, Elsevier Ltd, v. 48, p. 220–239, 2013. ISSN 08959811. Avaible form internet: <http://dx.doi.org/10.1016/j.jsames.2013.08.006>.

WESTIN, A. et al. The Neoproterozoic southern passive margin of the São Francisco craton: Insights on the pre-amalgamation of West Gondwana from U-Pb and Hf-Nd isotopes. *Precambrian Research*, p. 454–471, 2019.

WESTIN, A. et al. A paleoproterozoic intra-arc basin associated with a juvenile source in the Southern Brasilia Orogen: Application of U–Pb and Hf–Nd isotopic analyses to provenance studies of complex areas. *Precambrian Research*, v. 276, p. 178–193, 2016.

WHITE, R. W. et al. The effect of TiO_2 and Fe_2O_3 on metapelitic assemblages at greenschist and amphibolite facies conditions: mineral equilibria calculations in the system K_2O–FeO–MgO–Al_2O_3–SiO_2–H_2O–TiO_2–Fe_2O_3. *Journal of Metamorphic Geology*, v. 18, p. 497–511, 2000.

WHITE, R. W. et al. New mineral activity-composition relations for thermodynamic calculations in metapelitic systems. *Journal of Metamorphic Geology*, v. 32, n. 3, p. 261–286, 2014. ISSN 15251314.

WILLIAMS, M. et al. Format and philosophy for collecting, compiling, and reporting microprobe monazite ages. *Chemical Geology*, Elsevier, v. 225, n. 1-2, p. 1–15, 2006.

ZACK, T.; MORAES, R.; KRONZ, A. Temperature dependence of Zr in rutile: Empirical calibration of a rutile thermometer. *Contributions to Mineralogy and Petrology*, v. 148, n. 4, p. 471–488, 2004. ISSN 00107999.

5 The potential for using metagreywacke to study metamorphism of amphibolite facies conditions: a comparison study within the Luminárias Nappe, Southern Brasília Orogen (Southeastern Brazil)

Regiane A. Fumes[1]; George L. Luvizotto[1]; Renato Moraes[2]; Lara A. Patto[1]

[1] Department of Geology, São Paulo State University, Av. 24A, 1515, 13506-900, Rio Claro, Brazil

[2] Department of Mineralogy and Geotectonics, University of São Paulo, Rua do Lago, 562, 05508-080, São Paulo, Brazil

Abstract

Metagreywacke is a very common rock type in orogenic settings. It occurs in several domains within the Neoproterozoic Southern Brasília Orogen, that registers convergent events related to the Western Gondwana formation. Studied rocks derive from the Luminárias Nappe, which is composed of metapelite (Campestre Unit), quartzite and metagreywacke (Santo Antônio Unit) that occur in the northern portion of the structure. The potential use of the metagreywacke in metamorphic studies and the metamorphic P–T path of the Santo Antônio Unit was constrained using isochemical phase diagram, quantitative compositional mapping, and composition mineral contours. The metamorphic peak mineral assemblage of the metagreywacke is biotite + plagioclase + garnet + muscovite + ilmenite + quartz. Rutile is a prograde phase, but is replaced by ilmenite at metamorphic peak, while chlorite is a retrograde phase, as it replaced biotite and garnet. The garnet is almandine rich, preserves zoning, with lower almandine and pyrope contents in the core and lower spessartine and grossular contents in the rim. The peak assemblage is stable at temperatures of 570 °C to 650 °C and pressures of 0.7 GPa to 1.05 GPa. Prograde conditions of 540 °C and 0.9 GPa are obtained using the garnet core spessartine composition and the rutile occurrence. The compositional mineral contours of garnet rim, combined with those of muscovite and plagioclase, intercept at 630 °C and 1.0 GPa and indicate peak metamorphic conditions. Later crystallization of chlorite took place during retrograde conditions at 580 °C and 0.7 GPa, defining a single clockwise P–T path. The

calculated topology of metagreywacke pseudosection, in this study, resembles those of a typical metapelite, and the crystallization sequence of metamorphic index minerals, along a Barrovian gradient, with slightly distinguished mineral assemblages. The similarity and differences for the two rock types occurs, specially under amphibolite facies conditions. Therefore, the metagreywacke is a promising protolith for metamorphic studies, even if it presents marking differences from pelites. The constrained P–T path is similar to those presented in previous works carried out in the Luminárias Nappe, associated with the collisional setting in the Southern Brasília Orogen.

Keywords Biotite schist, Carrancas Group, Metagreywacke, Perple_X, XMapTools, Santo Antônio Unit

5.1 Introduction

Greywackes are sedimentary rocks that usually occur in flysch-like sequences Dzulynski e Walton (2011). These rocks are compositionally immature. Due to the rapid erosion associated with the mountain building of the orogens, the sedimentation of immature sediments, such as the greywackes, are common in the syn-orogenic units. In recent and old orogens, the (meta)greywacke could be the dominant siliciclastic rock type, even more abundant than (meta)pelite (Johnson; WHITE; POWELL, 2008). Therefore, it is important to investigate what kind of information can be extracted from metagreywackes in metamorphic studies.

Assessing the metamorphic conditions of greenschist and amphibolite facies of non-pelite metasedimentary rocks, such as the metagreywackes, with great precision, is an interesting task and usually requires the aid of advanced techniques, such as calculation of isochemical phase diagrams (or pseudosections) and compositional maps (LANARI; DUESTERHOEFT, 2019). Furthermore, the integration of isochemical phase diagrams and associated mineral isopleths with compositional maps allows for a better understanding of the metamorphic record of the rocks, not only to establish the metamorphic peak conditions, but also to understand the pressure (P)–temperature (T) path. The greywackes, after metamorphism, might produce a rock that is much richer, when compared with metapelites, in biotite and plagioclase, or even other Fe-Mg phases, such as amphibole in some cases. On the other hand, in most cases, their composition might follow similar guidelines as pelites. Greywackes have significant amounts of SiO_2 and most rocks may have quartz in excess, fair amounts of Al_2O_3, with production of aluminum-rich phases as garnet, staurolite, and aluminum-silicates polymorphs and, finally, the amount of K_2O is high enough to produce muscovite or K-feldspar in a wide P–T range. So, many metagreywackes can be envisaged as pelites enriched in biotite and plagioclase, so they may produce interesting sequences of metamorphic minerals, which are very useful to infer metamorphic conditions.

The southern Brasília Orogen is one of the Neoproterozoic collisional orogens related to the Western Gondwana formation (DARDENNE, 2000; FUCK et al., 2017; HEILBRON; CORDANI; ALKMIM, 2017) and the southernmost portion of this orogen is composed of several metasedimentary rocks, such as metagreywackes, metapelites and quartzites, organized in a stack of syn-metamorphic thick-skinned nappes (CAMPOS NETO et al., 2010). The Luminárias Nappe is one of them, in which metamorphic peak conditions took place under high-pressure greenschist to eclogite facies (TROUW; RIBEIRO; PACIULLO, 1980; TROUW et al., 1982; TROUW et al., 2000; SILVA, 2010; FUMES et al., 2019), but detailed studies on the characterization of the metamorphic P–T path of the Santo Antônio Unit, made up of metagreywacke rocks, have never been carried out in the Luminárias region. As the Luminárias is composed of metagreywackes and metapelites, it serves as an excellent example for comparative petrological study of all these rocks. Thus, understanding the metamorphic P–T path of the metagreywacke (the Santo Antônio Unit) may add key information to the tectonic evolution of the Luminárias Nappe and the southern Brasília Orogen, as well as to the understanding of metamorphic evolution of these rocks.

The aim of this work is to investigate the potential use of the metagreywacke in metamorphic studies. What are the advantages and the limitations in thermobarometry using metagreywackes? Furthermore, the metagreywacke from Santo Antônio Unit is used to investigate the metamorphic conditions and the P–T path of the Luminárias Nappe, for which we use microstructures, as well as metamorphic modelling and quantitative compositional mapping.

5.2 Geological setting

The Brasília Orogen occurs in the center / southeast region of Brazil (Fig. 5.1 a), and represents an Ediacaran-Cambrian collisional orogen related to the western Gondwana formation (BRITO NEVES; CAMPOS NETO; FUCK, 1999; CAMPOS NETO; CABY, 2000; TROUW et al., 2000). The Brasília Orogen is several hundred km long and is subdivided into northern and southern (location of the study area) portions, in respect to the Pirineus Syntaxis (ARAÚJO FILHO, 2000).

According to (CAMPOS NETO, 2000), the southernmost portion of the Brasília Orogen is divided (from top to base) in (Fig. 5.1 b): (i) granulite-migmatite-granite lower crust of the Socorro-Guaxupé Nappe, that derives from a magmatic arc root (CAMPOS NETO; CABY, 1999; CAMPOS NETO, 2000); (ii) metasedimentary rocks associated with forearc and accretionary prism segments that compose the Andrelândia Nappe System (TROUW et al., 1982; TROUW; RIBEIRO; PACIULLO, 1983; TROUW et al., 2000; CAMPOS NETO; CABY, 1999; CAMPOS NETO, 2000; CAMPOS NETO et al., 2007);

Figure 5.1 – Location of the studied area. a) Gondwana map (situation ~500 Myr ago) showing the location of the study area (red rectangle). Extracted from Spencer et al. (2013). b) Geological map of the Southern Brasília Orogen with the location of the Luminárias Nappe. Extracted from Frugis, Neto e Lima (2018).

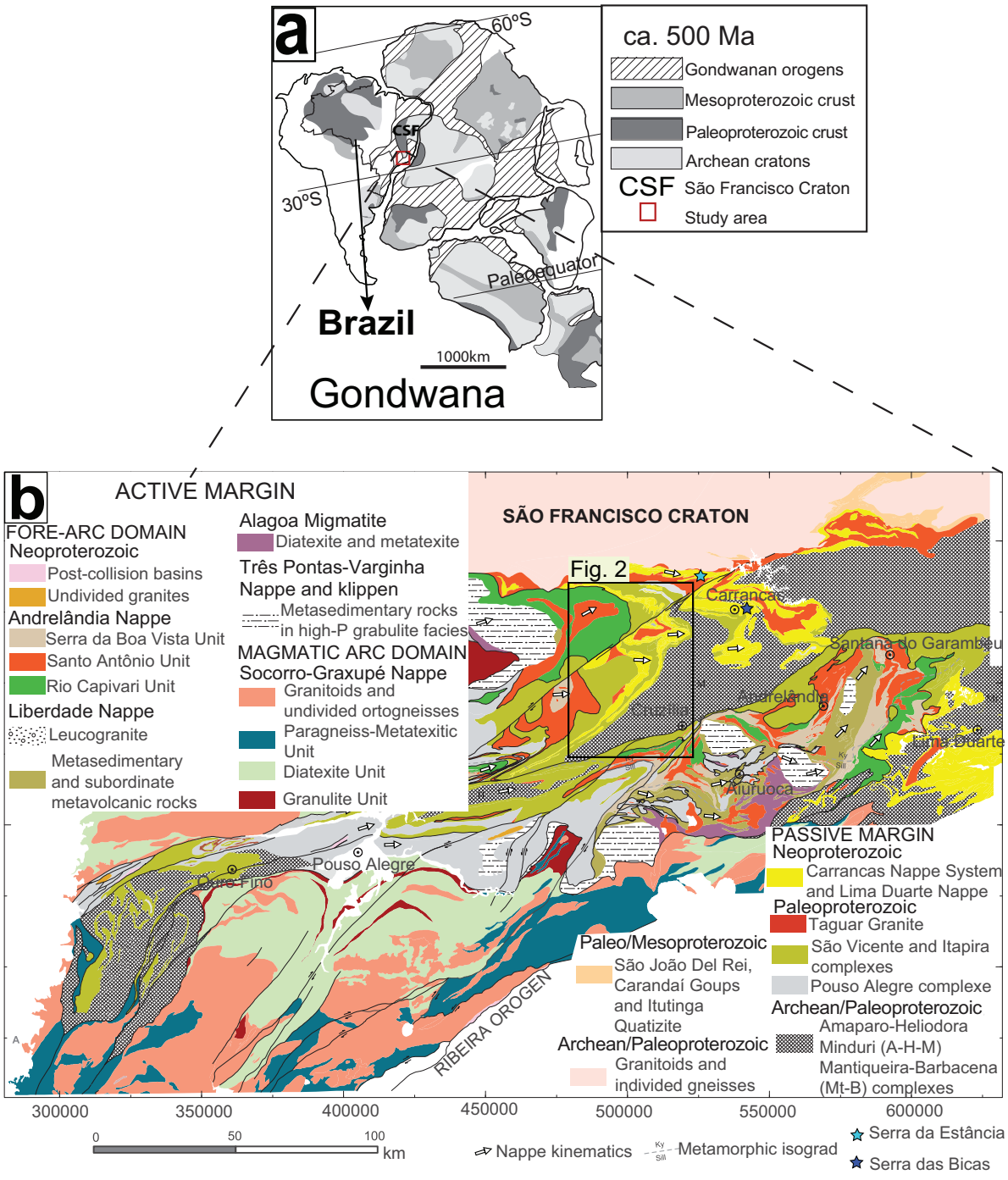

(iii) metasedimentary rocks interpreted as the western passive continental margin of Sanfranciscan Plate, e g., the Carrancas Nappe System and Lima Duarte Nappe, where the Luminárias Nappe is included (PACIULLO et al., 2000; PACIULLO; RIBEIRO; TROUW, 2003; TROUW et al., 2000; CAMPOS NETO et al., 2004; WESTIN et al., 2019).

The Carrancas Nappe System, where the study area is located, is predominantly

composed of paragneiss, quartzite, schist and minor amphibolite bodies (TROUW; RIBEIRO; PACIULLO, 1980; TROUW; RIBEIRO; PACIULLO, 1983). This system consists of two main pieces of nappes, the Luminárias Nappe and Carrancas Klippe (Fig. 5.1 b). The Luminárias Nappe is an elongated structure, 80 km long N-S, thrusted over older rocks (Fig. 5.2). The biotite gneiss from the São Vicente Unit occurs at the base of the Luminárias Nappe (WESTIN et al., 2016). The São Vicente Unit is overlain by (muscovite) quartzite from São Tomé das Letras Unit and metapelite from the Campestre Unit. The Santo Antônio Unit, the focus of this study, occurs at the top of the Luminárias Nappe and is composed of metagreywacke (plagioclase-bearing biotite schist) (TROUW et al., 2000; RIBEIRO et al., 1995). The basement rocks are represented by orthogneisses (SE of Luminárias Nappe) and are interpreted as parts of the São Francisco paleocontinent crust that was reworked during the orogenic processes (CIOFFI et al., 2016).

According to Campos Neto et al. (2007), Campos Neto et al. (2011) and Westin e Campos Neto (2013), the Santo Antônio Unit in the Andrelândia Nappe System (southeastern of Luminárias Nappe), was deposited in a syn–collisional orogenic foreland basin. The sediments of this basin were derived from a juvenile volcanic arc with Ediacaran age ca. 630-590 Ma and followed an immediate metamorphic peak at 610 Ma (CAMPOS NETO et al., 2007; CAMPOS NETO et al., 2011; WESTIN; CAMPOS NETO, 2013). According to Kuster et al. (2020), the Santo Antônio Unit was deposited in a relatively deep and fast subsiding basin during the early collisional stage of the Southern Brasília Orogen. Marimon et al. (2021) interpreted that the Santo Antônio Unit was deposited in a syn-collisional basin with maximum depositional age at 650 Ma. Although the depositional age is slightly older, it is not very different from those proposed earlier by Campos Neto et al. (2007), Campos Neto et al. (2011), Westin e Campos Neto (2013).

Fumes et al. (2019) describes that the metamorphic peak conditions in the metapelites from the Luminárias Nappe vary from high-pressure lower-amphibolite facies, in the northern portion, which occurred at 615 ±6 Ma [electron probe micro-analyzers (EPMA) total U–Th–Pb monazite–(Ce) ages], to eclogite facies in the southern portion at 632 ±4 Ma. In the Carrancas region, an investigation using pelites reveals that metamorphism varies from north to south, with transition from greenschist to amphibolite facies at the northern portion to conditions of high-pressure amphibolite facies at the south, close to eclogite facies. In Serra da Estância, the peak metamorphic conditions were calculated as 1.00 ±0.17 GPa and 577 ± °C and for Serra das Bicas 1.29 ±0.10 GPa and 608.5 ±19.5 °C. A sequence of kyanite + chloritoid, chloritoid + staurolite + chlorite, staurolite + kyanite + garnet and finally kyanite + garnet + biotite is observed from north to south (SILVA, 2010). The Santo Antônio Unit in the Carrancas Klippe is metamorphosed under greenschist facies, with chlorite, biotite, muscovite, and garnet as index minerals citeWestin2013. According to Motta e Moraes (2017), the metamorphic peak of the Santo Antônio Unit in the Andrelândia Nappe System, south of the Luminárias Nappe, is 668

Figure 5.2 – Geological map of the Luminárias Nappe (extracted and modified from Quéméneur et al. (2003), Nunes, Trouw e Castro (2008), Paciullo e Ribeiro (2008), Trouw et al. (2013a). This geological map of the Luminárias sheet is based on Almeida (1992) and mapping of undergraduate courses in the 80^{ths} of Federal University of Rio de Janeiro. The arrows in the legend of the biotite gneiss interlayered with schists and quartzite is due the different interpretations presented in the literature of the age of this unit: According Ribeiro et al. (1995), Paciullo et al. (2000) this unit is Neoproterozoic (Na_1 and Na_2), whereas according to Westin et al. (2016) the unit is Paleoproterozoic (São Vicente Complex). Geographical coordinates of analyzed samples are present in Table 5.1.

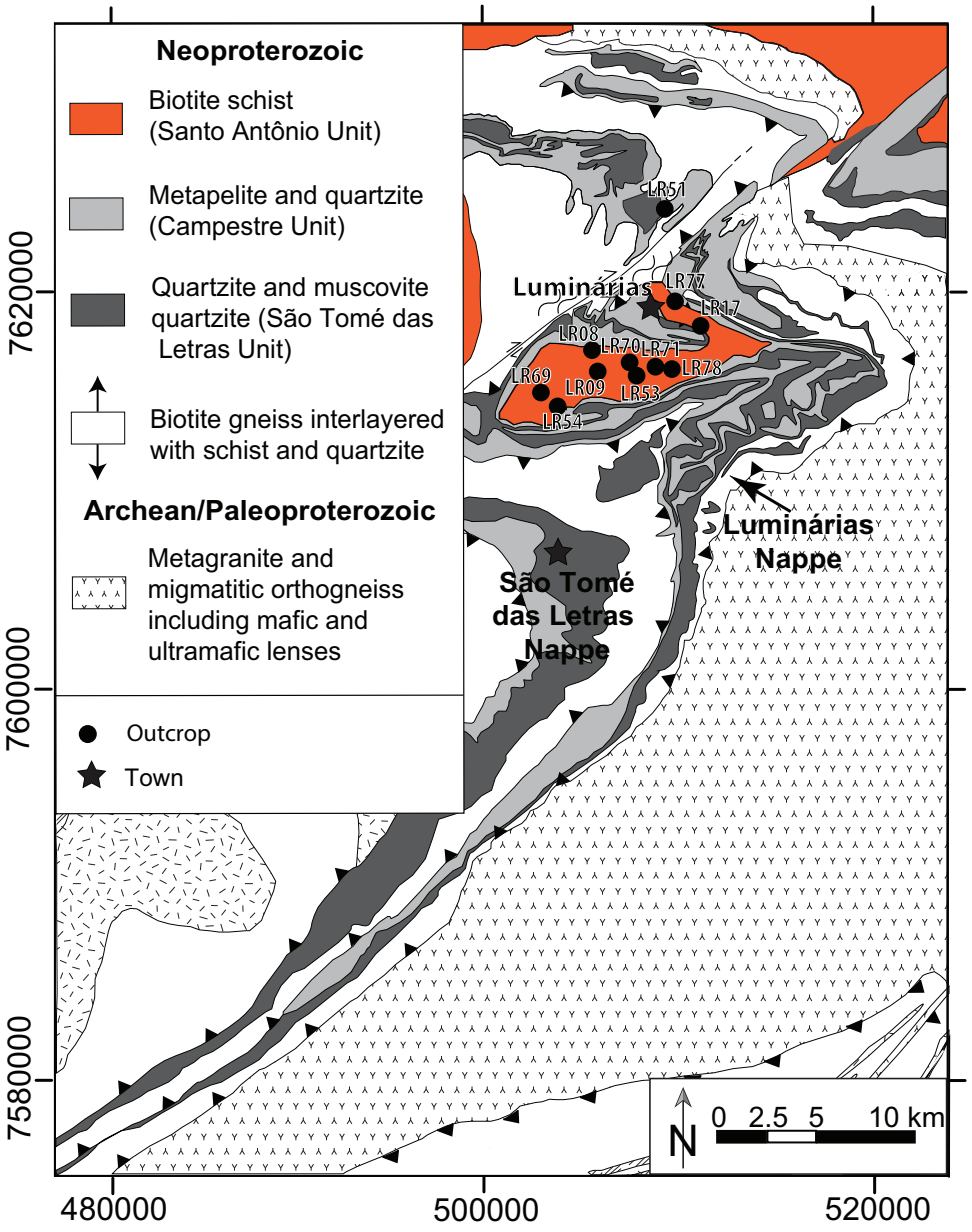

±15 °C and 0.9 ±0.07 GPa at 586 ±15 Ma. The Santo Antônio Unit at SW of the Luminárias Nappe presents a peak at ∼720 °C and 1.0 GPa, with anatexis due the water excess (BATISTA, 2015; BATISTA et al., 2018).

In the literature, two interpretations have been proposed for the tectonic evolution of the southeasternmost border of the Brasília Orogen and its relation with the Neoproterozoic Ribeira Orogen, including (i) the occurrence of an interference zone due to superposition

of structures and metamorphism related to collision in both orogens Trouw et al. (2000), Trouw et al. (2013), Peternel et al. (2005), Heilbron et al. (2008), Heilbron, Cordani e Alkmim (2017), Coelho et al. (2017); and (ii) the presence of only one set of deformational structures and metamorphism, exclusively related to the Brasília Orogen (CAMPOS NETO, 2000; CAMPOS NETO et al., 2004; CAMPOS NETO et al., 2007; WESTIN et al., 2016).

5.3 Materials and Methods

5.3.1 Whole-rock chemistry and thermodynamic modelling

Whole-rock chemical compositions were obtained by X-ray fluorescence. Representative sample powders were mixed with lithium tetraborate to obtain fused disks. The disks were analyzed with a Philips PW 2400 equipment. Loss on ignition was determined by the conventional gravimetric method.

Phase equilibria modelling was undertaken with the software Perple_X (version 6.8; Connolly (2005) and dataset version 6.2.2 from Holland e Powell (2011). Our calculations considered solution phase descriptions of biotite, chlorite, white mica, staurolite and garnet from White et al. (2014), of ilmenite from White et al. (2000), modified as described by White et al. (2014), of pyroxene from Holland, Green e Powell (2018), of epidote from Holland e Powell (2011) and of feldspar from (FUHRMAN; LINDSLEY, 1988). The phase diagram was based on the chemical model system MnO-Na_2O-CaO-K_2O-FeO-MgO-Al_2O_3-SiO_2-H_2O-TiO_2-O_2 (MnNCKFMASHTO), which represents the whole composition of a metagreywacke. The P and T intervals were 0.6 to 1.8 GPa and 500 to 700 °C, respectively. H_2O was set to be in excess for the whole P–T range.

A MnNCKFMASHTO isobaric (1.0 GPa) T–XO_2 isochemical phase diagram (Fig. 5.S1) was calculated to constrain the oxygen content used to the P–T isochemical phase diagram. The O_2 value of 0.5% mol was chosen due the predominance of ilmenite at the metamorphic peak and to produce small amounts of rutile, as observed in investigated samples.

5.3.2 Chemical analysis

Chemical mineral analysis and elemental maps were carried out using a JEOL JXA-8230 EPMA system operated in wavelength-dispersive X-ray spectrometry mode. Matrix correction was performed using the ZAF method.

Chemical compositions of garnet, chlorite, biotite, muscovite and plagioclase were obtained by EPMA point analyses that were carried out using a focused beam at 15 kV and 20 nA. The total counting times were 10s peak and 5s background for major elements

Table 5.1 – Location of the studied samples. Coordinates are in Universal Transverse Mercator (UTM) (Zone 23K, WGS84).

Outcrop/Sample	**UTM E (m)**	**UTM S (m)**
LR-08	507538	7619042
LR-09	507731	7617820
LR-17	511432	7620562
L5-53	508987	7618214
LR-54	505190	7616186
LR-69	504202	7616678
LR-70	509005	7618212
LR-71	510387	7618289
LR-77	510942	7621303
LR-78	511254	7618155

and 20s and 10 s background for minor elements. Natural reference minerals and synthetic oxides were used for calibration; these calibrant materials and detailed EPMA conditions are summarized in Table 5.S1. Mineral formulae were calculated with the AX software (HOLLAND, 2009).

For micro-scale elemental mapping, the EPMA system was operated at 15 kV and 100 nA. The beam size was set to 10 μm and the dwell time per pixel to 100 ms. Data were processed using the XMapTools 3.2.1 software (LANARI et al., 2014; LANARI; DUESTERHOEFT, 2019). Quantitative maps were produced by calibrating X-ray counts using results of quantitative point analyses placed within the map area. The mineral compositions described in the present paper, and used in the interpretations of the composition mineral contours, were based on these quantitative maps.

5.4 Results

5.4.1 Sample descriptions: microstructures and mineral assemblages

The metagreywacke from the Santo Antônio Unit crops out only in the northern portion of the Luminárias Nappe (Fig. 5.2 and Table 5.1). The rocks have lepidoblastic and inequigranular microstructure (Fig. 5.3). All the studied samples are similar in microstructure, composition and mineral modal proportion. The main foliation, Sn, is a continuous schistosity that is defined by the orientation of the muscovite, quartz, biotite and elongated plagioclase. This schistosity can be locally crenulated (Fig. 5.3d). The average grain size of the matrix minerals is ∼of 0.3 mm with garnet porphyroblasts reaching up to 5 mm. The rock matrix is composed of muscovite (30-35 vol%), quartz (20-40 vol%), biotite (10-20 vol%), plagioclase (5-15 vol%), chlorite (from traces up to 2 vol%), ilmenite (from traces up to 1 vol%), tourmaline (accessory), rutile (accessory), epidote (accessory) and apatite (accessory, see Fig. 5.3).

Figure 5.3 – Petrographic features of the biotite schist from the Luminárias Nappe. a and b) Photomicrograph from sample LR09 showing in the center a garnet porphyroblast with chlorite in the rim (plane-polarized light in a and crossed-polarized light in b). c) Back- scatter electron image from sample LR09 showing the biotite associated with the chlorite. d) Photomicrograph of sample LR08 showing the schistosity crenulated in the matrix of the biotite schist (plane-polarized light) e) Mineral distribution map from sample LR09 showing syn-tectonic to Sn garnet porphyroblasts with chlorite in the rim and the matrix composed of quartz, plagioclase, biotite and chlorite. f) Mineral distribution map from sample LR54 showing a syn-tectonic to Sn garnet porphyroblast and the matrix composed of white mica, quartz, plagioclase, biotite, ilmenite and apatite. Abbreviations according to Whitney e Evans (2010).

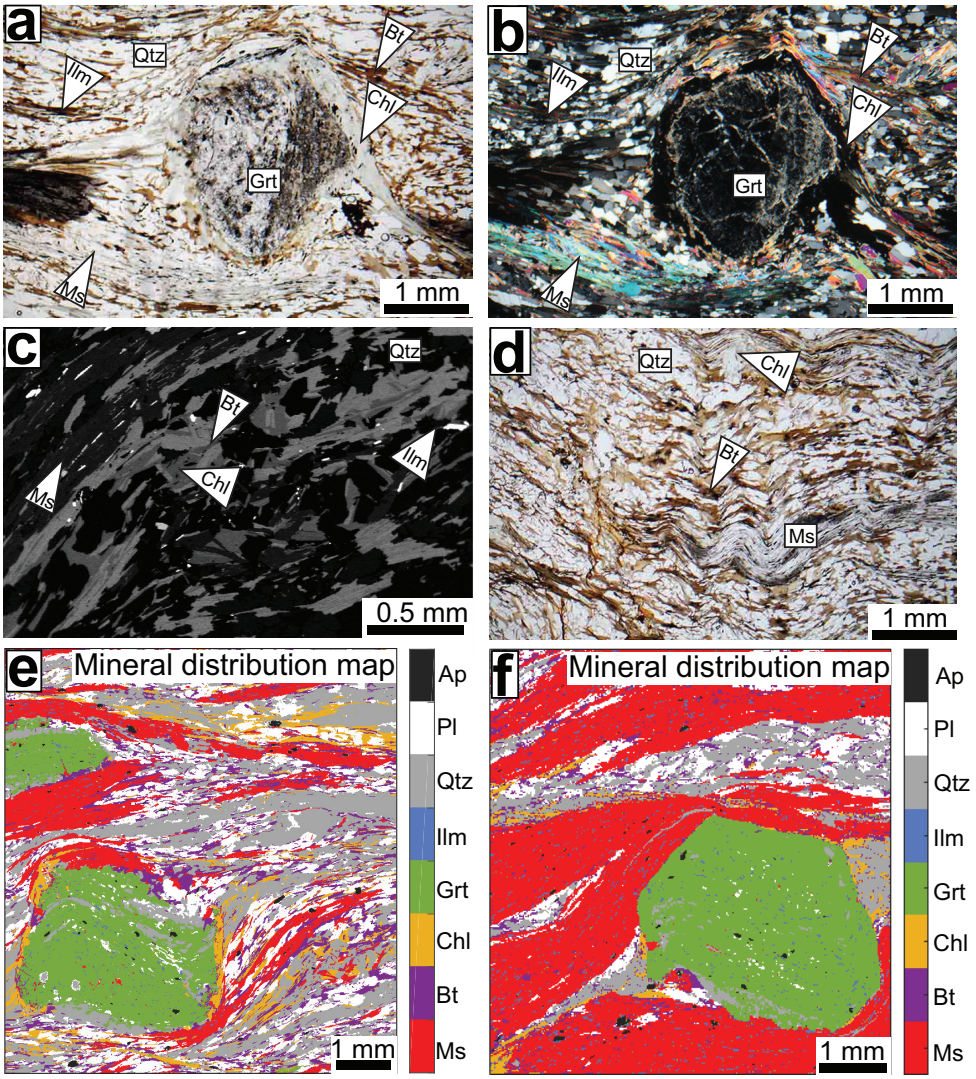

Quartz occurs both in the matrix and as inclusions in garnet. It often shows undulatory extinction and dynamic recrystallization by grain boundary migration and subgrain rotation. Plagioclase occurs in the matrix and as inclusion in the garnet (Figs. 5.3e,f). Muscovite is the most abundant mica and occurs in the matrix, as well as inclusion in garnet; biotite also occurs in the matrix and as inclusion in garnet, but only in the rims. Chlorite is observed in the matrix, crystallizing at the expense of biotite and surrounding garnet porphyroblasts (Figs 5.3a–c, e, f). The garnet porphyroblasts have curved inclusion trails defined by quartz, muscovite, plagioclase, ilmenite, rutile and biotite. Strain shadows

are common. These features allow for the interpretation of a syn-tectonic growth of the porphyroblasts during the formation of Sn (Figs. 5.3a, b, e, f). Ilmenite is the most abundant titanium phase. Rutile occurs rarely, and it is replaced by ilmenite, so the rutile is interpreted as a prograde phase. The peak mineral assemblage is biotite + plagioclase + garnet + muscovite + ilmenite + quartz and chlorite is a retrograde phase.

5.4.2 Compositional variability of metamorphic minerals

Representative chemical analyses of metamorphic minerals from samples LR09 and LR54 are listed in Table 5.2 and in Table 5.S2, while quantitative compositional mapping is presented in Figs. 5.4 and 5.5, and in Fig. 5.S3. Results of quantitative composition mapping open up the opportunity for direct observation of mineral compositions in the rocks. Mineralogical compositions of the two samples studied are fairly similar.

Quantitative compositional maps show an intense chemical zoning of garnet porphyroblasts (Figs. 5.4 and 5.5). The zoning is concentric, with the core presenting lower almandine and pyrope contents and higher spessartine and grossular contents with respect to the rim. The nominal almandine fraction varies from 55–67 mol% in the core to 65–78 mol% in the rim. End-member fractions of pyrope (6–8 mol% core; 8–11 mol% rim), spessartine (15–25 mol% core; 1–15 mol% rim) and grossular (11–14 mol% core; 7–11 mol% rim) vary accordingly (Figs. 4 and 5). The X_{Mg} value [Mg/(Mg+Fe)] in garnet varies from 0.06–0.10 (core) to 0.11–0.16 (rim; Figs. 5.4e, 5.5e). The molar Fe/Ca ratios vary from 2–6 (core) to 6–10 in the rim (Figs. 5.4f and 5.5f).

Muscovite is fairly homogeneous, with the exception of some domains (Figs. 5.S2a–h). The proportions of other end-members of white mica (paragonite, celadonite and Fe-celadonite) are less than 30 mol%. The X_{Fe} value [Fe/(Mg+Fe)] in muscovite varies from 0.40 to 0.52, with higher values in the rim of some muscovite agglomerates (Fig. 5.S2a). In some rare portions, however, the Fe contents in muscovite and paragonite are significantly lower (X_{Fe} 0.58 and 0.15, respectively). The Si^{4+} content in muscovite is 3.1 apfu, and Na+ varies in the range 0.1–0.2 apfu.

Biotite has a homogeneous composition and its X_{Fe} value is 0.52 (Figs. 5.S2i, m). Chlorite is also homogeneous and its X_{Fe} value is 0.48 (Figs. 5.S2j, n), while Si^{4+} is about 0.48 apfu (Figs. 5.S2k, o). The plagioclase composition varies from An0.13 to An0.19, with higher anorthite contents usually occurring in the core (Figs. 5.S2l, p).

5.4.3 Thermodynamic modelling

A *P–T* isochemical phase diagram was calculated for the bulk composition of sample LR09 (Fig. 6). The phases modelled in the phase diagram are garnet, chlorite, biotite, Al_2SiO_5, epidote, plagioclase, muscovite, quartz, staurolite ilmenite, clinopyroxene

Figure 5.4 – Fig. 4 Garnet composition maps (i.e., colour-coded distribution patterns based on nominal end-member fractions) showing the chemical zoning in sample LR54. a) Almandine map and chemical compositional profile. b) Spessartine map and chemical compositional profile. c) Pyrope map and chemical compositional profile. d) Grossular map and chemical compositional profile. e) X_{Mg} map and profile in garnet from sample LR54. f) Ratio of Fe/Ca map and chemical profile. Corresponding mineral distribution maps are shown in Figs. 5.3e, f. The dashed black lines in the maps indicate the location of the chemical compositional profiles.

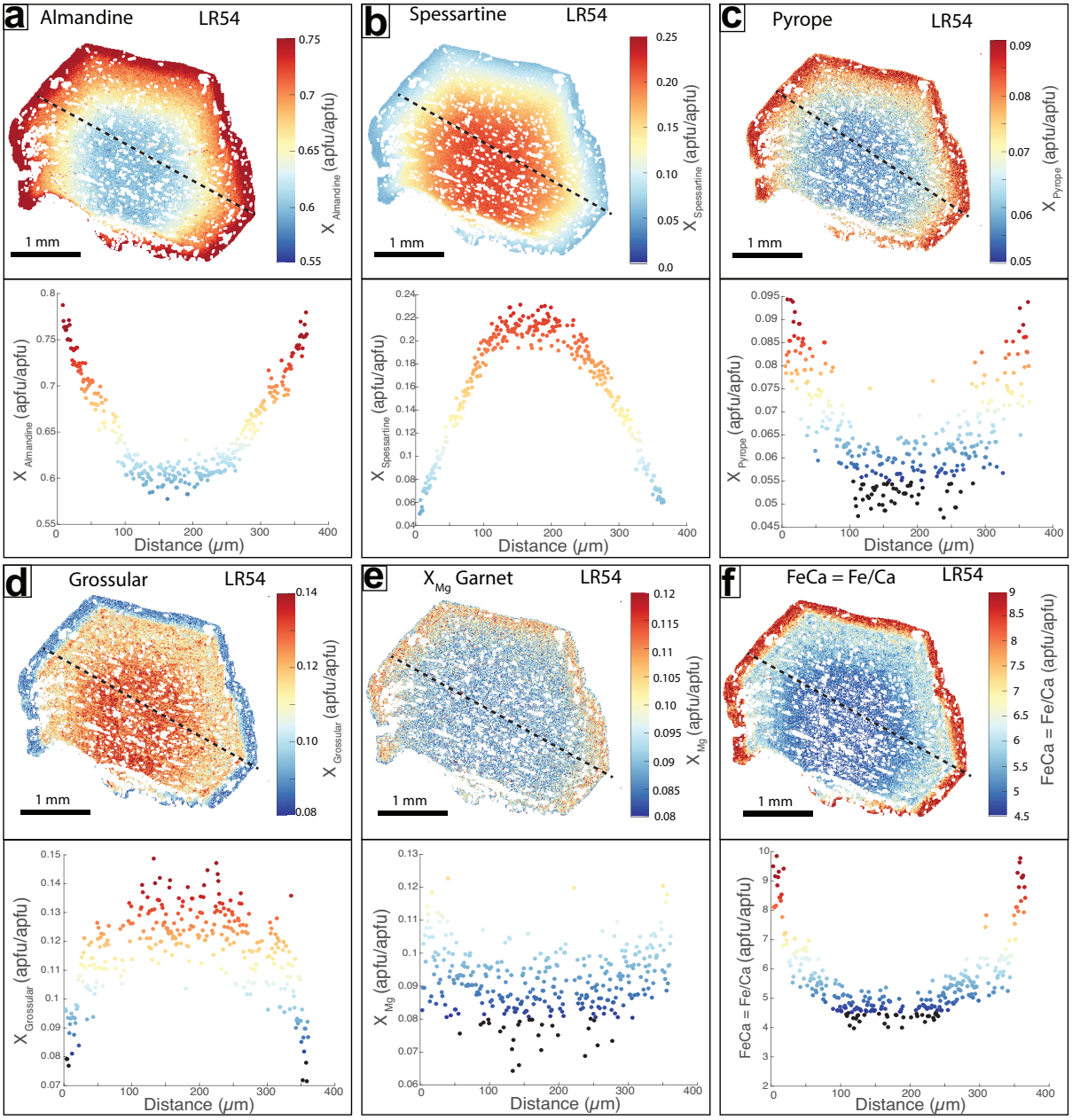

and rutile, with water as excess fluid.

Quartz, water and muscovite occur in all fields of the diagram (Fig. 5.6). Chlorite only occurs at temperatures below 580 °C and pressures lower than 0.75 GPa or higher than 1.1 GPa. Plagioclase occurs in all temperature ranges with exception of some fields at pressures higher than 1.0 GPa. Biotite is stable almost across the entire phase diagram, with exception of two fields, the first with pressures lower than 1.0 GPa and temperatures

Table 5.2 – Representative chemical compositions, calculated mineral formulae and calculated nominal end-member fraction for index metamorphic minerals.

Sample	LR09	LR09	LR54	LR54	LR09	LR54	LR09	LR54	LR09	LR54	LR54	LR09
Mineral	Grt	Grt	Grt	Grt	Bt	Bt	Chl	Chl	Ms	Ms	Fsp	Fsp
Location	Core	Rim	Rim	Core	-	-	-	-	-	-	-	-
Major oxides (wt%)												
SiO_2	37.31	37.43	37.12	37.33	36.23	36.26	24.51	24.70	46.89	47.22	65.53	63.91
TiO_2	0.18	0.10	0.01	0.13	1.74	1.59	0.06	0.07	0.34	0.21	0.00	0.00
Al_2O_3	20.04	21.10	21.31	20.89	18.25	18.67	22.12	22.62	35.40	35.46	22.58	23.37
Cr_2O_3	0.01	0.02	0.00	0.03	0.00	0.00	0.00	0.00	0.00	0.00	0.00	0.00
FeO	25.85	28.15	33.87	26.82	18.90	19.11	24.24	24.49	1.17	1.19	0.05	0.14
MnO	9.86	7.13	2.65	8.88	0.11	0.03	0.18	0.10	0.01	0.02	0.00	0.00
MgO	1.72	1.99	2.02	1.45	10.05	9.77	14.31	14.12	0.75	0.67	0.00	0.00
CaO	3.97	4.13	3.04	4.34	0.00	0.00	0.01	0.01	0.00	0.00	3.12	4.04
Na_2O	0.02	0.02	0.05	0.00	0.07	0.06	0.01	0.02	0.71	0.89	9.86	9.22
K_2O	0.00	0.00	0.00	0.02	8.80	8.65	0.02	0.01	9.83	9.26	0.05	0.06
Total	98.96	100.07	100.07	99.89	94.15	94.14	85.46	86.14	95.10	94.92	101.19	100.74
Calculated mineral formulae (apfu)												
Si	3.01	3.01	2.99	3.01	2.77	2.77	2.64	2.64	3.11	3.12	2.85	2.80
Ti	0.01	0.01	0.00	0.01	0.10	0.09	0.01	0.01	0.02	0.01	0.00	0.00
Al	1.99	2.00	2.03	1.99	1.65	1.68	2.81	2.85	2.77	2.77	1.16	1.21
Cr	0.00	0.00	0.00	0.00	0.00	0.00	0.00	0.00	0.00	0.00	0.00	0.00
Fe3	0.00	0.00	0.00	0.00	0.00	0.00	0.00	0.00	0.00	0.00	0.00	0.01
Fe2	1.74	1.89	2.28	1.81	1.21	1.22	2.18	2.19	0.07	0.07	0.00	0.00
Mn	0.67	0.49	0.18	0.61	0.01	0.00	0.02	0.01	0.00	0.00	0.00	0.00
Mg	0.21	0.24	0.24	0.18	1.15	1.11	2.30	2.25	0.07	0.07	0.00	0.00
Ca	0.34	0.36	0.26	0.38	0.00	0.00	0.00	0.00	0.00	0.00	0.15	0.19
Na	0.00	0.00	0.01	0.00	0.01	0.01	0.00	0.00	0.09	0.11	0.83	0.78
K	0.00	0.00	0.00	0.00	0.86	0.84	0.00	0.00	0.83	0.78	0.00	0.00
O (assumed)	12	12	12	12	11	11	14	14	11	11	8	8
Calculated end-member fractions (mol%)												
X_{Mg}	0.11	0.11	0.10	0.09	0.48	0.48	0.51	0.51	0.53	0.50		
X_{Alm}	0.59	0.64	0.77	0.61								
X_{Sps}	0.23	0.16	0.06	0.20								
X_{Gr}	0.12	0.12	0.09	0.13								
X_{Prp}	0.07	0.08	0.08	0.06								
X_{An}											0.145	0.19

X_{Gr} = grossular proportion (Ca/(Ca+Mg+Mn+Fe)), X_{Prp}= pyrope proportion (Mg/(Mg+Mg+Mn+Fe)), X_{Alm}= almandine proportion (Fe/(Fe+Mg+Mn+Fe)), X_{Sps}= spessartine proportion (Mn/(Mn+Mg+Mn+Fe)), X_{Mg}=Mg/Mg+Fe. X_{An}: anorthite proportion (Ca/(Ca+Na+K)).

lower than 580 °C, and the second with pressures lower than 0.7 GPa and temperatures higher than 580 °C. Staurolite is only stable from 580 to 660 °C and pressures below 1.0 GPa. The Al_2SiO_5 phases are stable in temperatures higher than 640 °C and pressures lower than 1.05 GPa, with sillimanite occurring in low pressures conditions and kyanite being stable at higher pressures. Epidote occurs at temperatures lower than 600 °C and pressure lower than 1.3 GPa. Clinopyroxene is stable at pressures higher than 1.0 GPa and temperatures lower than 660 °C, due to the breakdown of plagioclase. Ilmenite is stable in almost all ranges with the exception of one field, which occurs at pressure between 0.7 to 1.0 GPa and temperatures lower than 540 °C. Rutile is stable at low temperatures in all pressure ranges, therefore in temperatures higher than 530 °C the rutile only occurs at pressures higher than 1.0 GPa.

According to the isochemical phase diagram (Fig. 5.6), the mineral peak assemblage

Figure 5.5 – Garnet composition maps analogous to Fig. 4, showing the chemical zoning in sample LR09.

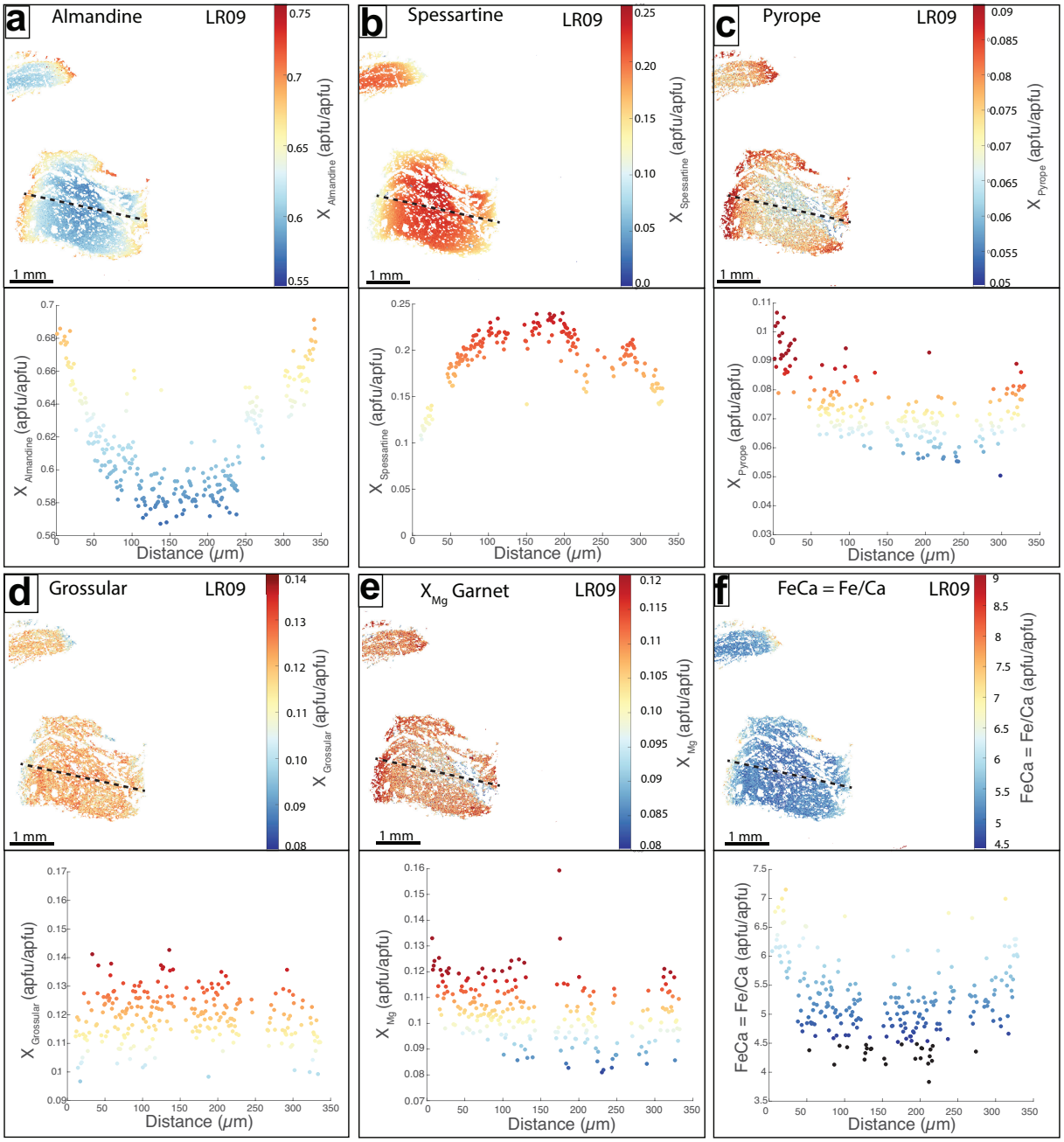

(biotite + plagioclase + garnet + muscovite + ilmenite + quartz) is stable at temperatures of 570–650 °C and pressures of 0.70–1.05 GPa. Rutile is interpreted as a prograde phase and indicates temperatures lower than 620 °C. Retrograde chlorite indicates cooling down to temperatures below 580 °C and pressures below 0.75 GPa.

The mineral composition and the chemical zoning in porphyroblasts may potentially preserve a detailed metamorphic record of the rock, if the chemical composition of the minerals has been relatively unmodified following the initial equilibration. Therefore, the composition mineral contours (i.e., isopleths) can be used to further constrain the P–T path of the rock. The nominal spessartine and grossular contents decrease from core

Figure 5.6 – Pressure-temperature (P–T) isochemical phase diagram calculated in the NCKFMASHTO model chemical system for sample LR09. The bulk composition used was SiO2 70.20 mol%, Al_2O_3 11.22 mol%, MgO 4.68 mol%, CaO 0.96 mol%, FeO 5.35 mol%, K_2O 2.68 mol%, Na_2O 2.05 mol%, MnO 0.08 mol%, TiO_2 0.75 mol%, O_2 0.5 mol%. The bold field represents the peak assemblage. Quartz and water are also present in all fields. Abbreviations according to Whitney e Evans (2010).

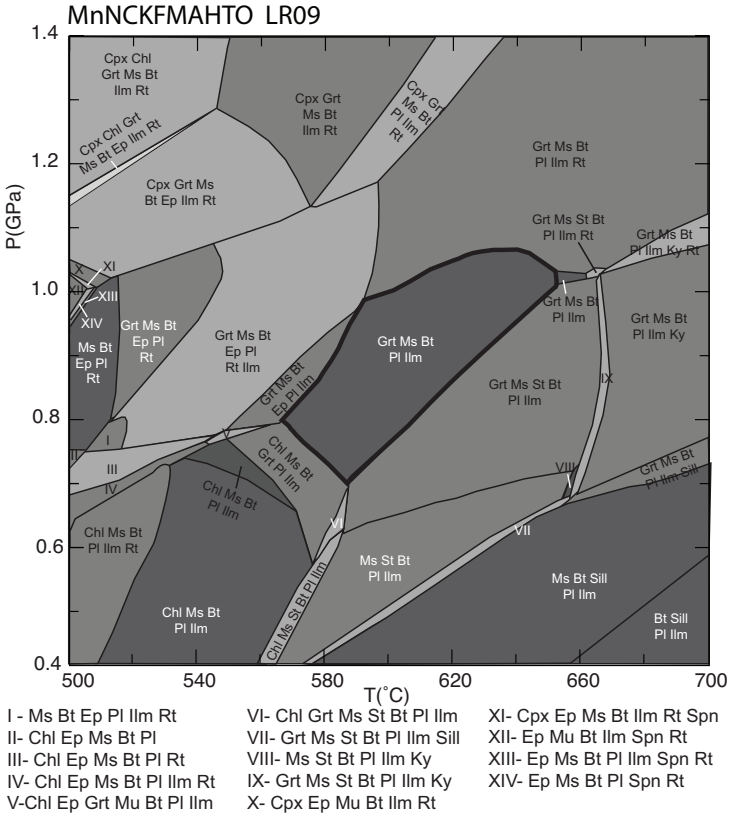

to rim, while almandine, pyrope and X_{Mg} increase. This pattern indicates its prograde crystallization (Fig. 5.7; see also Fig. 5.S3) from ~540 °C (garnet core) to 630 °C and 1.0 GPa (garnet rim; peak conditions). The higher anorthite contents is coherent with the peak conditions indicated by the garnet isopleths. On the other hand, the X_{Fe} value of biotite indicates retrograde conditions at lower pressures of ~0.7 GPa and temperatures of ~580 °C (Fig. 5.7).

5.5 Discussion

5.5.1 *P–T–t* path and regional correlations

Based on observed microstructures, isochemical phase diagram and composition mineral contours, a clockwise P–T path is obtained for the metagreywacke from the Santo Antônio Unit (Fig. 5.7). The garnet core records the prograde P–T conditions of 540 °C and 0.9 GPa followed by a heating to the metamorphic peak at 630 °C and 1.0 GPa (intersection of rim garnet composition; muscovite and anorthite composition mineral

contours). The metamorphic peak is followed by cooling and decompression stages, with chlorite crystallization at temperatures of ~580 °C and pressures of ~0.7 GPa.

Figure 5.7 – *P–T–t* path from the rocks from Santo Antônio Unit in the Luminárias Nappe, based on the isochemical phase diagram, garnet, biotite, feldspar and muscovite isopleths and mineral assemblages. Fields names see Fig. 5.4. Metamorphic facies boundaries according to Bucher e Grapes (2011).

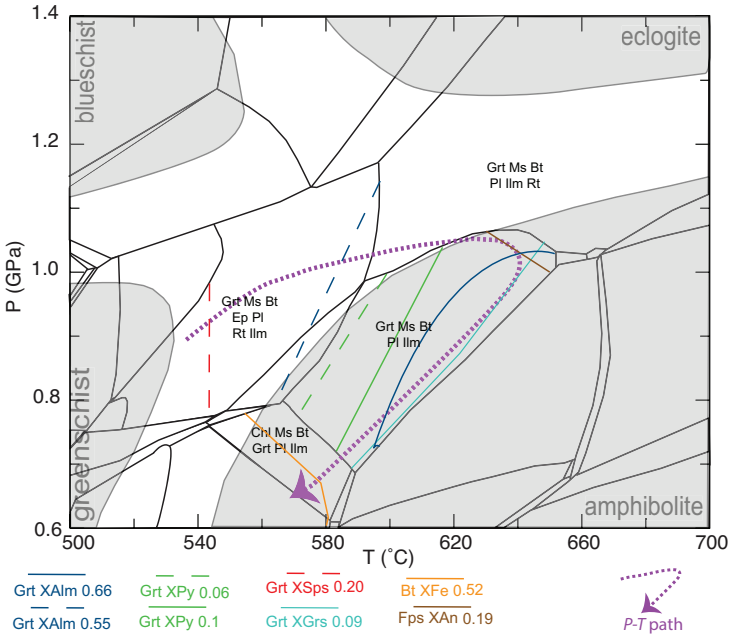

The use of quantitative composition maps allows for a detailed characterization of the chemical composition of the phases, including internal chemical zoning, and a direct correlation of the chemical composition of the phases with the rock fabric and textural domains. This approach is more precise than single spot analysis, given the relative uncertainties in the spot analysis are minimized by pixel integration (LANARI; ENGI; BERN, 2017; LANARI; DUESTERHOEFT, 2019; DUESTERHOEFT; LANARI, 2020). The integration of the quantitative compositional mapping with the composition mineral contours in the isochemical phase diagram has proven to be a powerful method to assess the *P–T* path of the studied unit.

The metamorphic record in the Santo Antônio Unit begins at greenschist facies and the *P–T* peak conditions occur at high-pressure amphibolite facies (Fig. 5.7). According to previous regional works developed in the area, the metamorphic peak ranges from greenschist facies, garnet zone, in the extreme north of the Luminárias Nappe, to amphibolite facies, in the south (RIBEIRO; HEILBRON, 1982; TROUW; PACIULLO; HEILBRON, 1984; TROUW et al., 2013; PETERNEL et al., 2005; SILVA, 2010; RENO et al., 2012). Fumes et al. (2019) described the metamorphic peak conditions in the Campestre Unit rocks. Nearby the occurrence of the rocks from the Santo Antônio Unit, present only in the northern portion of the nappe, varies from lower–amphibolite facies, peak conditions at 580 ±4 °C and ~0.9 GPa, to high-pressure amphibolite facies, peak conditions at 600

±15 °C and 1.1 ±0.3 GPa. Peak *P–T* conditions calculated for the studied rocks fall in the high-pressure amphibolite facies field. When compared to the literature data, the results show a slightly higher temperature (∼15 °C) and similar pressures as determined elsewhere (FUMES et al., 2019). If uncertainties are considered, conditions are the same as those of Campestre Unit rocks from the northern portion of the Luminárias Nappe. The Santo Antônio Unit only crops out along a small area in the northern portion of the nappe. Therefore, the metamorphic gradient described for the entire structure would not show up in such a restricted area. In all outcrops, the rock has the same metamorphic mineral assemblage. The peak *P–T* conditions of the Santo Antônio Unit in the Luminárias Nappe is lower than the peak condition calculated for this unit in the Andrelândia Nappe System (SE of the Luminárias Nappe), 668 ±15 15 °C and 0.9 ±0.07 GPa (MOTTA; MORAES, 2017). The same is true for rocks of the Santo Antônio Unit that occur southwest from the study area, 720 °C and 1.0 GPa (BATISTA, 2015; BATISTA et al., 2018). This increase of metamorphic conditions in the south of the Luminárias Nappe has been reported in several previous works (e. g. (PETERNEL et al., 2005; RENO et al., 2012; TROUW et al., 2013; HEILBRON; CORDANI; ALKMIM, 2017)) and is observed along the Brasília Orogen as a whole.

5.5.2 Comparison with the other units within the Luminárias Nappe

The pseudosection calculated for the metagreywacke rocks resemble those of a typical metapelite. Johnson, White e Powell (2008) have also noticed these features in partial melting studies of some greywackes. According to our modelling, if Barrovian pressure conditions (∼0.6 GPa at 500–700 °C) are considered the garnet crystallizes at ∼500 °C, the staurolite at 570 °C and the sillimanite at 660 °C (see again Fig. 5.6). Therefore, at the Barrovian gradient, index minerals in the investigated metagreywacke follow the same crystallization sequence observed in metapelites. Hence, metagreywackes have similar potential to register the metamorphic conditions as the pelites, despite the high plagioclase content and the lack of kyanite in this specific bulk composition. The bulk rock composition of the metagreywacke from the Santo Antônio Unit differs from the aluminous metapelite from the Campestre Unit in the Luminárias Nappe. The SiO_2/Al_2O_3 versus K_2O/Na_2O plot (Fig. 5.8) and the chemical index of alteration (CIA) diagram (Table 5.3) show that the bulk composition of the metagraywacke has higher SiO_2/Al_2O_3, lower K_2O/Na_2O and lower CIA than the metapelite samples. The bulk rock composition indicates that the depositional and tectonic settings were different for the two units, as indicated by previous studies in another areas (e.g. McLennan et al. (1990), Campos Neto et al. (2011), Westin e Campos Neto (2013).

Since metapelites are more mature sediments in respect to metagreywacke, the differences in the bulk rock composition result in slightly distinguished mineral assemblages.

Figure 5.8 – Comparation of bulk rock compositions between the Santo Antônio and Campestre Unit of the Luminárias Nappe. Plot of SiO_2/Al_2O_3 versus K_2O/Na_2O for the metagreywackes (Santo Antônio Unit) and metapelites (Campestre Unit). Data from the metapelite extracted from Fumes et al. (2019).

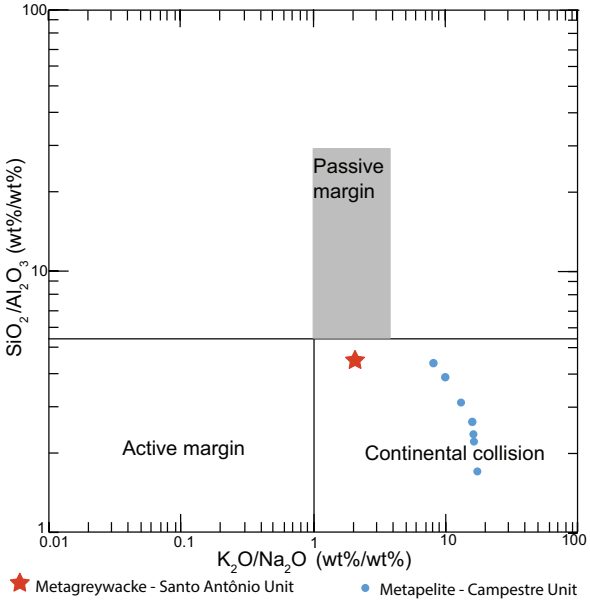

Table 5.3 – Chemical Index Alteration (CIA) for the metagreywackes (Santo Antônio Unit) and metapelites (Campestre Unit) of the Luminárias Nappe. Data from the metapelite extracted from Fumes et al. (2019).

Outcrop/Sample	Rock	CIA (mol%/mol%)
LR 04	metapelite	72.65
LR 09	metagreywacke	67.34
LR 10B	metapelite	77.96
LR 10C	metapelite	77.11
LR 10E	metapelite	81.26
LR 11	metapelite	80.29
LR 31A	metapelite	71.28
LR 44A	metapelite	73.10
LR 44C	metapelite	83.01

The metamorphic peak mineral assemblage in the aluminous metapelite from the Campestre Unit of the Luminárias Nappe (northern portion) is chlorite + kyanite + staurolite + muscovite + quartz + rutile (FUMES et al., 2019). Differently the peak assemblage in the metagreywacke from the same nappe (Santo Antônio Unit) is biotite + plagioclase + garnet + muscovite + ilmenite + quartz. Despite the distinct mineral assemblages, due the different chemical composition of the protoliths, both metapelite and greywacke have a high potential to be used in metamorphic studies under amphibolite facies in order to obtain the *P*–*T*–*t* path, given that with a minor modification in pressure and temperature

conditions the mineral assemblage is modified.

The peak assemblage in the metapelite (Campestre Unit) in the southern portion of the Luminárias Nappe is staurolite + kyanite + garnet + muscovite + quartz + rutile at 630 ±13 °C and 1.4 ±0.6 GPa (Fumes et al., 2019). The metagreywacke (Santo Antônio Unit) does not occur in the southern portion in the Luminárias Nappe. However, considering the isochemical phase diagram (Fig. 5.6), and assuming that the metagreywacke rocks were metamorphosed under the same conditions, the mineral assemblage in the metagreywacke would be just slightly different, and composed of Na-rich clinopyroxene + kyanite + garnet + muscovite + quartz + rutile.

As pointed out in previous works, the metagreywackes are also useful protoliths in metamorphic studies under high temperature conditions (Johnson; WHITE; POWELL, 2008; YAKYMCHUK; BROWN, 2014; TIAN; ZHANG; DONG, 2016), not only under amphibolite facies as studied in this work. Since the metagreywacke could be the dominant siliciclastic rock type in several orogens, even more abundant than metapelite (Johnson; WHITE; POWELL, 2008), the thermobarometry studies in these rocks are very useful to add information about the orogenic evolution. The widespread distribution of these rocks is a great advantage to use this protolith in metamorphic investigations.

5.5.3 Tectonic evolution of the units in the Luminárias Nappe

The Luminárias Nappe is composed of metasedimentary rocks that have been deposited in two environments: the metapelite and quartzite, deposited in the passive margin (PACIULLO et al., 2000; PACIULLO; RIBEIRO; TROUW, 2003; TROUW et al., 2000; CAMPOS NETO et al., 2004; WESTIN et al., 2019) and the metagreywacke, deposited in a younger synorogenic basin (CAMPOS NETO et al., 2007; CAMPOS NETO et al., 2011; WESTIN; CAMPOS NETO, 2013; MARIMON et al., 2021); see Fig. 5.9a). Regardless the differences in the depositional environment was different, metagreywackes were metamorphosed in the same collisional setting with similar P–T path than the metapelite (Fig. 5.9b).

The baric conditions observed in the metamorphic rocks from the Southern Brasília Orogen are of high-pressure (SILVA, 2010; MOTTA; MORAES, 2017), which is confirmed in this work. This high-pressure condition indicates a crustal thickening that may be coherent with the continental collision, which involves subduction of continental crust (CAMPOS NETO, 2000; DARDENNE, 2000; TROUW et al., 2000; HEILBRON; CORDANI; ALKMIM, 2017; TEDESCHI et al., 2017). The maximum burial depth of the metagreywacke from the Santo Antônio Unit in the Luminárias Nappes is estimated to be ∼35 km, from pressures of 1.0 GPa recorded (Fig. 5.9b). This depth recorded in the metamorphic peak is compatible with burial within an orogenic wedge, with latter exhumation to relatively shallow crustal depths (∼25 km) in the retrograde path (Fig.

Figure 5.9 – Proposed tectonic model. a) Model showing the depositional environments of the (meta)sedimentary units based on Marimon et al. (2021). b) Model showing continental collision associated with the metamorphic peak of rocks from Luminárias Nappe. c) Model showing the retrograde conditions of rocks from Luminárias Nappe. Model and isotherms based on crust-mantle decoupling combined with slab advance from Vanderhaeghe e Duchêne (2010). * P–T metamorphic peak conditions from this work and ** P–T metamorphic peak conditions from Fumes et al. (2019).

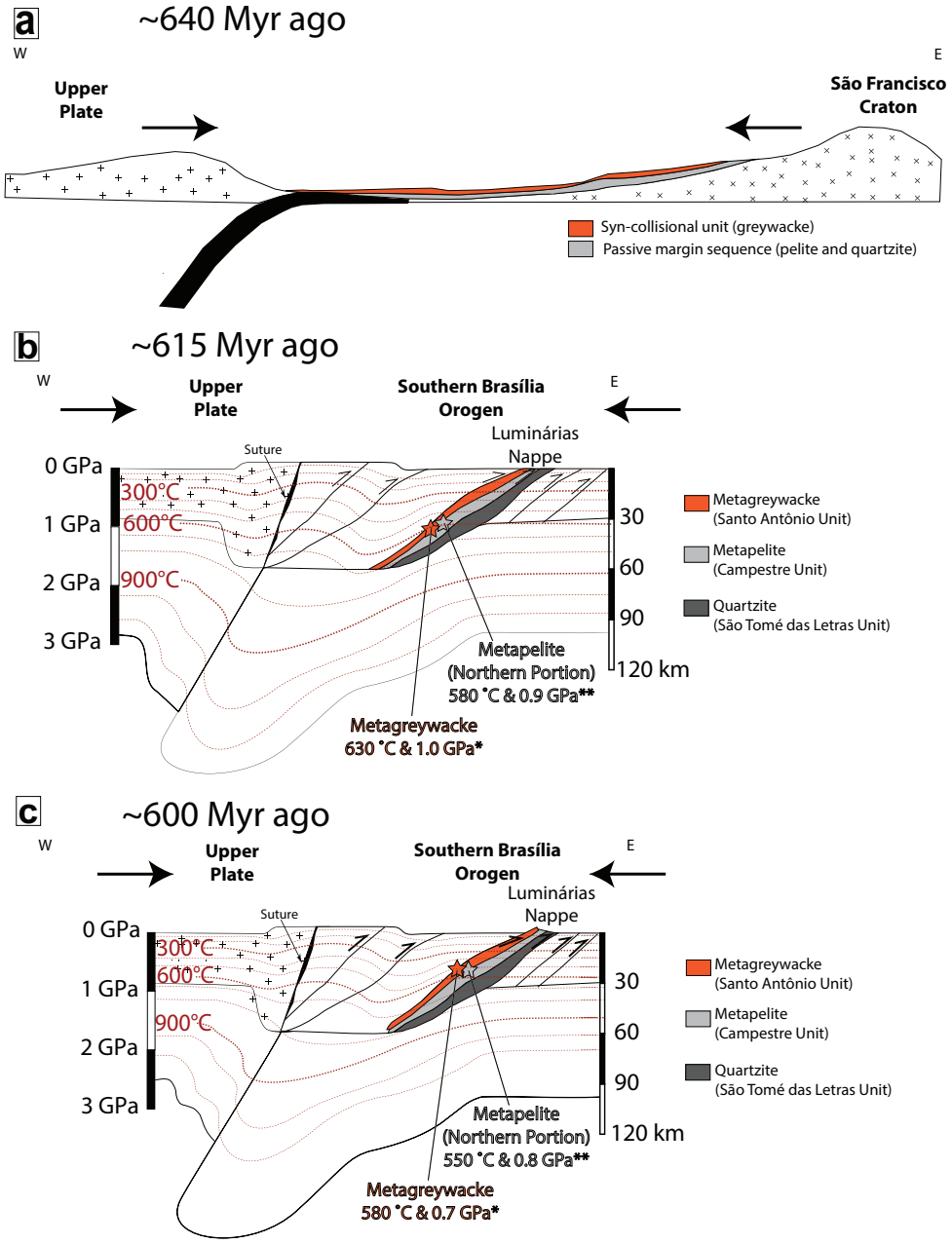

5.9c).

According to Fumes et al. (2019), Westin et al. (2021) the metapelites rocks from the Luminárias Nappe register a syn-collisional metamorphism ca. 630-615 Myr ago (Fig. 5.9b) and record a continuous exhumation/cooling path from 615 until 590 Myr ago (Fig. 5.9c). However, metamorphic age the Santo Antônio Unit in the Luminárias Nappe, is not available in the literature. Thus, since the metamorphic P–T path is similar to the

metapelites, we interpret the age of the metamorphism to be the same of the metapelite.

The rocks from the Luminárias Nappe, both from the Campestre Unit (quartzite and metapelite) and Santo Antônio Unit (metagreywacke), were metamorphosed under pressure conditions higher than the Barrovian gradient. The metamorphic peak is classified as intermediate dT/dP thermal gradient based on the Brown e Johnson (2018) classification.

5.6 Conclusions

In a general view, the metagreywacke present different bulk composition than the metapelites and this results in slightly different mineral assemblages. Despite that, both metapelite and greywacke are adequate to be used in metamorphic studies and might be used to infer and investigate metamorphic conditions, probably, with the same confidence.

The metagreywacke from the Santo Antônio Unit in the Luminárias Nappe, is metamorphosed under high-pressure amphibolite facies. The metamorphic study of the immature metasedimentary rocks from the Santo Antônio Unit based on quantitative compositional mapping and composition mineral contours in the isochemical phase diagram has proven to be a useful approach. The mineral peak assemblage is biotite + plagioclase + garnet + muscovite + ilmenite + quartz. Rutile is a prograde phase and chlorite is a retrograde phase. The metamorphic P–T path shows a single clockwise path with prograde conditions at greenschist facies, the peak at high-pressure amphibolite facies and retrograde conditions at also amphibolite facies at lower pressure conditions. The metagreywacke from Santo Antônio Unit records a similar metamorphic peak conditions and P–T path that the rocks from the metapelite from the Campestre Unit in the Luminárias Nappe.

Acknowledgements Daniel Godoy is thanked for the EPMA lab support in the Department of Geology of the São Paulo State University, UNESP, Brazil. The authors thank Sebastian Oriolo and Chun-Ming Wu for their constructive reviews that improved the presentation of this work. Journal editors Shah Wali Faryad and Lutz Nasdala are thanked for editorial handling of the manuscript and helpful suggestions for improvement of the manuscript. RAF, GLL and RM acknowledge the National Council for Scientific and Technological Development (Conselho Nacional de Desenvolvimento Científico e Tecnológico, CNPq); RM and GLL are research fellows of the CNPq (grant 305720/2001-1 to RM and grant 311606/2019-9 to GGL) and RAF had PhD scholarship (141604/2018-2). Further support was provided by the São Paulo Research Foundation (Fundação de Amparo à Pesquisa do Estado de São Paulo, FAPESP) through grants 2015/05230-0 and 2016/22627-3. This research was conducted within a post-graduation program, which was supported by the Brazilian Federal Agency for Support and Evaluation of Graduate Education (Coordenação de Aperfeiçoamento de Pessoal de Nível Superior, CAPES).

Reference

ALMEIDA, J. C. *Mapeamento geológico na Folha Luminárias (MG) 1:50.000 com ênfase na análise estrutural dos metassedimentos do Ciclo Deposicional Andrelândia.* Dissertação (Mestrado) — Universidade Federal do Rio de Janeiro, 1992.

ARAÚJO FILHO, J. O. The Pirineus Syntaxis: An example of the intersection of two Brasiliano fold-thrust belts in central Brazil and its implications for the tectonic evolution of western Gondwana. *Revista Brasileira de Geociências*, v. 30, n. 1, p. 144–148, 2000.

BATISTA, L. D. A. *Geração e transporte de fundidos em semi-pelitos: modelagem com dados de campo e pseudosseções*. Dissertação (Mestrado) — Universidade de São Paulo, 2015.

BATISTA, L. D. A. et al. Provenance and metamorphism in the western andrelândia nappe system: Coupling u-pb ages from zircon and monazite with forward metamorphic modelling and trace-element siganetures. In: *Anais do 49º Congresso Brasileiro de Geologia. Rio de Janeiro*. [S.l.: s.n.], 2018. p. 9005.

BRITO NEVES, B. B. de; CAMPOS NETO, M. D. C.; FUCK, R. A. From Rodinia to Western Gondwana: as Aproach to the Brasiliano-Pan African Cycle and orogenic collage. *Episodes-Newsmagazine of International Union of Geological Science*, v. 22, n. 155-166, 1999.

BROWN, M.; Johnson, T. Secular change in metamorphism and the onset of global plate tectonics. *American Mineralogist*, v. 103, n. 2, p. 181–196, 2018. ISSN 19453027.

BUCHER, K.; GRAPES, R. *Petrogenesis of metamorphic rocks*. [S.l.]: Springer Science & Business Media, 2011.

CAMPOS NETO, M. D. C. Orogenic Systems from Southwestern Gondwana: An Approach to Brasiliano-Pan African Cycle and Orogenic Collage in Southeastern Brazil. In: CORDANI, U. G. et al. (Ed.). *Tectonic Evolution of South America*. 1. ed. Rio de Janeiro: COMPANHIA DE PESQUISA DE RECURSOS MINERAIS, 2000. p. 335–365.

CAMPOS NETO, M. D. C. et al. Migração de Orógenos e Superposição de Orogêneses: Um Esboço da Colagem Brasiliana no Sul do Cráton do São Francisco, SE - Brasil. *Geologia USP - Serie Cientifica*, v. 4, n. 1, p. 13–40, 2004.

CAMPOS NETO, M. D. C. et al. Orogen migration and tectonic setting of the Andrelândia Nappe system: An Ediacaran western Gondwana collage, south of São Francisco craton. *Journal of South American Earth Sciences*, Elsevier Ltd, v. 32, n. 4, p. 393–406, 2011. ISSN 08959811. Avaible form internet: <http://dx.doi.org/10.1016/j.jsames.2011.02.006>.

CAMPOS NETO, M. D. C.; CABY, R. Neoproterozoic high-pressure metamorphism and tectonic constraint from the nappe system south of the Sao Francisco Craton, southeast Brazil. *Precambrian Research*, v. 97, n. 1-2, p. 3–26, 1999. ISSN 03019268.

CAMPOS NETO, M. D. C.; CABY, R. Lower crust extrusion and terrane accretion in the Neoproterozoic nappes of southeast Brazil. *Tectonics*, v. 19, n. 4, p. 669–687, 2000.

CAMPOS NETO, M. D. C. et al. Structural and metamorphic control on the exhumation of high-P granulites: The Carvalhos Klippe example, from the oriental Andrelândia Nappe System, southern portion of the Brasília Orogen, Brazil. *Precambrian Research*, v. 180, n. 3-4, p. 125–142, 2010. ISSN 03019268.

CAMPOS NETO, M. D. C. et al. Sistema de nappes andrelândia, setor oriental: litoestratigrafia e posição estratigráfica. *Revista Brasileira de Geociências*, v. 37, n. 4-Sup., p. 47–60, 2007.

CIOFFI, C. R. et al. Paleoproterozoic continental crust generation events at 2.15 and 2.08 ga in the basement of the southern brasília orogen, se brazil. *Precambrian Research*, Elsevier, v. 275, p. 176–196, 2016.

COELHO, M. B. et al. Constraining timing and P-T conditions of continental collision and late overprinting in the Southern Brasília Orogen (SE-Brazil): U-Pb zircon ages and geothermobarometry of the Andrelândia Nappe System. *Precambrian Research*, Elsevier B.V., v. 292, p. 194–215, 2017. ISSN 03019268. Avaible form internet: <http://linkinghub.elsevier.com/retrieve/pii/S0301926816305496>.

CONNOLLY, J. A. Computation of phase equilibria by linear programming: a tool for geodynamic modeling and its application to subduction zone decarbonation. *Earth and Planetary Science Letters*, Elsevier, v. 236, n. 1-2, p. 524–541, 2005.

DARDENNE, M. A. The Brasilia Fold Belt. In: *Tectonic Evolution of South Ameria*. [S.l.]: 31 Intern. Geol. Congr. Rio de Janeiro, 2000. p. 231–264.

DUESTERHOEFT, E.; LANARI, P. Iterative thermodynamic modelling—part 1: A theoretical scoring technique and a computer program (bingo-antidote). *Journal of metamorphic geology*, Wiley Online Library, v. 38, n. 5, p. 527–551, 2020.

DZULYNSKI, S.; WALTON, E. K. *Sedimentary features of flysch and greywackes*. [S.l.]: Elsevier, 2011.

FRUGIS, G. L.; NETO, M. d. C. C.; LIMA, R. B. Eastern Paranapanema and southern São Francisco orogenic margins: Records of enduring Neoproterozoic oceanic convergence and collision in the southern Brasília Orogen. *Precambrian Research*, Elsevier, v. 308, p. 35–57, 2018.

FUCK, R. A. et al. The Northern Brasília Belt. In: HEILBRON, M.; CORDANI, U. G.; ALKMIM, F. F. (Ed.). *São Francisco Craton, Eastern Brazil Tectonic Genealogy of a Miniature Continent*. [S.l.]: Springer Berlin Heidelberg, 2017. p. 205–220.

FUHRMAN, M. L.; LINDSLEY, D. H. Ternary-feldspar modeling and thermometry. *American mineralogist*, Mineralogical Society of America, v. 73, n. 3-4, p. 201–215, 1988.

FUMES, R. A. et al. Metamorphic modeling and petrochronology of metapelitic rocks from the Luminárias Nappe, southern Brasília belt (SE Brazil). *Brazilian Journal of Geology*, v.49, n. 2 2019.

HEILBRON, M.; CORDANI, U. G.; ALKMIM, F. F. *São Francisco Craton, Eastern Brazil: Tectonic Genealogy of a Miniature Continent*. [S.l.: s.n.], 2017. 331 p. ISBN 9783319017143.

HEILBRON, M. et al. Correlation of Neoproterozoic terrane between te Ribeira Belt, SE Brazil and its African countepart: comparative tectonic evolution and open questions. *Geological Society, London, Special Publications*, v. 294, p. 211–237, 2008.

HOLLAND, T. J.; GREEN, E. C.; POWELL, R. Melting of peridotites through to granites: a simple thermodynamic model in the system kncfmashtocr. *Journal of Petrology*, Oxford University Press, v. 59, n. 5, p. 881–900, 2018.

HOLLAND, T. J. B. *AX: A program to calculate activities of mineral endmembers from chemical analyses (usually determined by electron microprobe);*. 2009. Avaible form internet: <http://ccp14.cryst.bbk.ac.uk/ccp/web-mirrors/crush/astaff/holland/ax.html>.

HOLLAND, T. J. B.; POWELL, R. An improved and extended internally consistent thermodynamic dataset for phases of petrological interest, involving a new equation of state for solids. *Journal of Metamorphic Geology*, v. 29, n. 3, p. 333–383, 2011. ISSN 02634929.

JOHNSON, T.; WHITE, R.; POWELL, R. Partial melting of metagreywacke: a calculated mineral equilibria study. *Journal of Metamorphic Geology*, Wiley Online Library, v. 26, n. 8, p. 837–853, 2008.

KUSTER, K. et al. The neoproterozoic andrelândia group: Evolution from an intraplate continental margin to an early collisional basin south of the são francisco craton, brazil. *Journal of South American Earth Sciences*, Elsevier, v. 102, p. 102666, 2020.

LANARI, P.; DUESTERHOEFT, E. Modeling Metamorphic Rocks Using Equilibrium Thermodynamics and Internally Consistent Databases: Past Achievements, Problems and Perspectives. *Journal of Petrology*, v. 60, n. 1, p. 19–56, 2019. ISSN 14602415.

LANARI, P.; ENGI, M.; BERN, C. Local Bulk Composition Effects on Metamorphic Mineral Assemblages. *Reviews in Mineralogy and Geochemistry*, v. 83, p. 55–93, 2017.

LANARI, P. et al. Xmaptools: A matlab©-based program for electron microprobe x-ray image processing and geothermobarometry. *Computers & Geosciences*, Elsevier, v. 62, p. 227–240, 2014.

MARIMON, R. S. et al. Provenance of passive-margin and syn-collisional units: Implications for the geodynamic evolution of the southern brasília orogen, west gondwana. *Sedimentary Geology*, Elsevier, v. 413, p. 105823, 2021.

MCLENNAN, S. et al. Geochemical and nd sr isotopic composition of deep-sea turbidites: crustal evolution and plate tectonic associations. *Geochimica et cosmochimica acta*, Elsevier, v. 54, n. 7, p. 2015–2050, 1990.

MOTTA, R. G.; MORAES, R. Pseudo- and real-inverted metamorphism caused by the superposition and extrusion of a stack of nappes: a case study of the Southern Brasília Orogen, Brazil. *International Journal of Earth Sciences*, 2017. ISSN 1437-3254. Avaible form internet: <http://link.springer.com/10.1007/s00531-016-1436-7>.

NUNES, R.; TROUW, R. A. J.; CASTRO, E. *Mapa Gelógico - Folha Varginha – escala 1:100.000, Programa Geologia do Brasil*. [S.l.], 2008.

PACIULLO, F. V. P.; RIBEIRO, A. Mapa Geológico-Folha Nepumoceno. In: *CONTRATO - CPRM - UFRJ 067/P2/2005*. [S.l.: s.n.], 2008.

PACIULLO, F. V. P. et al. The Andrelândia Basin, a Neoproterozoic Intraplate Continental Margin, Southern Brasília Belt, Brazil. *Revista Brasileira de Geociências*, v. 30, n. 1, p. 200–202, 2000.

PACIULLO, F. V. P.; RIBEIRO, A.; TROUW, R. a. J. Geologia da Folha Andrelândia 1:100.000. *Geologia e recursos minerais do sudeste mineiro Projeto Sul de Minas - Etapa I*, p. 84–119, 2003.

PETERNEL, R. et al. Interferência Entre Duas Faixas Móveis Neoproterozóicas : O Caso Das Faixas Brasília E Ribeira No Sudeste Do Brasil. v. 35, n. 3, p. 297–310, 2005. ISSN 2317-4692.

QUÉMÉNEUR, J. J. G. et al. Mapa Geológico-Folha Lavras. In: *Geologia e Recursos Minerais do Sudeste Mineiro*. [S.l.: s.n.], 2003. p. 1:100.000.

RENO, B. L. et al. In situ monazite (U-Th)-Pb ages from the Southern Brasília Belt, Brazil: Constraints on the high-temperature retrograde evolution of HP granulites. *Journal of Metamorphic Geology*, v. 30, n. 1, p. 81–112, 2012. ISSN 02634929.

RIBEIRO, A.; HEILBRON, M. Estratigrafia e Metamorfismo dos Grupos Carrancas e Adrelândia, Sul de Minas Gerais. In: *Anais do XXXII Congresso Brasileiro de Geologia*. [S.l.: s.n.], 1982. p. 177–186.

RIBEIRO, A. et al. Evolução das Bacias Proterozóicas e o Termo-Tectonismo Brasiliano na Margem Sul do Cráton do São Francisco. *Revista Brasileira de Geociências*, v. 25, n. 4, p. 235–248, 1995.

SILVA, M. P. *Modelamento Metamórfico de Rocas das Fácies Xisto-Verde e Anfibolito com o Uso de Pseudosseções: Exemplo das Rochas da Klippe Carrancas, Sul de Minas Gerais*. Tese (Dissertação de mestrado) — Universidade de São Paulo, 2010.

SPENCER, C. J. et al. Not all supercontinents are created equal: Gondwana-rodinia case study. *Geology*, Geological Society of America, v. 41, n. 7, p. 795–798, 2013.

TEDESCHI, M. et al. Reconstruction of multiple PTt stages from retrogressed mafic rocks: Subduction versus collision in the Southern Brasília orogen (SE Brazil). *Lithos*, Elsevier, v. 294, p. 283–303, 2017.

TIAN, Z.; ZHANG, Z.; DONG, X. Metamorphism of high-p metagreywacke from the eastern himalayan syntaxis: phase equilibria and p–t path. *Journal of Metamorphic Geology*, Wiley Online Library, v. 34, n. 7, p. 697–718, 2016.

TROUW, R. A. J. et al. The Central Segment of the Ribeira Belt. In: CORDANI, U. G. et al. (Ed.). *Tectonic Evolution of South America*. 1. ed. [S.l.]: COMPANHIA DE PESQUISA DE RECURSOS MINERAIS, 2000. p. 287–310.

TROUW, R. A. J. et al. Análise de Deformação numa Área a SE de Lavras Minas Gerais. In: *Anais do XXXII Congresso Brasileiro de Geologia*. Salvador, Bahia: [s.n.], 1982. p. 187–198.

TROUW, R. A. J.; PACIULLO, F. V. P.; HEILBRON, M. Os Grupos São João Del Rei, Carrancas e Andrelândia Interpretados como a Continuição dos Grupos Araxá e Canastra. In: *Anais do XXXIII Congresso Brasileiro de Geologia*. Rio de Janeiro, RJ: [s.n.], 1984. p. 177–178.

TROUW, R. A. J. et al. *Mapa Geológico-Folha Caxambu. Projeto Sul de Minas - etapa 1, escala 1:100.000*. [S.l.], 2013.

TROUW, R. A. J. et al. A new interpretation for the interference zone between the southern Brasília belt and the central Ribeira belt, SE Brazil. *Journal of South American Earth Sciences*, v. 48, p. 43–57, 2013. ISSN 08959811.

TROUW, R. A. J.; RIBEIRO, A.; PACIULLO, F. V. P. Evolução Estrutural e Metamórfica de uma àrea a SE de Lavras - Minas Gerias. In: *Anais do XXXI Congresso Brasieliro de Geologia, Balneário de Camboriú, Santa Catarina*. Balneário de Camburiú: [s.n.], 1980.

TROUW, R. A. J.; RIBEIRO, A.; PACIULLO, F. V. P. Geologia Estrutural do Grupos São João del Rei, Carrancas e Andrelândia, Sul de Minas Gerais. *Anais da Academia brasileira de Ciências*, v. 55, n. 1, p. 71–87, 1983.

VANDERHAEGHE, O.; DUCHÊNE, S. Crustal-scale mass transfer, geotherm and topography at convergent plate boundaries. *Terra Nova*, Wiley Online Library, v. 22, n. 5, p. 315–323, 2010.

WESTIN, A.; CAMPOS NETO, M. D. C. Provenance and tectonic setting of the external nappe of the Southern Brasília Orogen. *Journal of South American Earth Sciences*, Elsevier Ltd, v. 48, p. 220–239, 2013. ISSN 08959811. Avaible form internet: <http://dx.doi.org/10.1016/j.jsames.2013.08.006>.

WESTIN, A. et al. The Neoproterozoic southern passive margin of the São Francisco craton: Insights on the pre-amalgamation of West Gondwana from U-Pb and Hf-Nd isotopes. *Precambrian Research*, p. 454–471, 2019.

WESTIN, A. et al. A paleoproterozoic intra-arc basin associated with a juvenile source in the Southern Brasilia Orogen: Application of U–Pb and Hf–Nd isotopic analyses to provenance studies of complex areas. *Precambrian Research*, v. 276, p. 178–193, 2016.

WESTIN, A. et al. The fast exhumation pattern of a neoproterozoic nappe system built during west gondwana amalgamation: Insights from thermochronology. *Precambrian Research*, Elsevier, v. 355, p. 106115, 2021.

WHITE, R. W. et al. The effect of TiO_2 and Fe_2O_3 on metapelitic assemblages at greenschist and amphibolite facies conditions: mineral equilibria calculations in the system K_2O–FeO–MgO–Al_2O_3–SiO_2–H_2O–TiO_2–Fe_2O_3. *Journal of Metamorphic Geology*, v. 18, p. 497–511, 2000.

WHITE, R. W. et al. New mineral activity-composition relations for thermodynamic calculations in metapelitic systems. *Journal of Metamorphic Geology*, v. 32, n. 3, p. 261–286, 2014. ISSN 15251314.

WHITNEY, D. L.; EVANS, B. W. Abbreviations for names of rock-forming minerals. *American mineralogist*, Mineralogical Society of America, v. 95, n. 1, p. 185–187, 2010.

YAKYMCHUK, C.; BROWN, M. Consequences of open-system melting in tectonics. *Journal of the Geological Society*, Geological Society of London, v. 171, n. 1, p. 21–40, 2014.

6 Changes in rutile geochemistry in quartzite through increasing *P–T* conditions

Regiane Andrade Fumes[1*]; George Luiz Luvizotto[1]; Renato Moraes[2]

[1]Department of Petrology and Metallogeny, São Paulo State University, Av. 24A, 1515, 13506- 900, Rio Claro, Brazil *Corresponding author e-mail: regiane.fumes@unesp.br

[2]Department of Mineralogy and Geotectonics, University of Sã °Co Paulo, Rua do Lago, 562, 05508-080, São Paulo, Brazil

Abstract

Low concentrations of Na, Ca, K, Fe, Mg and Al prevent the crystallization of index metamorphic minerals in quartzite, making *P-T* calculations a difficult task. Alternatively, single element thermometers, such as Zr-in-rutile may be applied. It is therefore important to evaluate if the thermometer can be applied to quartzite, since rutile may be detrital in the rock. In this work, we investigate changes in trace element composition in rutile from quartzite through increasing metamorphic conditions. Studied samples derive from a quartzite package (Luminárias Nappe, Brazil) where the metamorphic grade increases southward along the bedding, from high-pressure lower amphibolite facies (∼580 ^{o}C and 0.9 GPa) to eclogite facies (630 ±13 °C and 1.4±0.6 GPa). The Zr content in rutile, and particularly, the variability of Zr content is different at each metamorphic grade. Rutile grains from the lower grade samples show a large spread in Zr concentration and highest concentrations of Zr yield too high temperatures (up to 820 °C) to relate to the metamorphic overprint, and therefore are interpreted as an inherited detrital signature. A narrower spread in Zr concentration is observed in rutile grains from the highest-grade samples and calculated temperatures match previously presented data (638 °C). Therefore, it indicates that the Zr content in detrital rutile re-equilibrated at these conditions. The comparison between the Zr content in the rutile from quartzite with metapelite samples from the same area, shows that the resetting of the geothermometer in the latter seems to occur in slightly lower temperatures (∼50 °C lower). No correlation between metamorphic grade and concentrations of Si, Al, Cr, Sb, Sn, W and Ta in the rutile is observed, which indicates that re-equilibration did not take place for these elements. The behaviour of Zr is ascribed to the re-equilibration of the Zr-in-rutile thermometer. Diffusion, controlled by chemical potential gradient, is the main process responsible Zr re-equilibration in the detrital rutile. Dissolution-reprecipitation associated with fluid and deformation is the main process in the newly metamorphic rutile. Since it is not possible to assess the initial

concentration of trace element in detrital rutile, the degree of re-equilibration cannot be specified. Therefore, the application of low-grade quartzite for provenance studies using geochemistry of rutile needs to be further investigated.

Keywords: Zr-in-rutile thermometry, electron microprobe, single element thermometry, diffusion, HFSE

6.1 Introduction

Rutile has attracted significant attention in recent years, since it can be used in metamorphic studies to calculate crystallization temperature (ZACK; MORAES; KRONZ, 2004; WATSON; WARK; THOMAS, 2006; TOMKINS; POWELL; ELLIS, 2007); in provenance studies to differentiate between mafic and pelitic sources (ZACK; EYNATTEN; KRONZ, 2004; TRIEBOLD et al., 2007; TRIEBOLD; EYNATTEN; ZACK, 2012); to deduce the tectonic setting of sedimentary basins (PEREIRA et al., 2020); and in geochronological studies to calculate U-Pb ages (MEZGER; HANSON; BOHLEN, 1989; ZACK et al., 2011). Furthermore, rutile is a common accessory mineral in metamorphic and sedimentary rocks. It may also be present in mafic and ultramafic igneous rocks, although the high Fe contents may favor crystallization of ilmenite. It is also known to mirror host rock high field strength elements (HFSE) composition (ZACK et al., 2002).

Quartzite is a very common rock type in metasedimentary sequences. Although its protolith may be of different sources (e.g., chert, quartz vein, highly evolved igneous rock and detrital sediments), but quartzite usually represents the metamorphic product of mature detrital sedimentary rocks, where, besides quartz, only weathering resistant minerals such as rutile, tourmaline, zircon, apatite, ilmenite and magnetite occur. Quartzite is seldom used in metamorphic studies, since the lack, or very low concentration of elements such as Na, Ca, K, Fe, Mg and Al, prevents the crystallization of index metamorphic minerals. Some exceptions are sapphirine quartzite (HARLEY; MOTOYOSHI, 2000) and kyanite quartzite (ZHANG; LIOU; SHU., 2002) that may be used as a proxy for ultra-high temperature and ultra-high pressure rocks, respectively.

Previous studies have discussed the application of the Zr-in-rutile thermometry to quartzite and have shown that the Zr content in inherited rutile in quartzite may reset at higher temperature in comparison to crystallization temperature of rutile in metapelitic rocks (i.e., above ∼600 ^{o}C) (TRIEBOLD et al., 2007; LUVIZOTTO et al., 2009). The lack of Fe- Ca-bearing phases, which makes quartzite less reactive than other rock types, thus leads to a diminished ability to the retrogressive replacement of rutile by titanite or ilmenite (TRIEBOLD et al., 2007; LUVIZOTTO et al., 2009). The application of single-element thermometers, such as the Zr-in-rutile in rocks equilibrated at temperatures <600 ^{o}C requires caution, due slow-diffusion of HFSE elements and in such cases the attained

equilibrium must be demonstrated (CRUZ-URIBE et al., 2018). It is also important to take into consideration the whole geological evolution of the studied area and not only the *P-T* conditions, since fluid pressure, the amount of deformation and the time scale of the processes may play a significant role in the resetting of the geothermometer. For example, studies focusing on Ti-in-quartz thermometry have been carried out in quartzite (e.g. Kidder, Avouac e Chan (2013)), where the authors document resetting of Ti contents in quartz during deformation within the bulging regime, at temperature range of 360 ^{o}C.

Having the ability to extract meaningful pressure and temperature conditions from quartzite is particularly useful in areas with rocks where index metamorphic minerals are absent. Furthermore, if trace element composition of inherited rutile is preserved in low-grade quartzite, rutile trace element geochemistry, may be used in provenance studies to assess rock type (mafic or pelitic) and calculate temperature of source rocks (TRIEBOLD; EYNATTEN; ZACK, 2012).

In the present study we investigate trace element changes in rutile geochemistry through increasing *P-T* conditions, from lower amphibolite to eclogite facies. The aim is to evaluate under what *P-T* conditions resetting of trace element takes place in inherited rutile from quartzite. Particular attention is given to the resetting of Zr contents and the application of the Zr-in-rutile geothermometer. Possible causes involved in the resetting are investigate and discussed.

Studied samples derive from a continuous layer of rutile- and zircon-bearing quartzite from the Luminárias Nappe, Minas Gerais - Brazil, along which the regional metamorphic gradient increases from greenschist/lower-amphibolite facies to amphibolite/eclogite facies (TROUW; RIBEIRO; PACIULLO, 1980; RIBEIRO; HEILBRON, 1982; SILVA, 2010; FUMES et al., 2019). These are the metamorphic conditions where resetting of Zr in rutile is expected to occur (CHERNIAK; MANCHESTER; WATSON, 2007; TRIEBOLD et al., 2007; STENDAL et al., 2006; KOHN; PENNISTON-DORLAND; FERREIRA, 2016; CRUZ-URIBE et al., 2018), and so, this is a perfect area to conduct this investigation.

6.2 Geologic setting and sample description

The Neoproterozoic Southern Brasília Orogen is the result of an Ediacaran to Cambrian collision between the passive margin of São Francisco Plate and the active continental margin of the Paranapanema Plate (BRITO NEVES; CAMPOS NETO; FUCK, 1999; CAMPOS NETO, 2000; TROUW et al., 2000). In the southernmost portion of the Brasília Orogen, this collision is characterized by a syn-metamorphic stack of nappes, represented, from top to base by (CAMPOS NETO, 2000): (i) the Socorro-Guaxupé Nappe derives from the lower crust of a magmatic arc root and consists of granulite-migmatite-

granite association (CAMPOS NETO; CABY, 1999; CAMPOS NETO, 2000); (ii) the Andrelândia Nappe System (TROUW et al., 1982; TROUW; RIBEIRO; PACIULLO, 1983; TROUW et al., 2000; CAMPOS NETO; CABY, 1999; CAMPOS NETO, 2000; CAMPOS NETO et al., 2007), which is composed of highly deformed meta-sedimentary rocks associated with forearc and accretionary prism segments; (iii) the Carrancas Nappe System (CAMPOS NETO et al., 2004), which is composed of metasedimentary rocks interpreted as the passive continental margin of Sanfranciscan Plate (PACIULLO et al., 2000; PACIULLO; RIBEIRO; TROUW, 2003; TROUW et al., 2000; WESTIN et al., 2019).

The Carrancas Nappe System includes the Luminárias Nappe (Fig. 6.1) (TROUW et al., 2000; CAMPOS NETO et al., 2004). Rocks of the Carrancas Nappe System belong to the Carrancas Group (TROUW; RIBEIRO; PACIULLO, 1980), divided into two units: the basal São Tomé das Letras Unit, which is composed of quartzite and muscovite quartzite, and it is the unit from where the studied samples derive from, and the upper Campestre Unit, which is composed of schist and phyllite with frequent lenses of quartzite. In the Carrancas Nappe System, the maximum depositional age is ca. 920 Ma (VALERIANO et al., 2004; WESTIN; CAMPOS NETO, 2013; WESTIN et al., 2019; KUSTER et al., 2020; MARIMON et al., 2020).

A regional metamorphic gradient that extends throughout the Carrancas Group, with metamorphic conditions increasing southward from greenschist to amphibolite/eclogite facies, has long been described in the literature (TROUW; RIBEIRO; PACIULLO, 1980; RIBEIRO; HEILBRON, 1982; TROUW et al., 2000; RENO et al., 2012; TROUW et al., 2013; COELHO et al., 2017). However refined *P-T* conditions pointing that high pressures inside or close to eclogite facies were determined only recently (SILVA, 2010; FUMES et al., 2019). The Luminárias Nappe records a section of the regional metamorphic gradient (Fig. 6.1), where the metamorphic conditions increase along the geological beds. According to Fumes et al. (2019), three diagnostic mineral peak assemblages are present in metapelitic rocks from Luminárias Nappe: a) the Chl+Ky+St+ Ms+Qtz+Rt assemblage occurs in the northern portion at 580 ±4 °C and ∼0.9 GPa and indicate high-pressure lower amphibolite facies; b) the St+Bt+Grt+Ms+Qtz+Rt assemblage occurs in central portion at 600 ±15 °C and 1.1±0.3 GPa and indicates high-pressure amphibolite facies and c) the St+Ky+Grt+Ms+Qtz+Rt assemblage occurs in the southern portion at 630 ±13 °C and 1.4±0.6 GPa and indicates eclogite facies.

6.2.1 Sample description

Seven quartzite samples of ∼20 kg each (LR52a, LR22, LR30, LR33b, LR39, LR45 and LR46) were collected from the São Tomé das Letras Unit covering a 40 km long N-S transect (Fig. 6.1, Tab. 6.1), along which the metamorphic gradient increases southward.

Figure 6.1 – Location maps. a) Map of Brazil showing the location of the study area (grey rectangle). b) Simplified geological map of Luminárias Nappe showing sample location (UTM, WGS84, Zone 23K). Modified after Trouw et al. (2003), Quéméneur et al. (2003), Nunes, Trouw e Castro (2008), Paciullo e Ribeiro (2008). $^{*}P$-T conditions presented in the figure are those of Fumes et al. (2019).

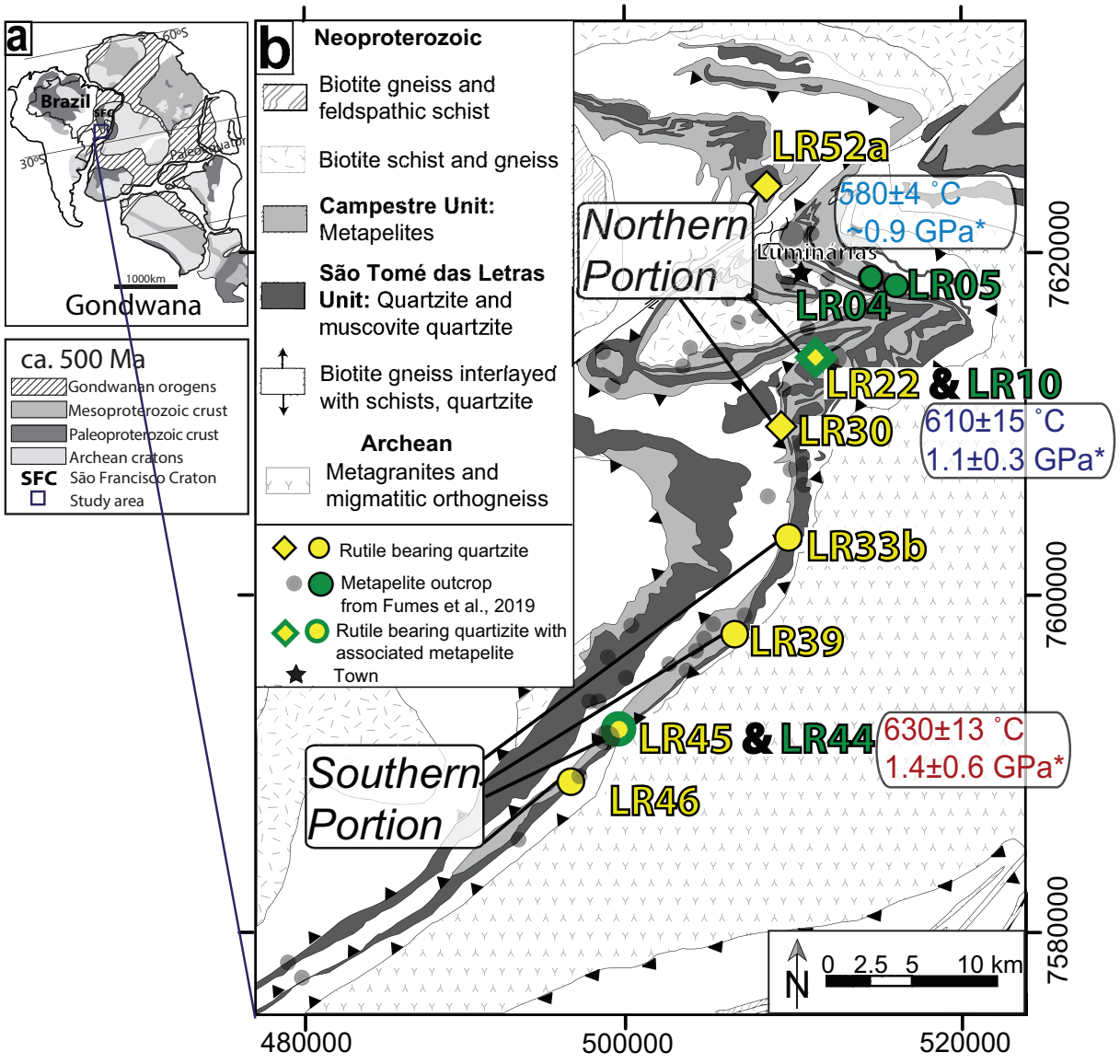

Table 6.1 – Location and metamorphic conditions of the studied quartzite samples. Corresponding metapelite samples studied by Fumes et al. (2019) and their peak mineral assemblage is also presented. Coordinates are in UTM (Zone 23K, WGS84).

Quartzite Sample	UTM E	UTM S	Metapelite Sample	Nappe Portion	T °C	P GPa	Min. Assemblage Metapelite*
LR-52a	511460	7625910	LR50**	Northern	580±4	∼0.9	Ky+Chl+Ctd+Ms
LR-22	513310	7615351	LR10**	Northern	600±15	1.1 ±0.3	St+Grt+Bt+Ms
LR-30	510406	7611675	LR32	Northern			Grt+St+Ms
LR-33b	511089	7604960	LR33	Southern			Grt+St+Ms
LR-39	506012	7598967	LR43	Southern			Ky+Grt+St+Ms
LR-45	501289	7593927	LR44**	Southern	630±13	1.4±0.6	Ky+Grt+St+Ms
LR-46	498605	7590930	LR47	Southern			Ky+Grt+Ms

* peak mineral assemblage according to Fumes et al. (2019).
** metamorphic modelling according to Fumes et al. (2019).

The irregular exposure pattern of the rocks from the São Tomé das Letras Unit is due to low-dipping geological beds (that may locally be folded) exposed on a steep topography (Fig. 6.1).

In order to assure an independent characterization of peak P-T conditions, samples derive from sites where nearby metapelitic schists have been collected and studied by Fumes et al. (2019). The P-T conditions of the studied samples, as well as their correlation with those studied by Fumes et al. (2019), is presented in Tab. 6.1. For the following description, studied samples are grouped according to their location along the Luminárias Nappe (Fig. 6.1), namely: northern portion samples (LR52a, LR22 and LR30) and southern portion samples (LR33b, LR39, LR45 and LR46). The studies were carried out on mineral separates in all samples.

6.2.1.1 Northern portion

Northern portion quartzite (LR52a, LR22 and LR30 samples) shows granular texture with inequigranular, polygonal shaped, quartz grains. Accessory minerals comprise less than 1 % in vol. (muscovite, zircon, rutile, magnetite, tourmaline, apatite and ilmenite). Average grain sizes are 200 μm for quartz and 150 μm for muscovite (Fig. 6.2a). Rock fabric is anisotropic, with oriented muscovite and elongated quartz grains, with tectonic foliation parallel to sedimentary bedding. Quartz grains have weak undulose extinction. Most of the rutile crystals from samples LR52a, LR22 and LR30 have round shapes (Figs. 6.3a and 6.3b). Few crystals have irregular shapes, including elongated ones in LR22 sample (Fig. 6.3c). In the LR52a sample, separated rutile crystals vary from 80 μm to 180 μm and zircon inclusions are frequent. In the LR22 sample, separated rutile crystals vary from 80 μm to 120 μm and and the grains often have inclusions of zircon and monazite. In the LR30 sample, separated rutile crystals vary from 90 μm to 250 μm (longest axis) and zircon inclusions and ilmenite lamellae occur. In thin section from the northern portion quartzite,

Figure 6.2 – Representatives transmitted light photomicrographs (cross polarized light) of studied quartzite and BSE images of rutile from thin section. a) Photomicrograph from northern portion quartzite showing polygonal inequigranular texture, medium-grained (Sample LR52a). b) BSE image of needle-shaped rutile in thin section (Sample LR52a). c) Photomicrograph from the southern portion quartzite showing granular texture (Sample LR33b).

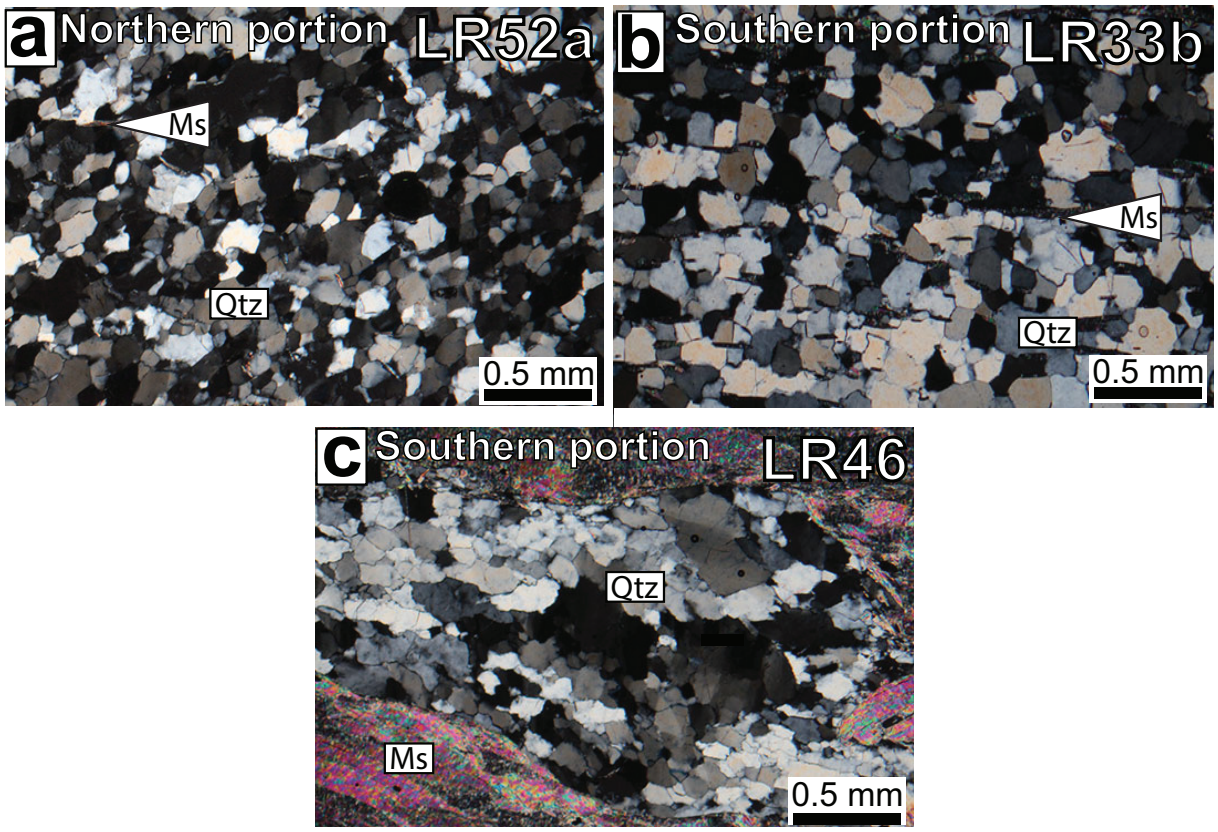

rutile also occurs as fine grained (average of 15 μm, longest axis), needle-shaped crystals (Fig. 6.2b). These grains are interpreted to have crystallized during metamorphism and, due to the small size, are not recovered during the heavy mineral separation process.

6.2.1.2 Southern portion

Southern portion quartzite (LR33, LR39, LR45 and LR46 samples) also has granular texture, with inequigranular and polygonal shaped quartz (Fig. 6.2c). The rock is coarser grained when compared to northern portion samples (Fig. 6.2e). Average grain size is 300 μm for quartz and 350 μm for muscovite (maximum grain size of 500 μm and 600 μm for quartz and muscovite, respectively). Samples have a slightly higher muscovite content (average of less than 3 vol. %) when compared to northern portion samples. We note that sample LR-46 is banded and in muscovite rich bands the concentration of this mineral reaches up to 15%. Accessory minerals are rutile, ilmenite, zircon, apatite, monazite, pyrite, tourmaline and magnetite. The rock displays a anisotropic fabric, defined by elongated quartz crystals and oriented muscovite crystals, when compared to northern portion quartzite. Tectonic foliation is parallel to bedding. Reduction of grain size by deformation, mainly by dynamic recrystallization of quartz, is locally observed in these samples. Quartz

Figure 6.3 – BSE images of representative rutile grains from crushed samples with concentrations of Zr and Nb in ppm. a) Rutile (Rt3) from LR52a sample with rounded detrital shape and zircon inclusion. b) Rutile (Rt6) from LR30 sample with detrital shape and zircon inclusion. c) Rutile (Rt9) from LR22 sample with elongated shape. d) Rutile (Rt13) from LR33b sample with zircon inclusion and ilmenite lamella. e) Rutile (Rt5) from LR39 sample with ilmenite lamella and detrital shape. f) Rutile (Rt17) from LR45 sample with elongated, euhedral shape. g) Rutile (Rt4) from LR46 sample with ilmenite lamella. Scale bar measures 50 μm in all images. Spots positions are indicated by the circles. Grains are labelled according to Table 6.S1.

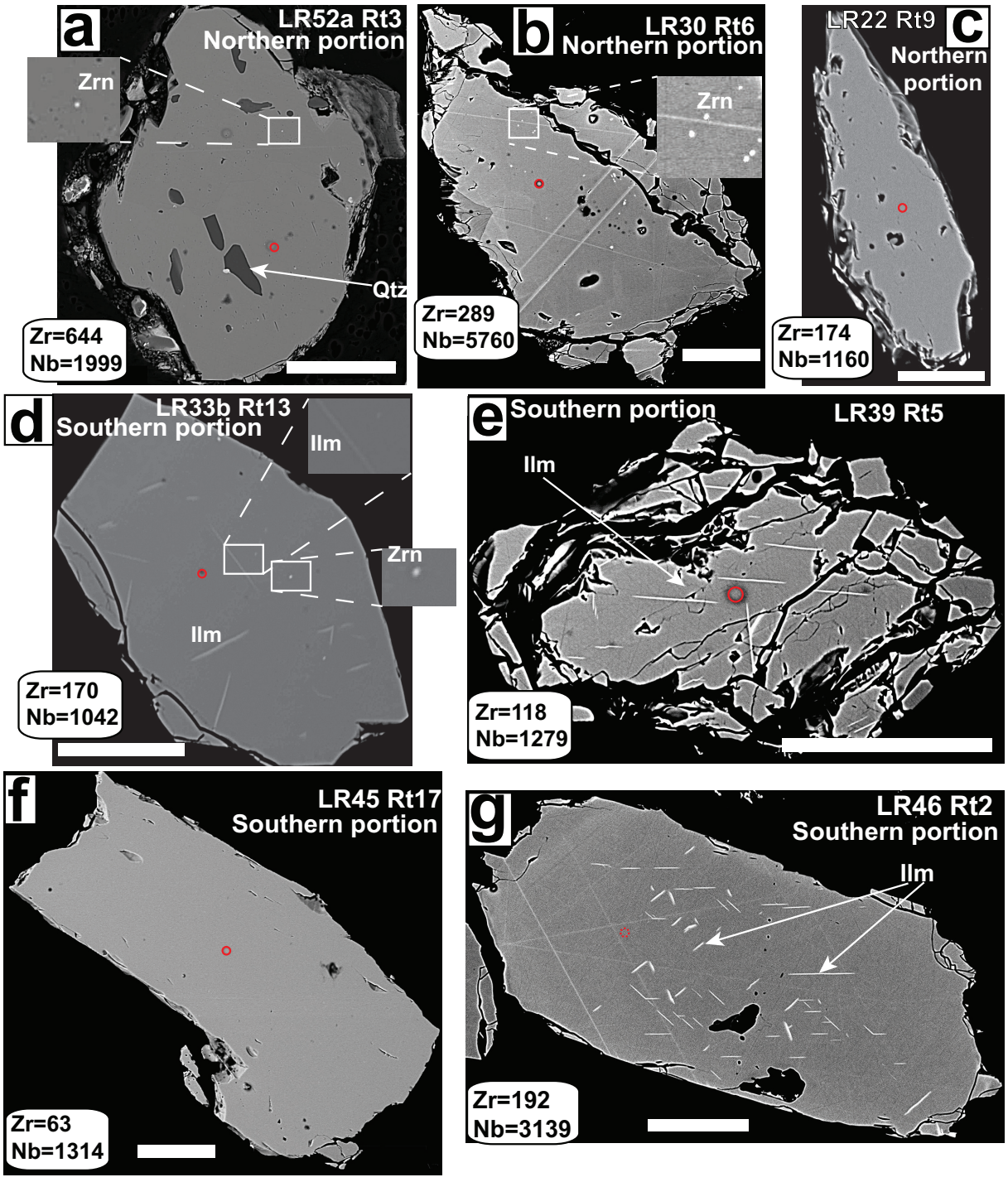

crystals have interlobate contacts and show intense undulose extinction. Irregular grain boundaries are interpreted to have formed in response to dynamic recrystallization of quartz associated with subgrain rotation and high-temperature (>500 °C) grain boundary migration, as described by Stipp et al., 2002.

In LR33 and LR39 samples most of the rutile crystals are rounded, pointing to preservation of the detrital shape (Fig. 6.3e), on the other hand, some grains have angular, euhedral, shapes (Fig. 6.3d). In LR45 and LR46 samples most of the rutile crystals have elongated and prismatic euhedral shapes (Fig. 6.3f and 6.3g) and few rutile crystals have rounded shape (Fig. 6.3g). Grain size varies from 50 μm to 120 μm in LR33 sample, 70 μm to 190 μm in LR39 sample, 100 μm to 340 μm at the longest axis in LR45 sample and 70 μm to 280 μm at the longest axis in LR46 sample. Ilmenite lamellae and zircon inclusion may occur in rutile grains from all samples (Fig. 6.3d). However, zircon inclusions in rutile grains are less frequent than in those from the northern portion.

In thin section from the LR33 sample, rutile is often in contact with muscovite and has irregular shape, occupying interstitial space between rock forming minerals (Fig. 6.2d). In thin section from the LR46 sample, subhedral rutile grains with irregular edges are also present (Fig. 6.2f). These grains are interpreted to have crystallized during metamorphism.

Large and rounded rutile crystals (70 μm to 340 μm, longest axis) present in quartzite, pointing to preservation of the detrital shape.

6.3 Methods

6.3.1 Sample preparation and imaging

Mineral separation followed the procedures of Triebold et al. (2007) and involved crushing and grain separation via sieving (63-200 μm fraction), heavy-liquid and magnetic separation. Minerals separate from the heavy, magnetic and non-magnetic fractions, were hand-picked under stereoscopic microscope. Grains were embedded in epoxy discs that were subsequently polished and coated with carbon. We note that a rutile with the average diameter of 100 μm relates via hydrodynamic equivalence to a typical fine- to medium-grained sand (quartz with grain size of $\sim$ 200 μm).

Grain mounts were observed under scanning electron microscope to identify sub-microscopic inclusions in rutile. Backscattered electron images (BSE) were collected using a JEOL JSM 6010 scanning electron microscope using 15 to 20 kV.

6.3.2 Electron Microprobe Analysis

Separated rutile grains from all samples (LR52a, LR22, LR30, LR33b, LR39, LR45 and LR46) were analyzed by Electron Microprobe.

Table 6.2 – Electron microprobe conditions applied for the rutile trace elements analysis

20 kV / 80 nA	Si	Al	Cr	Sb	Sn	W	Ta	Fe	Ti	Nb	Zr
Crystall	TAP	TAP	PETJ	PETJ	PETJ	LIFL	LIFL	LIFL	PETJ	PETJ	PETJ
Line	Kα	Kα	Kα	Lα	Lα	Lα	Lα	Kα	Kβ	Lα	Lα
Peak sec[a]	300	300	150	150	150	150	150	150	30	300	300
Bkg sec[b]	150	150	50	50	50	50	50	50	15	150	150
DL[c]	25	20	50	80	75	95	85	40	55	40	45

[a] Count time on peak position in seconds. [b] Count time on background position in seconds. [c] 2 σ detection limit, based on repeated measurement of variation on background, values in ppm.

Electron microprobe analyses of rutile were carried out at the Department of Geology of São Paulo State University in Rio Claro, Brazil with a JEOL JXA-8230 equipped with 5 wavelength-dispersive spectroscopy (WDS) detectors. Acceleration voltage was set to 20 kV and sample current to 80 nA. The following elements were analyzed: Si, Al, Cr, Sb, Sn, W, Ta, Fe, Ti, Hf, Nb and Zr. A summary of the operational conditions is presented in Table 6.2. The Sy and R10 rutile mineral standards (LUVIZOTTO et al., 2009) were routinely analyzed to evaluate the quality of the analyses. Furthermore, repeated analyzes on the Sy rutile were used to assure "true" zero concentration count rates on the peak, since this standard has virtually no trace elements (LUVIZOTTO et al., 2009). Si contents in rutile were used as a quality control to detect and avoid contamination associated with submicroscopic zircon inclusions following the method outlined by Zack, Moraes e Kronz (2004). Measurements with Si concentrations higher than 300 ppm were excluded from the dataset.

6.4 Results

6.4.1 Trace element in rutile

As an average, fifteen representative rutile crystals were analyzed for each of the seven samples. Trace element content in rutile is presented in Fig. 6.4 and the complete dataset is available as supplementary material in Table 6.S1. In twenty seven grains (Figure 6.S1), multiple analyses were performed in order to evaluate trace element intra-grain homogeneity. For grains with more than one analysis, only one representative result is presented in Fig. 6.4. Four out of twenty seven rutile grains show intra-grain variation of W, Al, Ta and Nb that is above the overall sample variation for the corresponding element (Figure 6.S1). Intra-grain variation of Zr is smaller than the overall sample variation for this element in all analyzed rutile grains. For Zr, the range of intra-grain variation (percentage difference from the average for each grain) is 9.4 - 121 %, for the northern portion samples, and 1.9 - 49.5 %, for the southern portion samples. The range of intra-grain variation for all analyzed elements is presented in Table 6.S2.

Concentrations of Hf are below the detection limit (DL) in all samples. Concentra-

Figure 6.4 – Box and whisker plots showing concentration (in ppm) of trace elements (W, Fe, Al, Nb, Ta, Cr and Zr) in rutile crystals from studied samples. Whiskers represent the 5th and 95th percentile and boxes represent the second (bottom-25%) and third quartile (top-75%). For rutile grains with more than one spot, only one representative analysis is plotted. The minimum and maximum values are plotted as 'x', the small squares represent the median value, and the lines represent the mean value. The numbers at the top-right of each box represent the number of analyses for that sample. For samples in which less than three analyses are above detection limits, the values of each analysis are plotted as small squares. Only analyses above the minimum detection limit are presented.

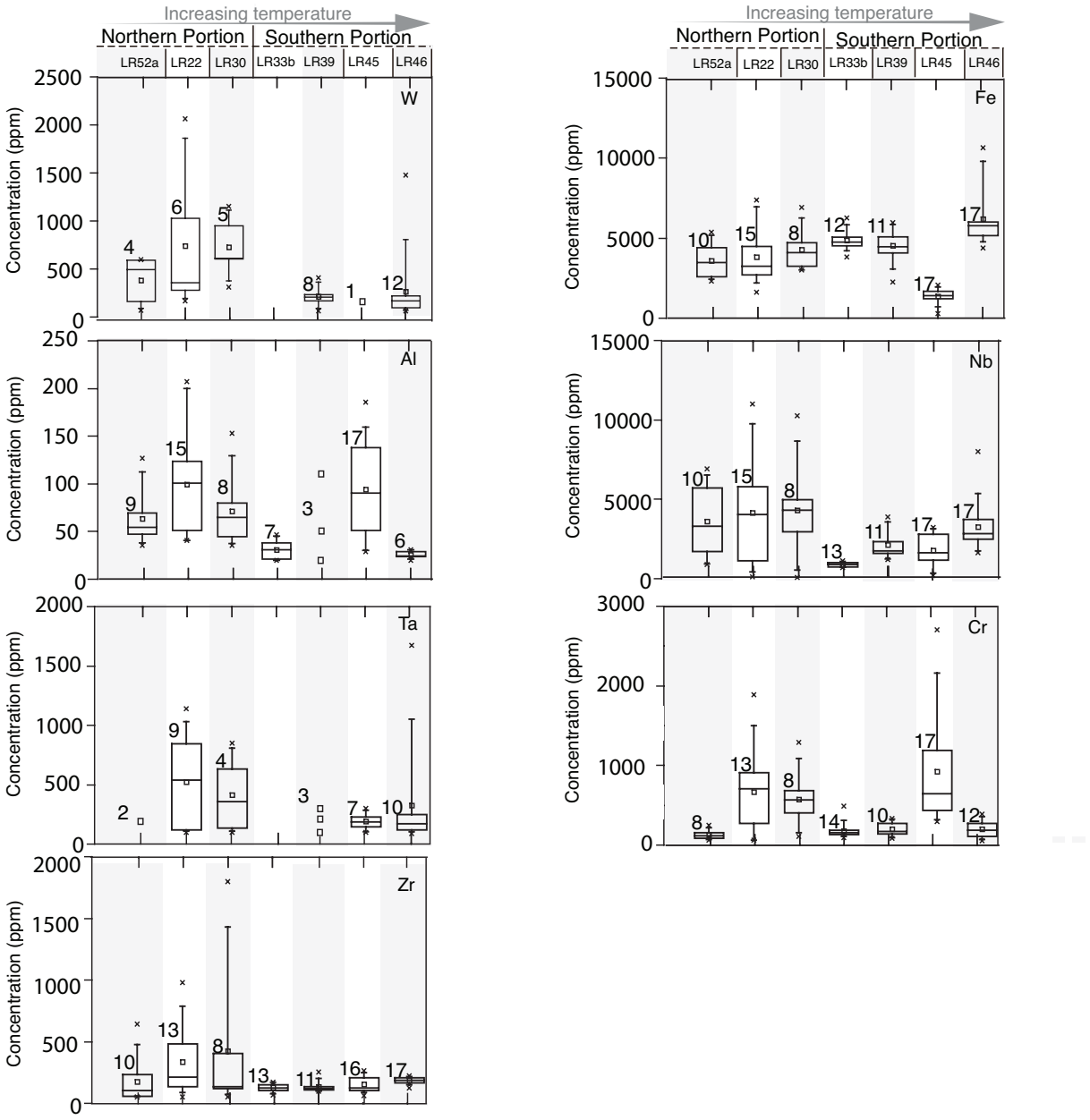

tions of Sb (110 out of 180) and Sn (129 out of 180) are often below DL. No distinctive pattern is displayed by these elements and, therefore, they are not shown in the Fig. 6.4. Rutile grains from two southern portion samples (LR33 and LR39) have several results above the DL for Sb and concentrations reach up to 480 ppm. Concentrations of Sb as high as 1030 ppm are obtained in rutile grains from LR46 sample and all results are above the DL. Only rutile grains from LR52a, LR22 and LR30 (northern portion), LR39 and LR45 (southern portion) samples have Sn concentrations above the DL, with an average of 94 ppm, 242 ppm, 165 ppm, 116 ppm and 175 ppm, for LR52a, LR22, LR30, LR39 and LR45 samples, respectively.

Rutile crystals from LR52a, LR22 and LR30 samples (northern portion) and LR46 sample (southern portion) record the highest contents of W (102-2070 ppm, Fig. 6.4). In LR33b sample, all analyses are below the DL for W. In the LR45 sample, concentration above the DL is only obtained for one grain. In the LR39 sample, most of the W analyses are above the DL and average concentration is within the 103-440 ppm range.

Contents of Fe obtained for almost all grains are above the DL (Fig. 6.4), reaching the highest concentration amongst all analyzed elements (average of ∼5180 ppm). A significant scatter in the contents of Fe within the same sample is observed. Consistently, lowest values are obtained in rutile grains from LR45 sample (average of ∼ 1560 ppm). With the exception of the latter, rutile grains from all other samples show similar patterns in terms of concentration and spread, although those from samples from the northern portion (LR52a, LR22 and LR30) have slightly lower contents. Some of the high values can be associated with secondary fluorescence of sub-microscopic ilmenite needles in rutile.

Most of the Al concentration data are above the DL. Results obtained for LR22, LR30, LR39 and LR45 samples show higher spread in concentration when compared to other samples. In all samples, Al contents vary between 21 to 740 ppm and the average is 80 ppm. In the LR46 sample, the Al content in rutile crystals from thin sections is higher than in the mineral separates and may reflect secondary fluorescence from nearby muscovite.

With the exception of one analysis, all rutile grains have Nb contents above the DL (40 ppm). Several analyses of Ta (Fig. 6.4) are below the DL (106 analyses below 85 ppm). For Nb, a larger spread in concentration (60-11000 ppm) is displayed by rutile grains from the northern portion samples. The same pattern is observed for Ta (LR22 and LR30 samples, 98-1700 ppm). In southern portion samples, the average Nb concentration is 2530 ppm and Ta concentration is 280 ppm. Two rutile crystals from the LR46 thin section record Nb content higher (8586 and 9482 ppm) than those from the mineral separate (maximum concentration of 7997 ppm).

Few rutile grains have Cr contents below the DL (50 ppm). Rutile from LR22, LR30 and LR45 samples show a higher variation in concentration of Cr (60-2700 ppm)

compared to the other samples (Fig. 6.4).

When compared to other trace element, Zr data show a distinct pattern (Fig. 6.4). Northern portion samples (LR52a, LR22 and LR30) show a large spread in Zr content. Some of the results are above 400 ppm and several analyses are below the DL (45 ppm). Samples from the southern portion display a much narrower spread in Zr concentration, with maximum concentration not exceeding 280 ppm. Zr contents in rutile crystals from thin sections and mineral separates are the same within the error.

6.5 Discussion

6.5.1 Trace elements systematics in rutile

Considering the distribution of the samples along the Luminárias Nappe and that metamorphic conditions increase southward, no clear correlation can be drawn between *P-T* conditions and contents of trace elements in the studied rutile grains, with the exception of Zr (Fig. 6.4).

It has been shown that the Nb and Cr contents of the whole rock is mirrored in associated rutile (ZACK; EYNATTEN; KRONZ, 2004; TRIEBOLD; EYNATTEN; ZACK, 2012), where a high Nb/Cr ratio points to a pelitic source. Results obtained for the studied samples show large intra- and inter-sample variation in concentrations of Nb and Cr (Fig. 6.4). Results suggest that the re-equilibration of Nb and Cr did not occur on the whole rock scale and rutile preserves its Nb/Cr detrital value. Calculations performed according to the method presented by Triebold, Eynatten e Zack (2012) indicate that the studied rutile grains have, with very few exceptions, a pelitic signature (Fig. 6.5), with positive values in the Triebold, Eynatten e Zack (2012) equation (x = 5*(Nb -500) - Cr)). Furthermore, analyzed grains have high contents of Nb (Fig. 6.4), which match values reported in the literature (TRIEBOLD et al., 2007; TRIEBOLD; Von Eynatten; ZACK, 2011) for rutile from pelitic rocks.

Studied grains show a large variation in Nb/Ta ratios (Fig 6.6). It has to be stressed that 51 out of 103 analyzed grains have Ta concentrations below the EPMA detection limit (85 ppm). Low concentrations of Nb are usually associated with low concentrations of Ta (Fig 6.6). Regarding the Nb/Ta ratio, 37 out of 51 rutile have sub-chondritic values (19.9; (MÜNKER et al., 2003)), with values as low as five. Few results (14 out of 51) are above the chondritic value, reaching up to 80.

6.5.2 Application of the Zr-in-rutile thermometry

Temperatures calculated for all analyzed rutile grains are presented in Fig. 6.7. Since the results obtained in the present work is compared to those of Fumes et al. (2019),

Figure 6.5 – Box and whisker plots showing of Pelitic / mafic discrimination line. Calculations are based on Nb and Cr concentrations and follow the method outlined by Triebold, Eynatten e Zack (2012). Positive values indicate pelitic source, whereas negative values indicate mafic source for the rutile grains. Whiskers represent the 5th and 95th percentile and boxes represent the second (bottom-25%) and third quartile (top-75%). For rutile grains with more than one spot, only one representative analysis is plotted. The minimum and maximum values are plotted as 'x', the small squares represent the median value, and the lines represent the mean value. The numbers at the top-right of each box represent the number of analyses for that sample. For samples in which less than three analyses are above detection limits, the values of each analysis are plotted as small squares. Only analyses above the minimum detection limit are presented.

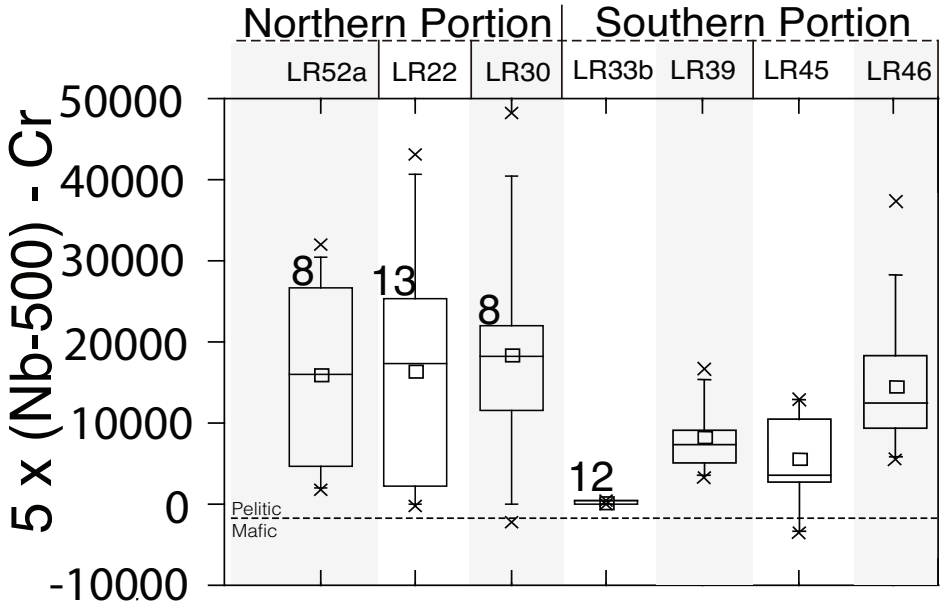

Figure 6.6 – Nb and Ta concentrations obtained for studied rutile grains. Nb versus Ta. Chondritic ratio from Münker et al. (2003). Only analyses above detection limits (85 ppm for Ta and 40 ppm for Nb) are plotted. The numbers in left side of each boxplots represents the number of analyses that are shown in the boxplot. When the numbers of analyses above detection limits are lower than three only the value of the analyze is plotted in squares. Only one representative analysis per grain is plotted.

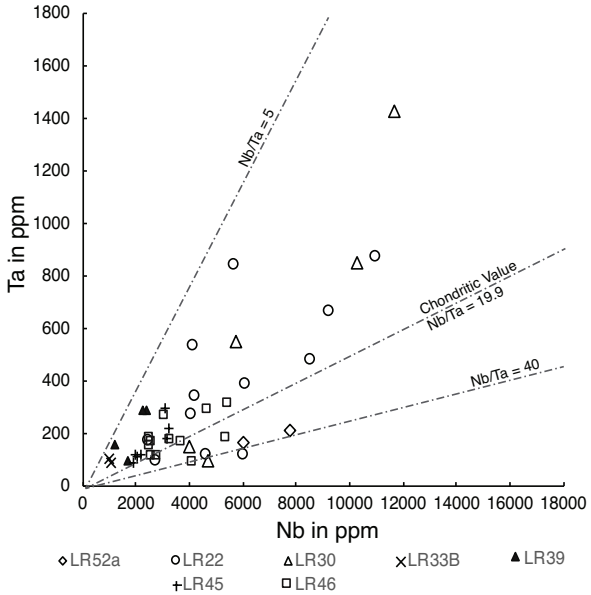

Figure 6.7 – Box and whisker plots showing concentration (in ppm) of Zr in rutile and Zr-in-rutile temperatures from quartzite and metapelite samples. The metapelite sample data are extracted from Fumes et al. (2019). The metapelite content is shown in green and the quartzite is in gray and black. The minimum and maximum values are plotted as 'x', the small squares represent the median value, and the lines represent the mean value. The numbers at the top-right of each box represent the number of analyses for that sample. For samples in which less than three analyses are above detection limits, the values of each analysis are plotted as small squares.

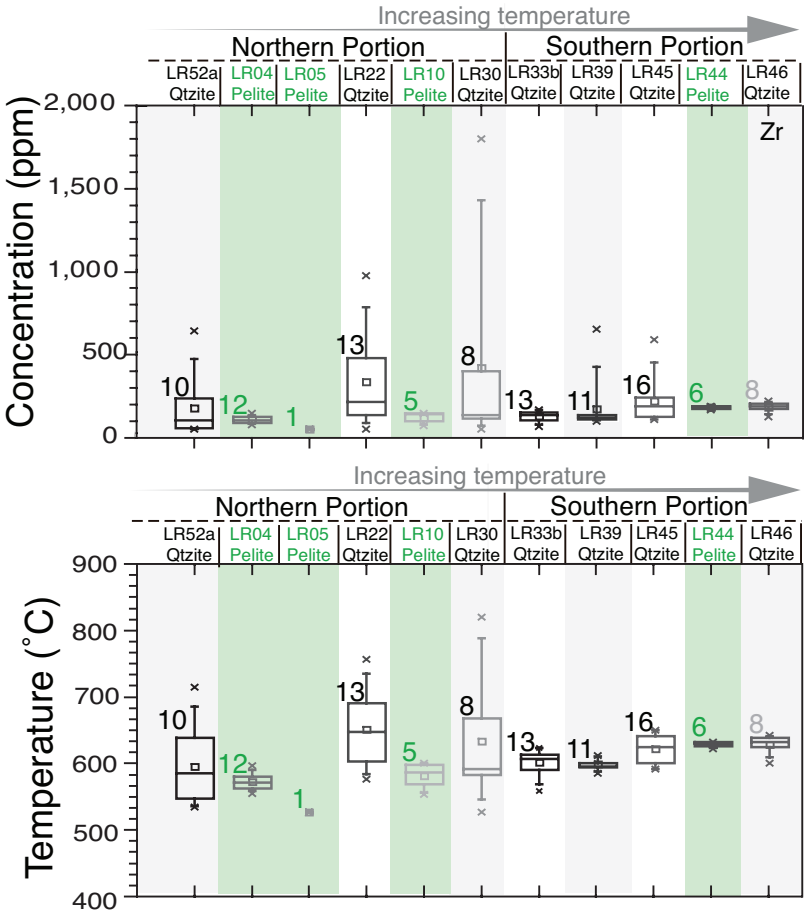

the same calibration used by the latter authors is used here, that is, Tomkins, Powell e Ellis (2007). The more recent calibration of Kohn (2020) would result in lower temperatures of ∼35 °C.

The Zr content in rutile grains from the northern portion (LR52a, LR22 and LR30 samples), as pointed out previously, show a large spread so is interpreted as a relict signature, reflecting T of the source rock. It is confirmed based on the preserve round shapes (Figs. 6.3a and 6.3b), indicating detrital shape in the northern portion samples. Therefore, P conditions under which the grains crystallized cannot be constrained. In order to give a rough T estimate, a pressure value of 1.0 GPa, based on the pressure peak conditions in the metapelite rocks in the Luminárias Nappe according to Fumes et al. (2019), was used in order to to give estimate for comparison reasons (Fig. 6.7). Although the pressure effect on the Zr-in-rutile thermometer is fairly small, a potential uncertainty of ∼40 °C is added to the temperature estimated for the northern portion samples, if a P

range of 0.5 GPa to 1.5 GPa is considered.

Temperature calculated at pressure of 1.4 GPa, according to Fumes et al. (2019) for southern portion samples show a much narrower spread in comparison to results obtained for the northern portion samples (Fig. 6.7). If the third quartile is taken into account, according to recommendation of Tomkins, Powell e Ellis (2007) values of 612 °C, 605 °C, 638 °C and 635 °C are obtained for samples LR33b, LR39, LR45 and LR46, respectively. Sample LR45 shows a larger spread when compared to the other samples from the southern portion (LR33b, LR39 and LR46). For LR33b and LR46 samples, T obtained for rutile grains from mineral separates (detrital grains) and thin sections (metamorphic grains) are identical within error (Fig. 6.7). These results strongly suggest that resetting of relict Zr signature in detrital rutile was attained at conditions of southern portion samples. Zr-in-rutile temperatures obtained for southern portion samples are in good agreement with the temperature presented in the literature for Luminárias Nappe rocks (FUMES et al., 2019).

Although minimum Zr re-equilibration T in detrital rutile from quartzite cannot be precisely determined, our data indicate that Zr re-equilibration was attained at 630 ^{o}C and 1.4 GPa, which is the highest P-T conditions for the metapelite from the southern portion), according to Fumes et al. (2019). Resetting temperature of Zr-in-rutile from our samples is similar to what was initially proposed in the literature (TRIEBOLD et al., 2007; STENDAL et al., 2006).

Diffusion coefficient for Zr in rutile is an important parameter in Zr resetting in rutile. Different diffusion coefficients for this element in rutile are present in the literature and vary by three orders of magnitude are high temperature (at ∼1100 ^{o}C) (CHERNIAK; MANCHESTER; WATSON, 2007; DOHMEN et al., 2018; SASAKI; PETERSON; HOSHINO, 1985). More diffusion studies are required to better understand this open question in the literature and the application to natural rutile. Another point is that all the diffusion experiments available are only performed at high temperatures and these results extend to lower temperatures. Diffusion of Zr in rutile values obtained in Dohmen et al. (2018), Sasaki, Peterson e Hoshino (1985) are similar and higher than Cherniak, Manchester e Watson (2007). According to (DOHMEN et al., 2018) at least some diffusion might occurs at the re-equilibration temperature of 630 ^{o}C. Dodson (1973) closure temperature calculated in Dohmen et al. (2018) for a rutile of ∼100 μm at a cooling rate of 10 ^{o}C/Ma is ∼of 600 ^{o}C, similar to that observed in our study. Dohmen et al. (2018) also point that the diffusion rates are influenced by the concentrations of trace elements in the rutile (e. g. the rutile diffusion coefficients are smaller by up to two orders of magnitude at concentrations of Nb higher than 100 ppm), however in our data we have a large spread in all others trace elements content in the rutile with exception of the Zr, so the resetting of Zr content in rutile was not dependent of the concentrations HFSE elements.

6.5.3 Mechanisms of trace elements resetting in rutile

Two types of rutile occur in the quartzite studied samples: detrital (Fig. 6.2f, g and Figs. 6.3 a to e) and metamorphic grains (Fig. 6.2b, d and f, Figs. 6.3 f and g), the latter is more abundant in the southern portion. Here are discussed the mechanisms that favoured the resetting of the Zr in the detrital rutile and also the crystallization of metamorphic rutile.

Several publications have focused on changes in rutile geochemistry after its crystallization under high-grade conditions (e. g. Kooijman et al. (2012), Ewing, Hermann e Rubatto (2013), Taylor-Jones e Powell (2015), Pape, Mezger e Robyr (2016), Kohn, Penniston-Dorland e Ferreira (2016), Pauly et al. (2016), Hart et al. (2018)). The process described in this work by which detrital rutile geochemistry is modified is similar to the ones discussed by the authors, since it involves geochemical changes, either by diffusion or recrystallization. Zr contents in rutile from granulite facies rocks usually show a large spread, and is interpreted as post-peak modification of rutile chemistry. According to Kooijman et al. (2012), Hart et al. (2018), the post-peak decrease of Zr concentration is related to diffusive cation exchange as result of decompression with cooling and/or the presence of fluid. However, Ewing, Hermann e Rubatto (2013) interpret that Zr resetting, also in granulite facies, occurs through recrystallization rather than diffusion, arguing that during the dissolution-reprecipitation process trace elements can be expelled from a grain wholesale. In contrast, diffusive exchange would affect mostly the grain rim. As discussed above, a large inter-grain variation in trace element contents, with the exception of Zr, is observed in the southern portion samples. Recrystallization, as proposed by Ewing, Hermann e Rubatto (2013), would favor re-equilibration of all trace elements, not only Zr. Furthermore, the large size and the round shape (relict detrital shape) of some grains disfavor recrystallization by dissolution-reprecipitation. The large rutile grains from southern portion samples show a small inter-grain spread in Zr concentration, flat rim-to-rim profiles and Zr-in-rutile temperatures calculated for these grains are in good agreement with those presented for the surrounding rocks (FUMES et al., 2019). All these characteristics point to diffusive resetting of Zr in inherited detrital grains in quartzite. The needle-shaped rutile from this portion may be formed by exsolution during cooling from Ti-rich, high-temperature quartz (CHERNIAK; WATSON; WARK, 2007; STORM; SPEAR, 2009), derived from the protolith. This feature corroborates the interpretation that high temperatures registered by the Zr-in-rutile thermometer represent those of the source rock. Needle-shaped rutile grains are too small to be analyzed by EPMA. They are also too small to be recovered during mineral separation.

According to Agangi et al. (2020) the Zr resetting in rutile probably requires fluid-assisted alteration and dissolution-reprecipitation processes at temperatures of greenschist and amphibolite facies metamorphism. In all studied samples the muscovite occurs, a

hydrated phase, and in the southern portion samples a slightly higher muscovite content is observed that suggests more fluid phases. Agangi et al. (2020) also suggests that the deformation can induce the intra-grain element mobility, affecting element concentrations. Deformational structures are observed in the samples, such as tectonic foliation, undulose extinction and dynamic recrystallization (subgrain rotation and grain boundary migration). Samples from the southern portion are more intensely deformed. The fluid presence and the deformation probably have favoured the Zr resetting in detrital rutile and also the dissolution-reprecipitation that crystallize the metamorphic rutile in the southern portion.

Therefore, the diffusion is the main mechanism in the modification of the geochemistry of detrital rutile in the southern portion. And dissolution-reprecipitation with fluid and deformation is the main process in the newly metamorphic rutile, both in the northern and southern portion. Either way, the presence of metamorphic rutile is evidence for mobilization on Ti on the whole rock scale

6.5.4 Comparison between trace elements in rutile from quartzite and metapelite

As pointed above, in the northern portion of the Luminárias Nappe, the Zr concentration in rutile grains from quartzite show a large spread. However, in rutile from metapelitic rocks from the same localities, the data from Fumes et al. (2019) indicate a small spread in Zr contents. On the other hand, in the southern portion, the concentration of Zr in rutile from both quartzite and metapelite are similar and show a small spread (Fig. 6.7).

According to Triebold et al. (2007), Luvizotto et al. (2009) the Zr content in rutile from quartzite may reset at higher temperature in comparison to crystallization temperature of rutile in metapelitic rocks (i.e., above $\sim$600 ^{o}C).

This idea is confirmed here, based on the Zr content in the metapelite and quartzite samples from the northern portion.

In the northern portion the metamorphic peak is calculated at 580 $\pm$4 °C (FUMES et al., 2019) - metapelite samples LR52, LR04 and LR05), that is $\sim$of 50 °C lower than in the southern portion. And all in the metapelite samples from this portion presents coherent Zr contents with the mineral assemblage, indicating that probably the Zr resetting in rutile.

Another difference between the rutile from quartzite and metapelite samples from the Luminárias Nappe is that in the quartzite samples detrital and metamorphic rutile grains are observed, meanwhile only metamorphic rutile occurs in the metapelite samples (see Fig. 5 in (FUMES et al., 2019)). The differences in the texture and in the temperature of Zr resetting in rutile between the quartzite and metapelite can be probably explained

due distinctive chemical system, the quartzite have very low concentration of elements such as Na, Ca, K, Fe, Mg and Al when compared with the metapelite. The more complex chemical system of the metapelite seems to favor the metamorphic recrystallization of the rutile and resetting of Zr content.

6.6 Concluding Remarks

- Our data show that Zr content in detrital rutile may re-equilibrate in quartzite. For the studied samples, minimum conditions are c.a. 630 ±30 ^{o}C and 1.4±0.6 GPa. Although these conditions cannot be taken as threshold temperature above which Zr-in-rutile temperatures in quartzite can generally be considered to record the temperature of metamorphism, our results indicate that rutile from high-grade quartzite may indeed be used to calculate peak metamorphic conditions. The re-equilibrate temperature in the quartzite is probably ∼of 50 ^{o}C higher than in the metapelite.

- Diffusion, driven by chemical potential gradient, is the main mechanism for trace element resetting of detrital in rutile in our studied samples. And dissolution-reprecipitation associated with fluid and deformation is the main process in the newly metamorphic rutile. The effect of neighboring phases on the chemical potential gradient is documented by high-Nb domains in rutile grains that are in contact with muscovite.

- Due to differences in diffusion coefficients, element distribution may vary within the grain. For example, zoned Nb and flat Zr profiles are observed in a single grain.

- The different behavior of Zr in respect to the other trace elements is accredited to equilibrium of the Zr-in-rutile geothermometer, where Zr, Ti and Si are buffered by the presence of zircon, rutile and quartz in the rock.

- The obtained results also indicate that re-equilibration of Si, Fe, Al, Cr, Sb, Sn, W, Nb and Ta in rutile from quartzite does not take place under conditions up to 630 ^{o}C and 1.4 GPa. Since the initial concentration of trace elements in detrital rutile cannot be determined, it is difficult to evaluate to what extent the trace elements concentrations were modified during metamorphism. Therefore, further studies on the application of low-grade quartzite for provenance studies using trace element geochemistry of rutile need to be carried out.

- The re-equilibration of Zr in rutile in the metapelite from the Luminárias Nappe seems to occur at slightly lower conditions than that occurs in the quartzite.

Acknowledgements: The authors acknowledge support from São Paulo Research Foundation (FAPESP) thought grants 2015/07750-0 and 2015/05230-0. GLL is supported by the National Council for Scientific and Technological Development (CNPq, Brazil) (Grant Number 311606/2019-9). R. A. Fumes acknowledge the National Council for Scientific and Technological Development-CNPq (PhD scholarship for RAF - 141604/2018-2) and the Brazilian Federal Agency for Support and Evaluation of Graduate Education (CAPES) for the financial support to the pos-graduation program. We are grateful to Daniela Rubatto, Alicia M. Cruz-Uribe and anonymous reviews for their detailed and insightful comments in the previous version of the work. The authors would like to thank Renato de Moraes, Mônica da Costa Pereira Lavalle Heilbron, Ticiano José Saraiva dos Santos, Maurício Pavan Silva and Cauê Rodrigues Cioffi for fruitful discussions. Juliana Okubo and Mauly Bottene are thanked for helping to improve the quality of the manuscript.

Reference

AGANGI, A. et al. Compositional modification and trace element decoupling in rutile: insight from the capricorn orogen, western australia. *Precambrian Research*, Elsevier, p. 105772, 2020.

BRITO NEVES, B. B. de; CAMPOS NETO, M. D. C.; FUCK, R. A. From Rodinia to Western Gondwana: as Aproach to the Brasiliano-Pan African Cycle and orogenic collage. *Episodes-Newsmagazine of International Union of Geological Science*, v. 22, n. 155-166, 1999.

CAMPOS NETO, M. D. C. Orogenic Systems from Southwestern Gondwana: An Approach to Brasiliano-Pan African Cycle and Orogenic Collage in Southeastern Brazil. In: CORDANI, U. G. et al. (Ed.). *Tectonic Evolution of South America*. 1. ed. Rio de Janeiro: COMPANHIA DE PESQUISA DE RECURSOS MINERAIS, 2000. p. 335–365.

CAMPOS NETO, M. D. C. et al. Migração de Orógenos e Superposição de Orogêneses: Um Esboço da Colagem Brasiliana no Sul do Cráton do São Francisco, SE - Brasil. *Geologia USP - Serie Cientifica*, v. 4, n. 1, p. 13–40, 2004.

CAMPOS NETO, M. D. C.; CABY, R. Neoproterozoic high-pressure metamorphism and tectonic constraint from the nappe system south of the Sao Francisco Craton, southeast Brazil. *Precambrian Research*, v. 97, n. 1-2, p. 3–26, 1999. ISSN 03019268.

CAMPOS NETO, M. D. C. et al. Sistema de nappes Andrelândia, setor oriental : litoestratigrafia e posição estratigráfica. *Revista Brasileira de Geociências*, v. 37, n. 4-suplemento, p. 47–60, 2007.

CHERNIAK, D.; MANCHESTER, J.; WATSON, E. Zr and Hf diffusion in rutile. *Earth and Planetary Science Letters*, Elsevier, v. 261, n. 1, p. 267–279, 2007.

CHERNIAK, D.; WATSON, E.; WARK, D. Ti diffusion in quartz. *Chemical Geology*, Elsevier, v. 236, n. 1-2, p. 65–74, 2007.

COELHO, M. B. et al. Constraining timing and P-T conditions of continental collision and late overprinting in the Southern Brasília Orogen (SE-Brazil): U-Pb zircon ages and geothermobarometry of the Andrelândia Nappe System. *Precambrian Research*, Elsevier B.V., v. 292, p. 194–215, 2017. ISSN 03019268. Avaible form internet: <http://linkinghub.elsevier.com/retrieve/pii/S0301926816305496>.

CRUZ-URIBE, A. M. et al. Assessing trace element (dis)equilibrium and the application of single element thermometers in metamorphic rocks. *Lithos*, Elsevier B.V., v. 314-315, p. 1–15, 2018. ISSN 18726143. Avaible form internet: <https://doi.org/10.1016/j.lithos.2018.05.007>.

DODSON, M. H. Closure temperature in cooling geochronological and petrological systems. *Contributions to Mineralogy and Petrology*, Springer, v. 40, n. 3, p. 259–274, 1973.

DOHMEN, R. et al. Diffusion of zr, hf, nb and ta in rutile: effects of temperature, oxygen fugacity, and doping level, and relation to rutile point defect chemistry. *Physics and Chemistry of Minerals*, Springer, v. 46, n. 3, p. 311–332, 2018.

EWING, T. A.; HERMANN, J.; RUBATTO, D. The robustness of the Zr-in-rutile and Ti-in-zircon thermometers during high-temperature metamorphism (Ivrea-Verbano Zone, northern Italy). *Contributions to Mineralogy and Petrology*, v. 165, n. 4, p. 757–779, 2013. ISSN 00107999.

FUMES, R. A. et al. Metamorphic modeling and petrochronology of metapelitic rocks from the Luminárias Nappe, southern Brasília belt (SE Brazil). *Brazilian Journal of Geology*, v. 49, n. 2, 2019.

HARLEY, S. L.; MOTOYOSHI, Y. Al zoning in orthopyroxene in a sapphirine quartzite: evidence for> 1120 °C UHT metamorphism in the Napier Complex, Antarctica, and implications for the entropy of sapphirine. *Contributions to Mineralogy and Petrology*, v. 138, n. 4, p. 293–307, 2000.

HART, E. et al. A window into the lower crust: Trace element systematics and the occurrence of inclusions/intergrowths in granulite-facies rutile. *Gondwana Research*, The Authors, v. 59, p. 76–86, 2018. ISSN 1342937X. Avaible form internet: <http://linkinghub.elsevier.com/retrieve/pii/S1342937X18300856>.

KIDDER, S.; AVOUAC, J. P.; CHAN, Y. C. Application of titanium-in-quartz thermobarometry to greenschist facies veins and recrystallized quartzites in the Hsüehshan range, Taiwan. *Solid Earth*, v. 4, n. 1, p. 1–21, 2013.

KOHN, M. J. A refined zirconium-in-rutile thermometer. *American Mineralogist: Journal of Earth and Planetary Materials*, Mineralogical Society of America, v. 105, n. 6, p. 963–971, 2020.

KOHN, M. J.; PENNISTON-DORLAND, S. C.; FERREIRA, J. C. Implications of near-rim compositional zoning in rutile for geothermometry, geospeedometry, and trace element equilibration. *Contributions to Mineralogy and Petrology*, Springer, v. 171, n. 10, p. 78, 2016.

KOOIJMAN, E. et al. Trace element systematics in granulite facies rutile: implications for Zr geothermometry and provenance studies. *Journal of Metamorphic Geology*, Wiley Online Library, v. 30, n. 4, p. 397–412, 2012.

KUSTER, K. et al. The neoproterozoic andrelândia group: Evolution from an intraplate continental margin to an early collisional basin south of the são francisco craton, brazil. *Journal of South American Earth Sciences*, Elsevier, v. 102, p. 102666, 2020.

LUVIZOTTO, G. L. et al. Rutile occurrence and trace element behavior in medium-grade metasedimentary rocks: Example from the Erzgebirge, Germany. *Mineralogy and Petrology*, v. 97, n. 3-4, p. 233–249, 2009. ISSN 09300708.

MARIMON, R. S. et al. U-pb and lu-hf isotope systematics on detrital zircon from the southern são francisco craton's neoproterozoic passive margin: Tectonic implications. *Journal of South American Earth Sciences*, Elsevier, v. 100, p. 102539, 2020.

MCDONOUGH, W. F.; SUN, S.-S. The composition of the earth. *Chemical geology*, Elsevier, v. 120, n. 3-4, p. 223–253, 1995.

MEZGER, K.; HANSON, G.; BOHLEN, S. High-precision UPb ages of metamorphic rutile: application to the cooling history of high-grade terranes. *Earth and Planetary Science Letters*, Elsevier, v. 96, n. 1-2, p. 106–118, 1989.

MÜNKER, C. et al. Evolution of planetary cores and the Earth-Moon system from Nb/Ta systematics. *Science*, v. 301, n. 5629, p. 84–87, 2003.

NUNES, R.; TROUW, R. A. J.; CASTRO, E. *Mapa Gelógico - Folha Varginha – escala 1:100.000, Programa Geologia do Brasil*. [S.l.], 2008.

PACIULLO, F. V. P.; RIBEIRO, A. Mapa Geológico-Folha Nepumoceno. In: *CONTRATO - CPRM - UFRJ 067/P2/2005*. [S.l.: s.n.], 2008.

PACIULLO, F. V. P. et al. The Andrelândia Basin, a Neoproterozoic Intraplate Continental Margin, Southern Brasília Belt, Brazil. *Revista Brasileira de Geociências*, v. 30, n. 1, p. 200–202, 2000.

PACIULLO, F. V. P.; RIBEIRO, A.; TROUW, R. a. J. Geologia da Folha Andrelândia 1:100.000. *Geologia e recursos minerais do sudeste mineiro Projeto Sul de Minas - Etapa I*, p. 84–119, 2003.

PAPE, J.; MEZGER, K.; ROBYR, M. A systematic evaluation of the zr-in-rutile thermometer in ultra-high temperature (uht) rocks. *Contributions to Mineralogy and Petrology*, Springer, v. 171, n. 5, p. 44, 2016.

PASSCHIER, C. W.; TROUW, R. A. *Microtectonics*. [S.l.]: Springer Science & Business Media, 2005.

PAULY, J. et al. Prolonged Ediacaran–Cambrian metamorphic history and short-lived high-pressure granulite-facies metamorphism in the HU Sverdrupfjella, Dronning Maud Land (East Antarctica): evidence for continental collision during Gondwana assembly. *Journal of Petrology*, Oxford University Press, v. 57, n. 1, p. 185–228, 2016.

PEREIRA, J. et al. Detrital rutile ages can deduce the tectonic setting of sedimentary basins. *Earth and Planetary Science Letters*, Elsevier, v. 537, p. 116193, 2016.

QUÉMÉNEUR, J. J. G. et al. Mapa Geológico-Folha Lavras. In: *Geologia e Recursos Minerais do Sudeste Mineiro*. [S.l.: s.n.], 2003. p. 1:100.000.

RENO, B. L. et al. In situ monazite (U-Th)-Pb ages from the Southern Brasília Belt, Brazil: Constraints on the high-temperature retrograde evolution of HP granulites. *Journal of Metamorphic Geology*, v. 30, n. 1, p. 81–112, 2012. ISSN 02634929.

RIBEIRO, A.; HEILBRON, M. Estratigrafia e Metamorfismo dos Grupos Carrancas e Adrelândia, Sul de Minas Gerais. In: *Anais do XXXII Congresso Brasileiro de Geologia*. [S.l.: s.n.], 1982. p. 177–186.

RUDNICK, R. L.; GAO, S. Composition of the continental crust. *Treatise on geochemistry*, v. 3, p. 659, 2003.

SASAKI, J.; PETERSON, N.; HOSHINO, K. Tracer impurity diffusion in single-crystal rutile (tio2- x). *Journal of Physics and Chemistry of Solids*, Elsevier, v. 46, n. 11, p. 1267–1283, 1985.

SILVA, M. P. *Modelamento Metamórfico de Rocas das Fácies Xisto-Verde e Anfibolito com o Uso de Pseudosseções: Exemplo das Rochas da Klippe Carrancas, Sul de Minas Gerais*. Tese (Dissertação de mestrado) — Universidade de São Paulo, 2010.

STENDAL, H. et al. Derivation of detrital rutile in the yaounde region from the neoproterozoic pan-african belt in southern cameroon (central africa). *Journal of African Earth Sciences*, Elsevier, v. 44, n. 4-5, p. 443–458, 2006.

STIPP, M. et al. The eastern Tonale fault zone: a 'natural laboratory' for crystal plastic deformation of quartz over a temperature range from 250 °C to 700 °C *Journal of structural geology*, Elsevier, v. 24, n. 12, p. 1861–1884, 2002.

STORM, L.; SPEAR, F. Application of the titanium-in-quartz thermometer to pelitic migmatites from the adirondack highlands, new york. *Journal of Metamorphic Geology*, Wiley Online Library, v. 27, n. 7, p. 479–494, 2009.

TAYLOR-JONES, K.; POWELL, R. Interpreting zirconium-in-rutile thermometric results. *Journal of Metamorphic Geology*, v. 33, n. 2007, p. 115–122, 2015.

TOMKINS, H. S.; POWELL, R.; ELLIS, D. J. The pressure dependence of the zirconium-in-rutile thermometer. *Journal of Metamorphic Geology*, v. 25, n. 6, p. 703–713, 2007. ISSN 02634929.

TRIEBOLD, S. et al. Deducing source rock lithology from detrital rutile geochemistry: An example from the Erzgebirge, Germany. *Chemical Geology*, v. 244, n. 3-4, p. 421–436, 2007. ISSN 00092541.

TRIEBOLD, S.; EYNATTEN, H. von; ZACK, T. A recipe for the use of rutile in sedimentary provenance analysis. *Sedimentary Geology*, Elsevier B.V., v. 282, p. 268–275, 2012. ISSN 00370738. Avaible form internet: <http://dx.doi.org/10.1016/j.sedgeo.2012.09.008>.

TRIEBOLD, S.; Von Eynatten, H.; ZACK, T. A recipe for the use rutle in sedimentary provenance analysis. *Sedimentary Geology*, v. 282, p. 268–275, 2011.

TROUW, R. A. J. et al. The Central Segment of the Ribeira Belt. In: CORDANI, U. G. et al. (Ed.). *Tectonic Evolution of South America*. 1. ed. [S.l.]: COMPANHIA DE PESQUISA DE RECURSOS MINERAIS, 2000. p. 287–310.

TROUW, R. A. J. et al. Análise de Deformação numa Área a SE de Lavras Minas Gerais. In: *Anais do XXXII Congresso Brasileiro de Geologia*. Salvador, Bahia: [s.n.], 1982. p. 187–198.

TROUW, R. A. J. et al. Mapa Geológico-Folha Caxambu. In: CODEMIG (Ed.). *Geologia e Recursos Minerais do Sudeste Mineiro*. [S.l.: s.n.], 2003. p. 1:100.000.

TROUW, R. a. J. et al. A new interpretation for the interference zone between the southern Brasília belt and the central Ribeira belt, SE Brazil. *Journal of South American Earth Sciences*, v. 48, p. 43–57, 2013. ISSN 08959811.

TROUW, R. A. J.; RIBEIRO, A.; PACIULLO, F. V. P. Evolução Estrutural e Metamórfica de uma àrea a SE de Lavras - Minas Gerias. In: *Anais do XXXI Congresso Brasieliro de Geologia, Balneário de Camboriú, Santa Catarina*. Balneário de Camburiú: [s.n.], 1980.

TROUW, R. A. J.; RIBEIRO, A.; PACIULLO, F. V. P. Geologia Estrutural do Grupos São João del Rei, Carrancas e Andrelândia, Sul de Minas Gerais. *Anais da Academia brasileira de Ciências*, v. 55, n. 1, p. 71–87, 1983.

VALERIANO, C. M. et al. U-Pb Geochronology of Southern Brasília Belt (SE Brazil): sedumentary provenance, Neoproterozoic orogeny and assembly of Western Gondwana. *Precambrian Research*, v. 130, p. 7–11, 2004.

WATSON, E. B.; WARK, D. a.; THOMAS, J. B. Crystallization thermometers for zircon and rutile. *Contributions to Mineralogy and Petrology*, v. 151, n. 4, p. 413–433, 2006. ISSN 00107999.

WESTIN, A.; CAMPOS NETO, M. D. C. Provenance and tectonic setting of the external nappe of the Southern Brasília Orogen. *Journal of South American Earth Sciences*, Elsevier Ltd, v. 48, p. 220–239, 2013. ISSN 08959811. Avaible form internet: <http://dx.doi.org/10.1016/j.jsames.2013.08.006>.

WESTIN, A. et al. The Neoproterozoic southern passive margin of the São Francisco craton: Insights on the pre-amalgamation of West Gondwana from U-Pb and Hf-Nd isotopes. *Precambrian Research*, p. 454–471, 2019.

ZACK, T.; EYNATTEN, H. von; KRONZ, A. Rutile geochemistry and its potential use in quantitative provenance studies. *Sedimentary Geology*, v. 171, n. 1-4, p. 37–58, 2004.

ZACK, T. et al. Trace element abundances in rutiles from eclogites and associated garnet mica schists. *Chemical Geology*, v. 184, n. 1-2, p. 97–122, 2002.

ZACK, T.; MORAES, R.; KRONZ, A. Temperature dependence of Zr in rutile: Empirical calibration of a rutile thermometer. *Contributions to Mineralogy and Petrology*, v. 148, n. 4, p. 471–488, 2004. ISSN 00107999.

ZACK, T. et al. In-situ U/Pb rutile dating by LA-ICP-MS: 208Pb correction and prospects for thermochronological applications. *Contributions to Mineralogy and Petrology*, v. 162, p. 515–530, 2011.

ZHANG, R. Y.; LIOU, J. G.; SHU., J. F. Hydroxyl-rich topaz in high-pressure and ultrahigh-pressure kyanite quartzites, with retrograde woodhouseite, from the Sulu terrane, eastern China. *American Mineralogist*, v. 87, n. 4, p. 445–453, 2002.

7 Overall discussions

7.1 Evaluation of the application of trace elements geothermometers to amphibolite facies and granulite facies rocks

In this work, Zr-in-rutile and Ti-in-quartz thermometry have been applied to high-pressure metamorphic rocks (metapelite and quartzite) that were formed under amphibolite, eclogite and granulite facies conditions. Results obtained for the lower metamorphic grade rocks (Chapters 6 and 4) allow for discussions regarding the closure and resetting temperatures of trace elements in rutile. On the other hand, at higher metamorphic grades, the post-crystallization changes in the rutile and quartz chemistry is an important issue, since Zr in rutile and Ti in quartz results often show large spread (Chapters 3).

7.1.1 Trace elements thermometers in the Luminárias Nappe

As previously presented, in the Luminárias Nappe the metamorphic grade varies from HP amphibolite facies (northern portion) to eclogite facies (southern portion) and the nappe is composed, predominantly, of metapelite, quartzite and metagreywacke. Rutile from metapelite and quartzite has been analyzed. The trace elements in rutile from the metapelite are present in the Chapter 4 and the data from quartzite in the Chapter 6.

Metamorphic peak temperature in the Luminárias Nappe rocks is close to the resetting temperature of Zr in rutile, at of ∼550-650 °C (CHERNIAK; MANCHESTER; WATSON, 2007; TRIEBOLD et al., 2007; TRIEBOLD; EYNATTEN; ZACK, 2012; KOOIJMAN; MEZGER; BERNDT, 2010; KOHN; PENNISTON-DORLAND; FERREIRA, 2016; CRUZ-URIBE et al., 2018). Figure 7.1 presents Zr-in-rutile data as well as the location of the studied quartzite and metapelite samples. In the northern portion of the Luminárias Nappe, the Zr contents in rutile from the quartzite show a large spread. However, in the metapelite from the same localities, results show a small spread. In the southern portion both samples show a small spread in Zr contents in rutile.

According to this data, the bulk rock composition influences on how trace elements behave in rutile. For example, while rutile is metamorphically crystallized in metapelite from the northern portion of the Luminarias Nappe, and its Zr content indicates the crystallization temperature, detrital rutile from quartzite from the same area are not re-equilibrated and/or re-crystalized and keeps it source rock Zr signature. On the other hand, rutile from metapelite and quartzite from the higher grade rocks from Luminárias

Nappe, have similar Zr contents and indicate that the Zr content in detrital rutile from quartzite was able to re-equilibrate.

The chemical diffusion is the main mechanism in the modification of the geochemistry of rutile and the whole rock chemical system interferes in the diffusion. The present data shows that the metapelitic system favours the chemical diffusion at HP amphibolite facies and thus the crystallization and/or re-crystallization of rutile when compared with the quartzite system.

The Zr-in-rutile temperatures in the metapelite samples are coherent with the peak mineral assemblages observed and the metamorphic modelling in the rocks from the Lumimárias Nappe. The Ti-in-quartz geothermometer was applied to a metapelite from the southern portion of the Luminárias Nappe (LR44). The Ti-in-quartz and the Zr-in-rutile isopleths intercept each other at *ca.* 630 ± 13 °C and 1.4 GPa, indicating metamorphic peak conditions that agree with those obtained by metamorphic modeling using pseudosection.

7.1.2 Trace elements thermometry in the Passos Nappe

Although Zr-in-rutile is regarded as a robust geothermometer for metamorphic peak temperatures in granulite facies (KOOIJMAN et al., 2012; EWING; HERMANN; RUBATTO, 2013; TAYLOR-JONES; POWELL, 2015, for example), the Zr content in rutile from granulite often presents a large spread and requires a careful study to extract peak and retrograde temperatures. This large spread in Zr content in rutile is also observed in our dataset on the granulitic rocks from the Passos Nappe.

Several works agree that part of the high–T assemblage is retained in high Zr content crystals (CLARK et al., 2019; EWING; HERMANN; RUBATTO, 2013; HART et

Figure 7.1 *(following page)* – a) Map of Brazil showing the location of the study area (grey rectangle). b) Simplified geological map of Luminárias Nappe showing sample location, included quartzite and metapelite samples with analyzed rutile (UTM, WGS84, Zone 23K). Modified after Trouw et al. (2003), Quéméneur et al. (2003), Nunes, Trouw e Castro (2008), Paciullo e Ribeiro (2008). *P-T conditions presented in the figure are those of Fumes et al. (2019). c) Boxplots showing concentration (in μg/g) of the Zr in rutile grains from Luminárias Nappe. Quartzite samples plotted in black and gray and from metapelite in green. In samples LR33b and LR46 data from separated rutile grains (SEP - black) and from thin section (TS - gray) are individualized. Whiskers represent the 5^{th} and 95^{th} percentile. Boxes represent the second (bottom-25%) and third quartile (top-75%). For rutile grains with more than one spot, only one representative analysis is plotted. The numbers in the left side of each boxplots represent the number of analyses that are shown in the graph, the points plotted as x represent the minimum and maximum values, the small squares represent the median value and the line represent the mean value. When the numbers of analyses above detections limits are lower than three only the value of the analyses are plotted in squares.

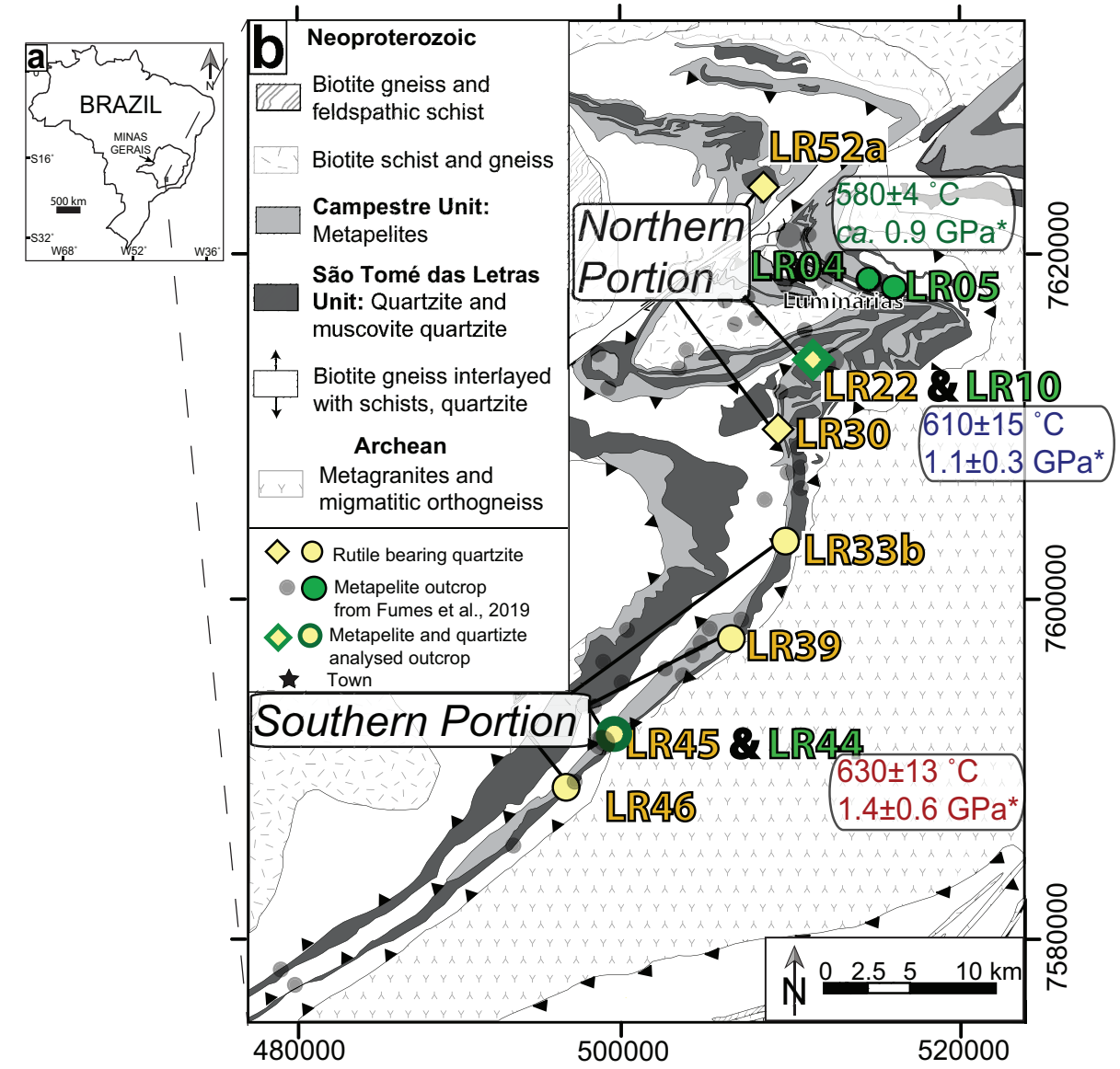
a
BRAZIL
MINAS GERAIS
S16°
S32°
W68°
W52°
W36°
500 km
b
Neoproterozoic
Biotite gneiss and feldspathic schist
Biotite schist and gneiss
Campestre Unit: Metapelites
São Tomé das Letras Unit: Quartzite and muscovite quartzite
Biotite gneiss interlayed with schists, quartzite
Archean
Metagranites and migmatitic orthogneiss
Rutile bearing quartzite
Metapelite outcrop from Fumes et al., 2019
Metapelite and quartizte analysed outcrop
Town
Northern Portion
Southern Portion
LR52a
580±4 °C
ca. 0.9 GPa*
LR04
LR05
Luminárias
LR22 & LR10
LR30
610±15 °C
1.1±0.3 GPa*
LR33b
LR39
LR45 & LR44
LR46
630±13 °C
1.4±0.6 GPa*
N
0 2.5 5 10 km
480000
500000
520000
7620000
7600000
7580000

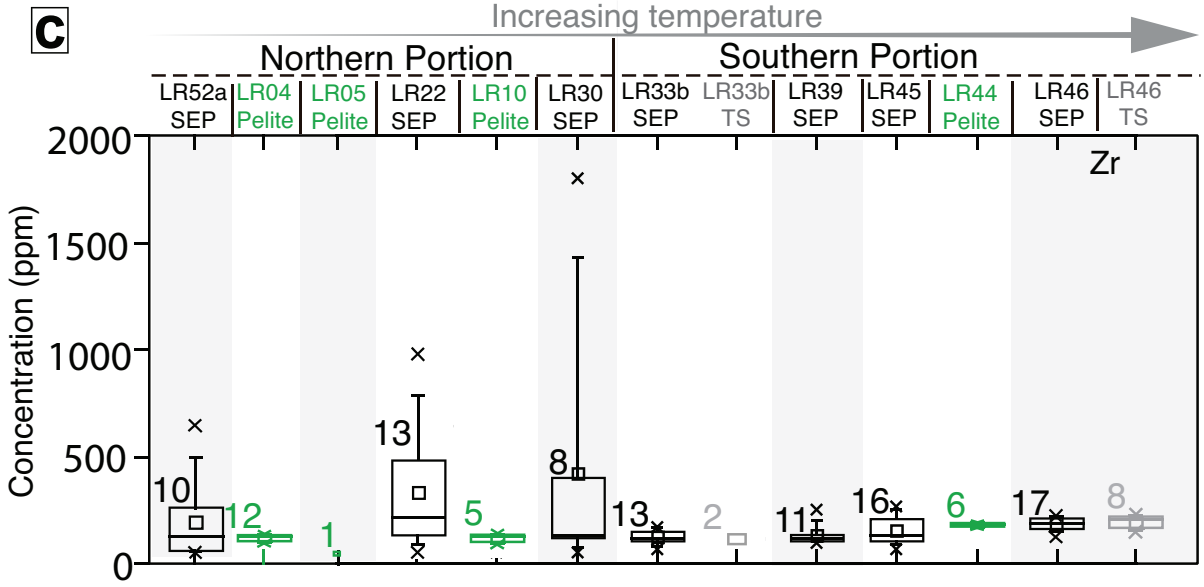
c
Increasing temperature
Northern Portion
Southern Portion
LR52a SEP
LR04 Pelite
LR05 Pelite
LR22 SEP
LR10 Pelite
LR30 SEP
LR33b SEP
LR33b TS
LR39 SEP
LR45 SEP
LR44 Pelite
LR46 SEP
LR46 TS
Zr
Concentration (ppm)
2000
1500
1000
500
0
10
12
1
13
5
8
13
2
11
16
6
17
8

al., 2018; KOHN; PENNISTON-DORLAND; FERREIRA, 2016; KOOIJMAN et al., 2012; PAPE; MEZGER; ROBYR, 2016; PAULY et al., 2016; TAYLOR-JONES; POWELL, 2015). Therefore, to constrain the conditions of granulite facies metamorphism, and following the recommendation of Luvizotto et al. (2009), Hart et al. (2018), the Zr contents above the 90^{th} percentile were used to calculate temperature. The values of contents of Zr in rutile above the 90^{th} ranges from 1660μg/g to 1847 μg/g, giving temperatures ranging from 821 °C to 834 °C (at 1.2 GPa). These are interpreted as the minimum peak temperature, since we cannot determine the extent to which rutile composition has been modified after its crystallization, but are consistent with the peak assemblage in the pseudosections calculated for samples SSPDH10 and SSPDH2 (Chapters 3).

In the HP granulite from the Passos Nappe the Ti in quartz concentration data also present a large spread. Quartz is usually involved in several reactions in metapelitic rocks, during prograde and retrograde metamorphism. As this mineral is crystallized, recrystallized and consumed in these several reactions, the cathodoluminescence mapping is an indispensable tool to evaluate the Ti distribution in quartz. This tool was used in our study and, for the first time, cathodoluminescence maps were processed within quantitative analysis using the XMapTools software (LANARI et al., 2014; LANARI; DUESTERHOEFT, 2019) to generate quantitative maps of Ti-in-quartz and of temperature.

In our samples, a decrease of the Ti content towards the rim of the quartz crystals is systematically observed, similarly to the observations of Kendrick e Indares (2018). According to these authors, the low content of Ti in the retrograde quartz is related with the disequilibrium between quartz and rutile during the retrograde path, which causes Ti-undersaturation of quartz. The Ti incorporation in quartz is sensitive to post-peak P and T variations (NACHLAS; HIRTH, 2015; THOMAS et al., 2015) and the dynamic recrystallization enhances the kinetics of Ti equilibration in quartz (GRUJIC; STIPP; WOODEN, 2011; KOHN; NORTHRUP, 2009; NACHLAS; HIRTH, 2015), favoring post crystallization modification of quartz compositions. Therefore, in order to constrain temperatures based on the Ti-in-quartz content, it is important: (i) to choose an appropriate P (THOMAS et al., 2010); (ii) to observe the textural features of the quartz in the sample and (iii) to study the recrystalization patterns of the mineral.

In the HP granulite from the Passos Nappe the large quartz crystals that are associated with K-feldspar and plagioclase in the leucossome and, therefore, it is interpreted as crystallized from a melt. These large quartz grains tend to have higher Ti contents than smaller grains. Furthermore, lower Ti contents are observed in the outer rim as well as in fractures along the crystals. Hence, the highest Ti contents are interpreted to represent the T of melt crystallization shortly after metamorphic peak conditions. Low Ti contents at the rim of large quartz crystals and in small grains are attributed to post crystallization changes associated with dynamic recrystallization, mostly by grain boundary migration

and less frequently by bulging recrystallization. Based on peak P of 1.2 GPa, the T results range from ∼654 °C to 837 °C, while, at retrograde P of 0.7 GPa the results would range from ∼555 °C to 719 °C. The highest T calculated for 1.2 GPa is in good agreement with peak conditions constrained in the pseudosection and the lower contents of Ti in quartz are probably related to the retrograde conditions.

7.2 Insights in the tectonic evolution of the southern Brasília Orogen

Metamorphic and petrochronological data collected in the Passos and Luminárias Nappe bring valuable information on the tectonic evolution of the southern Brasília Orogen. In both nappes, the passive margin sedimentary and syn-collisional rocks are metamorphosed under high pressure conditions, related to the West Gondwana amalgamation in the late Neoproterozoic (DARDENNE, 2000; FUCK et al., 2017; HEILBRON; CORDANI; ALKMIM, 2017). Although the nappes occurs in the same regional setting the, metamorphic peak conditions are different (HP amphibolite to eclogite facies - Luminárias Nappe; HP granulite facies in the top Unit from the Passos Nappe), indicating that the specific tectonic setting and the P-T-t followed for each nappe will also be different.

7.2.1 Tectonic evolution in the Luminárias Nappe

Metamorphic studies were carried out in the three units that compose the Luminárias Nappe. The nappe is composed of metasedimentary rocks that have been deposited in two environments: the metapelite (Carrancas Unit) and quartzite (São Tomé das Letras Unit), deposited in the passive margin (PACIULLO et al., 2000; PACIULLO; RIBEIRO; TROUW, 2003; TROUW et al., 2000; CAMPOS NETO et al., 2004; WESTIN et al., 2019) and the metagreywacke (Santo Antônio Unit), deposited in a younger synorogenic basin (CAMPOS NETO et al., 2007; CAMPOS NETO et al., 2011; WESTIN; CAMPOS NETO, 2013; MARIMON et al., 2021). Regardless if the depositional environment was different, the three units were metamorphosed in the same collisional setting with similar P–T paths (Figure 7.3 b and c). The best diagram to differentiate the metapelite rocks from the metagreywacke are the present in the plot in Fig. 5.8, since the major differences are in the Ca and Na contents that are not considered in the AFM plot (Fig. 7.S1).

The baric conditions observed in the metamorphic rocks from the Southern Brasília Orogen are of high-pressure (SILVA, 2010; MOTTA; MORAES, 2017); CARVALHO et al., 2020) (Figure 7.2), which is confirmed in this work. These high-pressure conditions indicates a thick-skinned tectonic setting that is coherent with the continental collision, which involves subduction of continental crust (CAMPOS NETO, 2000; DARDENNE, 2000; TROUW et al., 2000; FUCK et al., 2017; HEILBRON; CORDANI; ALKMIM, 2017; TEDESCHI et al., 2017). Geothermal gradients in Luminárias Nappe varies from

45 °C/kbar (southern portion) to 64 °C/kbar (northern portion) and these values can be correlated with continental-continental collision setting (BROWN, 2007; BUCHER; GRAPES, 2011; SIZOVA; GERYA; BROWN, 2014; BROWN; JOHNSON, 2018). The maximum burial depth of the metassedimenatry rocks from the Luminárias Nappes is estimated to be ∼50 km, from pressures of 1.4 GPa recorded (Figure 7.3 c). This depth recorded in the metamorphic peak is compatible with burial within an orogenic wedge, with latter exhumation to relatively shallow crustal depths (∼25 km) in the retrograde path.

Figure 7.2 – Metamorphic map nearby Luminárias Nappe from Peternel et. al., 2005 with the *P-T* conditions from *this work, [1]Silva, 2010 and [2]Carvalho et al., 2020.

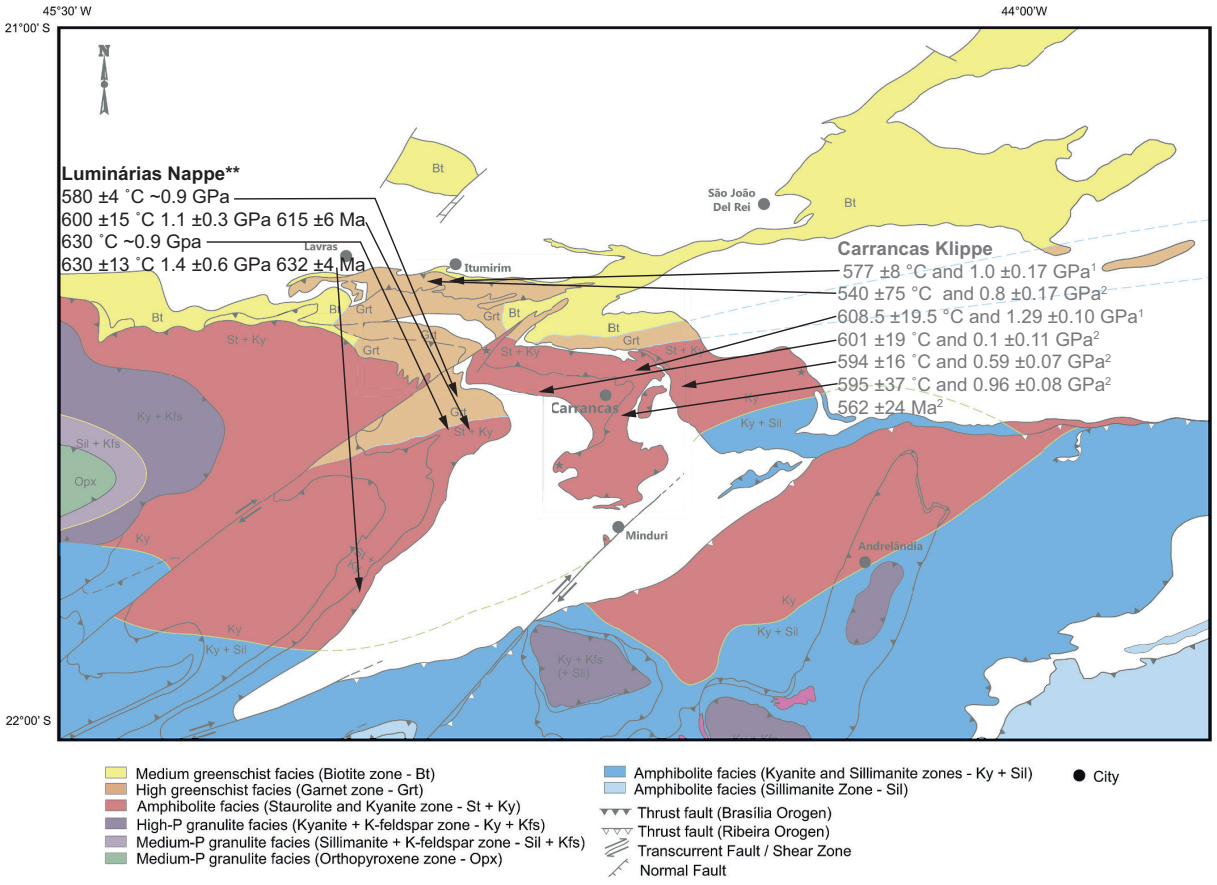

Metamorphic peak conditions in the Luminárias Nappe vary from high-pressure lower-amphibolite facies at 580 ± 4 °C and ∼0.9 GPa in the northern portion to eclogite facies at 630 ± 13 °C and 1.4 ± 0.6 GPa in the southern portion ((Figure 7.2) and Figure 7.3 c) (detailed description in the Chapter 6, 5 and 4). This metamorphic gradient is oblique to the main geological contacts. Monazite ages in the metapelitic rocks from Luminárias are neoproterozoic and ranges from 615 ± 6 Ma to 632 ± 4 Ma which are similar to the ages observed in the southern Brasília Orogen (VLACH; GUALDA, 2000; CAMPOS NETO et al., 2004; VALERIANO et al., 2004; CAMPOS NETO et al., 2007; CAMPOS NETO et al., 2010; CAMPOS NETO et al., 2011; TROUW; TAVARES; ROBYR, 2008; RENO; BROWN; PICCOLI, 2010; RENO et al., 2012; WESTIN et al., 2016; COELHO et

al., 2017; ROCHA et al., 2017; ROCHA et al., 2018; TEDESCHI et al., 2017; TEDESCHI et al., 2018).

The divergent interpretations presented in the literature regarding the contact between the Brasília Orogen and Ribeira Orogen extends to the Luminárias Nappe region. According to Campos Neto (2000), Campos Neto et al. (2004), Campos Neto et al. (2007), Campos Neto et al. (2011), Westin et al. (2016), Westin et al. (2019) the contact between the orogens are abrupt and the tectonic evolution of Luminárias Nappe and region is related entirely with the Brasília Orogen. However, Peternel et al. (2005), Trouw et al. (2000), Trouw et al. (2013), Heilbron et al. (2008), Heilbron, Cordani e Alkmim (2017), Coelho et al. (2017) propose an interference zone between the Ribeira and Brasília Orogen, which affected the tectonic evolution of the rocks. Unfortunately the range of monazite ages obtained in the present work (615 ± 6 Ma — included crystals, 600 ± 8 Ma — matrix crystals for LR10E sample and 632 ± 4 Ma — matrix and included crystals for LR44C sample) are not conclusive, since it can be correlated to the Brasília Orogen (metamorphic ages from 630 to 607 (ROCHA et al., 2017; MORA; NETO; BASEI, 2014; COELHO et al., 2017; TEDESCHI et al., 2017; TEDESCHI et al., 2018) and the Ribeira Orogen (620–520 Ma according to Machado et al. (1996), Santos et al. (2007), Heilbron, Cordani e Alkmim (2017)). The oldest ages obtained are, therefore, in agreement with processes associated with the Brasília orogeny, while younger ages may be related to retrometamorphism or to processes associated with the Ribeira orogeny. Although a single clockwise metamorphic path was documented for the Luminárias Nappe rocks (Santo Antônio Unit and Carrancas Unit). This observation would favor the hypothesis of only one orogenic belt. The oblique position of the metamorphic gradient in relation to the geological bedding/contacts could be explained by extrusion processes during the tectonic evolution of the area.

Figure 7.3 – Simplified sketch of the tectonic evolution of the Southern Brasília Orogen in the latitudes of the Lumiárias Nappe (b, c and d) and Passos Nappe (e, f and g). a) Tectonic map with the delimitation of the tectonic units in the area of the geological sections, according to Valeriano (2017) (see Figure 2.1 b from a more detailed map). b) Model showing the depositional environments of the (meta)sedimentary units of the Luminárias Nappe based on Marimon et al. (2021). c) Model showing continental collision associated with the metamorphic peak of rocks from Luminárias Nappe. Model and isotherms based on crust-mantle decoupling combined with slab advance from Vanderhaeghe e Duchêne (2010). The star represents the P–T metamorphic peak conditions based on this work. Tectonic evolution of the Southern Brasília Orogen in the latitude of the Passos Nappe interpreted in this study at 635 Ma (e), 615 Ma (f) and 590-570 Ma (g).

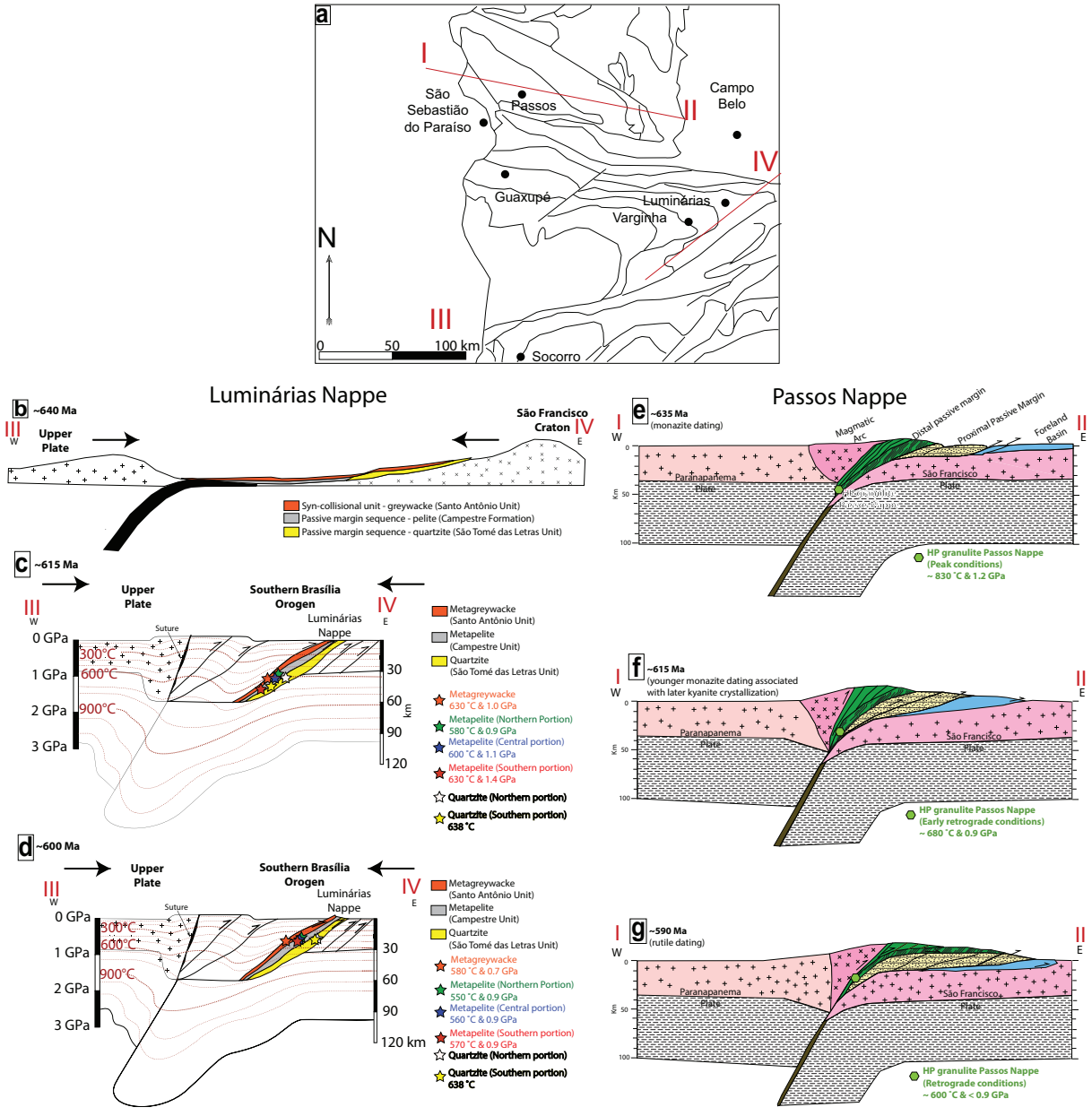

7.2.2 Tectonic evolution of the HP granulite of the Passos Nappe

This study focused on the HP granulite facies rocks that occur at the uppermost portion of the Passos Nappe. Since an inverted metamorphic gradient is described for the Passos Nappe (SIMÕES, 1995; ZANARDO, 1992; LUVIZOTTO, 2003), the studied rocks register the highest metamorphic grade. Although never studied in detail, the occurrence of HP granulite has been shown in maps from previous studies (VALERIANO et al., 2004; VALERIANO, 2017).

Simões (1995) uses the deflection of isotherms during subduction to explain the inverted thermal gradient and continuous expulsion of high pressure rocks to shallow crustal levels, due a strong non coaxial shear, to explain the inverted pressure gradient. However, our calculated geothermal gradient (18 °C/km or 690 °C/GPa) is coherent with a continental-continental collision setting (BROWN, 2007; BUCHER; GRAPES, 2011; SIZOVA; GERYA; BROWN, 2014; BROWN; JOHNSON, 2018) and not a subduction zone as proposed in Simões (1995). It has to be noticed that only one unit from the Passos Nappe is studied in the present work, and our interpretations may not be valid for the Passos Nappe as a whole. The geothermal gradient recorded by the studied granulites is similar to that observed in retroeclogite from the Pouso Alegre region (south of the Passos Nappe) (TEDESCHI et al., 2017), which is also interpreted as related to a continental collision setting. Luvizotto (2003) describes retroeclogite occurences near to the studied granulites. The rocks are similar to those studied by Tedeschi et al. (2017) and may have faced a similar tectonic evolution.

The metamorphic conditions and age obtained for the upper unit of the Passos Nappe (Chapter 3) suggest that these rocks can be correlated with the Andrelândia Nape System rocks (CAMPOS NETO, 2000; CAMPOS NETO et al., 2010; CIOFFI et al., 2012; CIOFFI et al., 2019; MOTTA; MORAES, 2017; RENO et al., 2009; RENO et al., 2012). Although the present work is the first to systematically investigate the high-pressure granulite from Passos Nappe, a correlation of these rocks with the ones from the Andrelândia Nappe System has previously been previously presented in the literature (RENO et al., 2012; TROUW; PACIULLO; HEILBRON, 1984). Probably the lower units from the Passos Nappe could also be correlated with others units from the Southern Brasília Orogen, e. g., with the Andrelândia rocks that are metamorphosed under lower conditions. In the Passos Nappe there is a gradual transition from low grade metamorphism in the lower part to high pressure granulite facies in the upper part, all within a single nappe in which the protoliths are interpreted to be derived from a passive margin sedimentary basin. In the Andrelândia Nappe System, several nappes are separated by basement slices and thrust faults. These nappes were originally defined, mapped (TROUW et al., 2000) and stacked based on these structures. Some authors (CAMPOS NETO et al., 2010; FRUGIS; NETO; LIMA, 2018, , for example) interpret

these different nappes as derived from different sedimentary basins; the upper part of the stack would be derived from a fore arc basin related to the upper plate, the active margin of the Paranapanema paleocontinent. However, other authors (COELHO et al., 2017; TROUW et al., 2013, ,for example) maintain the interpretation that the whole stack is derived from the passive margin of the São Francisco Paleocontinent, similar to the interpretation of the Passos Nappe presented here. It is, however, noteworthy that the retrograde replacement of kyanite by sillimanite, is widely observed in the metasedimentary high-pressure Andrelândia Nappe rocks (CAMPOS NETO et al., 2010; CIOFFI et al., 2012; MOTTA; MORAES, 2017; RENO et al., 2012; TROUW et al., 2013). However, sillimanite is absent in all studied high-pressure granulites from the Passos Nappe and other nappes to the north. The widespread occurrence of late metastable sillimanite in the Andrelândia Nappe System could be explained, at least in part, by the partial superposition of Ribeira Orogen metamorphism on the system (COELHO et al., 2017; TROUW et al., 2013), or just by the following decompression, without the effect of this tectonic superposition (CAMPOS NETO et al., 2010; CIOFFI et al., 2012; MOTTA; MORAES, 2017). Exhumation of the Passos Nappe may have occurred at slightly higher pressure than the Andrelândia Nappe, with rocks cooling inside the kyanite field.

The studied rocks result from the metamorphism of continental margin sediments in the deep root of this Cryogenian-Ediacaran continent-continent collisional zone, at ca. 635 Ma, related with the early phases of West Gondwana formation (Figure 7.3 d). The retrograde path (Figure 7.3 f and g) records exhumation to ∼600 °C at < 0.9 GPa at a relatively slow integrated cooling rate, of ∼6 °C/Ma. This slow cooling rate can be partially explained by the retention of heat producing elements (U, Th and K) in the middle and deep orogenic crust, allowing for high-pressure granulite rocks to overcome the enthalpy barrier of melting (YAKYMCHUK; BROWN, 2019).

The slow cooling rates in the high-pressure granulite of the Passos Nappe corroborate previous descriptions of long-lived metamorphism and deformation, which lasted at least 30 my, in the Southern Brasília Orogen more to the south (CIOFFI et al., 2019; COELHO et al., 2017; ROCHA et al., 2017; TEDESCHI et al., 2018; TROUW et al., 2000). Muscovite K-Ar ages of ca. 570-580 Ma in the Passos Nappe are described by VALERIANO et al. (2000) and record the final cooling stages upon exhumation to the upper crust (∼300 °C). The cooling rate of this final stage of the retrograde P–T–t path is faster (∼15 °C/Ma) than calculated for the earlier phase.

Reference

BROWN, M. Metamorphic conditions in orogenic belts: a record of secular change. *International Geology Review*, Taylor & Francis, v. 49, n. 3, p. 193–234, 2007.

BROWN, M.; JOHNSON, T. Secular change in metamorphism and the onset of global plate tectonics. *American Mineralogist*, v. 103, n. 2, p. 181–196, 2018. ISSN 19453027.

BUCHER, K.; GRAPES, R. *Petrogenesis of metamorphic rocks*. [S.l.]: Springer Science & Business Media, 2011.

CAMPOS NETO, M. D. C. Orogenic Systems from Southwestern Gondwana: An Approach to Brasiliano-Pan African Cycle and Orogenic Collage in Southeastern Brazil. In: CORDANI, U. G. et al. (Ed.). *Tectonic Evolution of South America*. 1. ed. Rio de Janeiro: COMPANHIA DE PESQUISA DE RECURSOS MINERAIS, 2000. p. 335–365.

CAMPOS NETO, M. D. C. et al. Migração de Orógenos e Superposição de Orogêneses: Um Esboço da Colagem Brasiliana no Sul do Cráton do São Francisco, SE - Brasil. *Geologia USP - Serie Cientifica*, v. 4, n. 1, p. 13–40, 2004.

CAMPOS NETO, M. D. C. et al. Orogen migration and tectonic setting of the Andrelândia Nappe system: An Ediacaran western Gondwana collage, south of São Francisco craton. *Journal of South American Earth Sciences*, Elsevier Ltd, v. 32, n. 4, p. 393–406, 2011. ISSN 08959811. Avaible form internet: <http://dx.doi.org/10.1016/j.jsames.2011.02.006>.

CAMPOS NETO, M. D. C. et al. Structural and metamorphic control on the exhumation of high-P granulites: The Carvalhos Klippe example, from the oriental Andrelândia Nappe System, southern portion of the Brasília Orogen, Brazil. *Precambrian Research*, v. 180, n. 3-4, p. 125–142, 2010. ISSN 03019268.

CAMPOS NETO, M. D. C. et al. Sistema de nappes andrelândia, setor oriental: litoestratigrafia e posição estratigráfica. *Revista Brasileira de Geociências*, v. 37, n. 4-Sup., p. 47–60, 2007.

CHERNIAK, D.; MANCHESTER, J.; WATSON, E. Zr and Hf diffusion in rutile. *Earth and Planetary Science Letters*, Elsevier, v. 261, n. 1, p. 267–279, 2007.

CIOFFI, C. R. et al. Geochemical signatures of metasedimentary rocks of high-pressure granulite facies and their relation with partial melting: Carvalhos Klippe, Southern Brasília Belt, Brazil. *Journal of South American Earth Sciences*, v. 40, p. 63–76, 2012. ISSN 08959811.

CIOFFI, C. R. et al. Titanite petrochronology of the southern Brasília Orogen basement: Effects of retrograde net-transfer reactions on titanite trace element compositions. *Lithos*, Elsevier, v. 344, p. 393–408, 2019.

CLARK, C. et al. Testing the fidelity of thermometers at ultrahigh temperatures. *Journal of Metamorphic Geology*, Wiley Online Library, v. 37, n. 7, p. 917–934, 2019.

COELHO, M. B. et al. Constraining timing and P-T conditions of continental collision and late overprinting in the Southern Brasília Orogen (SE-Brazil): U-Pb zircon ages and geothermobarometry of the Andrelândia Nappe System. *Precambrian Research*, Elsevier B.V., v. 292, p. 194–215, 2017. ISSN 03019268. Avaible form internet: <http://linkinghub.elsevier.com/retrieve/pii/S0301926816305496>.

CRUZ-URIBE, A. M. et al. Assessing trace element (dis)equilibrium and the application of single element thermometers in metamorphic rocks. *Lithos*, Elsevier B.V., v. 314-315, p. 1–15, 2018. ISSN 18726143. Avaible form internet: <https://doi.org/10.1016/j.lithos.2018.05.007>.

DARDENNE, M. A. The Brasilia Fold Belt. In: *Tectonic Evolution of South Ameria*. [S.l.]: 31 Intern. Geol. Congr. Rio de Janeiro, 2000. p. 231–264.

EWING, T. A.; HERMANN, J.; RUBATTO, D. The robustness of the Zr-in-rutile and Ti-in-zircon thermometers during high-temperature metamorphism (Ivrea-Verbano Zone, northern Italy). *Contributions to Mineralogy and Petrology*, v. 165, n. 4, p. 757–779, 2013. ISSN 00107999.

FRUGIS, G. L.; NETO, M. d. C. C.; LIMA, R. B. Eastern Paranapanema and southern São Francisco orogenic margins: Records of enduring Neoproterozoic oceanic convergence and collision in the southern Brasília Orogen. *Precambrian Research*, Elsevier, v. 308, p. 35–57, 2018.

FUCK, R. A. et al. The Northern Brasília Belt. In: HEILBRON, M.; CORDANI, U. G.; ALKMIM, F. F. (Ed.). *São Francisco Craton, Eastern Brazil Tectonic Genealogy of a Miniature Continent*. [S.l.]: Springer Berlin Heidelberg, 2017. p. 205–220.

FUMES, R. A. et al. Metamorphic modeling and petrochronology of metapelitic rocks from the Luminárias Nappe, southern Brasília belt (SE Brazil). *Brazilian Journal of Geology*, 2019.

GRUJIC, D.; STIPP, M.; WOODEN, J. L. Thermometry of quartz mylonites: Importance of dynamic recrystallization on ti-in-quartz reequilibration. *Geochemistry, Geophysics, Geosystems*, Wiley Online Library, v. 12, n. 6, 2011.

HART, E. et al. A window into the lower crust: Trace element systematics and the occurrence of inclusions/intergrowths in granulite-facies rutile. *Gondwana Research*, The Authors, v. 59, p. 76–86, 2018. ISSN 1342937X. Avaible form internet: <http://linkinghub.elsevier.com/retrieve/pii/S1342937X18300856>.

HEILBRON, M.; CORDANI, U. G.; ALKMIM, F. F. *São Francisco Craton, Eastern Brazil: Tectonic Genealogy of a Miniature Continent*. [S.l.: s.n.], 2017. 331 p. ISBN 9783319017143.

HEILBRON, M. et al. Correlation of Neoproterozoic terrane between te Ribeira Belt, SE Brazil and its African countepart: comparative tectonic evolution and open questions. *Geological Society, London, Special Publications*, v. 294, p. 211–237, 2008.

KENDRICK, J.; INDARES, A. The Ti Record of Quartz in Anatectic Aluminous Granulites. *Journal of Petrology*, n. July, p. 1–23, 2018. ISSN 0022-3530.

KOHN, M. J.; NORTHRUP, C. J. Taking mylonites' temperatures. *Geology*, Geological Society of America, v. 37, n. 1, p. 47–50, 2009.

KOHN, M. J.; PENNISTON-DORLAND, S. C.; FERREIRA, J. C. Implications of near-rim compositional zoning in rutile for geothermometry, geospeedometry, and trace element equilibration. *Contributions to Mineralogy and Petrology*, Springer, v. 171, n. 10, p. 78, 2016.

KOOIJMAN, E.; MEZGER, K.; BERNDT, J. Constraints on the U–Pb systematics of metamorphic rutile from in situ LA-ICP-MS analysis. *Earth and Planetary Science Letters*, Elsevier, v. 293, n. 3-4, p. 321–330, 2010.

KOOIJMAN, E. et al. Trace element systematics in granulite facies rutile: implications for Zr geothermometry and provenance studies. *Journal of Metamorphic Geology*, Wiley Online Library, v. 30, n. 4, p. 397–412, 2012.

LANARI, P.; DUESTERHOEFT, E. Modeling Metamorphic Rocks Using Equilibrium Thermodynamics and Internally Consistent Databases: Past Achievements, Problems and Perspectives. *Journal of Petrology*, v. 60, n. 1, p. 19–56, 2019. ISSN 14602415.

LANARI, P. et al. Xmaptools: A matlab©-based program for electron microprobe x-ray image processing and geothermobarometry. *Computers & Geosciences*, Elsevier, v. 62, p. 227–240, 2014.

LUVIZOTTO, G. *Caracterização metamórfica das rochas do Grupo Araxá na região de São Sebastião do Paraíso, sudoeste de Minas Gerais*. Dissertação (Mestrado) — Instituto de Geociências e Ciências Exatas da Universidade Estadual Paulista, 2003.

LUVIZOTTO, G. L. et al. Rutile occurrence and trace element behavior in medium-grade metasedimentary rocks: Example from the Erzgebirge, Germany. *Mineralogy and Petrology*, v. 97, n. 3-4, p. 233–249, 2009. ISSN 09300708.

MACHADO, N. et al. Ages of detrical zircon from Archean-Paleoproterozoic sequences: implication for greenstone belt setting and evolution of Transamazonian foreland basin in Quadrilátero Ferrífero, southeast Brazil. *Earth and Planetary Science Letters*, v. 141, p. 259–276, 1996.

MARIMON, R. S. et al. Provenance of passive-margin and syn-collisional units: Implications for the geodynamic evolution of the southern brasília orogen, west gondwana. *Sedimentary Geology*, Elsevier, v. 413, p. 105823, 2021.

MORA, C. A. S.; NETO, M. d. C. C.; BASEI, M. A. S. Syn-collisional lower continental crust anatexis in the Neoproterozoic Socorro-Guaxupé Nappe System, southern Brasília Orogen, Brazil: Constraints from zircon U–Pb dating, Sr–Nd–Hf signatures and whole-rock geochemistry. *Precambrian Research*, Elsevier, v. 255, p. 847–864, 2014.

MOTTA, R. G.; MORAES, R. Pseudo- and real-inverted metamorphism caused by the superposition and extrusion of a stack of nappes: a case study of the Southern Brasília Orogen, Brazil. *International Journal of Earth Sciences*, 2017. ISSN 1437-3254. Avaible form internet: <http://link.springer.com/10.1007/s00531-016-1436-7>.

NACHLAS, W.; HIRTH, G. Experimental constraints on the role of dynamic recrystallization on resetting the Ti-in-quartz thermobarometer. *Journal of Geophysical Research: Solid Earth*, Wiley Online Library, v. 120, n. 12, p. 8120–8137, 2015.

NUNES, R.; TROUW, R. A. J.; CASTRO, E. *Mapa Gelógico - Folha Varginha – escala 1:100.000, Programa Geologia do Brasil*. [S.l.], 2008.

PACIULLO, F. V. P.; RIBEIRO, A. Mapa Geológico-Folha Nepumoceno. In: *CONTRATO - CPRM - UFRJ 067/P2/2005*. [S.l.: s.n.], 2008.

PACIULLO, F. V. P. et al. The Andrelândia Basin, a Neoproterozoic Intraplate Continental Margin, Southern Brasília Belt, Brazil. *Revista Brasileira de Geociências*, v. 30, n. 1, p. 200–202, 2000.

PACIULLO, F. V. P.; RIBEIRO, A.; TROUW, R. a. J. Geologia da Folha Andrelândia 1:100.000. *Geologia e recursos minerais do sudeste mineiro Projeto Sul de Minas - Etapa I*, p. 84–119, 2003.

PAPE, J.; MEZGER, K.; ROBYR, M. A systematic evaluation of the zr-in-rutile thermometer in ultra-high temperature (uht) rocks. *Contributions to Mineralogy and Petrology*, Springer, v. 171, n. 5, p. 44, 2016.

PAULY, J. et al. Prolonged Ediacaran–Cambrian metamorphic history and short-lived high-pressure granulite-facies metamorphism in the HU Sverdrupfjella, Dronning Maud Land (East Antarctica): evidence for continental collision during Gondwana assembly. *Journal of Petrology*, Oxford University Press, v. 57, n. 1, p. 185–228, 2016.

PETERNEL, R. et al. Interferência Entre Duas Faixas Móveis Neoproterozóicas : O Caso Das Faixas Brasília E Ribeira No Sudeste Do Brasil. v. 35, n. 3, p. 297–310, 2005. ISSN 2317-4692.

QUÉMÉNEUR, J. J. G. et al. Mapa Geológico-Folha Lavras. In: *Geologia e Recursos Minerais do Sudeste Mineiro*. [S.l.: s.n.], 2003. p. 1:100.000.

RENO, B. L. et al. Eclogite–high-pressure granulite metamorphism records early collision in West Gondwana: new data from the Southern Brasília Belt, Brazil. *Journal of the Geological Society*, Geological Society of London, v. 166, n. 6, p. 1013–1032, 2009.

RENO, B. L.; BROWN, M.; PICCOLI, P. M. $^{40}Ar/^{39}Ar$ thermochronology of high-pressure granulite nappes in the southern Brasília Belt, Brazil: Implications for Nappe Exhumation. *American Journal of Science*, American Journal of Science, v. 310, n. 10, p. 1294–1332, 2010.

RENO, B. L. et al. In situ monazite (U-Th)-Pb ages from the Southern Brasília Belt, Brazil: Constraints on the high-temperature retrograde evolution of HP granulites. *Journal of Metamorphic Geology*, v. 30, n. 1, p. 81–112, 2012. ISSN 02634929.

ROCHA, B. C. et al. Timing of anatexis and melt crystallization in the Socorro – Guaxupé Nappe , SE Brazil : Insights from trace element composition of zircon , monazite and garnet coupled to U — Pb geochronology. v. 277, p. 337–355, 2017.

ROCHA, B. C. et al. Magmatic inheritance vs. UHT metamorphism: Zircon petrochronology of granulites and petrogenesis of charnockitic leucosomes of the Socorro–Guaxupé nappe, SE Brazil. *Lithos*, v. 314-315, p. 16–39, 2018. ISSN 18726143.

SANTOS, T. Bento dos et al. Thermochronological evidence for long-term elevated geothermal gradients in Ribeira Belt, SE Brazil. In: *Goldschmidt Conference 2007*. [S.l.: s.n.], 2007.

SILVA, M. P. *Modelamento Metamórfico de Rocas das Fácies Xisto-Verde e Anfibolito com o Uso de Pseudosseções: Exemplo das Rochas da Klippe Carrancas, Sul de Minas Gerais*. Tese (Dissertação de mestrado) — Universidade de São Paulo, 2010.

SIMÕES, L. *Evolução tectono-metamórfica da nappe de Passos, sudoeste de Minas Gerais*. Tese (Doutorado) — IG-Universidade de São Paulo, 1995.

SIZOVA, E.; GERYA, T.; BROWN, M. Contrasting styles of Phanerozoic and Precambrian continental collision. *Gondwana Research*, Elsevier, v. 25, n. 2, p. 522–545, 2014.

TAYLOR-JONES, K.; POWELL, R. Interpreting zirconium-in-rutile thermometric results. *Journal of Metamorphic Geology*, v. 33, n. 2007, p. 115–122, 2015.

TEDESCHI, M. et al. Reconstruction of multiple PTt stages from retrogressed mafic rocks: Subduction versus collision in the Southern Brasília orogen (SE Brazil). *Lithos*, Elsevier, v. 294, p. 283–303, 2017.

TEDESCHI, M. et al. Protracted zircon geochronological record of UHT garnet-free granulites in the Southern Brasília orogen (SE Brazil): Petrochronological constraints on magmatism and metamorphism. *Precambrian Research*, Elsevier, v. 316, n. August, p. 103–126, 2018. ISSN 03019268. Avaible form internet: <https://doi.org/10.1016/j.precamres.2018.07.023>.

THOMAS, J. B. et al. TitaniQ under pressure: The effect of pressure and temperature on the solubility of Ti in quartz. *Contributions to Mineralogy and Petrology*, v. 160, n. 5, p. 743–759, 2010. ISSN 00107999.

THOMAS, J. B. et al. TitaniQ recrystallized: experimental confirmation of the original Ti-in-quartz calibrations. *Contributions to Mineralogy and Petrology*, v. 169, n. 3, 2015. ISSN 0010-7999. Avaible form internet: <http://link.springer.com/10.1007/s00410-015-1120-0>.

TRIEBOLD, S. et al. Deducing source rock lithology from detrital rutile geochemistry: An example from the Erzgebirge, Germany. *Chemical Geology*, v. 244, n. 3-4, p. 421–436, 2007. ISSN 00092541.

TRIEBOLD, S.; EYNATTEN, H. von; ZACK, T. A recipe for the use of rutile in sedimentary provenance analysis. *Sedimentary Geology*, Elsevier B.V., v. 282, p. 268–275, 2012. ISSN 00370738. Avaible form internet: <http://dx.doi.org/10.1016/j.sedgeo.2012.09.008>.

TROUW, R. A. J. et al. The Central Segment of the Ribeira Belt. In: CORDANI, U. G. et al. (Ed.). *Tectonic Evolution of South America*. 1. ed. [S.l.]: COMPANHIA DE PESQUISA DE RECURSOS MINERAIS, 2000. p. 287–310.

TROUW, R. A. J.; PACIULLO, F. V. P.; HEILBRON, M. Os Grupos São João Del Rei, Carrancas e Andrelândia Interpretados como a Continuição dos Grupos Araxá e Canastra. In: *Anais do XXXIII Congresso Brasileiro de Geologia*. Rio de Janeiro, RJ: [s.n.], 1984. p. 177–178.

TROUW, R. A. J. et al. Mapa Geológico-Folha Caxambu. In: CODEMIG (Ed.). *Geologia e Recursos Minerais do Sudeste Mineiro*. [S.l.: s.n.], 2003. p. 1:100.000.

TROUW, R. A. J. et al. A new interpretation for the interference zone between the southern Brasília belt and the central Ribeira belt, SE Brazil. *Journal of South American Earth Sciences*, v. 48, p. 43–57, 2013. ISSN 08959811.

TROUW, R. A. J.; TAVARES, F. M.; ROBYR, M. Rotated garnets: a mechanism to explain the high frequency of inclusion trail curvature angles around 90^o and 180^o. *Journal of Structural Geology*, v. 30, n. 8, p. 1024–1033, 2008. ISSN 01918141.

VALERIANO, C. M. The Southern Brasília Belt. In: HEILBRON, M.; CORDANI, U. G.; ALKMIM, F. (Ed.). *São Francisco Craton, Eastern Brazil. Regional Geology Reviews*. Switzerland: Springer International Publishing, 2017. cap. The Southe, p. 189–203. ISBN 9783319017150.

VALERIANO, C. M. et al. U-Pb Geochronology of Southern Brasília Belt (SE Brazil): sedumentary provenance, Neoproterozoic orogeny and assembly of Western Gondwana. *Precambrian Research*, v. 130, p. 7–11, 2004.

VALERIANO, C. M. et al. Southern brasilia belt (se brazil): tectonic discontinuities, k-ar data and evolution during the neoproterozoic brasiliano orogeny. *Revista Brasileira de Geociências*, v. 30, n. 1, p. 195–199, 2000.

VANDERHAEGHE, O.; DUCHÊNE, S. Crustal-scale mass transfer, geotherm and topography at convergent plate boundaries. *Terra Nova*, Wiley Online Library, v. 22, n. 5, p. 315–323, 2010.

VLACH, S.; GUALDA, G. A. R. Microprobe monazite dating and the ages of some granitic and metamorphic rocks from southeastern Brazil. *Revista Brasileira de Geociências*, v. 30, n. 1, p. 214–218, 2000.

WELLER, O.; ST-ONGE, M. Record of modern-style plate tectonics in the Palaeoproterozoic Trans-Hudson orogen. *Nature Geoscience*, Nature Publishing Group, v. 10, n. 4, p. 305, 2017.

WESTIN, A.; CAMPOS NETO, M. D. C. Provenance and tectonic setting of the external nappe of the Southern Brasília Orogen. *Journal of South American Earth Sciences*, Elsevier Ltd, v. 48, p. 220–239, 2013. ISSN 08959811. Avaible form internet: <http://dx.doi.org/10.1016/j.jsames.2013.08.006>.

WESTIN, A. et al. The Neoproterozoic southern passive margin of the São Francisco craton: Insights on the pre-amalgamation of West Gondwana from U-Pb and Hf-Nd isotopes. *Precambrian Research*, p. 454–471, 2019.

WESTIN, A. et al. A paleoproterozoic intra-arc basin associated with a juvenile source in the Southern Brasilia Orogen: Application of U–Pb and Hf–Nd isotopic analyses to provenance studies of complex areas. *Precambrian Research*, v. 276, p. 178–193, 2016.

YAKYMCHUK, C.; BROWN, M. Divergent behaviour of Th and U during anatexis: Implications for the thermal evolution of orogenic crust. *Journal of Metamorphic Geology*, v. 37, n. 899-916, 2019.

ZANARDO, A. *Análise petrográfica, estratigráfica e microestrutural da região de Guaxupé-Passos-Delfinópolis (MG)*. Tese (Doutorado) — Universidade Estadual Paulista, São Paulo, Brazil, 1992.

8 General conclusions

The present thesis contributes to understanding the metamorphic and tectonic evolution of southern Brasília Orogen, based on the data obtained for the Passos Nappe and the Luminárias Nappe. The main conclusions are described below.

- The combination of metamorphic modelling, trace elements geothermometers (Zr-in-rutile and Ti-in-quartz) and geochronology (EPMA monazite and LA-ICP-MS rutile dating) is an efficient procedure to access the metamorphic evolution of high pressure rocks under different facies.

- Rocks from the Unit H of the Passos Nappe (uppermost unit in the São Sebastião do Paraíso area) are metamorphosed under HP granulite facies. The P–T–t path is clockwise, the peak conditions took place at ∼830 ^{o}C and 1.2 GPa and the retrograde conditions at ∼600 ^{o}C and 0.9 GPa. The age of the metamorphic peak is ca. 635 Ma, constrained by monazite dating. The U-Pb rutile age of ca. 590 Ma indicates cooling down to 600 ^{o}C (rutile closure temperature). This data indicate a slow cooling rate for the granulite.

- The high pressure granulite facies rocks from Passos Nappe can be correlated with the rocks from the Andrelândia Nappe System (south of Passos Nappe).

- Rocks from the the Luminárias (both Carrancas Group and Santo Antônio Unit) record a metamorphic gradient that varies from HP lower amphibolite facies, in the northern portion, to eclogite facies in the southern portion. The both rocks were metamorphosed along a single clockwise metamorphic P–T–t path.

- Zr content in detrital rutile re-equilibrated in quartzite from the Luminárias Nappe. Minimum conditions of the re-equilibrium are *c.a.* 630 ± 30 ^{o}C and 1.4 ± 0.6 GPa. These conditions may indicate the threshold temperature above which rutile starts to record the temperature of metamorphism in quartzite.

- The age of the metamorphic peak from Luminárias Nappe is 615 ± 6 Ma for the central portion of Luminárias (LR10E sample) and 632 ± 4 Ma for the southern portion (LR44C sample) according to the included monazite.

- The high pressure rocks from Passos and Luminárias Nappe are tightly correlated with collisional continental setting during the southern Brasília Orogen tectonic evolution.

- The application of trace elements thermometers requires caution in the evaluations of the data, since a large spread in concentration is observed in HP amphibolite, eclogite and HP granulite facies. The third quartile of the Zr-in-rutile seems to be a coherent choice of value in both metamorphic facies. To evaluate and choose coherent Ti-in-quartz values it is essential to observe the cathodoluminescence (blue filter) *versus* the textural features of the quartz.

9 Supplementary Material

Additional supporting information may be found online in the follow links.

9.1 Supplementary Material of the Chapter 3

Supplementary Material - Chapter 3 - Folder

Figure 3.S1: Mineral compositional maps for sample SSPDH12. **Link**

Figure 3.S2: Standardization graphs from the compositional maps obtained from the cathodoluminescenc maps and Ti-in-quartz composition. **Link**

Figure 3.S3: Garnet isomodes. **Link**

Figure 3.S4: Kyanite isomodes. **Link**

Figure 3.S5: Biotite and rutile isomodes. **Link**

Table 3.S1: Microprobe mineral chemistry analyses of garnet, plagioclase and biotite from Sample SSPDH10. **Link**

Table 3.S2: Trace element composition of analyzed rutile grains. **Link**

Table 3.S3: T in quartz content in granulite samples. **Link**

Table 3.S4: Summary of whole rock compostion of the studied samples. **Link**

Table 3.S5: EPMA monazite major and trace element composition, Corrected concentrations of Th, U and Pb and calculated ages for the analyzed monazite. **Link**

Table 3.S6: Rutile dating data from samples SSPDH12, MG161 and SSPDH10. **Link**

9.2 Supplementary Material of the Chapter 4

Table 4.S1: Location of all studied samples with mineral assemblages in the schist samples. **Link**

9.3 Supplementary Material of the Chapter 5

Supplementary Material - Chapter 5 - Folder

Figure 5.S1: Calculated MnNCKFMASHTO isobaric (1.0 GPa) T–XO_2 isochemical phase diagram. **Link**

Figure 5.S2: Composition maps. **Link**

Figure 5.S3: Pressure–temperature isochemical phase diagram with garnet, biotite, feldspar and muscovite isopleths. **Link**

Table 5.S1: Electron microprobe conditions applied for the chemical analysis. **Link**

Table 5.S2: Chemical compositions, calculated atom per formula unit and calculated nominal end-member fraction for index metamorphic minerals. **Link**

9.4 Supplementary Material of the Chapter 6

Supplementary Material - Chapter 6 - Folder

Figure 6.S1: Pressure–temperature isochemical phase diagram with garnet, biotite, feldspar and muscovite isopleths. **Link**

Table 6.S1: Trace element composition of analyzed rutile grains. **Link**

Table 6.S2: Table showing the range of intra-grain variation of rutile grains with more than one analyses. **Link**

9.5 Supplementary Material of the Chapter 7

Figure 7.S1: AFM diagram from the Luminárias Nappe rocks. **Link**

Appendix

APPENDIX A – Conference abstracts

A.1 Application of rutile thermometry to quartzite: a new tool in metamorphic studies - Goldschmidt 2017 - Paris - France

Goldschmidt2017 Abstract

Application of rutile thermometry to quartzite: a new tool in metamorphic studies

R.A. FUMES [1] AND G.L. LUVIZOTTO [1]

[1] Department of Petrology, São Paulo State University, Av. 24A, 1515, 13506-900, Rio Claro, Brazil. (rafumes@rc.unesp.br, georgell@rc.unesp.br)

Quartzite represents a poor chemical system and is fairly unreactive when compared to other metamorphic rocks. Thus, it is seldom used in metamorphic studies. Geothermometers based on the equilibrium ZrO_2-TiO_2-SiO_2 might be used to assess temperature in this rock, since Zrn, Rt and Qtz are often present. However, it has been shown [1,2] that quartzite may preserve chemical composition of inherited Rt grains. A set of quartzites interbedded with schists from an area where the metamorphic gradient is oblique to the geological contacts (Lumiárias *Nappe* - Brazil) is used to evaluate the application of Zr-in-Rt thermometry to quartzites. Independent *P-T* data on the metapelite (pseudosections, Zr-in-Rt and Ti-in-Qtz) confirm a metamorphic gradient with conditions increasing from north (550 ˚C, 1.0 GPa) to south (640 ˚C, 1.5 GPa). Trace elements of Rt grains (heavy mineral separate, 63-200μm fraction) from seven quartzite samples (ca. 20kg each) that span the whole metamorphic gradient were analyzed by EPMA (JEOL 8230) at the São Paulo State University. In all samples, Nb/Cr in Rt is high and indicates pelitic signature. Zr contents in Rt from the lower-grade portion (< 580 ˚C) show a large spread. Higher grade samples show a smaller spread (Fig. 1). Other elements, such as Cr and Nb follow the same pattern. A slight increase in Zr content, marking the metamorphic gradient, is observed. Detailed BSE imaging shows that size and shape of Rt do not correlate with its chemical composition. In conclusion, the Zr-in-Rt geothermometer may be applied to quartzites and equilibration occurs at about 580 ˚C (1.2 GPa), opening new possibilities in metamorphic studies.

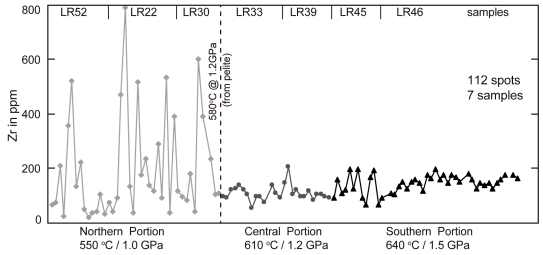

Figure 1: Zr content in rutiles (EPMA). *P-T* data from pelites.

[1] Triebold *et al*. (2007) *Chem. Geol*. **244**, 421-436. [2] Luvizotto *et al*. (2009) Miner. Petrol. **97**, 233-249.

A.2 P-T constraints on high-pressure granulites from southern Brasília belt: Ti-quartz and Zr-in-Rutile thermometry - Goldschmidt 2017 - Paris - France

Goldschmidt2017 Abstract

P-T constraints on high-pressure granulites from southern Brasilian Belt: Ti-quartz and Zr-in-Rutile thermometry

G.L. LUVIZOTTO [1*], R.A. FUMES [1], R. MORAES[2], E.R.M. FERRAZ [1]

[1] Department of Petrology, São Paulo State University, Av 24A, 1515, 13506-900, Rio Claro, Brazil. (*georgell@rc.unesp.br)

[2] Geoscience Institute, University of São Paulo, Rua do Lago, 562, 05508-080, São Paulo, Brazil.

HP and UHP rocks are important tools to understand Earth Dynamics. However, assessing peak metamorphism and *P-T* history of such rocks is not an easy task. Pelitic HP-granulites have the assemblage Grt+Ky+KFs±Rt and the lack of Opx/Cpx has led to misclassification of some of these rocks as amphibolite facies. One major problem in determining peak *P-T* conditions is the diffusion, during cooling, of elements that are important for exchange thermometers. Although net transfer barometers are less affected by cooling, pelitic granulites have low concentration of Na and Ca and important minerals for barometric calculations are not formed (Plag, Cpx, Opx). It is the case of the studied rocks, a set of Pelitic HP-granulites that derive from a Neoproterozoic nappe system (Passos Nappe) related to the formation of Gondwana (Brasilia Orogen). Ti-in-quartz and Zr-in-Rutile thermometry was used to determine peak P-T conditions, since they are less prone to resetting. Analyses were carried out by EPMA at the São Paulo State University using a JEOL8230. Ti content in Qtz show a smaller spread when compared to Zr in rutile. Rt grains that have small Zrn inclusions and record lower Zr contents are responsible for the dispersion of the data. Highest Zr contents are interpret to represent peak conditions. The interception of both thermometers on a *P-T* space indicates conditions of 850 to 870 ^{o}C and 1.4 to 1.8 GPa for the studied rocks.

A.3 Evaluation of Zr-in-Rt and Ti-in-Qtz thermobarometry in granulites - Goldschmidt 2018 - Boston - EUA

Goldschmidt2018 Abstract

Evaluation of Zr-in-Rt and Ti-in-Qtz thermobarometry in granulites

R.A. FUMES [1], G.L. LUVIZOTTO [1*], R. MORAES[2]

[1] Department of Petrology, São Paulo State University, Av 24A, 1515, 13506-900, Rio Claro, Brazil. (*rafumes@rc.unesp.br)

[2] Geoscience Institute, University of São Paulo, Rua do Lago, 562, 05508-080, São Paulo, Brazil.

Recent papers have shown that highest contents of Zr-in-Rt may be used to calculate peak *T* [1] in high-grade Rt+Zrc+Qtz bearing rocks. Several mechanisms have been presented in the literature to explain lower contents of Zr in Rt that are often registered in HT-UHT rocks [1, 2]. More importantly, low Zr contents cannot be used to assess cooling temperatures [2]. Studies have shown that Ti incorporation in Qtz is sensitive to post-peak variation of *P* and *T* [3,4]. Furthermore, dynamic recrystallization enhances the kinetics of Ti equilibration in Qtz [4]. We present Zr-in-Rt and Ti-in-Qtz concentration data on HP metapelitic granulite (Rt+Grt+Ky+Kfs+Qtz+Zrc) samples from the Passos Nappe, Minas Gerais, Brazil, that have faced varying degrees of post-peak retrometamorphism. Although a large inter-grain spread in Zr content (450 to 2090 ppm) in Rt grains from all studied samples is observed, temperature calculated using highest content is ca. 850 ºC at 16 kbar and match those calculated based on peak mineral assemblage and pseudosection modelling. A large inter-grain spread in Ti content (32 to 134) in Qtz grains is also observed, however, highest values (all above 70 ppm) are recorded by the most retrogressed sample. This sample has an intensely oriented fabric where the presence of Ms indicates the foliation formed after metamorphic peak. There is no correlation between Ti content in Qtz and texture (i.e., included in Grt or in matrix). We interpret highest Ti contents in Qtz to represent re-equilibration during decompression and not metamorphic peak conditions. As a consequence, although some Rt grains are able to keep high Zr contents, *P* estimates based on both Zr-in-Rt and Ti-in-Qtz thermobarometer would not represent peak condition in rocks where post-peak retrogression took place. In the studied samples, lower Ti contents (ca. 40 ppm) in less retrogressed samples may indeed indicate metamorphic peak conditions at ca. 850 ºC and 18-20 kbar.

[1] Taylor-Jones & Powell (2015) *J Metamorph Geol.* 115:33. [2] Kohn *et al.* (2016) *Contrib Mineral Petrol.* 171:78. [3] Thomas et al. (2015) *Contrib Mineral Petrol.* 169:27. [4] Nachlas & Hirth (2015) J. Geophys. Research. 8120:120.

A.4 Idades de monazita no granulito de alto alumínio da Nappe de Passos no sul do Orógeno Brasília - Simpósio de Geologia do Sudeste 2019 - Campinas - Brasil

Núcleo
São Paulo

IDADES DE MONAZITA NO GRANULITO DE ALTO ALUMÍNIO DA NAPPE DE PASSOS NO SUL DO ORÓGENO BRASÍLIA

Regiane Andrade Fumes[1], George Luiz Luvizotto[2]

[1] Universidade Estadual Paulista (UNESP), Instituto de Geociências e Ciências Exatas, Campos de Rio Claro, e-mail: regiane.fumes@unesp.br
[2] Universidade Estadual Paulista (UNESP), Instituto de Geociências e Ciências Exatas, Campos de Rio Claro, e-mail: george.luvizotto@unesp.br

O Orógeno Brasília é uma faixa móvel neoproterozoica associada à formação do Gondwana ocidental que registra a história completa da abertura e fechamento de um oceano até a colisão continental. O Orógeno Brasília Sul (porção ao sul da Sintaxe dos Pirineus) é composto essencialmente por rochas metassedimentares com metamorfismo e deformação aumentando, em geral, de leste (borda cratônica) para oeste. A Nappe de Passos ocorre no extremo sul do Orógeno Brasília Sul e é composta por rochas metassedimentares plataformais e de sedimentação imatura em ambiente de plataforma profunda a talude continental. É descrito um metamorfismo invertido para as rochas da nappe, variando desde fácies xisto verde na unidade basal atingindo fácies granulito na unidade superior. Nesse trabalho, são apresentadas idades de monazita para as rochas metassedimentares de fácies granulito de alta pressão da porção superior da Nappe de Passos. As análises de monazita foram realizadas no Laboratório de Microssonda Eletrônica (JEOL8230 SUPERPROBE) do Departamento de Petrologia e Metalogenia da UNESP em Rio Claro. Foram analisados mapas de Ca, Y, U e Th nos cristais de monazita selecionados, os quais foram utilizados para guiar as análises quantitativas. Três cristais de monazita, com idade conhecida, foram utilizados como padrão interno (Moacir, Madmon e Zack). As quatro amostras de granulito de alto alumínio analisadas apresentam granulação grossa e texturas de anatexia. São compostas por porfiroblastos de granada e cianita em uma matriz de quartzo, feldspato potássico, plagioclásio, biotita, apatita, clorita, rutilo, zircão, ilmenita e monazita. A foliação é uma xistosidade marcada pela orientação dos minerais da matriz. A paragênese do pico metamórfico é granada+cianita+K-feldspato+rutilo±plagioclásio, com condições previamente calculadas de 1.5 GPa e 830 ^{o}C. A monazita ocorre tanto na matriz das rochas quanto inclusa na granada e na cianita. Cristais de monazita inclusos em granada apresentam idades sutilmente mais antigas (633 ±5 a 640 ±10 Ma) e teores mais elevados de Y quando comparados com cristais da matriz (629 ±8 a 635 ±8 Ma). As idades obtidas são compatíveis com os dados publicados na literatura para as rochas do Orógeno Brasília Sul e indicam idade mínima de 640 ±10 Ma para o pico metamórfico que ocorreu fácies granulito de alta pressão, sob condições de pressão e temperatura de crosta inferior.

Apoio: CNPq.
Palavras-chave: Microssonda eletrônica, Neoproterozoico, Gondwana.

A.5 Cooling rates in high pressure granulite from Southern Brasília Orogen (SE-Brazil) - Goldschmidt 2020 - Virtual, Global

Goldschmidt2020 Abstract

Cooling rates in high pressure granulite from Southern Brasília Orogen (SE-Brazil)

R.A. FUMES [1*], G.L. LUVIZOTTO [1], C. M. VALERIANO[2] AND R. MORAES[3]

[1]Department of Geology, São Paulo State University, 13506-900, Rio Claro, Brazil. (*regiane.fumes@unesp.br)
[2]Faculdade de Geologia, Rio de Janeiro State University, 20550-900, Rio de Janeiro, Brazil
[3]Geoscience Institute, University of São Paulo, 05508-080, São Paulo, Brazil

A combination of U-Th-Pb$_T$ monazite EPMA dating and LA-ICP-MS rutile dating is used to assess the cooling rates of high-pressure granulite from the Passos Nappe (SE - Brazil). These rocks have a pelitic protolith and record a peak assemblage of garnet + kyanite + rutile + K-feldspar + melt formed at 860 ˚C and 1.8 GPa. Retrograde conditions of 800 ˚C and 1.0 GPa are marked by grossular content, anorthite composition and biotite crystallization. Metamorphic peak conditions occurred *ca*. 635 Ma, based on monazite dating, whereas rutile ages of *ca*. 590 Ma record the late retrograde stage (at *ca*. 600 ˚C), associated with late chlorite replacing biotite. Muscovite K-Ar ages in the Passos Nappe of *ca.* 570-580 Ma record the final cooling stages upon exhumation to the upper crust (*ca.* 300 ˚C) [1]. The studied rocks result from the metamorphism of continental margin sediments in the deep root of this Cryogenian-Ediacaran continent-continent collisional zone, which is related with the early phases of western Gondwana formation. The retrograde path records exhumation to 600 ˚C at < 1.0 GPa at a relatively slow integrated cooling rate, of *ca.* 6 ˚C/Ma (to the peak in 635 Ma to retrograde in 590 Ma). This slow cooling rate can be partially explained by the increase of melt production during the decompression. The cooling rate of the final stage of the retrograde *P*–*T*–t path, based on the muscovite age, is faster (*ca.* 15 ˚C/Ma) than calculated for the earlier phase. We infer that channel flow occurred in the presence of melt during the metamorphic peak (*ca.* 630 Ma), transitioning to localized fault slice tectonics during later stages of the *P*–*T*–t path, at *ca.* 590 Ma at lower temperatures (e.g. [2]). This interpretation would be consistent with switching from a slow cooling rate during initial exhumation in a viscous channel to faster cooling in a fault-block dominated regime.

[1] Valeriano *et al.* (2000). *Revista Brasileira de Geociências* **30(1)**, 195–199. [2] Chakraborty *et al.* (2017) *Lithos* **282-283**, 464-482

A.6 Quantitative mapping of Ti-in-quartz for thermobarometry: application to high-pressure granulite - GSA 2020 - Connects Online

Quantitative mapping of Ti-in-quartz for thermobarometry: application to high-pressure granulite

R.A. FUMES [1*], P. LANARI [2], G.L. LUVIZOTTO [1]

[1]Department of Geology, São Paulo State University, 13506-900, Rio Claro, Brazil. ([*]regiane.fumes@unesp.br)
[2]Institute of Geological Sciences, University of Bern, Baltzerstrasse 1 + 3, Bern 3012, Switzerland

In high-grade rocks such as high-pressure granulites, the Ti content of quartz commonly shows a large variability in composition. This apparent complexity requires a careful evaluation of the chemical data, if possible combined with a detailed microstructural study. Only then, meaningful temperatures can be derived using Ti-in-quartz thermometry. In this study, we demonstrate that cathodoluminescence (CL) mapping is essential for this purpose, since the CL emission (captured using a blue filter) on quartz is proportional to the Ti content. Quantitative maps of TiO_2 were produced by combining qualitative CL maps with spot analyses obtained by Electron Probe Micro-analyzer (EPMA). This mapping approach produces temperature maps which raise the possibility of recovering detailed records of *T* conditions in a microstructural context. Measurements of Ti in quartz, were performed simultaneously with a JEOL JXA8230 EPMA using three WDS spectrometers, whereas CL maps were acquired using a coupled panchromatic CL system. The XMapTools software was used for calibration and to generate temperature maps (calibration of Thomas et al., 2010). Results obtained for the high-pressure granulite from the Passos *Nappe* (SE – Brazil) Southern Brasília Orogen show an heterogenous distribution of Ti in quartz. The Ti content decreases towards the rim of crystals, from 134 ppm to 26 ppm. These rocks have a pelitic protolith; they recorded metamorphic peak conditions at high-pressure granulite facies followed by a phase of near isothermal decompression. Highest temperatures obtained for 1.0 GPa (~ 800 ˚C) are in good agreement with early retrograde conditions. This result indicates that Ti-in-quartz thermometry shows, in the studied sample, the temperature of quartz formation, which occurred during melt crystallization. The described method is appropriate to retrieve quartz-forming reactions and the associated conditions in granulitic rocks.

Thomas et al. (2010). *Contrib. Mineral. Petrol.*, ***160*(5)**,743–759

Geological Society of America Abstracts with Programs. Vol 52, No. 6, 2020 doi: 10.1130/abs/2020AM-356156